



PhD-FSTM-2024-001
The Faculty of Science, Technology and Medicine

DISSERTATION

Presented on 22/01/2024 in Esch-sur-Alzette

to obtain the degree of

DOCTEUR DE L'UNIVERSITÉ DU LUXEMBOURG

EN SCIENCES DE L'INGÉNIEUR

by

Hooman ESLAMI

Born on 22 October 1991 in Kerman (Iran)

DESIGN AND ANALYSIS OF A MODULAR, FLEXIBLE, REUSABLE, PREFABRICATED TIMBER-CONCRETE COMPOSITE FLOOR SYSTEM

Dissertation defence committee

Prof. Dr. Danièle WALDMANN, dissertation supervisor
Professor, Technische Universität Darmstadt

Prof. Dr. Frank SCHOLZEN, Chairman
Professor, Université du Luxembourg

Prof. Dr. Norman TEFERLE, Vice Chairman
Professor, Université du Luxembourg

Prof. Dr. Marc OUDJENE
Professor, Université de Laval

Dr. Laddu Bhagya JAYASINGHE
Postdoctoral Scientist, Ludwig-Maximilians-Universität München

Blank page

I. Acknowledgment

This doctoral project began under the ECO4SD research project at the University of Luxembourg in the Faculty of Science, Technology, and Medicine as part of the Doctoral Programme in Engineering Sciences. Supported by the "Investissement pour la croissance et l'emploi" program—European Regional Development Fund, the research project concluded in 2022, while this specific research continued until 2023.

I am foremost grateful to my supervisor, Prof. Dr. Danièle Waldmann-Diederich, for including me in her admirable research team and for her unwavering encouragement and trust. Her consistent support, guidance, and confidence in my work have been instrumental in starting and continuing my doctoral research journey.

My sincere thanks go to the members of my supervision committee (CET), Prof. Dr. Felix Norman Teferle and Prof. Dr. Frank Scholzen, for their continuous support and constructive feedback guiding my research. Dr. Laddu Bhagya Jayasinghe deserves heartfelt appreciation for his significant role in my achievements. His scientific support, mentorship, and companionship have been invaluable. I also thank Prof. Dr. Marc Oudjene for agreeing to be a member of my defense jury.

I owe a debt of thanks to Prof. Dr. Markus Schäfer and Prof. Dr. Christoph Odenbreit, who were my professors during my master's studies and continued to be a source of inspiration and support during my PhD studies. I appreciate the support of Prof. Dr. Ludger Wirtz, who kindly accepted to be my manager during the last two years of my Ph.D.

I must express my gratitude to all the professors involved in the ECON4SD project. Moreover, I show appreciation to my fellow doctoral researchers in this project, Dr. Akbarieh Arghavan, Dr. Marielle Ferreira Silva, Dr. Jovan Fodor, and Dr. Michael Rakotonjanahary, who rapidly included and accompanied me in the research project. Also, I appreciate the help of Mr. Alfredo

Romero, a fellow Ph.D. and friend at the University of Luxembourg, in some tests on the timber material. I thank the former doctoral researcher and friend, Dr. Shilton Rica, for inspiring me to start my PhD journey.

I express my appreciation to my colleagues and friends, including Dr. Vishojit Bahadur Thapa, Dr. Dolgion Erdenebat, Dr. Gael Chew Ngapeya, Dr. Patrick Pereira Dias, Dr. Lorenc Bogoviku, Mr. Tarik Camo, Mr. Sinan Kaassamani, Ms. Anna Tokareva, and Ms. Suzanne Biwer for their daily support and companionship, making my time at the University of Luxembourg genuinely memorable.

My gratitude again extends to Prof. Teferle and Ms. Biwer, the Doctoral Programme Coordinator and the Doctoral Programme Administrator, respectively, for their dedicated efforts to improve doctoral students' personal and professional development. My sincere thanks go to all the staff at the University of Luxembourg who supported me during my Ph.D., including Dr. Silvia Venditti, Ms. Heidi Backstroem, Ms. Rita Giannini, Ms. Odile Marois, Ms. Adamantia Galani, and Mr. Shayan Weber.

I extend my gratitude to the structural laboratory team at the University of Luxembourg, including Mr. Gilbert Klein, Mr. Marc Seil, Mr. Ed Weyer, and Mr. Ken Adam, for their amicable and beneficial help, invaluable advice, and flexibility. I also appreciate the team at the Technical University of Darmstadt, namely Dr. Eftychia Apostolidi, Mr. Yves Kibnowski, Mr. Eric Rauschenbach, Mr. Max Fritzsche, and Mr. Maximilian Rupp, for their fast-paced support during my experiments in Darmstadt which was truly incredible.

Special thanks to Mr. Mehdi Saeidi, Mr. Alireza Yaghma Carbonel, and Ms. Anna Dontsova, students who contributed to this work through their semester projects and master theses under my supervision.

I want to dedicate a paragraph here to all the professors and administration support staff at BIHE University who sacrificed their time and put their careers and personal lives in danger to serve young students like me whose fundamental rights to have higher education were refused by the Iranian government solely due to their personal beliefs. I shall not mention their names for their safety, but I remember their sacrifices every step of my career.

Finally, my most profound appreciation goes to my parents, family, and friends for their continuous support during challenging times and celebrations of every small achievement. I feel fortunate to have you by my side, and without your support, navigating the difficulties and completing this work would have been impossible.

Luxembourg, December 12th, 2023

Hooman ESLAMI

II. Abstract

The timber-concrete floor system (TCC) has gained more attention in the last few decades as the construction industry has focused more on reducing its environmental impact. Combining concrete in compression and timber in tension zones of a bending section enables the designers to benefit from the advantages of both materials while reducing concrete consumption and improving the stiffness and strength of plain timber floors. However, research on demountable and reusable TCC floor systems, which can reduce the environmental impact and improve the sustainability capacity of the floor system one step further, is limited. Therefore, this research is focused on finding a reversible means of connection between concrete and timber and a floor system concept that could be prefabricated, demounted and reused in a straightforward manner.

This dissertation presents a background and literature review on TCC floor systems and sustainability. Then, the research project results are presented in a compilation of 5 papers. The first paper compares the environmental impacts of a TCC slab with similar reinforced concrete and steel-concrete composite slabs. The paper also highlights the environmental benefits of reusing timber in TCC slabs. The second paper presents a case study in Luxembourg that compares the environmental impacts of two functionally identical buildings with different structural materials: one in masonry concrete and the other one in timber. In the third paper, a material model for timber as a structural material is presented, which gives the possibility to numerically simulate the orthotropic behavior of timber and model its failure under compression and tension. The modular prefabricated TCC floor system that is demountable and reusable is presented in the fourth paper, and a downscaled experiment was performed on the bending behavior of the slab. The paper further investigates different notched shear connections within a numerical parametric study. The fifth paper investigates the shear

behavior of six real-scaled samples of the demountable notched connection. The effects of different loading setups and reuse on the results were studied.

Lastly, a real-scaled bending experiment is presented in Chapter 4. Three CLT-concrete composite slabs and one CLT slab were tested under a 10-meter span bending setup. The results confirmed the floor system's high strength and stiffness and the ease in fabrication and demounting of the floor system.

III. List of Publications

This dissertation is mainly based on the investigations and studies presented in the following publications:

- H. Eslami, A. Yaghma, L. Bhagya Jayasinghe, and D. Waldmann, “Influence of different end-of-life cycle scenarios on the environmental impacts of timber-concrete composite floor systems,” in *World Conference on Timber Engineering (WCTE 2023)*, Oslo, Norway: World Conference on Timber Engineering (WCTE 2023), 2023, pp. 982–988. doi: [10.52202/069179-0134](https://doi.org/10.52202/069179-0134).
- H. Eslami, A. Yaghma, L. Bhagya Jayasinghe, and D. Waldmann, “Comparative life cycle assessment of light frame timber and reinforced concrete masonry structural systems for single-family houses in Luxembourg,” *Heliyon*, vol. 10, no. 4, Feb. 2024, doi: 10.1016/j.heliyon.2024.e26083.
- H. Eslami, L. B. Jayasinghe, and D. Waldmann, “Nonlinear three-dimensional anisotropic material model for failure analysis of timber,” *Engineering Failure Analysis*, vol. 130, p. 105764, Dec. 2021, doi: 10.1016/j.engfailanal.2021.105764.
- H. Eslami, L. B. Jayasinghe, and D. Waldmann, “Experimental and Numerical Investigation of a Novel Demountable Timber–Concrete Composite Floor,” *Buildings*, vol. 13, no. 7, p. 1763, Jul. 2023, doi: 10.3390/buildings13071763.
- H. Eslami, L. B. Jayasinghe, and D. Waldmann, “Experimental and numerical study on shear behavior of a demountable CLT-concrete composite shear connection,” *Construction and Building Materials*, vol. 425, p. 135982, Apr. 2024, doi: 10.1016/j.conbuildmat.2024.135982.

IV. Table of Contents

I.	Acknowledgment	III
II.	Abstract	VI
III.	List of Publications	VIII
IV.	Table of Contents	IX
V.	List of Figures	XII
VI.	List of Tables	XIV
VII.	Abbreviations	XV
1	Introduction.....	1
1.1	Motivation.....	1
1.2	ECON4SD research project	1
1.3	Background	4
1.4	Aim of the study	6
1.5	Outline of the thesis	7
2	Review of the Literature.....	9
2.1	Environmental impact of construction materials.....	9
2.1.1	Life cycle Assessment	9
2.1.2	Design for deconstruction	12
2.2	Timber as a structural material.....	13
2.2.1	Timber material model	17
2.3	Timber-concrete composite floor system	21
2.3.1	Mechanical fasteners.....	25

2.3.2	Steel profiles	26
2.3.3	Notches	27
2.3.4	Continuous connections	28
2.4	<i>Push-out test</i>	28
3	Results	32
3.1	<i>Paper I</i>	33
3.2	<i>Paper II</i>	49
3.3	<i>Paper III</i>	82
3.4	<i>Paper IV</i>	128
3.5	<i>Paper V</i>	162
4	CCC slab under bending.....	203
5	Discussion	212
5.1	<i>Paper I</i>	212
5.2	<i>Paper II</i>	213
5.3	<i>Paper III</i>	215
5.4	<i>Paper IV</i>	216
5.5	<i>Paper V</i>	217
6	Conclusion and outlook.....	218
7	Bibliography.....	223
8	Annexes.....	229
8.1	<i>Drawings of CCC bending experiment</i>	229
8.2	<i>Drawings of Push-out experiment</i>	233

8.3	<i>Drawing of downscaled bending test</i>	237
-----	---	-----

V. List of Figures

FIGURE 1. ECON4SD PROJECT MEMBERS AND WORK PACKAGES.	2
FIGURE 2. (A) CONTRIBUTIONS AND (B) NEEDS BETWEEN THE WORK PACKAGES OF THE ECON4SD PROJECT. FIGURE SOURCE [7].....	3
FIGURE 3. OUTLINE OF THE THESIS.....	8
FIGURE 4. LIFE CYCLE ASSESSMENT FRAMEWORK ACCORDING TO ISO 14040 [35].....	10
FIGURE 5. BUILDING ASSESSMENT INFORMATION BASED ON EN 15978 [39].....	12
FIGURE 6. MURRAY GROVE BUILDING. FIGURES FROM [43].....	15
FIGURE 7. FORTÉ BUILDING. FIGURES FROM [44].	15
FIGURE 8. TREET BUILDING. FIGURES FROM [45].	16
FIGURE 9. BROCK COMMONS TALLWOOD HOUSE. FIGURES FROM [46].	16
FIGURE 10. HAUT BUILDING. FIGURE FROM [47].	17
FIGURE 11. ORTHOTROPIC AXES OF TIMBER.	18
FIGURE 12. COMPARISON OF COMPOSITE SLAB UNDER THE SAME LOADING WITH A) FULL COMPOSITE ACTION, B) PARTIAL COMPOSITE ACTION, AND C) NO COMPOSITE ACTION.....	22
FIGURE 13. THE FORCE AND MOMENT AT A TCC CROSS-SECTION. FIGURE IS BASED ON [79].....	23
FIGURE 14. SOME MECHANICAL FASTENERS AS SHEAR CONNECTIONS: (A) PERPENDICULAR SELF-TAPPING SCREWS; (B) INCLINED SELF-TAPPING SCREWS; (C) COACH SCREW WITH A CIRCULAR GROOVE IN TIMBER. CONNECTIONS WERE REBUILT BASED ON [83,85].....	26
FIGURE 15. EXAMPLE STEEL PROFILES AS SHEAR CONNECTIONS: (A) FOLDED STEEL PLATE EMBEDDED IN CONCRETE AND GLUED IN TIMBER; (B) STEEL PLATE EMBEDDED IN CONCRETE AND SCREWED TO TIMBER BEAM WITH VULCANIZED RUBBER LAYER; (C) STEEL TUBE WITH COACH SCREW. CONNECTIONS WERE REBUILT BASED ON [86,87].....	27
FIGURE 16. A NOTCHED SHEAR CONNECTION. THE CONNECTION WAS REBUILT BASED ON [88]	28
FIGURE 17. PERFORATED STEEL PLATE AS A SHEAR CONNECTION FOR A TTC SLAB. THE CONNECTION WAS REBUILT BASED ON [89].	28
FIGURE 18. SYMMETRIC PUSH-OUT TEST SETUP WITH (A) TIMBER AND (B) CONCRETE CORE.	29
FIGURE 19. ASYMMETRIC PUSH-OUT TEST SETUP WITH LOADING ON (A) TIMBER AND (B) CONCRETE	29
FIGURE 20. LOADING PROCEDURE OF THE PUSH-OUT TEST ACCORDING TO EN 26891 [91].	30
FIGURE 21. TYPICAL LOAD-SLIP RESULTS FROM A PUSH-OUT TEST.....	31

FIGURE 22. THE CCC SLAB DESIGNED FOR THE BENDING EXPERIMENT. DIMENSIONS ARE IN MILLIMETERS.	203
FIGURE 23. SLABS BEFORE CASTING CONCRETE.	204
FIGURE 24. SIX-POINT BENDING EXPERIMENT SETUP. DIMENSIONS ARE IN MILLIMETERS.	205
FIGURE 25. DISPLACEMENT SENSORS IN THE BENDING EXPERIMENT USED FOR 1) VERTICAL DEFLECTION (w1-w4), B) END-SPAN SLIP (H1 AND H12), C) SEPARATION OF THE CONCRETE AND TIMBER AT THE MID-SPAN (v1 AND v2), AND D) SLIP AT EACH NOTCHED CONNECTION (H2-H11, H13 AND H14).....	205
FIGURE 26. LOADING PROCEDURE OF THE BENDING EXPERIMENT FOR A) CCC B1, B) CLT B1, C) CCC B2, AND D) CCC B3.	206
FIGURE 27. FAILURE MODES OF THE SPECIMENS: A) FLEXURAL FAILURE OF THE CLT PANEL IN CLT-B1, B) FLEXURAL FAILURE OF THE CLT PANEL AND TENSILE CRACK OPENING IN CONCRETE IN CCC B2, C) FLEXURAL FAILURE OF THE CLT PANEL IN CCC-B3, D) CONCRETE CRUSHING UNDER COMPRESSION AT THE NOTCH, E) SHEAR CRACK OPENING IN CONCRETE AT NOTCH, F) SHEAR CRACK PROPAGATION AT THE CONCRETE FROM NOTCH TO CONCRETE SURFACE, G) SHEAR CRACKS IN TIMBER AT NOTCH, H) TIMBER CRUSHING UNDER COMPRESSION AT NOTCH, I) FINGER JOINT FAILURE IN THE TENSILE ZONE UNDER BENDING AT THE MIDSPAN.	207
FIGURE 28. LOAD-DEFLECTION RESULTS OF THE BENDING EXPERIMENT FOR A) CCC-B1, B) CLT-B1, C) CCC-B2, AND D) CCC-B3.	208
FIGURE 29. END-SPAN SLIP OF A) CCC-B1, B) CCC-B2 AND C) CCC-B3.	209
FIGURE 30. DEMOUNTED CCC-B2 SLAB AFTER FAILURE.	210
FIGURE 31. DEMOUNTING CONCRETE SLAB FROM CCC-B1 AFTER THE FIRST LOADING CYCLE.....	211

VI. List of Tables

TABLE 1. THE RESULTS FROM THE SIX-POINT BENDING EXPERIMENT.	210
--	-----

VII. Abbreviations

BIM – Building Information Modeling

CCC – CLT-Concrete Composite

CDM – Continuum Damage Mechanics

CDP – Concrete Damage Plasticity

CLT – Cross-Laminated-Timber

DfD – Design for Deconstruction

ECON4SD – Eco-Construction for Sustainable Development

EoL – End-of-Life

EPD – Environmental Product Declaration

EPS – Expanded Polystyrene

EWP – Engineered Wood Products

FE – Finite Element

Glulam – Glued Laminated Timber

GWP – Global Warming Potential

LCA – Life cycle Assessment

LVL – Laminated Veneer Lumber

NLFM – Non-Linear Fracture Mechanics

OSB – Oriented Strand Board

PE – Primary Energy

RC – Reinforced Concrete

SCC – Steel-Concrete Composite

TCC – Timber-Concrete Composite

WP –Work Package

1 Introduction

1.1 Motivation

The construction industry is a major contributor to energy consumption, resource depletion, and greenhouse gas emissions. Construction and demolition activities generate a substantial portion of total waste, accounting for over one-third of waste production in Europe [1]. This sector contributes to approximately 40% of Europe's primary energy (PE) consumption, accounts for 39% of energy-related carbon dioxide emissions, and is responsible for 36% of the world's total energy use [2–4]. In alignment with the Paris Agreement, the European Green Deal has set ambitious goals to achieve climate neutrality within the European Union by 2050 [5]. However, addressing these commitments in the face of significant carbon emissions and rapid population growth poses a formidable challenge [6]. Consequently, the imperative to reduce the environmental impacts stemming from the construction industry has become increasingly pressing over the past few decades.

1.2 ECON4SD research project

The Eco-Construction for Sustainable Development (ECON4SD) project represented a paradigm shift in how architects and engineers collaborate to create energy and resource-efficient buildings. This multidisciplinary research project, co-funded by the EU in partnership with the University of Luxembourg, sought to revolutionize sustainable construction concepts, focusing on materials such as concrete, steel, and timber [7].

The project's fundamental goals were to promote adaptability, flexibility, and modularity both in building conceptual and structural design, with a particular emphasis on modular and detachable buildings. The project recognized that structural elements and aging materials are crucial in a building's service life. The project pursued to illustrate the transformation of

buildings into sources of materials and components, shifting away from contributing to End-of-Life (EoL) waste. This approach aimed to minimize energy and resource consumption throughout the buildings' entire life cycle. Moreover, the project required the design of easily maintained, repaired, removed, and reused components, aligning with circular economy principles.

The project comprised a team of researchers, including six doctoral candidates, a postdoctoral researcher, and professors from the School of Civil Engineering and Architecture at the University of Luxembourg. They collaborated across seven working packages (WP), each addressing specific aspects of sustainable construction. The WPs and members are presented in Figure 1.

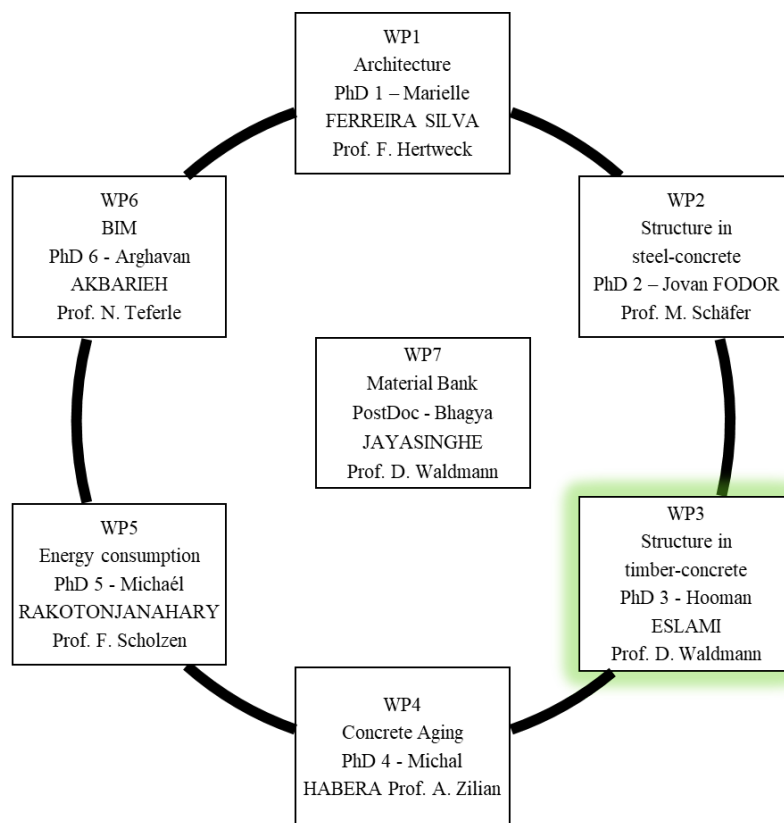


Figure 1. ECON4SD project members and work packages.

The needs and contributions of the WPs are demonstrated in Figure 2. WP1 focuses on flexible architecture, aiming to develop architectural typologies that facilitate deconstruction,

reconstruction, and adaptability to different needs. WP2 and WP3 are dedicated to optimizing structural components in steel-concrete and timber-concrete systems, respectively, emphasizing modularity and reusability. WP4 delves into concrete aging, addressing the durability of components. WP5 tackles energy efficiency and life cycle optimization of building elements, considering heating, ventilation, and cooling. WP6 explores Building Information Modeling (BIM) and data acquisition for eco-construction and sustainable development, aiming to create a digital library (Material data bank) for component tracking and labeling. Finally, WP7 focuses on centralizing project information, analyzing results, and developing a material and component bank.

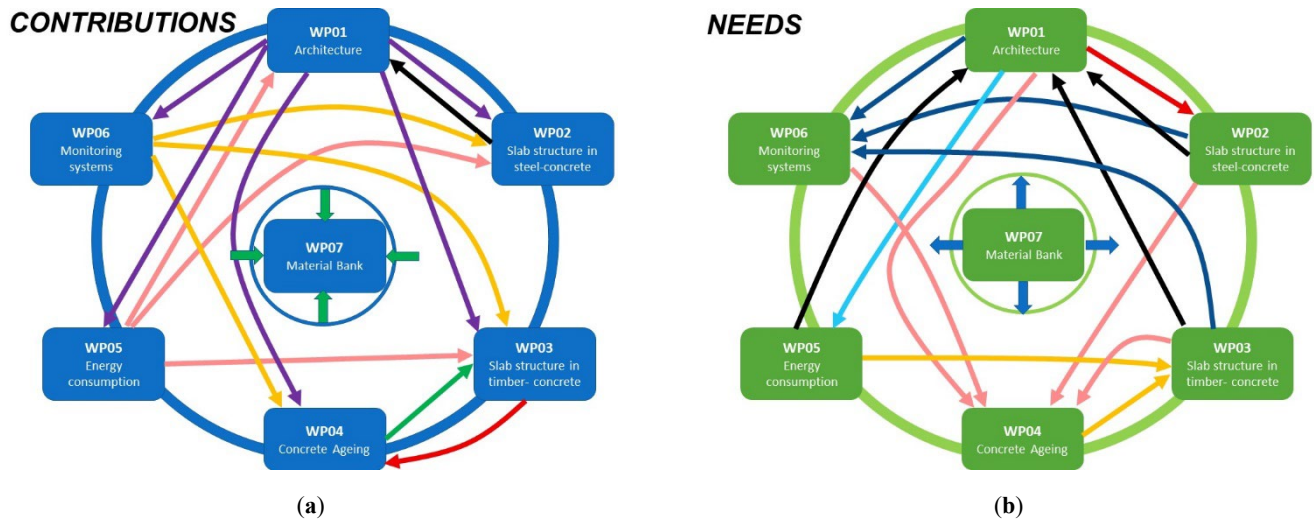


Figure 2. (a) contributions and (b) needs between the work packages of the ECON4SD project. Figure source [7].

This dissertation is based on the findings from the investigation of WP3. The WP3 focused on designing a reversible means of composite connection between concrete and timber to further improve the current sustainability performance of Timber-Concrete Composite (TCC) systems by enabling partial reuse and effective recycling of both materials.

1.3 Background

The balance of environmental impacts in buildings has shifted over time. Previously, energy consumption during the operational stage was the dominant factor contributing to these impacts [8]. Traditionally, this stage accounted for more than 70% of a building's energy consumption [9]. However, as buildings have become more energy-efficient and moved towards nearly zero-energy standards, the significance of energy use during the operational stage has decreased [10–12]. A study conducted in Belgium [13] illustrates this shift, indicating that in conventional residential buildings with regular energy performance, the operational stage could contribute between 69% and 89% of the total life cycle impact, depending on the house type. In contrast, this proportion has notably reduced in modern low-energy houses, ranging from 35% to 61%. This change signifies a transition where the embodied energy in construction materials now plays a more substantial role in determining a building's environmental impact.

The manufacturing processes of conventional construction materials such as steel and concrete are energy-consuming and contribute significantly to carbon dioxide emissions [14]. Consequently, in the last decades, substantial attention has been devoted to fostering the usage of timber and engineered wood products (EWPs) [15]. They are more sustainable due to their low embodied energy, high carbon storage, and renewability [16]. Other characteristics of timber, such as its high strength-to-density ratio, desirable aesthetic, and low thermal conductivity, made it a good solution for substituting steel and concrete in structural elements [17–19].

However, in the context of timber-based solutions like slabs and beams, certain unfavorable characteristics, such as springiness, vibration, and inadequate sound insulation, pose challenges for designers [20,21]. These limitations have driven an increased adoption of timber in hybrid structures, often combined with concrete [22]. TCC floors, a notable example, feature a

concrete slab placed atop a timber section, usually in the form of a joist or slab, connected through a shear connection mechanism [23]. The effectiveness of this shear connection determines the level of composite behavior between the two components when subjected to bending forces [24]. Notably, the concrete element primarily resists compression forces, while the timber component bears tension forces. A well-optimized TCC system can significantly enhance the bending capacity of conventional timber floors, often by a factor of 3 to 5 [25]. This approach not only reduces the amount of concrete employed but also results in lighter self-weight and diminished carbon dioxide emissions. Research findings underscore that TCC slabs can exhibit a substantial 30% [26] to 70% [27] reduction in global warming potential (GWP) compared to concrete slabs with equivalent flexural properties. Consequently, numerous researchers have directed their efforts toward developing innovative TCC slabs and shear connection methodologies [28,29]. Within TCC slabs, the timber component may involve either traditional joists or modern panel-type EWPs, with the latter gaining prominence, especially in response to the growing demand for prefabrication and swift on-site assembly [30].

The shear connection in a TCC slab plays a pivotal role in determining its stiffness and strength and in shaping the fabrication method employed. Typically, these shear connections are affixed to the timber beam or panel and subsequently embedded within the wet in-situ concrete. Consequently, this approach is known as dry-wet fabrication. Such connections generally result in a permanent bond between the two materials, which, in turn, hampers efforts related to prefabrication, maintenance, deconstruction, and material reuse. Separating timber from concrete under these circumstances demands increased effort and energy. In contrast, a "dry-dry" shear connection system has been developed wherein the concrete is precast and then mechanically attached to the timber component. This dry-dry arrangement facilitates

prefabrication and disassembly processes, ultimately enhancing the sustainability of TCC floor systems.

While there has been considerable research on the topic of prefabrication in TCC slabs, it's worth noting that disassembly aspects have received relatively limited attention within the scope of these studies.

1.4 Aim of the study

The primary objective of this study is to develop a sustainable solution for building floor systems that effectively reduce the embodied energy and carbon footprint associated with the construction industry. More specifically, the study aims to establish a reversible method of connection for TCC systems, enabling prefabrication, deconstruction, partial material reuse, and recycling, all while minimizing environmental impact.

To accomplish the objectives of the project, the research focuses on three core research questions:

1. What are the environmental implications of different solutions, and how do different life cycle scenarios impact these solutions in the context of sustainable construction focusing on building floor systems?
2. How can a modular TCC system be designed to facilitate and optimize processes related to prefabrication, transportation, installation, maintenance, disassembly, modular reuse, deconstruction, and material reuse or recycling?
3. What are the key parameters that influence the design of the system, and how can the mechanical performance of such a system be characterized effectively to ensure its reliability and adaptability in diverse conditions?

1.5 Outline of the thesis

The outline of the thesis is demonstrated in Figure 3. Following the introduction chapter, Chapter 2 of the thesis provides an in-depth literature review covering various aspects, including the environmental impacts of the structural materials, timber as a structural material, TCC floor systems, existing shear connections and their attributes. Chapter 3 presents the results of this study in the form of 5 publications. The first two papers address the first research question. Paper I compares the environmental impacts of a TCC slab and its steel-concrete and reinforced-concrete counterparts. Then, the influence of different EoL scenarios on the TCC system is considered. Paper II discusses a case study in Luxembourg that compares the environmental impacts between a timber building and a concrete building. Additionally, the study explores the influence of reusable slabs in the context of the timber building.

Paper III focuses on developing a three-dimensional material model for the numerical simulation of timber. This model enables the modeling of timber, its mechanical behavior, as well as the analysis of failures and damages. This chapter is vital as it forms the foundation for the numerical studies conducted in Paper IV and Paper V, characterizing the TCC system and shear connection.

The last two papers tackle the second and third research questions. Paper IV introduces an innovative design for a modular and prefabricated TCC system featuring a demountable shear connection. The paper outlines a numerical and experimental investigation of a downscaled model of this slab concept. It assesses the slab's manufacturing process, potential bending characteristics, and key factors influencing its load-bearing capacity, stiffness, and failure behavior. A real-scaled shear test and further numerical study on the proposed shear connection are presented in Paper V.

Chapter 4 presents the results from a six-point bending experiment with 10 meters span. The discussion in Chapter 5 examines the integrity, interconnection, and relevancy of the papers in Chapter 3, followed by a comparison to studies published later in the literature. Chapter 6 serves as the final segment of the thesis, including the conclusion, limitations, and outline of prospective studies.

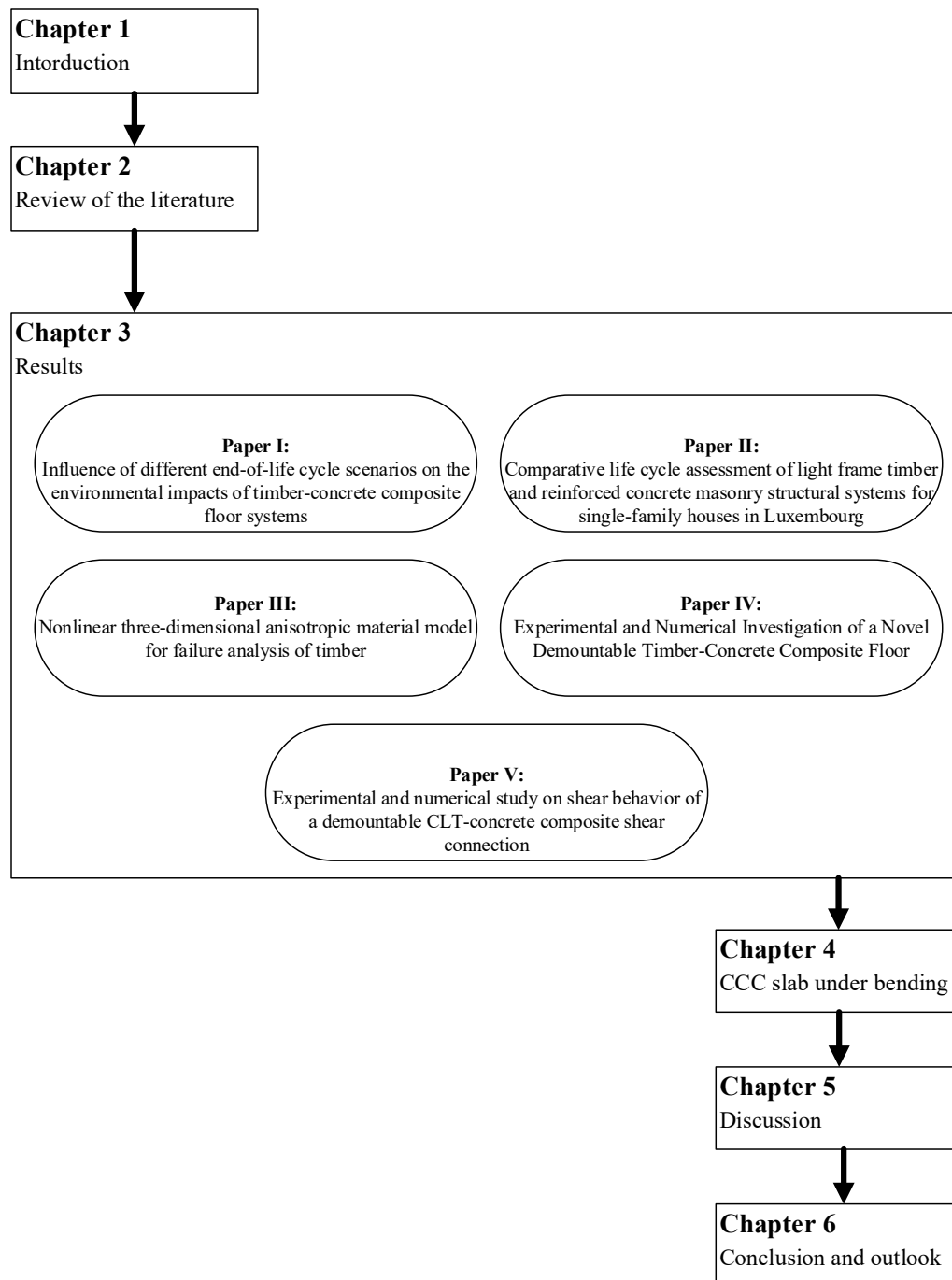


Figure 3. Outline of the thesis.

2 Review of the Literature

2.1 Environmental impact of construction materials

As mentioned, the building sector is one of the main contributors to energy consumption, waste production, and resource depletion. Hence, it has a significant environmental impact on the planet. In this section, firstly, Life cycle Assessment (LCA), a method for determining the environmental impact of all products, including buildings, is explained. Then, the concept of circular economy in building and Design for Deconstruction (DfD) is discussed.

2.1.1 Life cycle Assessment

The growing awareness and concern regarding environmental protection and the associated negative impacts of products have driven the development and adoption of methods to address these concerns. Among these methods, the most prominent is LCA, which comprehensively, systematically, and through a multidisciplinary approach, quantifies the environmental burdens and their potential impacts across the entire life cycle of a product [31]. LCA has been the foremost tool for assessing a building's environmental performance in buildings assessment. Recently, in several countries, the authorities made it mandatory to register the environmental impacts of new buildings or building materials [32]. For example, France, which since 1974 has put several regulations for reducing the energy consumption of buildings, including thermal regulation TR2012, has already moved toward an approach to reduce the environmental impacts of the whole life cycle of the buildings with environmental regulation RE2020 [33].

LCA is an analytical technique to assess the environmental impacts associated with all stages of a product's life cycle. This comprehensive evaluation encompasses various stages, depending on the scope of the study, such as raw material extraction, material processing, manufacturing, transportation, use, disposal, reuse, recycling, and refurbishing [34].

In an LCA study, an inventory of the required energy and materials attributed to all life cycle stages of the building is calculated, and all the resulting emissions and environmental impacts are accumulated. ISO 14040 [35] provides general standard guidance and defines the procedures for conducting an LCA with a framework that consists of four distinct steps, as presented in Figure 4.

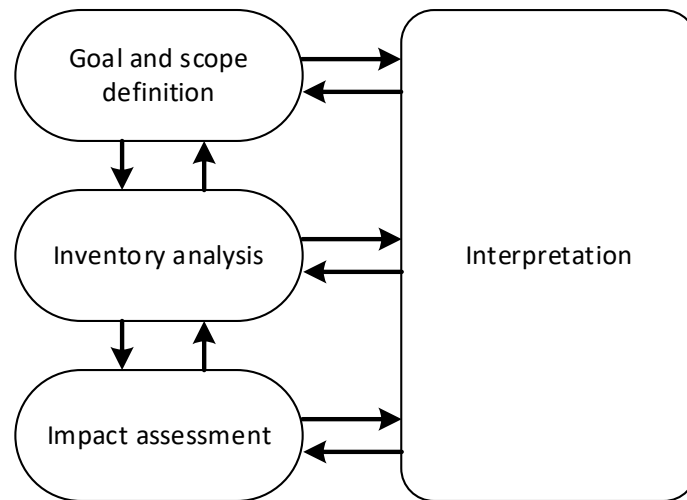


Figure 4. Life cycle assessment framework according to ISO 14040 [35].

- **Goal and scope definition**

In this stage, the reason and intended application of the LCA study should be decided. The goal definition clarifies the reason that the study is performed and the questions it will answer. According to the goal, the scope of the study is assigned, which determines the functional unit and system boundary [36]. The functional unit is used to relate the studied impact parameter of the product to one unit. It is a quantification of the performance of the studied product system. The system boundary defines a framework comprising a range of products and processes linked to manufacturing the product under investigation. Moreover, it specifies the quantity and category of energy and material inputs, along with the production of waste and emissions, that are integrated into determining the embodied

energy for a particular product. The system boundary for a building can be cradle-to-gate, cradle-to-site, cradle-to-grave, or cradle-to-cradle [37].

- **Inventory analysis**

When the goal and scope are defined, the inventory analysis gathers information about the input and output flows of resources, materials, products, emissions and waste to and from the system boundary of the studied product. The inventory collects all quantifiable items without consideration of their environmental impact. Therefore, the outcome of this step is the life cycle inventory, a list of quantified flows for the system associated with the functional unit [36].

- **Impact Assessment**

In this step, the impact on the environment of all the flows from the life cycle inventory is evaluated and categorized into categories such as damage to human health, climate change, global warming, acidification, eutrophication, etc. The impact categories must be chosen according to the study's goal and the needed results for the report to be as transparent and explicit as possible [38].

- **Interpretation**

In this step, the life cycle inventory and impact assessment results are interpreted by having the goal and scope definition in mind. The interpretation step transforms raw data into actionable insights, helping individuals and organizations make informed decisions to reduce environmental impacts and improve sustainability [36].

The assessment of the building's environmental impacts can be determined based on the life cycle of the building, which is categorized by EN 15978 [39] into 4 stages: production, construction process, use, and EoL, which are referred to as stage A, B, C, and D, respectively.

As illustrated in Figure 5, each stage refers to several sub-stages that define all the processes and activities of that stage. Additionally, supplementary information about the potential loads and benefits beyond the system boundary is considered in stage D. It is recommended to present the potential environmental benefits and loads from stage D separately from the other stages to ensure the emissions and energy consumption sources stay transparent [40].

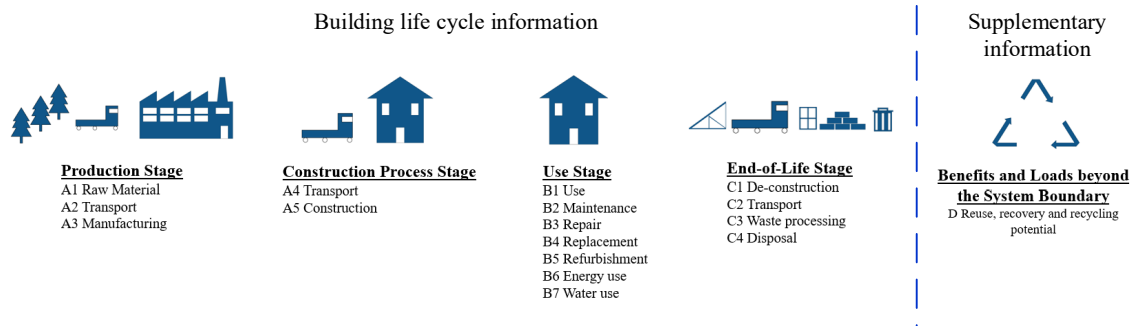


Figure 5. Building assessment information based on EN 15978 [39].

2.1.2 Design for deconstruction

A method to enhance the sustainability of a building is to consider, during the design stage, not only the possibilities for adjustment and restoration but also the disassembly and reuse of the components and materials at the end of the use stage of the life cycle [41]. This method is called DfD. According to [42], three strategies are necessary in designing buildings to promote DfD in the built environment:

- Employing assembly techniques conducive to easy disassembly (e.g., prioritizing fasteners over adhesives, selecting screws and bolts instead of nails and welding).
- Minimizing the weight of individual components.
- Avoiding the use of composite materials when separating individual constituents is problematic.

By implementing these principles, the recovery of materials and components for reuse or recycling becomes feasible with less effort and energy requirements.

2.2 Timber as a structural material

Timber has garnered significant attention in the construction industry over the past few decades due to the growing demand for sustainable and reusable building materials. Its appeal lies in its high strength-to-weight ratio, minimal carbon footprint, effective heat insulation properties, and aesthetic charm. Additionally, its lightweight nature facilitates swift transportation and assembly, expediting construction timelines. Furthermore, timber boasts easy recyclability, reusability, or potential for heat generation through incineration. However, it is not solely sustainability that has driven the increased adoption of timber and timber buildings. The advent of innovative EWPs has expanded the possibilities of timber usage in diverse dimensions.

EWPs are wood materials created by binding or fixing wood strands, fibers, veneers, or lumber with adhesives, heat, and pressure. Some of the advantages of EWPs compared to solid timber are:

- **Enhanced Dimensional Stability:** EWPs are less prone to warping, shrinking, or expanding when exposed to changes in temperature and humidity compared to solid wood.
- **Larger Cross-Sections:** EWPs can be manufactured in larger dimensions, allowing for the creation of larger cross-sections than what can be obtained from solid wood. Additionally, panel-like cross-sections are also possible in larger dimensions compared to solid timber.
- **Longer Spans:** On paper, the gluing method and finger jointing techniques remove the limits on the span length of EWPS.
- **Uniform Properties:** EWPs are engineered to have consistent strength, stiffness, and other properties, reducing the variability often associated with solid timber. This uniformity allows for more predictable performance in structural applications.

- **Sustainability:** Many EWPs are made from smaller, fast-growing trees or wood residues, which can be sourced sustainably. This efficient use of wood resources contributes to the overall sustainability of the timber industry.
- **Reduced Waste and increased efficiency:** It is possible to use lower-grade wooden materials that cannot be used as structural materials separately in EWPs in combination with higher-grade timber.

Some of the common EWPs used in the construction industry are:

- **Oriented Strand Board (OSB):** OSB is made from wood strands oriented in layers, bonded with adhesive, and then compressed into sheets. OSB is often used in residential and commercial construction for sheathing, flooring, and roofing.
- **Laminated Veneer Lumber (LVL):** LVL is created by bonding thin wood veneers with adhesive to form beams or structural elements. LVL is commonly used for beams, floors and other structural components.
- **Glued Laminated Timber (Glulam):** Glulam is made by bonding layers of dimension lumber with adhesives. It's widely used for structural beams, columns, and arches in buildings.
- **Cross-Laminated Timber (CLT):** CLT is a relatively newer EWP consisting of an odd number of timber boards stacked at right angles and bonded together to form large panels. CLT is increasingly used in construction for walls, floors, and roofs.

Thanks to these advantages and the ready availability of modern EWPs in construction, engineers have been empowered to design mid and high-rise mass timber structures. Numerous buildings, either fully or partially constructed with timber, exemplify this trend. For instance:

- Murray Grove: 9-story building in Hackney, London (2009)

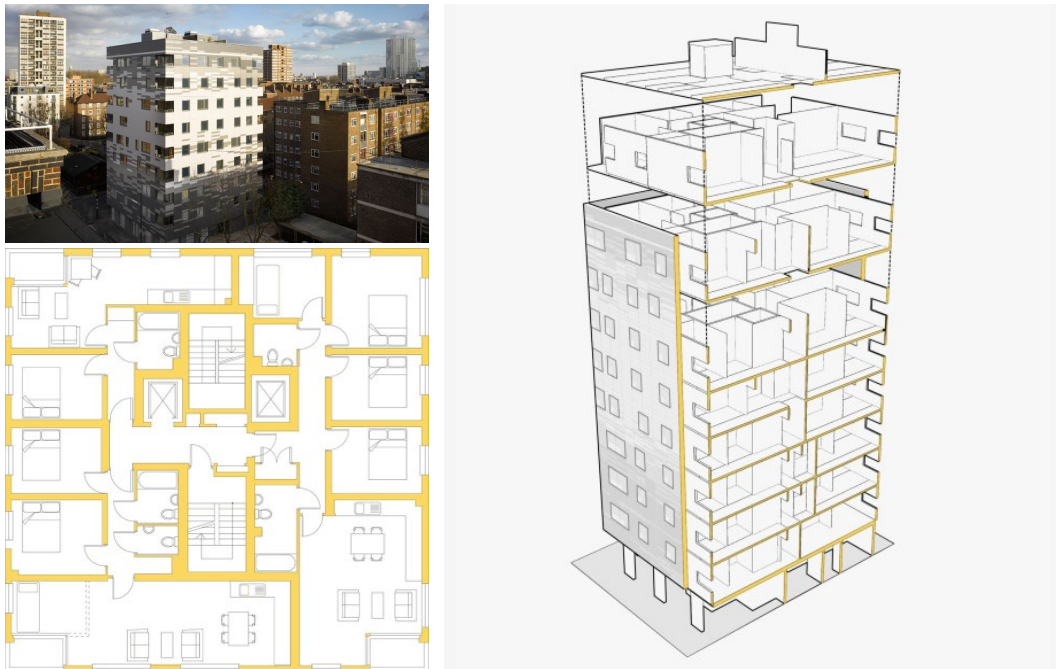


Figure 6. Murray Grove building. Figures from [43].

- Forté: 10-story building in Melbourne, Australia (2012)



Figure 7. Forté building. Figures from [44].

- Treet: 14-story building in Bergen, Norway (2015)

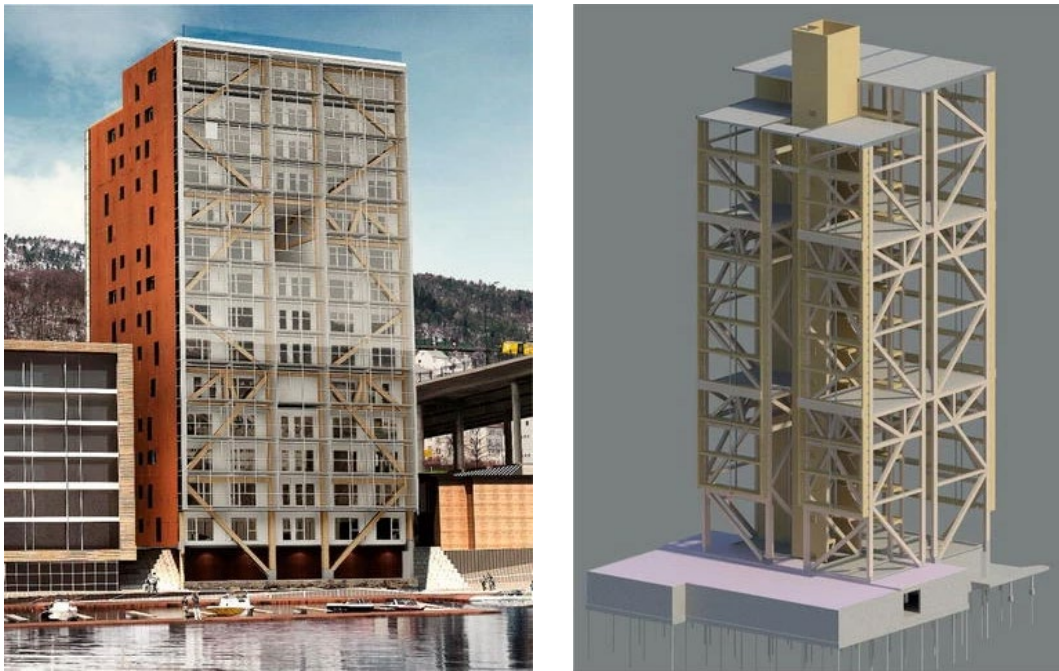


Figure 8. Treet building. Figures from [45].

- Brock Commons Tallwood House: 18-story building in Vancouver, Canada (2017)



Figure 9. Brock Commons Tallwood House. Figures from [46].

- Haut: 21-story building in Amsterdam, Netherlands (2022)



Figure 10. Haut building. Figure from [47].

When observing these buildings, it becomes evident that Glulam and CLT are predominantly employed in mass timber constructions. The construction of such buildings and the gradual replacement of concrete and steel with timber are becoming increasingly prevalent. Nevertheless, particular challenges associated with wooden structures can be mitigated and enhanced by utilizing timber as a hybrid structural material alongside other construction materials.

2.2.1 Timber material model

As the use of timber in the construction industry increases, developing new accurate and efficient computational models for timber material behavior becomes more critical. Modeling timber material behavior is complicated because of its behavior under different stresses in different directions. Timber is an orthotropic material with unique and different mechanical properties in three mutually perpendicular axes. These axes are longitudinal (parallel to grain), radial, and tangential based on the timber grain direction [48], as illustrated in Figure 11.

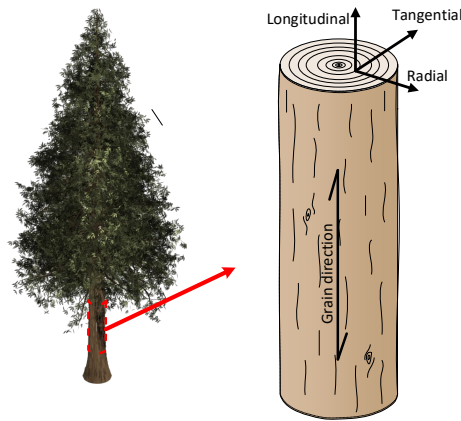


Figure 11. Orthotropic axes of timber.

Moreover, timber's strength depends on whether it is under tension, compression or shear. This is also true for the behavior of the material. Under tension and shear, the behavior of timber is relatively linear elastic followed by a brittle failure. In compression, timber behaves as linear elastic until it starts to deform more plastic with strain hardening before a ductile failure.

In the literature, different methods have been tried to model the complicated material behavior of timber. Some 2D finite element (FE) models were developed about two decades ago to determine the load-bearing capacity of dowel-type timber joints [49–52] by studying the initiation of fracture and its growth based on Linear Elastic Fracture Mechanics (LEFM) and Non-linear Fracture Mechanics (NLFM) to model the brittle failure of timber.

In general, the available material models in the literature that simulate the nonlinear behavior of timber can be categorized into three categories [53,54]:

1. Elastic-plastic models

The elastic-plastic models were mainly used to determine timber behavior in compression by bilinear [55,56] or trilinear [57] stress-strain curves. Researchers used different yield criteria in tandem with classical flow theory. Kharouf et al. [58] introduced a 2D orthotropic material model based on Hill's yield criterion [59] with anisotropic hardening to represent

timber behavior under compression. Yet, it overlooked brittle failures in tension and shear. Oudjene and Khalifa [60] proposed a 3D anisotropic elastic-plastic model with hardening also based on Hill's criterion addressing strength disparities in compression and tension, brittle tension behavior, and densification in compression. Studies like [61,62] utilized the Tsai-Wu criterion [63] for a 2D FE model of timber, while Xu et al. [27] incorporated the Hoffman failure criterion with Hill's criterion for an orthotropic 3D constitutive model of timber but struggled to precisely capture timber's load-deformation behavior. Mackenzie-Helnwein et al. proposed four-surfaced representing four basic failure modes to create a comprehensive failure surface, which considers timber's specific failure modes as brittle tensile failure parallel to the grain, brittle tensile failure perpendicular to the grain, ductile compressive behavior perpendicular to the grain, and compressive failure parallel to the grain direction. Although the results from multi-surface models are accurate, they raise issues such as numerical instabilities as complicated constitutive laws are used.

2. Elastic-damage models

In elastic-damage material models, the linear behavior of timber is modeled, and the nonlinear behavior is determined by the Continuum Damage Mechanics (CDM). CDM is a framework in engineering mechanics that deals with material deterioration at the continuum scale. It quantifies the progressive loss of load-bearing capacity in stressed materials as they accumulate strain [64]. It is adaptable, allowing different damage rate equations to address various damage mechanisms [65] to describe microflow initiation, propagation, and coalescence leading to macroscopic fractures [66].

The roots of CDM can be traced back to foundational work by Kachanov in 1986 [67], and the first practical application was when Chaboche and Lesne [68] used it to predict fatigue in steel [69]. Since then, CDM has matured considerably and is widely employed in

numerical simulation methods across various engineering applications. Its ability to capture the intricate interplay of damage mechanisms and their effects on material behavior makes it an essential tool for predicting and managing material degradation in structural design and analysis [70].

Studies [71–73] used CDM to model strain hardening and softening, stiffness degradation, and failure in timber. They inserted damage variables into Hooke's fundamental equation to degrade the stiffness matrix.

3. Elastic-plastic in combination with damage models

The studies in the third group used a combination of elastic-plastic and CDM to model the behavior of timber. These models [74,75] often rely on Hill's criterion [59] for yield surfaces or damage criteria and describe timber's behavior under different loading conditions. Xu et al. [76] used an anisotropic elastic-plastic model with isotropic hardening to describe timber's compressive behavior and the CDM method to describe the brittle behavior of timber under tension and shear. A timber model within a plasticity and CDM framework was created by [77], considering anisotropic plasticity, isotropic hardening, isotropic damage, and large plastic deformations. However, it did not differentiate between tension and compression strength parameters. Another study [78] developed a cyclic timber behavior model using the Hofmann criterion for plasticity and Hill's criterion for damage.

Nevertheless, they assumed isotropic damage, preventing the identification of individual failure modes. Benvenuti et al. [53] proposed a multi-surface elastic-damaging-plastic constitutive model with two plastic activation functions and three damage variables. This model effectively addressed ductile and brittle failure modes but was limited to plane stress cases for simplicity.

2.3 Timber-concrete composite floor system

In TCC floor systems, a shear connection mechanically connects a concrete slab to a supporting timber beam or panel. In this system, timber resists bending and tensile stress, whereas concrete efficiently handles compressive stress through composite action and bending moment distribution. This integrated approach capitalizes on both materials' strengths while mitigating their weaknesses. Timber offers several advantages: lightweight, renewable, and environmentally sustainable. It excels at bearing tensile forces, which concrete is less suited for. Conversely, concrete significantly enhances the strength and stiffness of the timber floor while also reducing vibrations and improving sound insulation and thermal mass. This hybrid system not only proves cost-effective but also aligns with sustainable construction practices, making it an environmentally friendly choice.

In this system, the timber component can be a joist, panel-type solid timber or EWP. The concrete can either be cast in situ or precast concrete slabs. The two materials are connected by shear connections. This connection can be achieved through various means, such as using mechanical fasteners like nails, screws, or toothed metal plates embedded into the timber. Alternatively, it can involve cutting notches in the timber, directly gluing timber to concrete, and many other methods available in the literature. The connection between timber and concrete determines the degree of composite action in the floor system. The degree of composite action between timber and concrete can vary based on the stiffness of the shear connection and the frequency of occupied connections. This variation leads to relative slip at their contact point during bending, as illustrated in Figure 12, ranging from two extremes: freely slipping, indicating no composite action, to no slip, signifying full composite action. The smaller the slip between the two materials, the higher the degree of composite action. The bending moment at the cross-section of a TCC composite system is shown in Figure 13. The

total bending results from the sum of bending in concrete M_1 and timber M_2 and the moment from the eccentric force resulted by composite action N as:

$$N_1 + N_2 = N, \quad M = M_1 + M_2 + (N \times r) \quad (1)$$

where N_1 and N_2 are the composite forces in concrete and timber, respectively, and r is the eccentricity.

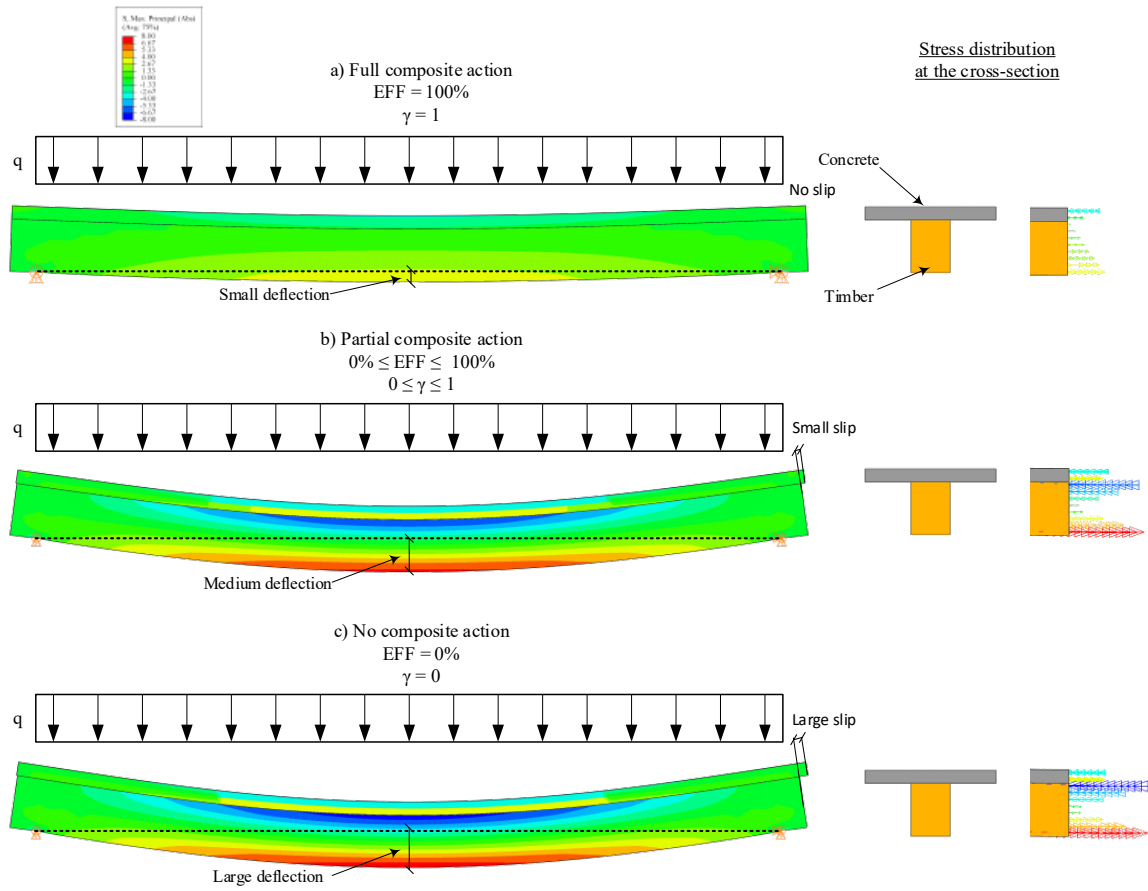


Figure 12. Comparison of composite slab under the same loading with a) full composite action, b) partial composite action, and c) no composite action

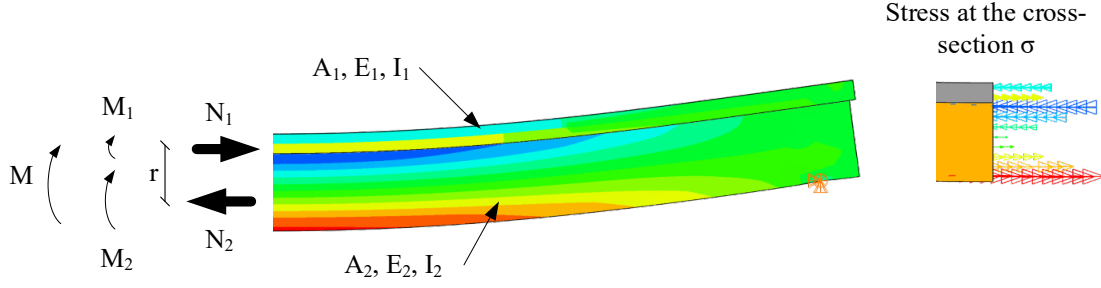


Figure 13. The force and moment at a TCC cross-section. Figure is based on [79].

In TCC slabs, it is difficult to achieve fully composite action due to the shear connections, which are mostly not entirely rigid. Consequently, there will be a slip between the two materials. Therefore, most of the TCC slabs perform partial composite action. For a TCC slab with a full composite connection, the bending stiffness can be calculated as:

$$(EI)_{\infty} = E_c I_c + E_c A_c a_c^2 + E_t I_t + E_t A_t a_t^2 \quad (2)$$

In this equation, the subscripts c and t denote concrete and timber. At the same time, E , I , A , and a represent Young's modulus, the second moment of inertia, the area of the cross-section, and the distance from the centroid of the element to the neutral axis of the composite section, respectively.

The theoretical bending stiffness with no composite action between timber and concrete can also be calculated similarly:

$$(EI)_0 = E_c I_c + E_t I_t \quad (3)$$

The efficiency of the deflection of the slab can determine the efficiency of the shear connection system. As the deflection of a composite slab increases with the decrease of the composite action, Gutkowski et al. [80] defined the efficiency of the slab as:

$$EFF = \frac{\Delta_N - \Delta_I}{\Delta_N - \Delta_C} \times 100 \quad (4)$$

where Δ_N , Δ_C and Δ_I represent the deflection of no composite, full composite, and the actual deflection of the TCC slab, respectively. The efficiency of the TCC composite slab can also be determined by the efficiency of its bending stiffness γ [81] as:

$$\gamma = \frac{(EI)_{real} - (EI)_0}{(EI)_\infty - (EI)_0} \quad (5)$$

where EI_0 , EI_∞ and EI_{real} represent the bending stiffness of no composite, full composite, and the actual bending stiffness of the TCC slab, respectively. The shear connection directly influences the efficiency of the TCC slab, hence its bending stiffness and deformation.

Ceccotti [79] calculated the effective bending stiffness for simply supported beams considering the composite system's efficiency by the γ -method. The method is commonly used for a linear-elastic design of TCC slab, also outlined in annex B of Eurocode 5 [82]. If the used shear connection has a slip modulus of K and is installed with a distance of s with a span length of l , the bending stiffness can be determined as:

$$(EI)_{eff} = E_c I_c + \gamma_c E_c A_c a_c^2 + E_t I_t + \gamma_t E_t A_t a_t^2 \quad (6)$$

and

$$\gamma_c = \frac{1}{1 + \frac{\pi^2 E_c A_c s^3}{K l^2}} \quad (7)$$

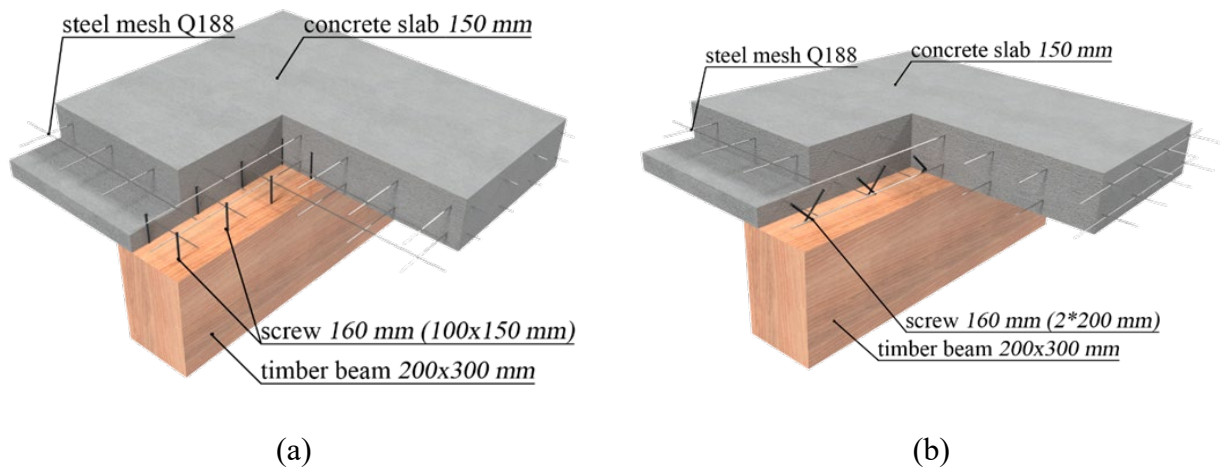
$$\gamma_t = 1 \quad (8)$$

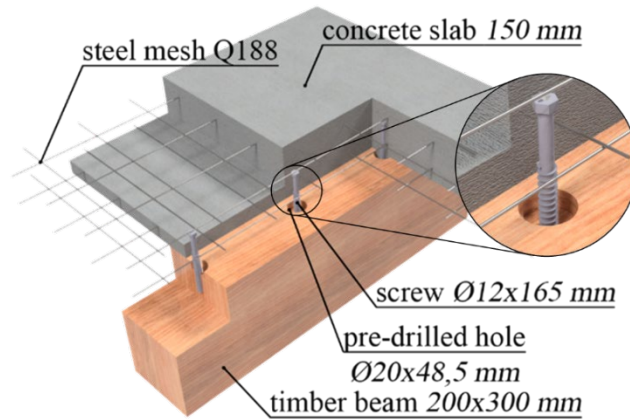
In this equation, γ_c can change from 0 for no composite to 1 for full composite. As can be seen, the shear connection significantly impacts the efficiency of a TCC slab. Some of the more common shear connections and their mechanical attributes are described in the following section.

2.3.1 Mechanical fasteners

Mechanical fasteners such as nails, self-tapping screws, coach screws, threaded bars, and dowels have been used as one of the most common shear connections in TCC floors. They are inexpensive and easy to install, but their stiffness and strength are not noticeable compared to other types of shear connections.

Figure 14 demonstrates three examples of mechanical fasteners used as shear connections. Self-tapping screws are used in Figure 14(a) and (b) with perpendicular and inclined cross setups, respectively [83]. Experiments [83,84] show that an inclined cross-screw setup performs better in stiffness and strength than perpendicularly installed screws. Figure 14(c) demonstrates coach screws combined with a circular plug in the timber [85]. Since the diameter of this kind of screw is larger than regular screws, predrilled hole is needed to avoid timber splitting. Also, the plug needs to be cut in the timber beam. Therefore, installing such a connection is more complicated than self-tapping screws.





(c)

Figure 14. Some mechanical fasteners as shear connections: (a) perpendicular self-tapping screws; (b) inclined self-tapping screws; (c) Coach screw with a circular groove in timber. Connections were rebuilt based on [83,85].

2.3.2 Steel profiles

Different steel profiles can be used as shear connections, as shown in Figure 15. Figure 15(a) is a steel plate that is split and folded into two sides embedded in concrete and, on the other side, glued within a slot milled in the timber beam [86]. Figure 15(b) shear connection includes plates screwed to the sides of the timber beam [87]. On the top of each plate, two steel angles are bolted to the plate and embedded in concrete. Figure 15(c) shows that the shear connection consists of a steel tube inserted in a predrilled hole [86]. The steel profile shear connections are generally stiffer and more robust than those with mechanical fasteners. However, their fabrication takes more time and effort. The main advantage of this type of connection is its suitability for prefabrication. Subsequently, the concrete, along with the connection, can be transported to the construction site and installed on the timber beam.

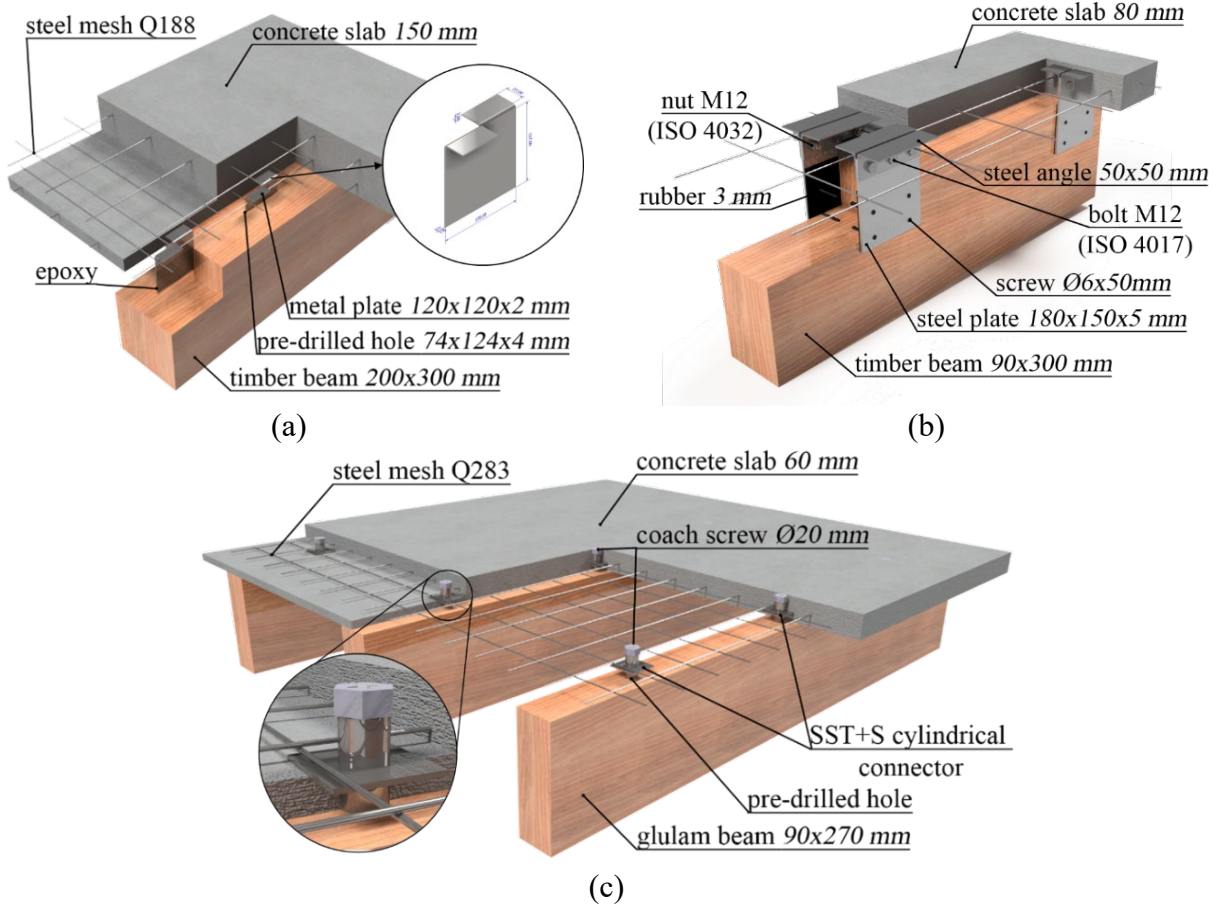


Figure 15. Example steel profiles as shear connections: (a) folded steel plate embedded in concrete and glued in timber; (b) steel plate embedded in concrete and screwed to timber beam with vulcanized rubber layer; (c) steel tube with coach screw. Connections were rebuilt based on [86,87].

2.3.3 Notches

Notched shear connections can consist of different groove shapes in timber, usually accompanied by a steel fastener, as demonstrated in Figure 16. The shear force between the two materials transfers by their direct contact at the notch, and the presence of a fastener can enhance both shear transfer and the ductility of the connection [29]. The construction of notched shear connections is a relatively simple process, as the timber notch can be cut using CNC machinery, and concrete can be cast directly on top of the timber beam. Their stiffness and strength are higher than mechanical fasteners and steel connections. With proper consideration for the steel fasteners, they have the potential to be employed in prefabricated TCC slabs.

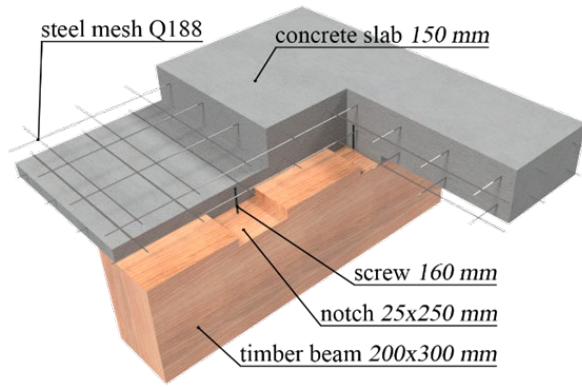


Figure 16. A notched shear connection. The connection was rebuilt based on [88]

2.3.4 Continuous connections

Continuous shear connections, such as those involving direct epoxy gluing of concrete to timber or the perforated steel plates embedded in concrete and glued within pre-milled timber slots (Figure 17), are acknowledged for their substantial stiffness. They possess the capacity to achieve full or near-full composite action within TCC slabs.

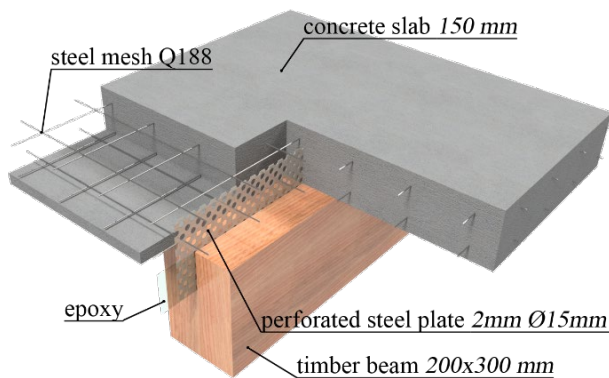


Figure 17. Perforated steel plate as a shear connection for a TTC slab. The connection was rebuilt based on [89].

2.4 Push-out test

A push-out test determines the mechanical properties of a shear connection. In a push-out test, the shear connection is loaded in a setup to determine the slip, stiffness, strength, and behavior under shear force. The setup of the push-out tests can be categorized into two main groups: symmetric and asymmetric. In the symmetric setup recommended in the upcoming Eurocode

5 for TCC push-out tests and widely used in Steel-Concrete Composite (SCC) joint tests [90], a core of timber or concrete is pushed against two outer elements from the other material. The symmetric setup avoids the eccentric reaction from the shear connection. However, since imperfections of materials and fabrication usually exist, lateral supports are required, as shown in Figure 18.

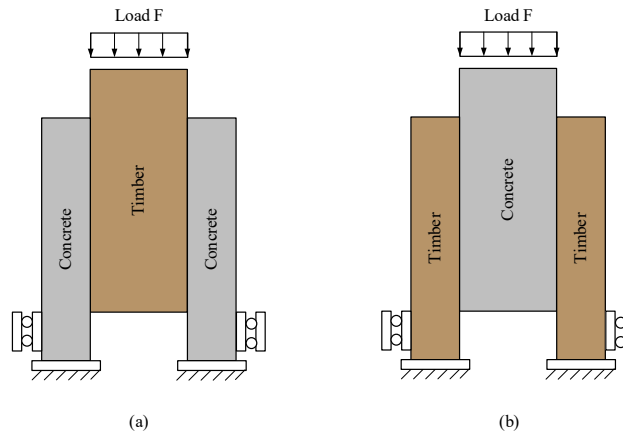


Figure 18. Symmetric push-out test setup with (a) timber and (b) concrete core.

In the asymmetric setup, only one element is pushed against the other. The setup introduces a moment as soon as the load is applied. Therefore, roller supports are needed in addition to the lateral support, as shown in Figure 19.

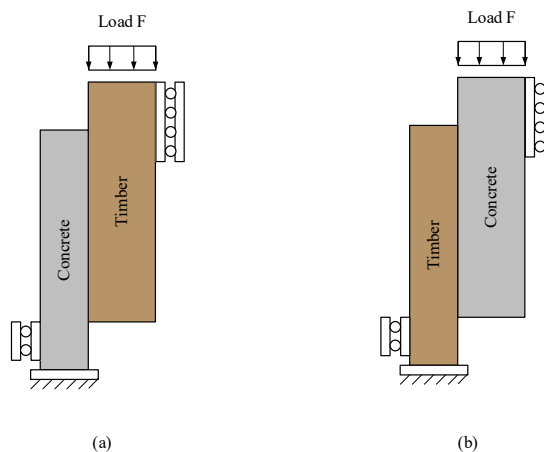


Figure 19. Asymmetric push-out test setup with loading on (a) timber and (b) concrete

Although there is no existing standard for the TCC push-out test, it is common to use the loading procedure from EN 26891 [91], which is shown in Figure 20. The calculation or the previous test determines the estimated load F_{est} . Then, the specimen is loaded and unloaded with 40% of F_{est} . After the first loading cycle, the specimen is loaded to the ultimate load, F_u . F_{est} must be updated if F_u differs more than 20% from F_{est} .

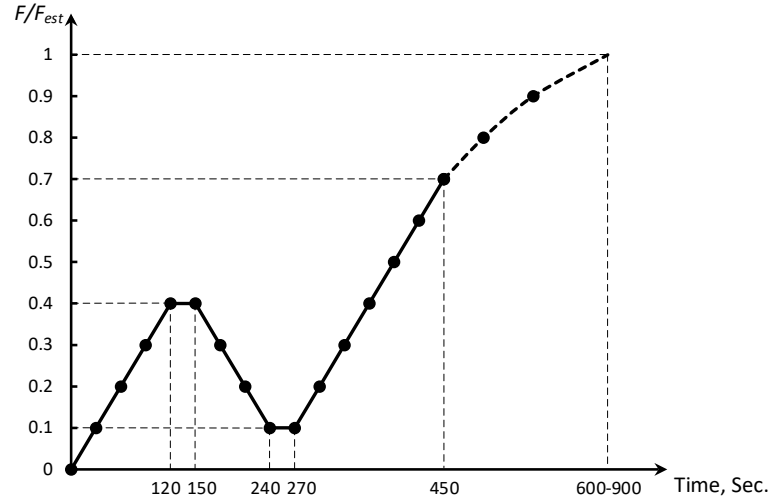


Figure 20. Loading procedure of the push-out test according to EN 26891 [91].

The results of the push-out test are usually demonstrated as a load-slip graph. These results show the stiffness of the shear connection in different loading stages, as presented in Figure 21. The stiffness of the connection is presented as slip modulus with [N/mm] units. The initial slip modulus is the secant slope of a line passing 0 and 40% F_{est} of the load-slip graph in the first loading cycle, denoted as K_i . In the second cycle, 40%, 60%, and 80% of F_{est} slope represent the slip modulus at service load, ultimate load, and close to failure mode, respectively.

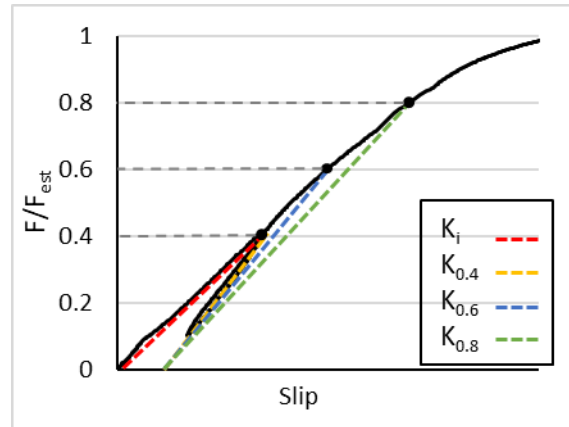


Figure 21. Typical load-slip results from a push-out test.

3 Results

This chapter will introduce the papers that have been published containing the results and studies related to this research project. The outcomes of this research are documented in a total of five papers, including one conference paper and four journal articles. Collectively, these publications offer in-depth insights into the findings and investigations of this study.

3.1 Paper I

The paper “Influence of different End-of-Life cycle scenarios on the environmental impacts of timber-concrete composite floor systems” [27] was presented at the World Conference on Timber Engineering 2023 (WCTE2023) in Oslo, Norway and published in the proceeding of the conference. The author of this dissertation served as the first author, and his contribution included conceptualization, methodology, analysis, investigation, the original draft preparation and visualization.

INFLUENCE OF DIFFERENT END-OF-LIFE CYCLE SCENARIOS ON THE ENVIRONMENTAL IMPACTS OF TIMBER-CONCRETE COMPOSITE FLOOR SYSTEMS

Hooman Eslami¹, Alireza Yaghma², Laddu Bhagya Jayasinghe³, Daniele Waldmann⁴

ABSTRACT: Timber-concrete composite (TCC) floor systems attracted attention in the construction industry because of their low environmental impacts while demonstrating decent load-bearing capacity. However, the environmental impacts of possible end-of-life scenarios of TCC floors have not been extensively studied. To address this gap, a comprehensive life cycle assessment (LCA) study was conducted on three different slabs: a Reinforced concrete slab, a Steel concrete composite slab, and a CLT-concrete composite slab. The study revealed that the CLT-concrete composite slab has the lowest Global Warming Potential (GWP) among the three slabs. Subsequently, a more detailed LCA is performed on the CLT-concrete composite slab considering three different end-of-life scenarios of the CLT: 1. Energy recovery via incineration, 2. The prevailing scenario in Europe (a combination of energy recovery, recycling, and disposal), and 3. Reuse. The results show all three scenarios are beneficial in terms of GWP whereas the 3rd scenario is the most beneficial one.

¹ Hooman Eslami, FSTM University of Luxembourg, Luxembourg, Hooman.eslami@uni.lu

² Alireza Yaghma Carbonel, FSTM University of Luxembourg, Luxembourg

³ Laddu Bhagya Jayasinghe, FSTM University of Luxembourg, Luxembourg

⁴ Daniele Waldmann, Massivbau TU Darmstadt, Germany, waldmann@massivbau.tu-darmstadt.de

KEYWORDS: Timber-concrete composite floor system, Life cycle assessment, Environmental impact, Reusable slab

1 INTRODUCTION

The construction industry is a major consumer of global resources and contributes greatly to waste generation and greenhouse gas emissions [1, 2]. In the last few decades, with the aim to reduce the environmental impacts of the construction industry, the use of renewable and more environmentally friendly materials such as timber and engineered wood products have gained more attention due to their green properties such as low carbon footprint and low embodied energy. Previous studies have shown that Timber-Concrete Composite (TCC) floor systems are promising sustainable solutions since they have decent structural behavior while having low environmental impacts [3].

TCC slabs have several advantages over conventional Reinforced Concrete (RC) slabs. By replacing concrete with timber, the environmental impacts of the floor system can be reduced about 30 to 50 percent [4]. Moreover, TCC can be used for resource-saving and lightweight constructions. These advantages can be expanded if the TCC slabs are designed to ensure the concrete is only subjected to compression and that all or most of the timber is stressed in tension. Consequently, TCC slabs should be designed so that shear between the timber and concrete components is transferred effectively through a proper shear connector system. The degree of composite action of the slab depends on the efficiency of the shear transfer system between the two materials. Furthermore, the connection system influences the sustainability of the TCC slab since it manipulates the fabrication, installation, maintenance, and End-of-Life (EoL) scenario. Hence, important aspects of sustainability such as prefabrication, deconstruction, recycling, and reuse must be considered during the design of the shear connection. A shear connection system that bonds the two materials permanently makes the

deconstruction, reuse, or recycling difficult while a demountable shear connection facilitates these processes. This encouraged researchers to develop new shear connections suitable for prefabrication [5–7] and deconstruction [8, 9]. Having these new solutions which facilitate the recycling and reuse of TCC slabs, it is important to evaluate and compare the environmental impact of different EoL cycle possibilities for TCC floor systems.

This paper aims to study the environmental impacts of different floor systems for identical loading and span length. Then, a comparison between different EoL scenarios for the timber used in TCC floors is studied to identify the best solution considering the environmental impacts.

2 ASSESSMENT OF THE ENVIRONMENTAL IMPACT

Life-Cycle Assessment (LCA) is a common method that is used for the analysis of the environmental impact of products [10]. It is an analysis technique that evaluates the environmental impacts of different stages of a designed product during its life cycle. In an LCA study, an inventory of the energy and materials which are used for the product is determined and the corresponding potential environmental impacts are calculated to improve the environmental profile of a product or compare it to another one.

Many studies evaluate the environmental impacts, considering the Global Warming Potential (GWP) and Primary Energy (PE), for some or all of the life cycle stages of a designed product [11]. GWP is a metric to quantify the total global warming effect of a substance over a specified time horizon. The GWP of a substance is defined as the ratio of the cumulative radiative forcing over a specified life cycle stage due to the emission of a unit mass of a substance, relative to the equivalent emissions of CO₂. PE states to the energy that is first extracted from natural sources and then used to generate electricity, heat, or power for other purposes. The sources of primary energy include renewable energy sources such as wind, solar, hydro, and geothermal,

as well as non-renewable energy like coal, oil, and natural gas [12]. For construction materials and components, the stages which are mostly considered are Production and Construction (A), Use(B), End of Life (C), and Benefits and Loads (D) [13]. The considered stages in this study are demonstrated in Figure 1 which are the most relevant ones to the floor systems.

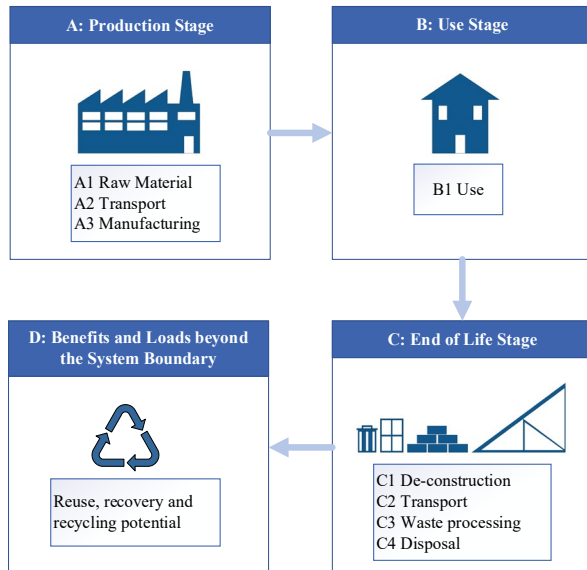


Figure 1. Life cycle stages of construction materials and components. Based on [13].

Stage A includes the extraction and processing of the raw materials, as well as their transportation to the manufactory where the floor component is produced. The construction process stage is not considered here because it does not have a noticeable influence compared to the other stages on a component level of analysis. Stage B only considers the use phase, assuming that the floor systems will not require any maintenance, repair, replacement, refurbishment, energy, or water during their service life. Stage C includes the deconstruction of the component, transportation, waste processing, and disposal. Stage D depends on the method that is used to derive benefits from the materials or components through reuse, recovery, or recycling. Although all the stages influence the environmental impacts of construction materials, stages A, C, and D are the decisive ones since stage B has no or a very small contribution to the environmental impacts.

Depending on the scope of an LCA analysis, different stages are considered in a study. A cradle-to-grave (CTG) scope considers stages A, B, and C, whereas a cradle-to-cradle (CTC) scope includes stages A, B, C, and D. The CTG approach examines the environmental impacts of a product from the extraction of raw materials to its disposal. On the other hand, the CTC approach takes into account the possibility of reusing, recovering or recycling the materials and components of the product at the end of its life. This approach considers the grave of a structure as the new cradle for its materials and components, enabling them to be used again in the manufacturing process of new products, reducing waste and the need for additional raw materials.

3 ASSESSMENT OF DIFFERENT FLOOR SYSTEMS

The Eco-Construction for Sustainable Development (ECON4SD) project at the University of Luxembourg has the objective of advancing toward a sustainable and circular society. This initiative aims to accomplish this goal by developing innovative architectural and structural design models that are resource and energy-efficient. The underlying purpose of this project is to create constructions that utilize sustainable practices, thereby minimizing their environmental impact. This paper study the environmental impacts of different possible floor systems to find a suitable floor system for the prototype 3 building in the ECON4SD project [14], which is a demountable building made of standard prefabricated modules. Each module has a length of 10.8 meters, a width of 10.8 meters, and a height of 3 meters. The building is made by adding these modules and expanding the building horizontally and vertically as it is shown in Figure 2. The architectural concept is designed for adaptive usage over the life cycle such as residential, office, and public buildings. After each life cycle, the building can be modified for a new purpose or can be demounted and reused in another building site.

To find a suitable floor system for this prototype building, 3 different floor systems are designed statically. Then, the environmental impacts of the floor systems are compared through a cradle-to-grave LCA analysis. The proposed floor systems are Reinforced Concrete (RC), Steel-Concrete Composite (SCC), and Timber-Concrete Composite (TCC). The floor systems which are depicted in Figure 3, are designed for an office building loading condition and a 10.8 meters single-span system. The design considers both load-bearing capacity and serviceability of the floor for a lifespan of 50 years. Since the building is meant for prefabrication and demounting, floor modules are designed as prefabricated slabs with 1.8 meters in width.

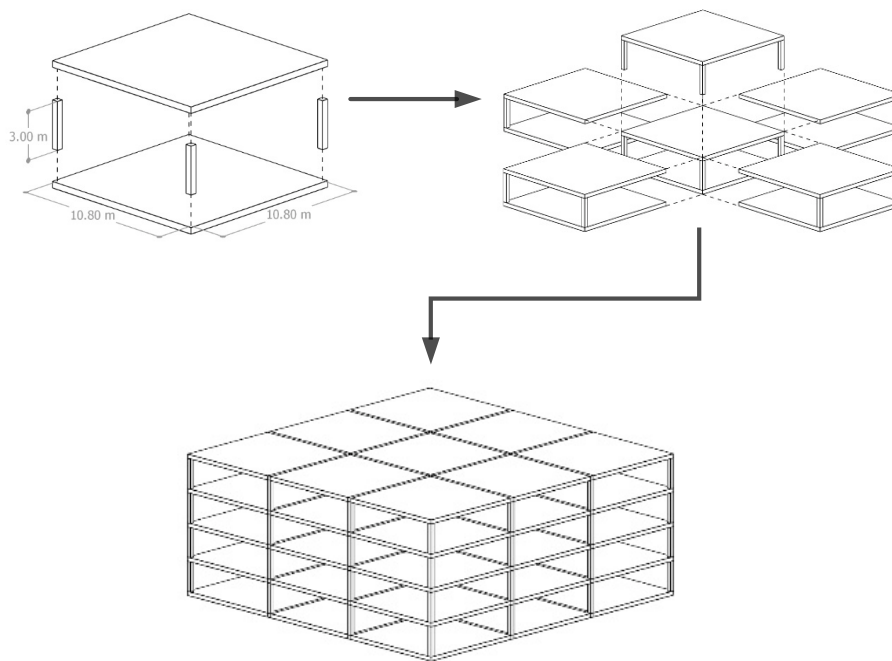
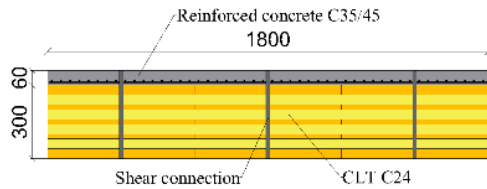


Figure 2. Architectural concept and standard module expansion for ECON4SD building prototype 3. From: [14].

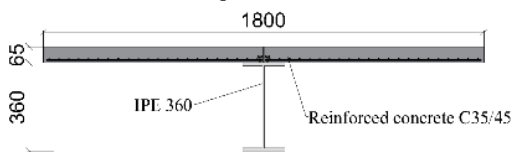
The TCC slab includes a 60 mm deep concrete slab on top of a Cross-Laminated Timber (CLT) panel with a thickness of 300 mm. CLT is a type of engineered wood product that is made from layers of solid-sawn lumber and is used in construction as floors, walls, roofs, etc. The layers are stacked in alternating orthogonal directions and then glued together under pressure to form a solid, stable panel. The CLT and concrete are connected by shear connections. The SCC slab

is made of an IPE 360 steel profile with a 65 mm deep concrete slab. The RC floor has the highest thickness of 440 mm and The TCC has the lowest thickness of 360 mm.

CLT-Concrete Composite Slab



Steel-Concrete Composite Slab



Reinforced Concrete Slab

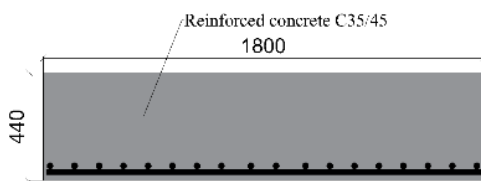


Figure 3. The investigated floor systems (dimensions in mm).

Based on the designed floor systems, all material quantities required for each slab module are calculated. Then, the ÖKOBAUDAT German database [15] which provides data on the environmental impacts of the construction products, is used to calculate the GWP and PE of all the materials in each stage except for CLT whose environmental impact is extracted from Stora Enso environmental product declaration [16]. Figure 4 and Figure 5 show the results of the LCA analysis in GWP and PE, respectively. For each floor system, the results are calculated for all stages and the total CTG is presented. The GWP results for the TCC and SCC floors are similar with a small advantage for the TCC slab while the result for the RC slab is about 3 times higher than the other two floors. This is due to the high CO₂ footprint of cement in the production stage. For TCC, the production stage of timber contributes to removing CO₂ from

the environment while the EoL stage releases CO₂ back into the environment due to incineration. Since the steel in the SCC slab will be recycled in stage C, the CO₂ contribution comes mostly from the production stage. Stage B contribution for all the slabs is negligible since it counts only the insignificant recovered CO₂ by concrete carbonation during the utilization stage.

The results for PE are different since the SCC slab requires about 30% less energy compared to the TCC slab. Yet, the RC slab requires the highest PE with about 2 times more than the TCC slab. The majority of the demanded PE is used in the production stage for all of the slabs. Only for the TCC slab, there is recovered PE which belongs to the heat recovery of the timber by incineration in stage C. Figure 5 also demonstrates the proportion of the renewable and non-renewable energy. Although the TCC slab requires more primary energy, it is mostly acquired from renewable energy. This is contrary to the SCC slab. Therefore, one can claim that the TCC slab is more sustainable compared to the other two slabs in a cradle-to-grave LCA analysis.

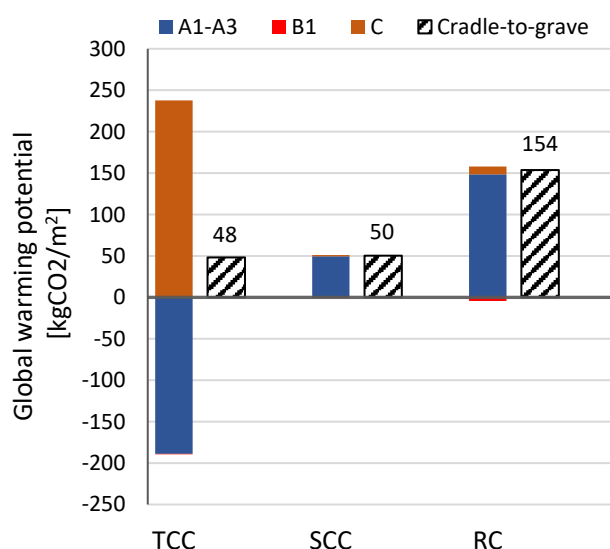


Figure 4. CTG global warming potentials of TCC, SCC, and RC slabs.

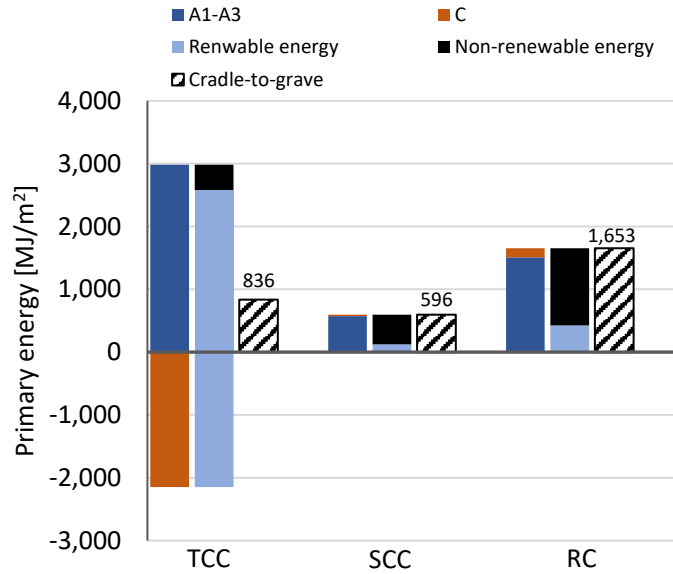


Figure 5. CTG primary energy of TCC, CLT, and RC slabs.

To have a cradle-to-cradle LCA, the potential GWP and PE relevant to stage D of each slab are calculated to determine the loads and benefits of each substance from its reuse, recycling, or recovery. For both GWP and PE measures, as it is shown in Figure 6 and Figure 7, respectively, the TCC slab stands significantly more beneficial than the other two slabs. For GWP this goes from 6 times compared to the RC slab up to 12 times better compared to the SCC slab. For PE the same trend exists when comparing TCC with RC and SCC slabs with 18 times and 53 times more recovered energy, respectively.

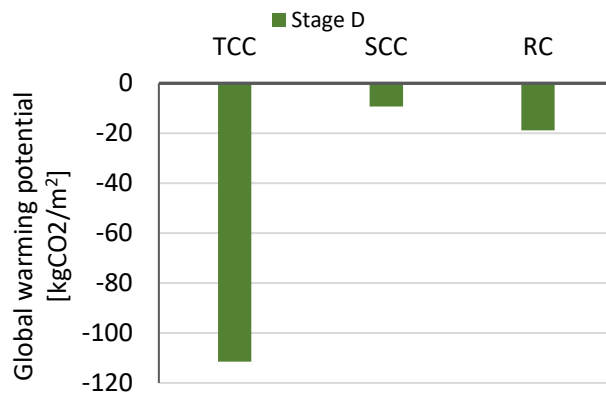


Figure 6. Comparison of the GWP from benefits and loads beyond the system boundary for TCC, SCC, and RC floor system.

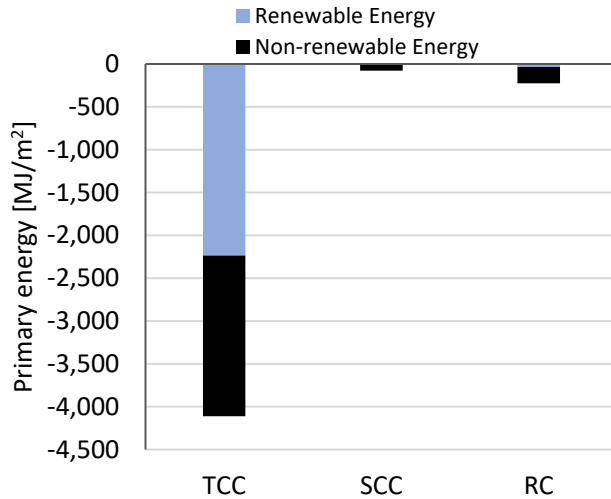


Figure 7. Comparison of the PE from benefits and loads beyond the system boundary for TCC, SCC, and RC floor system.

4 COMPARISON OF POSSIBLE END-OF-LIFE SCENARIOS FOR TCC

Knowing the TCC floor system has sustainable advantages compared to SCC and RC floors, different possible EoL cycle scenarios can be studied to compare their benefits toward finding a more sustainable solution. The assumed EoL cycle stages are shown in Figure 8. Since the production and use stages are identical, only stages C and D vary between the scenarios. For all the scenarios, the materials in the TCC slab are considered for de-construction (C1), transportation (C2), and waste processing (C3). The steel parts such as reinforcements and the bolts are recycled and the concrete is downcycled. Then, three different scenarios are studied for the CLT panel. The first scenario is identical to the one in the previous part which considers the benefits of timber for full energy recovery by incineration of wood to generate steam heat energy or electricity. On the other hand, a study [17] shows that in Europe on average 37% of wood products go to disposal while 33 % is recycled and the rest is used to produce energy. For disposal, the wood is interred in a landfill where the methane produced from its decomposition can also be harnessed to produce electricity. As for recycling, wood waste can be processed into engineered wood products and paper [18]. Therefore, the second scenario is

considered the prevailing scenario in Europe with the combination of the mentioned proportions for disposal, recycling, and energy production. Then again, the environmental impact of a component can be reduced significantly when it is designed for deconstruction and reuse which is the aim of the ECON4SD building prototype 3. Therefore, the third scenario considers that the CLT panel of the composite slab is fully reused with the assumption that the shear connection allows for such operation.

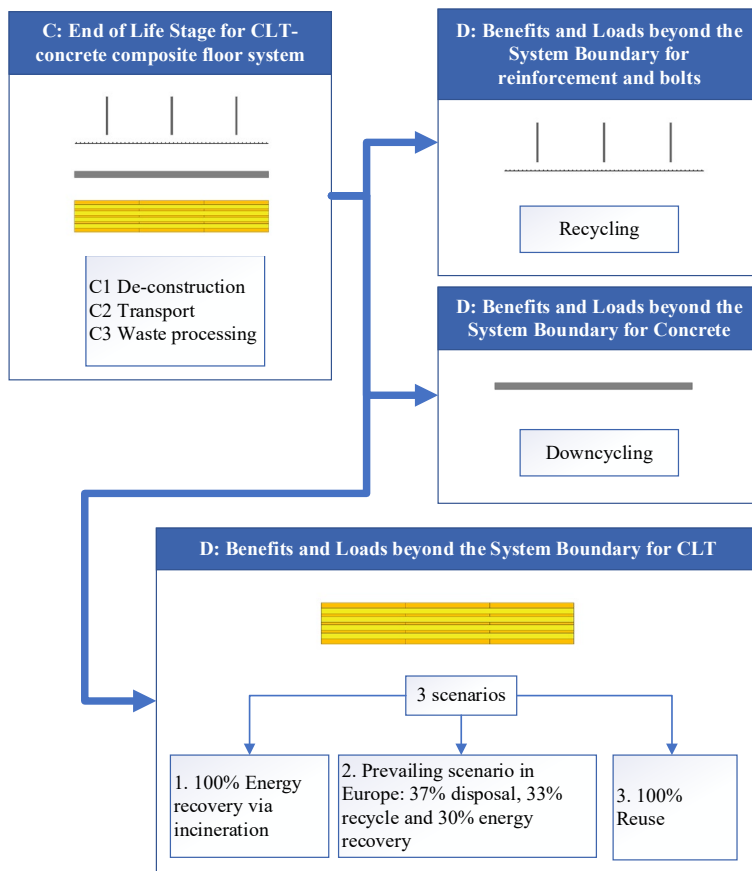


Figure 8. End-of-life scenarios of CLT-concrete composite floor system.

Although the different EoL scenarios do not affect the environmental impact in C1 and C2 stages, they influence the C3 stage. This impact can be seen in Figure 9 and Figure 10 with the CTG calculation of the GWP and PE. The second scenario has about two times more GWP than the other two scenarios. The third scenario has about 25% less GWP than the first scenario. Considering PE, the renewable required energy is almost the same for all scenarios. However,

regarding the non-renewable PE, the third scenario is again the most sustainable solution demanding about 15% and 7% less PE compared to the first and second scenarios, respectively.

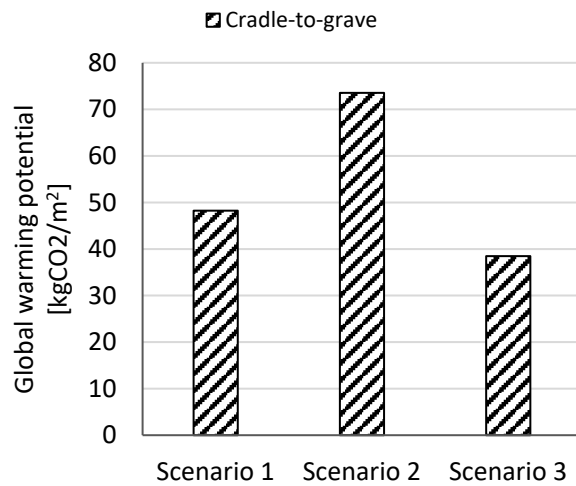


Figure 9. Cradle-to-grave GWP of the three different EoL scenarios for the TCC floor system.

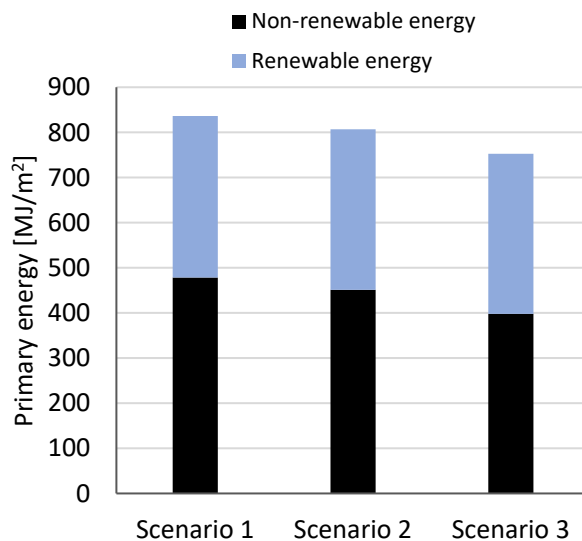


Figure 10. Cradle-to-grave PE of the three different EoL scenarios for the TCC floor system.

The benefits and loads of the three scenarios in stage D are compared in Figure 11 and Figure 12 as recovered GWP and PE, respectively. The first and second scenarios have almost the same GWP potential benefits while the GWP for the third scenario is more than 2 times higher compared to the other two scenarios. The maximum possible recovered primary energy is from

the first scenario followed by the third and second scenarios. This is due to the recovered energy from the incineration of the timber in the first scenario. However, the third scenario has the most renewable energy. Therefore, among the three scenarios, the third scenario has the least environmental impact and the most benefits beyond the system boundary.

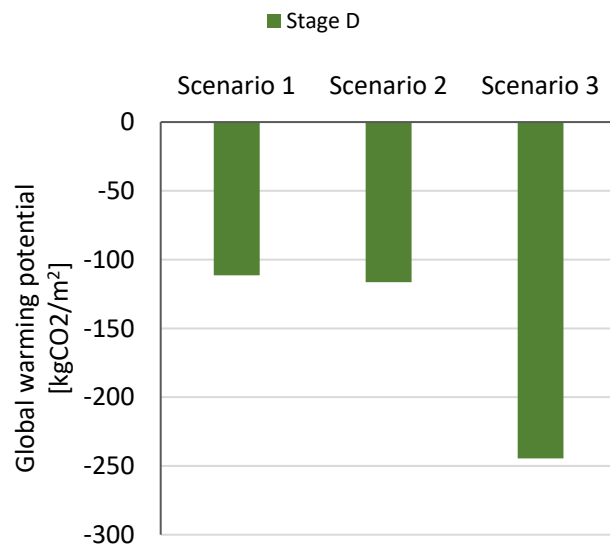


Figure 11. Stage D potential benefits for GWP of the three different EoL scenarios for the TCC floor system.

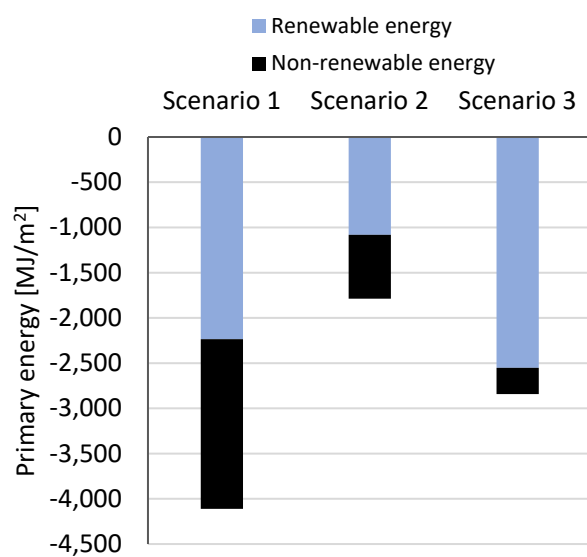


Figure 12. Stage D potential PE recovery of the three different EoL scenarios for the TCC floor system.

5 CONCLUSION

Three different floor systems are designed for the prototype building of the ECON4SD project considering the same loading condition and life span. The results show that:

- The global warming potential of the TCC floor system is one-third of the RC floor.
- The demanded primary energy of the TCC floor system is half of the RC floor.
- The TCC floor has significantly higher environmental benefits in stage D of the LCA compared to the other two floor systems.

Additionally, three different EoL cycle scenarios are compared for the CLT panel including full energy recovery, the prevailing scenario in Europe with a combination of energy recovery, disposal and recycling, and full reuse of the CLT. The comparison shows that reusing the CLT is the most sustainable solution since it has the lowest GWP and required PE. Also, the environmental benefits of the reuse scenario are more sustainable considering both GWP and PE measures. Therefore, for the studied building, a demountable and reusable TCC floor system is the most sustainable solution.

REFERENCES

- [1] Jayasinghe L. B., Waldmann D.: Development of a BIM-based web tool as a material and component bank for a sustainable construction industry. *Sustainability*, 12(5), 2020, 1766, doi: 10.3390/su12051766.
- [2] Abd Rashid A. F., Yusoff S.: A review of life cycle assessment method for building industry. *Renewable and Sustainable Energy Reviews*, 45:244-248, 2015. doi: 10.1016/j.rser.2015.01.043.
- [3] Holschemacher K., Hoffmann L., Heiden B.: Environmental impact of timber-concrete composite slabs in comparison to other floor systems. In: *World Conference on Timber Engineering*, 2021
- [4] Basaglia B., Lewis K., Shrestha R., Crews K.: A comparative life cycle assessment approach of two innovative long span timber floors with its reinforced concrete equivalent in an Australian context. In *International Conference on Performance-based and Life-cycle Structural Engineering*, pages 1433–1442, 2015. doi: <https://doi.org/10.14264/uql.2016.714>.

- [5] E. Lukaszewska, M. Fragiacomio, and H. Johnsson, "Laboratory Tests and Numerical Analyses of Prefabricated Timber-Concrete Composite Floors," *J. Struct. Eng.*, vol. 136, no. 1, pp. 46–55, Jan. 2010, doi: 10.1061/(ASCE)ST.1943-541X.0000080.
- [6] B. Shi, W. Zhu, H. Yang, W. Liu, H. Tao, and Z. Ling, "Experimental and theoretical investigation of prefabricated timber-concrete composite beams with and without prestress," *Engineering Structures*, vol. 204, 2020, doi: 10.1016/j.engstruct.2019.109901.
- [7] S. Yilmaz, S. Demir, and N. Vural, "Experimental investigation of a prefabricated timber-concrete composite floor structure: Notched-slab approach," *Advances in concrete construction*, vol. 12, no. 1, pp. 13–23, Jul. 2021, doi: 10.12989/ACC.2021.12.1.013.
- [8] N. Khorsandnia, H. Valipour, J. Schänzlin, and K. Crews, "Experimental Investigations of Deconstructable Timber–Concrete Composite Beams," *J. Struct. Eng.*, vol. 142, no. 12, Dec. 2016, doi: 10.1061/(ASCE)ST.1943-541X.0001607.
- [9] M. Derikvand and G. Fink, "Bending properties of deconstructable cross-laminated timber-concrete composite floor elements," *Wood Material Science & Engineering*, pp. 1–8, May 2022, doi: 10.1080/17480272.2022.2077658.
- [10] A. Luximon and L. Jiang, "The Role of Footwear Fitting and Comfort in the Environmental Impact of Footwear," in *Advances in Physical Ergonomics and Human Factors*, Cham, 2016, pp. 183–190.
- [11] Algren M., Fisher W., Landis A.E.: Chapter 8 - Machine learning in life cycle assessment. In J. Dunn and P. Balaprakash, editors, *Data Science Applied to Sustainability Analysis*, pages 167–190. Elsevier, 2021, doi: 10.1016/B978-0-12-817976-5.00009-7.
- [12] Shahzad, U. (2012). The need for renewable energy sources. *energy*, 2, 16-18.
- [13] Enzo S.: Environmental product declaration in accordance with ISO 14025 and EN 15804 for: CLT, 2021.
- [14] Silva M. F., Jayasinghe L. B., Waldmann D., Hertweck F.: Recyclable architecture: prefabricated and recyclable typologies," *Sustainability*, 12(4), 2020, doi: 10.3390/su12041342.
- [15] B. a. C. Federal Ministry of the Interior, "oekobaudat.de," [Online]. Available: <https://www.oekobaudat.de/en.html>.
- [16] The International EPD system, "S-P-02033 EPD CLT (Cross Laminated Timber)." Stora Enso Oyj, May 11, 2020. Accessed: Feb. 13, 2023. [Online]. Available: <https://www.storaenso.com/-/media/documents/download-center/certificates/wood-products-approvals-and-certificates/epd/stora-enso-epd-clt-2021.pdf>
- [17] Besserer A., Troilo S., Girods P., Rogaume Y., Brosse N.: Cascading recycling of wood waste: a review. *Polymers* 13, 1751, 2021.
- [18] J. Morris, "Recycle, Bury, or Burn Wood Waste Biomass?: LCA Answer Depends on Carbon Accounting, Emissions Controls, Displaced Fuels, and Impact Costs: Recycle, Bury, or Burn Wood Waste Biomass?," *Journal of Industrial Ecology*, vol. 21, no. 4, pp. 844–856, Aug. 2017, doi: 10.1111/jiec.12469.

3.2 Paper II

The paper “Comparative life cycle assessment of light frame timber and reinforced concrete masonry structural systems for single-family houses in Luxembourg” [92] was published in Heliyon journal. The author of this dissertation served as the first author and his contribution included conceptualization, methodology, formal analysis, investigation, the original draft preparation, data curation and visualization.

Comparative life cycle assessment of light frame timber and reinforced concrete masonry structural systems for single-family houses in Luxembourg

Hooman Eslami^a, Alireza Yaghma^a, Laddu Bhagya Jayasinghe^b, Daniele Waldmann^{c*}

^a Faculty of Science, Technology, and Medicine (FSTM), University of Luxembourg,

^b Department of Earth and Environmental Sciences, Ludwig-Maximilians-Universität München, Germany

^c Institute for Solid Structures, Technical University of Darmstadt, Germany

*Corresponding author: waldmann@massivbau.tu-darmstadt.de, Franziska-Braun Str. 3, 64287 Darmstadt, Germany

Abstract

The building sector is responsible for significant global greenhouse gas emissions and energy consumption. This, combined with the rapid population growth, makes achieving the European commitments on climate change more challenging. In Luxembourg, most of the residential buildings are single-family houses, making them one of the main contributors to construction waste production and CO₂ emissions. This study compares the environmental impacts of a three-story reinforced concrete masonry single-family house with a functionally identical timber building in Luxembourg constructed on the same site. Specifically, the paper compares the greenhouse gas emissions and the embodied energy in timber and concrete houses. A comprehensive cradle-to-grave life cycle assessment was conducted using Building Information Modelling (BIM) models to analyze the global warming potential and primary energy requirements. Environmental product declarations from the producers and ÖKOBAUDAT German database were used to determine the environmental impacts of the materials. The results show that the timber building outperforms the concrete building,

exhibiting approximately 43.5% lower global warming potential, while the concrete building demonstrates a noteworthy 15.6% reduction in primary energy demand. These findings align with the average outcomes of seven similar studies discussed in this paper, which are 33.2% and 4.7%, respectively. Moreover, the timber building is 78.6% lighter compared to the concrete one. Evaluation of benefits and loads beyond the system boundary from the potential reuse, recycling, and recovery of the materials reveals that the timber building provides 3.6 and 4 times greater advantages in terms of global warming potential and primary energy, respectively, compared to the reinforced concrete masonry building. Additionally, the study explores the impact of reusing the floors in the timber building. The cradle-to-grave LCA reveals that reusing the timber slabs improves the building's global warming potential and primary energy by 2.4% and 1.2%, respectively. However, when considering the potential benefits and loads beyond the system boundary, the reuse of the floor system exhibits a 38.9% surge in advantages concerning global warming while reducing the benefits in term of primary energy by 28.1%. The findings advocate for a policy promoting timber construction and reuse in Luxembourg, aiming to achieve the net-zero emission target by 2050.

Keywords: Life cycle assessment; Environmental impact; Timber building; Reinforced concrete masonry building; CO₂ emissions;

1. Introduction

1.1 Background

The construction industry has a notable share in global resource and energy consumption, waste production, and greenhouse gas emissions. The sector contributes to about 40% of Europe's primary energy use, 39% of energy-related carbon dioxide emissions, and 36% of global energy consumption [1–4]. The European Green Deal aims to become climate neutral by 2050 in European Union in line with the Paris Agreement [5]. The significant carbon footprint and

population growth make it challenging to address these commitments on climate change [6]. Therefore, the need to decrease the environmental impacts of the construction industry has become more critical in the last few decades.

The environmental impacts of a building can be reduced by optimizing the effects of the operational stage along with the selection of materials and construction methods [7,8]. Conventionally, the operational stage accounted for over 70% of the energy consumption of the building [9]. However, with the improvement of the energy standard of the buildings and moving toward nearly zero-energy buildings, the contribution of the use stage to the overall environmental impacts has dropped [10–13]. A study in Belgium [14] reveals that in conventional energy performance residential buildings, the use stage accounts for 69% to 89% of the total life cycle impact, contingent upon the house type. However, in modern low-energy houses, this proportion has reduced from 35% to 61%.

Reinforced concrete has been the dominant building material in the construction sector for the last century due to its favorable properties, including compression strength, cost-effectiveness, durability, and fire resistance [15]. Cement is the primary binding component of concrete. It is the third-largest source of anthropogenic CO₂ emissions, accounting for about 8% of total global carbon emissions [16]. Concrete and steel continue to be the primary construction materials for new buildings. However, the recent upsurge in environmental awareness within the construction industry has drawn significant attention to timber as a preferred structural material [17]. Timber offers benefits such as renewability, low environmental impacts, and construction benefits like fast erection and ease of prefabrication [18,19]. The development of new engineered wood products (EWP) made it possible to use timber in various structural elements. Materials such as cross-laminated timber (CLT), laminated veneer lumber timber (LVL), glued laminated timber (Glulam), and oriented stranded board (OSB) have found their way into mid and high-rise buildings [20–22].

The increase in timber consumption has led to concerns about the existence of sufficient timber resources [23]. In Europe, only 73% of the annual wood growth increment is harvested, which includes the 550 million cubic meters of roundwood production [24]. It is estimated that there is enough wood in the forests to sustain the construction sector until 2050 [25]. Thus, the rising consumption of wood should not raise concerns about resource scarcity.

1.2 Life cycle assessment

A commonly used tool to assess the environmental impacts of products and services is Life Cycle Assessment (LCA) [26–28]. According to ISO 14040 [29], LCA investigates the environmental dimensions and potential impacts across a product's complete life cycle, including the raw material acquisition, manufacturing, utilization, and disposal stages. Vital environmental impact classifications involve the utilization of resources, human well-being, and ecological ramifications. LCA allows decision-makers and industries to evaluate and improve the emissions associated with their products and services. It follows a standardized procedure that evaluates different emissions and energy requirements at each stage of a product's life cycle. For a building, these stages can be chosen depending on the scope of the study from production and construction (A), use (B), and EoL (C) stages. Moreover, the potential benefits from recycling, recovery, and reuse of the materials can be evaluated in benefits and load beyond the system stage (D) [30]. For this purpose, all inputs and outputs of material and energy are compiled and quantified throughout the considered stages in a life cycle inventory. This inventory is used to determine the environmental impacts of the building. Two parameters that are common in the environmental evaluation of buildings are Global Warming Potential (GWP) and Primary Energy (PE) [31]. GWP quantifies the overall global warming effect of the product or building over its life cycle relative to the equivalent amount of CO₂ [32]. PE counts for all the energy extracted from renewable or non-renewable sources. The energy can be used in the form of heat, electricity, and power for different purposes in the

various stages of the life cycle of the building elements [33]. These parameters quantify the environmental impacts regarding resource depletion and climate change for each building. The outcomes can serve as indicators for the comparison of different buildings. An LCA study can be classified as cradle-to-gate (including stage A), cradle-to-grave (including stages A, B, and C), or cradle-to-cradle (including stages A, B, C, and D). In a cradle-to-cradle boundary, the potential environmental benefits from stage D are presented separately to maintain distinguishability from other stages. This ensures transparency regarding emissions and energy consumption sources [34,35].

1.3 LCA limitations

LCA analysis is data-intensive [36] and subject to case-by-case variation due to the use of different system boundaries and databases, which can hinder comparing LCA results of different buildings. Many producers establish environmental certificates such as the Environmental Product Declaration (EPD), which quantify the data on the environmental performance of materials, products, or services over their lifespan [37,38]. Hence, comparing the environmental impacts of different buildings has become more feasible using these EPDs and standard LCA methods.

A comparative LCA can be used to analyze the environmental impact of different building materials for the same building. However, it is essential to note that the results of these studies can vary due to differences in design codes, transportation distances, construction methods, and waste processing, which can vary between countries and construction sites. These variabilities add complexity to conducting these studies. The intricate nature of such studies hinders the direct comparison between the overall environmental impacts of buildings with different construction materials. It is rarely possible to find identical buildings with different

construction materials within the same region according to the same codes and construction conditions. Therefore, having two similar buildings to compare is a unique opportunity.

1.4 Review of literature

Table 1 summarizes seven LCA studies that compared the environmental impacts of buildings with alternative structural materials. These studies compared a timber building to a comparable concrete building, with two of them additionally examining a sheet metal building and a timber-concrete hybrid. The alternative buildings were functionally identical, which means the number of floors, floor planning, usage, and energy grade of the buildings were equivalent. Four of the seven studies considered a cradle-to-gate system boundary, while the rest considered a cradle-to-grave. The life cycle span considered in these studies varied between 50 to 100 years. The studies considered various building types ranging from two-story single-family houses to 12-story residential and office buildings. The environmental impacts of the operational stage and non-load-bearing elements such as furniture, doors, windows, and mechanical installations were not considered in any of the studies. The results of the studies show that in all cases, the GWP of the timber building is noticeably less significant than the alternative in concrete or steel. When comparing a timber building to a reinforced concrete building can have from 6% to 84% lower GWP. The compared buildings were not all constructed and some comparisons were based on a solely designed alternative building. Therefore, related factors to the construction such as construction time, required logistics, and actual costs were impossible to be compared.

Table 1. Summary of seven comparative LCAs between buildings with alternative structural materials.

Reference	System boundary	Service life	Compared buildings	GWP [kg CO ₂ eq./m ²]	Embodied energy [MJ/m ²]	Building size
Robertson et al. (Canada 2012) [20]	Cradle-to-gate	50 years	Timber / RC	126 / 420	11660 / 8110	5-story: 14233 m ²
Canadian Wood Council (Canada 1999) [39]	Cradle-to-grave	-	Timber / Concrete / Sheet metal	288 / 354 / 433	1181 / 1801 / 2602	Single-family house: 216 m ²
Skullestad et al. (Norway 2016) [40]	Cradle-to-gate	60 years	Timber / RC	26 to 67 / 121 to 270	-	Four buildings from 3-story: 2613 m ² to 21-story: 11823 m ²
Liang et al. (USA 2020) [41]	Cradle-to-site	-	Timber / RC	193 / 237	2868 / 2673	12-story: 8360 m ²
Andersen et al. (Norway 2021) [6]	Cradle-to-grave	100 years	Timber / RC	454 / 904	-	8 story: 3973 m ² / 5-story: 2449 m ²
Chen et al. (China 2021) [42]	Cradle-to-gate	80 years	Timber / RC	221 / 296	10711 / 7058	8-story: 3524 m ²
Rinne et al. (Finland 2022) [43]	Cradle-to-grave	50 years	Timber / RC / Hybrid	168 / 178 / 179	-	5-story: 7250 m ²

1.5 Structure of the paper

A census in 2013 showed that in Luxembourg 83.5% of the residential buildings are single-family houses [44] from which only 10% are built in timber [45]. This illustrates the capacity to promote greater adoption of timber construction in Luxembourg. To the authors' knowledge, no prior research has been done in Luxembourg to compare the environmental impacts of timber and concrete buildings. Hence, this is the first study to conduct a comparative LCA

using local resources and databases pertinent to Luxembourg and its vicinity. The aim is to unveil the potential advantages of advancing timber-based single-family housing in the region.

This study compares two 3-floor single-family houses in reinforced concrete masonry and timber built in Luxembourg on the same building site. The two buildings are functionally identical with the difference of having a mirrored floor plan. A BIM model was created for each building to assess their environmental impacts to gather the necessary life cycle inventory data. The results obtained from the BIM models were then post-processed in spreadsheets to evaluate the environmental impacts of each building. The study also investigated the potential impact of reusing floors in the timber building. The analysis emphasizes the potential of integrating circular economy principles by exploring the benefits of material reuse, leading to diminished reliance on new materials and mitigated associated environmental impacts. By assessing the environmental impacts of this reuse scenario, the study aimed to provide the potential benefits of incorporating circular economy principles into the construction industry.

2. Materials and methods

2.1 Case study buildings

The buildings are located on the Schoenfels hills, approximately 15 km north of Luxembourg City in Luxembourg. Initially, both buildings were planned to be built in reinforced concrete masonry. Still, after finishing the foundation and basement construction, the owner decided to build one of the buildings in light-frame timber. Hence, the foundation of the timber building was over-designed since it was initially intended for a reinforced concrete masonry building. The construction was finished in late 2022. Figure 1 shows the front view of the reinforced concrete masonry building and light frame timber building which from now on will be mentioned as concrete building and timber building, respectively. Both buildings have the same surface area of 389 m² from which 274 m² are heated. The two buildings are functionally

identical with identical basement and roof structures, differing only in their structural system and insulation from the first floor to the roof. Both buildings have a rectangular raft foundation of 9 m by 15 m with a thickness of 30 cm and the basement level is partially buried. The height of the basement level is 2.35 meters. The rest of the floors have a height of 2.5 meters. The details of the external walls, internal walls, and floor systems are shown in Figure 2, Figure 3, and Figure 4.

In the concrete building, in-situ C25/30 concrete was used for the slabs and the staircase wall. The walls in the basement level are made of reinforced shuttering blocks of 24 cm. Exterior walls above the basement level were made of 24 cm hollow masonry blocks. The exterior walls were insulated with a 22cm layer of expanded polystyrene (EPS). The walls are covered by plaster layers from the interior and exterior. The interior walls were made of hollow blocks covered from both sides by layers of plaster. The floor system includes plaster, concrete, PUR insulation, screed, and wooden flooring.

For the timber building, solid C24 class timber and class 4 OSB boards were used for the load-bearing frames. The walls and slabs were prefabricated. For the walls, different layers of wooden-based insulations including fiberboards (STEICO flex [46]) and air-injected wood fibers (STEICO zell [47]) were used. The floor system consists of gypsum boards as false ceiling, solid timber joists topped with OSB, PUR insulation, screed, and wood flooring.



Figure 1. Front view of the concrete (left) and timber (right) buildings.

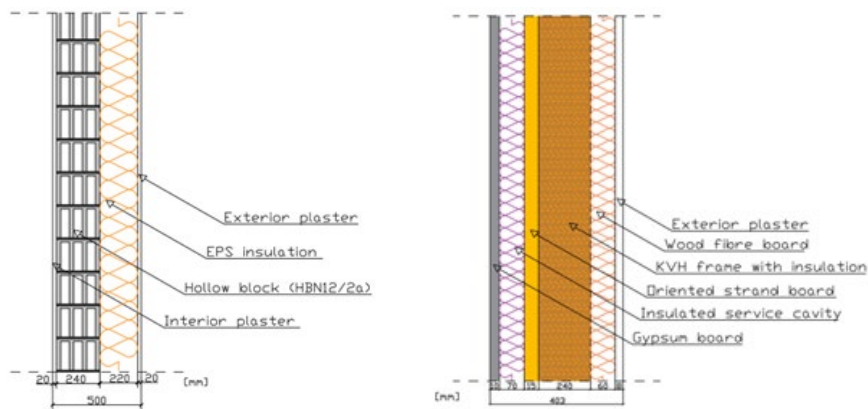


Figure 2. Section view of the external wall of the concrete (left) and the timber (right) building.

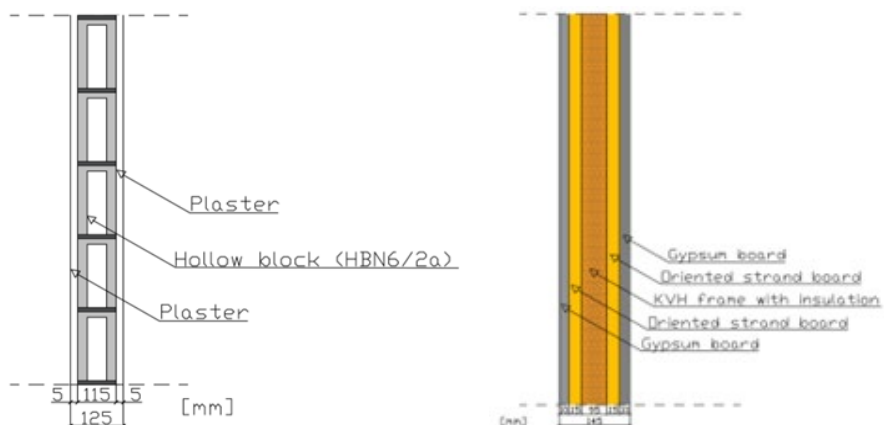


Figure 3. Section view of the internal wall of the concrete (left) and timber (right) building.

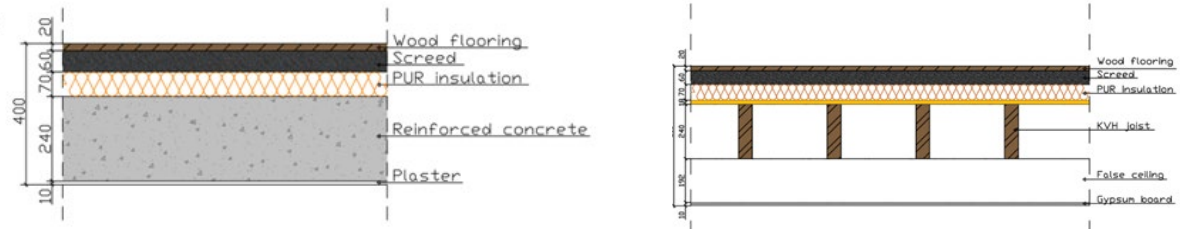


Figure 4. Section view of the slab of the concrete (left) and timber (right) buildings.

2.2 Construction and logistics

Construction of the buildings was started along with the demolition of the previous building on the site and earthworks. After the earthworks, the sequence of the building's construction continued as casting the foundation, placing the basement walls, and casting the concrete of the first slab. Once the first slab was made, the concrete and timber buildings had different construction agenda. The construction of the concrete building continued by placing the load-bearing walls and the concrete slab of the first and second floor consequently and the walls up to the roof. Afterward, the prefabricated roof structure was put in place. Lastly, the insulation and façade were installed. For the timber building, once the foundation and basement were constructed, the prefabricated timber walls and floors were delivered to the building site. They were assembled on-site, including the walls and the floors of the first and second floors and the roof structure. Following the erection of the prefabricated walls, the insulations were installed. However, unlike the concrete building, the façade was already prefabricated on the exterior walls of the timber building.

As Figure 5 shows, the construction time of the timber building was about 52% faster compared to the concrete building. Prefabrication is the main reason for the faster construction of the timber building. The timber building needed 10 days for prefabrication which was done in parallel with other construction processes. The number of required trucks for the transportation

of the structural materials to the building site is presented in Figure 6. The concrete building required twice more trucks compared to the timber building.

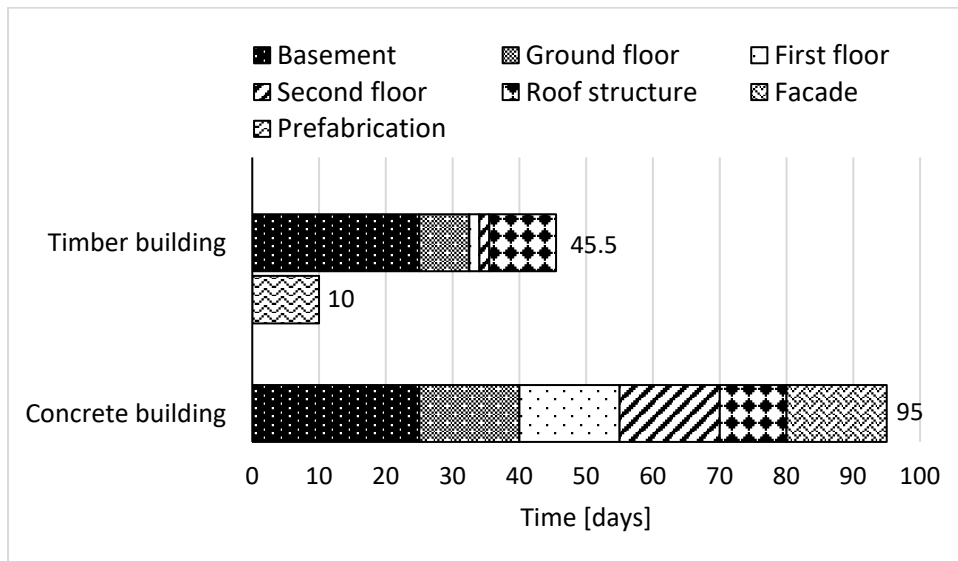


Figure 5. Construction time of the concrete and timber building.

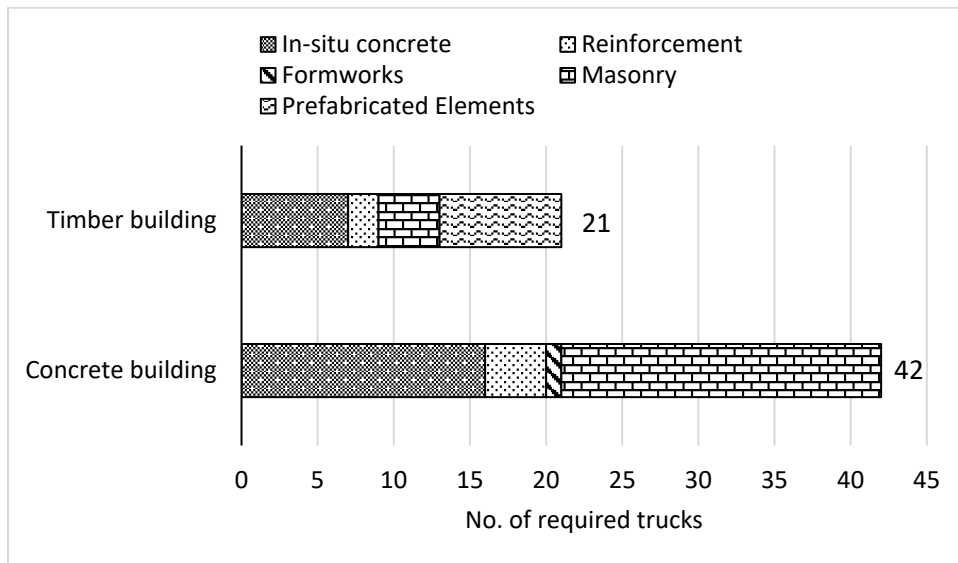


Figure 6. Number of required trucks for the structural materials of the buildings.

2.3 Assessment workflow

To facilitate decision-making regarding buildings and infrastructure, an adaptive LCA calculation workflow is essential to address the complexities of environmental impact

calculations [48]. In this context, a BIM-based LCA calculation can prove beneficial. Figure 7 illustrates the procedural framework adopted for the LCA study. The workflow was started by 3D modeling of the buildings in Revit (depicted in Figure 8) based on the 2D drawings offered by the construction company. On the other hand, the environmental data for each material was extracted from the EPD provided by the manufacturing company or by a similar producer. These environmental data, including the GWP and PE, were defined as project parameters within the 3D BIM model. The related project parameters for each material and element were defined for modules A, B, C, and D separately. A material takeoff schedule was generated from the model after finalizing the model and specifying all necessary attributes. This schedule offers the pertinent attributes and quantities of the materials utilized in the model. Then, the schedule from the model was exported to a spreadsheet for postprocessing. In the case of the timber building, two different scenarios were investigated. As timber environmental benefits increase when the storage period of used timber in buildings increases and the rotation period of timber source decreases [6], the second scenario considers the environmental impacts and the potential benefits of a reusable floor system. For this purpose, reusable timber was defined as a new material with corresponding environmental impacts. The BIM model facilitated the calculation of life cycle inventory and impact assessment, enabling the straightforward consideration of various scenarios.

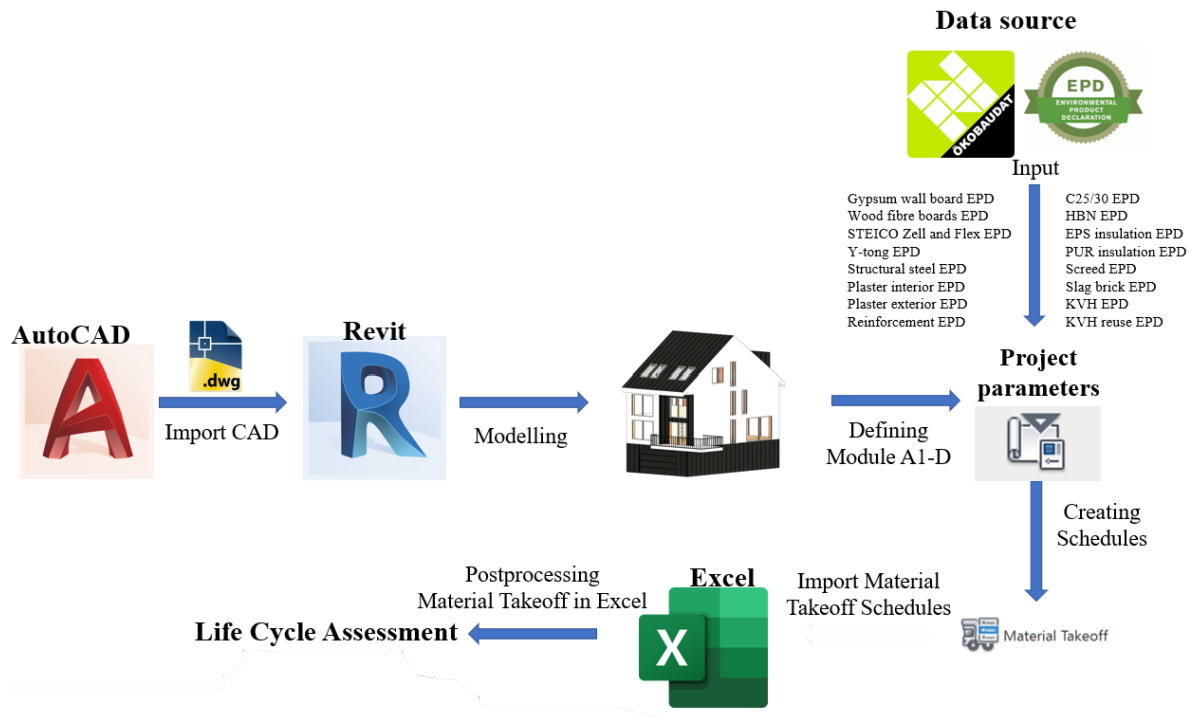


Figure 7. The workflow of the life cycle assessment.

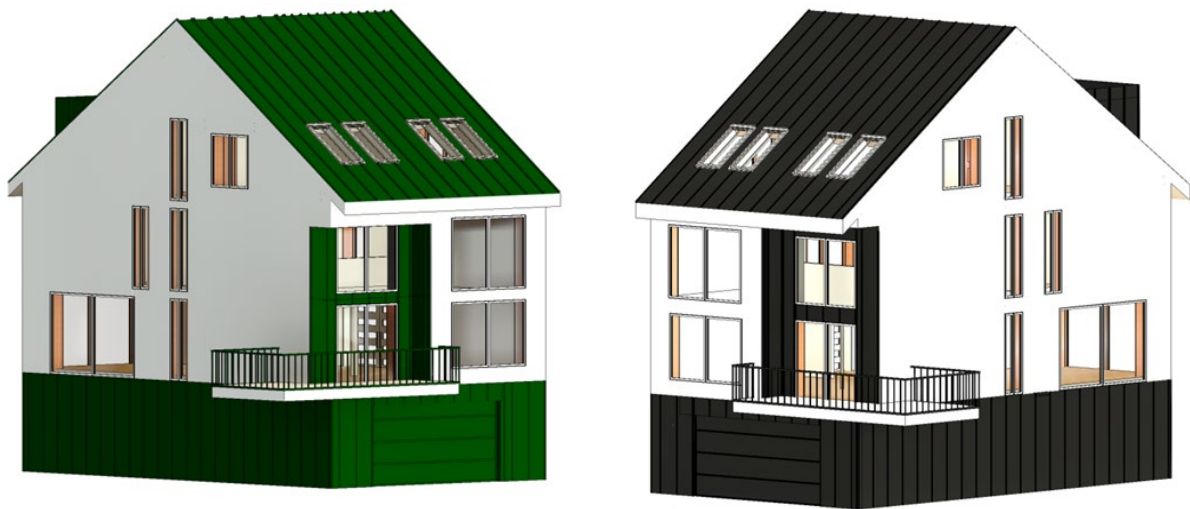


Figure 8. The BIM model of the concrete (left) and the timber (right) building.

2.4 Goal and scope

This study aims to perform a comparative consequential LCA on a light timber frame and a reinforced concrete masonry building. The two buildings are functionally identical and constructed at the same site and with the same environmental conditions. Therefore, the study

brings the opportunity to compare the environmental impacts of a single-family house in timber and concrete in Luxembourg country and its vicinity. To have a comprehensive approach that ensures no significant environmental impacts are overlooked, a cradle-to-grave LCA boundary was considered for this study. Additionally, the potential benefits and loads beyond the system boundary were considered to have an overview of the impact of the EoL stage.

The LCA study is performed according to EN 15978:2011 [30]. The system boundary is shown in Figure 9, which includes the production (modules A1-A3), construction process (modules A4-A5), use (module B1), and the EoL stage (modules C1-C4). Some modules within the use stage including maintenance (B2), repair (B3), replacement (B4), refurbishment (B5), energy use (B6), and water use (B7) are assumed identical for both buildings as they have the same energy class (Energiepass A [49]). Therefore, these modules are excluded from the system boundary. The benefits beyond the system boundary (module D) are calculated and presented for comparison. From a geographical perspective, the system boundary pertains to Europe, where 70% of energy is derived from fossil fuels, whereas only 18% of the energy consumed comes from sustainable sources [50]. In addition, the life span of the cradle-to-grave analysis is 50 years equal to the design service life of the buildings.

The functional unit is defined as 1 m² of the floor area of a single-family house during its 50 years lifespan. The functional unit allows the quantification of the environmental impacts to compare the results with similar buildings.

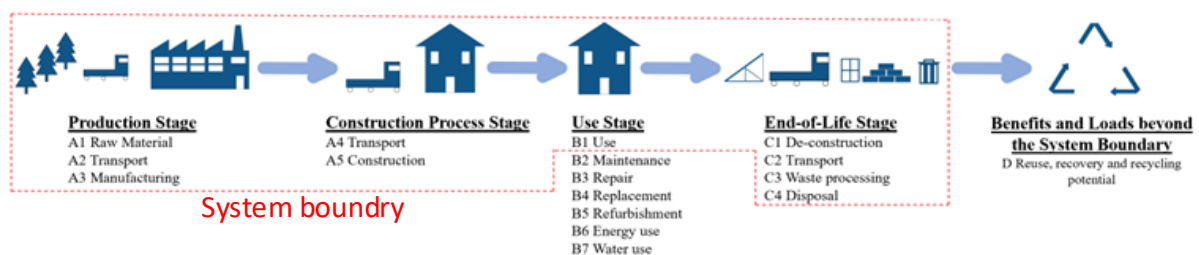


Figure 9. System boundary of the LCA (the figure is modified from [51]).

2.5 Life cycle inventory

2.5.1 Production stage

This stage comprises three modules: A1, A2, and A3. Module A1 deals with extracting the raw materials necessary to produce the construction materials under investigation. This module includes activities such as mining, quarrying, or harvesting of resources required for the manufacturing process. Module A2 focuses on the transportation of raw materials from their extraction sites to the manufacturing facility and the production site. Module A3 deals with the manufacturing and production processes involved in transforming raw materials into construction materials. The EPD provides the necessary data about energy consumption in each module, such as fuel and electricity, global warming potential, and other environmental impacts.

2.5.2 Construction process stage

Module A4 considers the environmental impacts associated with the transportation of the products from the manufacturing facilities to the building site. This module takes into account the distance between the factory and the construction site, which is provided in Table 1 for each product. The transport distances for the timber building are on average higher since the wood products mainly come from neighboring countries. Module A5 considers the installation of the construction products during the construction process at the building site.

Table 2. Transportation distance from the production to the buildings site.

Product	Distance [km]	
	Concrete building	Timber building
Masonry	25	25
Concrete	20	20
KVH	-	60
Wood fiberboard	-	60
OSB	-	60
Plaster-exterior	30	60
Gypsum wallboard	30	30
Plaster-interior	30	-
Y-tong	-	30
EPS	30	30
PUR	30	30
Screed	20	30
Reinforcement	10	10
Steel column	-	30

2.5.3 Use stage

The use stage considers the environmental impact of the usage of the building during its service life, including modules B1 to B7. This study assumes that the buildings do not require maintenance, repair, replacement, and refurbishment since only the structural parts and insulation are considered for the LCA analysis. Moreover, energy and water consumption are neglected during service life since both buildings have the same occupancy and energy class. Therefore, the only module considered from the use stage is B1, which reflects the carbonation of the concrete elements and masonry blocks [15]. Nevertheless, other materials have no environmental impact in the use phase.

2.5.4 End-of-life stage

At the end of the use stage and when the elements reach their planned service life, they will be deconstructed and transported for waste treatment to get sorted and prepared for incineration,

recycling, reuse, or landfill. The EoL scenario of each product is determined based on its EPD.

For each product, the EoL can be seen in Table 2.

Table 3. The end-of-life scenario of the used products in the building.

Product	EoL scenario
Masonry	Downcycling
Concrete	Downcycling
KVH	Incineration
Steico zell	Incineration
Steico flex	Incineration
Wood fiberboard	Incineration
OSB	16% incineration, 17% landfill, and 67% recycling
Plaster-exterior	Landfill
Gypsum wallboard	Recycling
Plaster-interior	Landfill
Y-tong	Downcycling
EPS	Incineration
PUR	Incineration
Screed	90% downcycling and 10% landfill
Reinforcement	90% recycling and 10% landfill
Steel column	98% recycling, 1 % energy recovery, and 1% landfill

2.5.5 Benefits and loads beyond the system boundary

Module D represents the potential benefits and loads from reusing, recycling, incinerating, or landfilling the products and materials. This can be energy recovery of wooden-based products and structural parts, downcycling of concrete and masonry blocks to aggregates, and recycling of steel parts. No benefit or load beyond the system is considered for some materials such as plasterboards.

2.6 Life cycle impact assessment

In this study, the environmental impacts are considered as GWP and PE, measured in kilograms of carbon dioxide equivalent (kg CO₂-eq) and megajoules (MJ), respectively. The CO₂-eq is a unit for measurement of the total global warming effect from all emitted greenhouse gases by

a product converted to the equivalent warming effect of CO₂ over the same period [52]. The data on GWP and PE of the used product in this study are extracted from the EPD provided by the producer. Where the EPD was unavailable, the EPD of a similar product from the ÖKOBAUDAT database was used. ÖKOBAUDAT is a standardized German database for the ecological assessment of buildings offered by the Federal Ministry for Housing, Urban Development, and Building [53]. This resource provides regularly updated generic and specific environmental declaration datasets and adheres to the EN15804 standard [34]. The German database is pertinent to Luxembourg's reality because of comparable environmental regulations and being in the same region. The environmental impact attributes for each material were assigned to the related project parameter in the BIM model. By extracting the relevant quantities from the model, the impact assessment was performed in a spreadsheet considering each stage of the life cycle of the buildings.

3. Results and discussion

3.1 Mass flow of materials

The mass quantities of the two buildings are extracted from the Revit models and are presented for comparison in Figure 10. It is observed that the concrete building is 4.7 times heavier than the timber buildings. In the concrete building, the load-bearing components comprise a significant proportion, accounting for 86.9% of the total mass, equivalent to 290 tons. Conversely, the load-bearing parts in the timber building constitute 43.2% of the total mass or 30 tons. These findings highlight the substantial disparity in mass distribution between the two buildings, with the concrete structure placing greater emphasis on load-bearing components relative to the timber building.

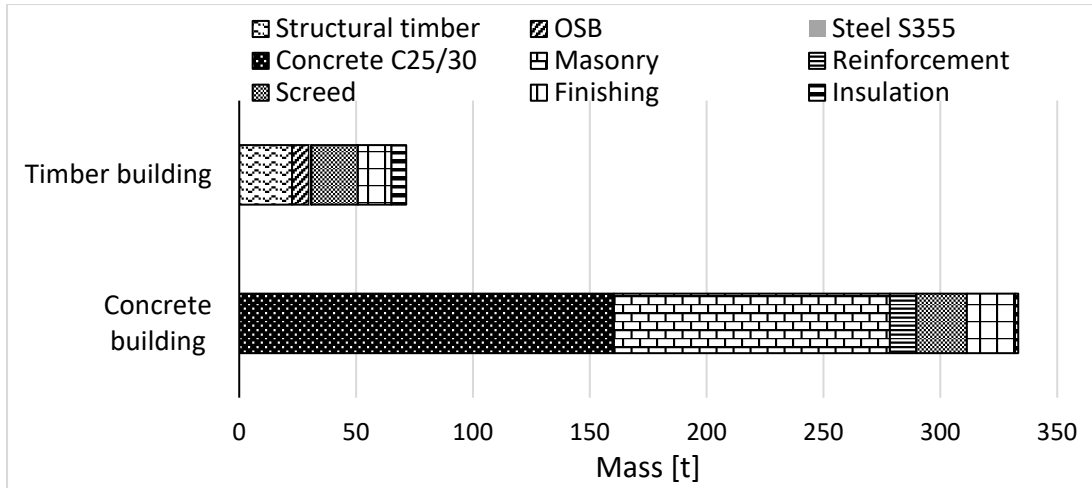


Figure 10. Comparison of the mass of the concrete and timber buildings.

3.2 Cradle-to-grave environmental impacts

The cradle-to-grave environmental impact of both studied buildings considering GWP and PE are shown in Figure 11 and Figure 12, respectively. Also, Figure 13 presents the environmental impacts per square meter of the buildings for each stage and the cradle-to-grave life cycle. The GWP of the concrete building is 77.1% higher than the timber building. The primary contributors to emissions in the concrete building are the structural components, accounting for 61.4% of the total GWP. In contrast, the corresponding figure for the timber building is only 26.1%. The most significant contributors to the GWP for the timber building are the insulation and finishing parts, with 59.3%. For the concrete building, this number is 29.7%. Regarding the non-structural parts, the GWP for both buildings is comparable, except for the finishing, which is 62.6% higher for the timber building compared to the concrete building. This is due to the high amount of gypsum fiber boards used in the timber building. However, the overall GWP value for finishing and insulation in the timber building is only 13% higher compared to the concrete building. This highlights the need for increased emphasis on finishings to reduce GWP in timber buildings effectively. For the timber building, the emissions are mostly related to the EoL stage due to the incineration of the wood-base

components, although 66% of it is recovered in the production stage. In the case of the concrete building, all stages except for the use stage contribute to emissions, with the production stage being the dominant contributor responsible for 80% of emissions. These findings are consistent with those of Burdova et al. [54], who similarly observed the substantial contribution of structural materials in single-family house buildings.

The overall PE for the timber building is about 15.6% higher than the concrete building. The variation arises primarily from finishings, where PE coming from the timber building's finishing is 211% higher compared to the concrete building. Except for finishing, the primary contributors to PE in both buildings exhibit comparable proportional contributions. This again confirms the possibility of diminishing environmental impacts in timber buildings by focusing on improvements in finishing components. The timber building demands about 2.7 times more energy during production than the concrete building, mostly recovered during the EoL stage by incineration and energy recovery of the wooden materials. Despite higher PE requirements for the timber building relative to the concrete one, approximately 69% of PE in the former is derived from renewable sources. In contrast, only 17% of PE in concrete buildings is sourced from renewable sources.

Figure 14 illustrates the benefits and loads beyond the system boundary. The benefits from module D of the timber building's life cycle in terms of GWP and PE are about 4.5 and 5 times greater compared to the ones from the concrete building, respectively. This emphasizes the importance of incorporating the contribution of module D to harness the environmental advantages timber buildings offer. The majority of the benefits for the concrete building come from downcycling of concrete, recycling of the reinforcement, and incineration of the insulations. In contrast, for timber buildings, the benefits are primarily a result of incineration and energy recovery of all the wooden-based structural and insulation components.

Timber construction accounts for only 10% of the overall construction in Luxembourg [45]. However, as Luxembourg strives to achieve net-zero emissions by 2050 [55], the results from this study highlight the potential of a policy promoting timber construction to accelerate the realization of this goal.

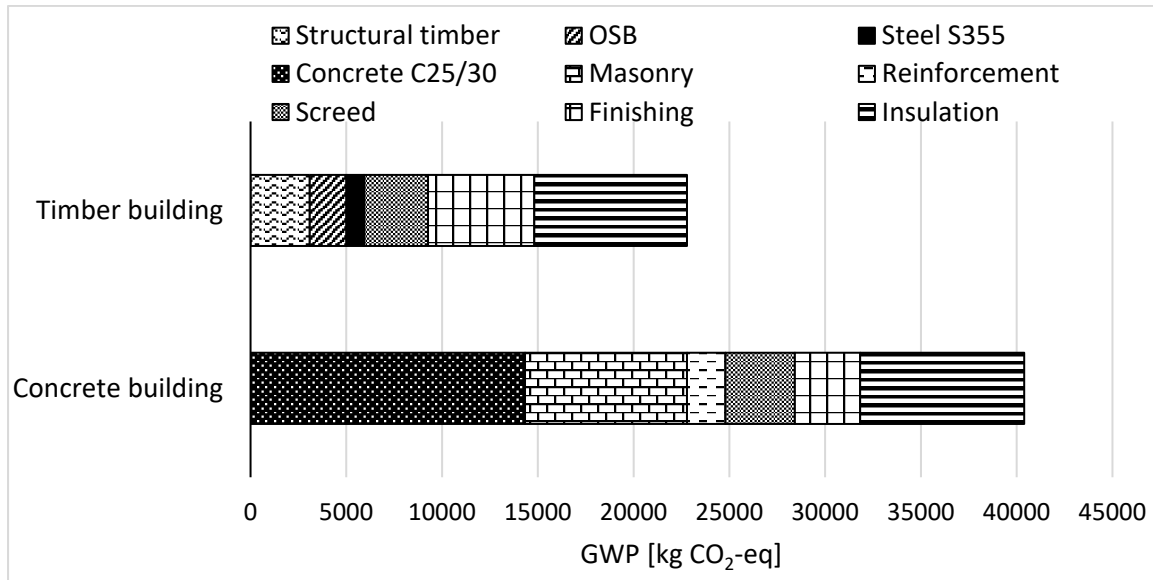


Figure 11. Comparison of the global warming potential of concrete and timber buildings.

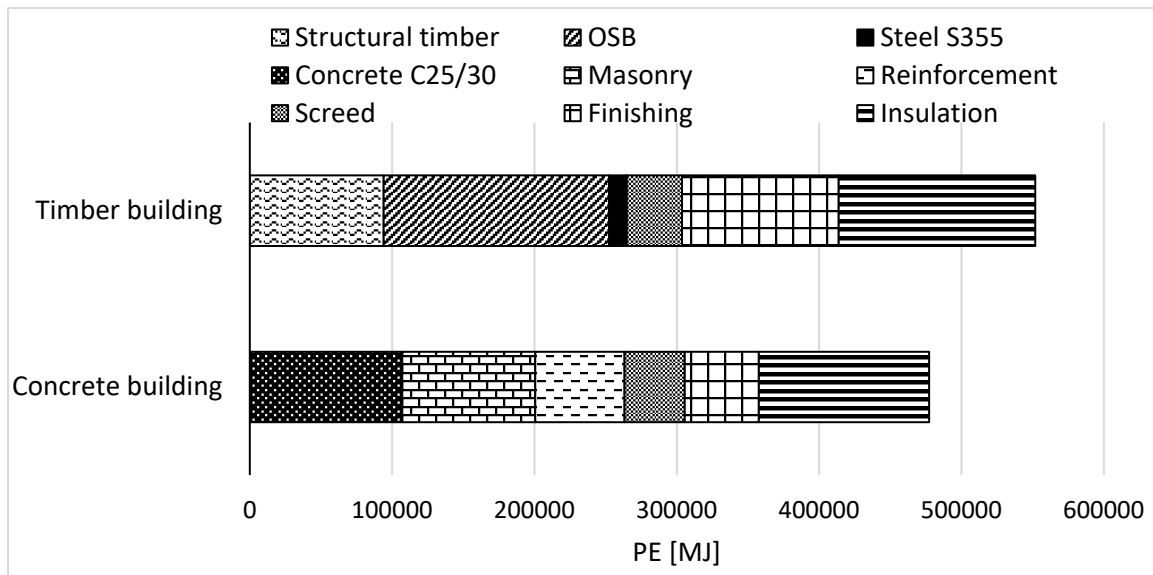


Figure 12. Comparison of the primary energy of the concrete and timber buildings.

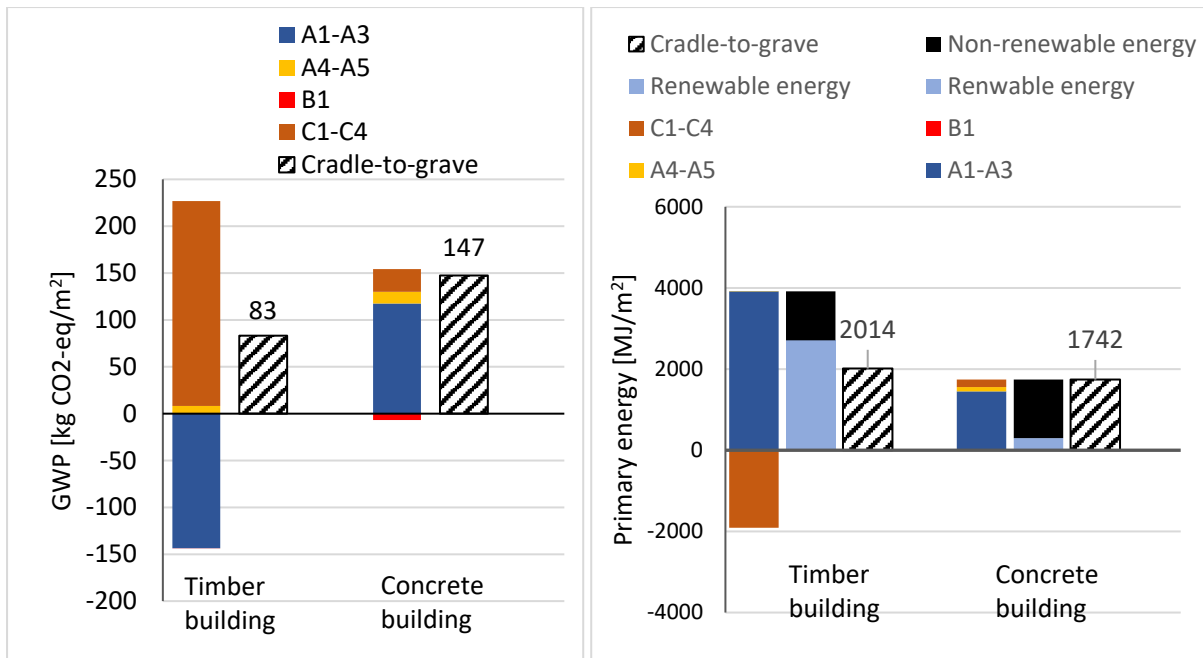


Figure 13. Cradle-to-grave GWP (left) and PE (right) of the timber and concrete buildings.

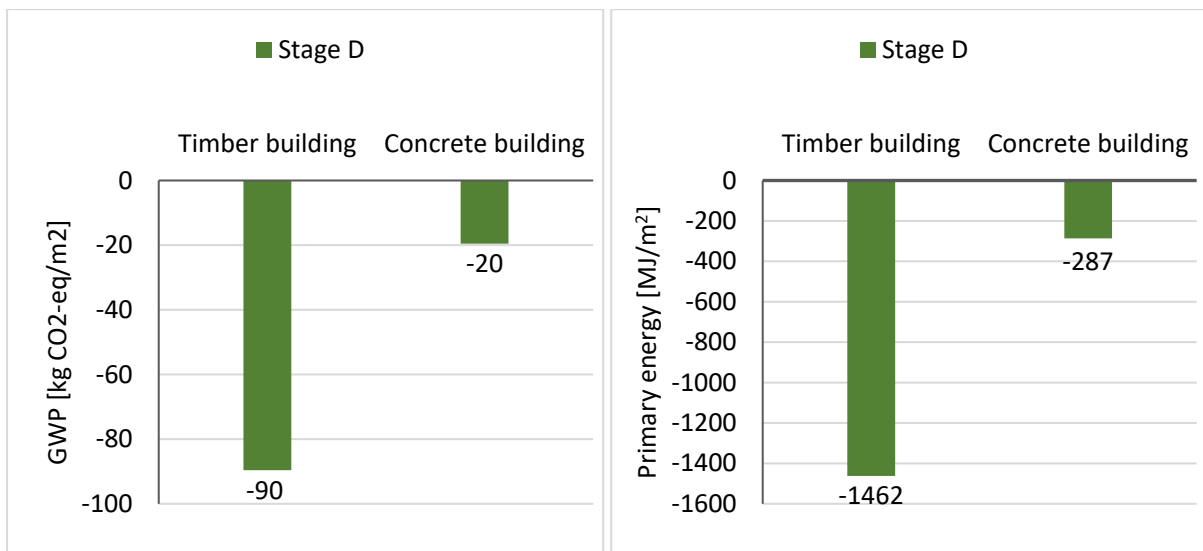


Figure 14. Comparison of the GWP from benefits and loads beyond the system boundary of the concrete and timber buildings.

3.3 Reusable slab scenario

Deconstruction and reuse of the structural component including timber buildings, can reduce the environmental impacts [56]. It is possible and practiced in various buildings to reuse old structural timber elements for new constructions or buildings rehabilitation within a similar or

different structural system [57,58]. Timber-framed buildings, particularly the studied timber building with its prefabricated floor systems designed for indoor environments, are well-suited for deconstruction and subsequent reuse. Hence, this section examines the possibility of reuse and its potential environmental advantages. To this end, a second scenario was investigated for the timber building. In this scenario, the floor system was reused at the end of its life cycle instead of being incinerated as in the first scenario. The rest of the building remained the same in the second scenario. The results of this analysis are demonstrated in Figure 15 and Figure 16. The figures show that the reusable floor system slightly reduces the GWP and PE of the buildings by 2.4% and 1.2%, respectively.

In module D of the life cycle, the reusable slab increases the potential benefits in GWP by 39%, as less material needs to be produced. However, the PE of the building with a reusable floor system decreases by 29% since the timber is not incinerated and thermal energy and electricity are not produced.

The results demonstrate that reusable slabs can significantly benefit the environmental impacts of buildings. As Tam et al. [59] highlighted, reuse can eliminate waste production when the product is repurposed for the same purpose. However, certain limitations exist, such as the high cost of reuse [60] and the need for performance testing from authorities to mitigate the risks associated with further reuse [61]. Therefore, implementing a potential policy to encourage the reuse of construction materials in Luxembourg can yield significant benefits.

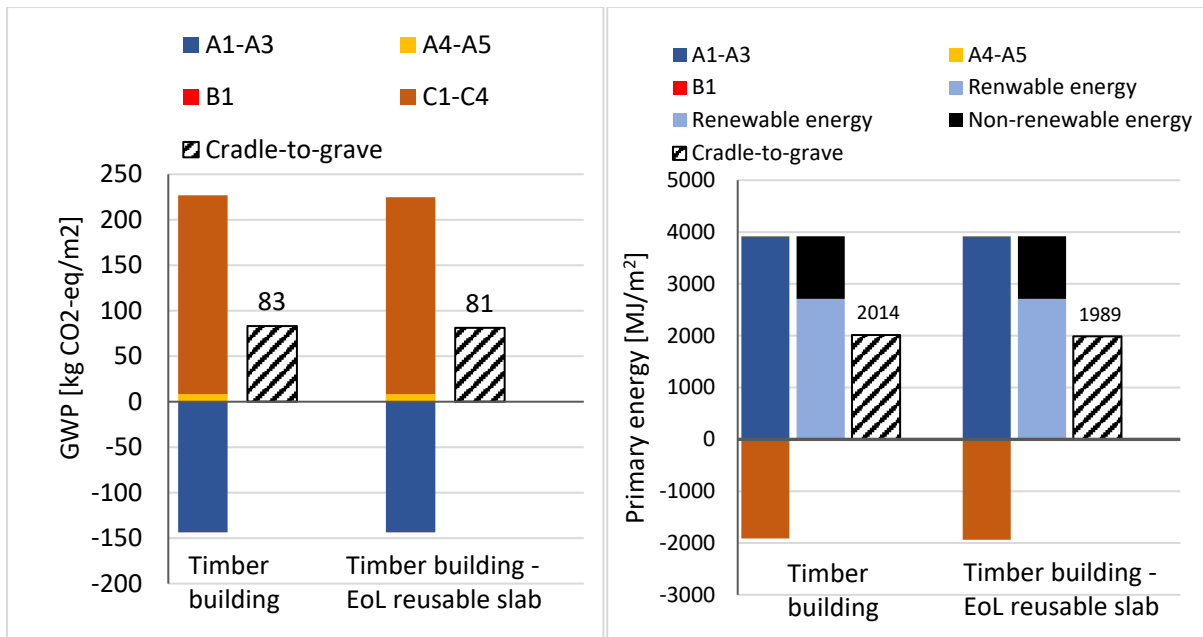


Figure 15. Cradle-to-grave GWP (left) and PE (right) of the timber building and timber building with a reusable floor system.

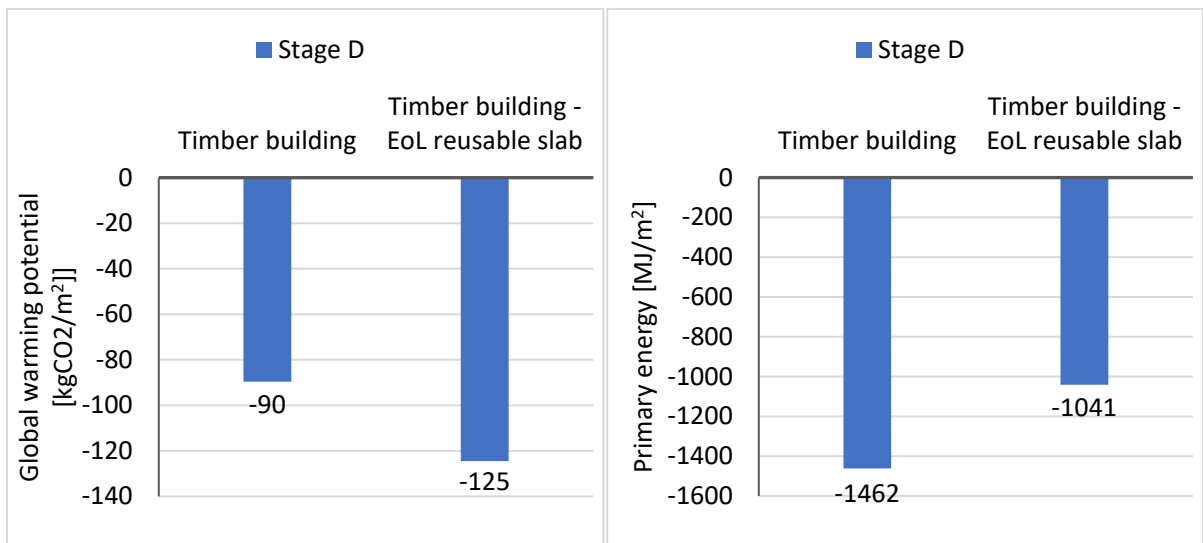


Figure 16. Comparison of the GWP (left) and PE (right) from benefits and loads beyond the system boundary of the timber building and timber building with a reusable floor system.

4. Conclusion

The construction industry is a significant contributor to waste production and CO₂ emissions. In Luxembourg, the majority of the residential buildings are single-family houses. Thus, it is necessary to study the environmental impacts of such buildings to strive toward net-zero

emission goals. This study compared the cradle-to-grave environmental results of two typical single-family houses in Luxembourg, one constructed with light-frame timber and another with reinforced concrete masonry.

The study showed that the construction of the timber building was significantly faster, with a 52% reduction in construction time compared to the concrete building. This can be attributed to the prefabrication process of timber construction. Moreover, the concrete building is 4.7 times heavier than the timber alternative. The Load-bearing parts are 290 tons in the concrete building, while in the timber building, they are only 30 tons.

Additionally, the results from the GWP comparison showed that:

1. Concrete building emits 77.1% higher GWP than timber building.
2. Primary emission contributors in the concrete building are structural components, comprising 61.4% of total GWP, while for the timber building, the contribution is only 26.1%.
3. Insulation and finishing parts contribute to 59.3% of the overall GWP in the timber building. For the concrete building, this proportion is 29.7%.
4. The rise in GWP in finishing parts of the timber building can be attributed to gypsum fiber boards.

Consequently, it is crucial to investigate the possibility of development in finishing components within timber buildings to diminish their GWP effectively. The results from the PE comparison showed that:

- The timber building's overall PE is approximately 15.6% higher than the concrete building.

- The finishing components of the timber building require 211% more PE than the concrete building.
- Except for finishings, primary PE contributors in both buildings show comparable proportional contributions.

Once more, this reaffirms the potential to reduce environmental effects in timber buildings through enhancements in finishing components.

The study also evaluated the recycling, recovery, and reuse (module D) of the buildings. In this stage, the timber building demonstrated significant potential benefits, with 4.5 times the GWP benefits and 5 times the PE benefits compared to the concrete building. This indicates that the timber building has better end-of-life prospects regarding environmental impacts.

A second scenario was evaluated for the timber building in which the floor system is reused instead of being recycled and incinerated at the end of the life cycle. The results indicated that the reusable floor system slightly improved the GWP and PE of the buildings by 2.4% and 1.2%, respectively. When accounting for module D, the reusable floor system improved the GWP benefits by 39% while increasing PE loads beyond the system by about 29%.

The major limitation of this study is its inherent case-specific nature in LCA analysis, relying on direct comparisons, which restricts its generalization to other cases. Considering reuse, the study is limited to the environmental impact and did not evaluate its technical and cost aspects. Overall, the findings suggest that the timber building has advantages in terms of construction speed, transportation impacts, and end-of-life prospects. Hence, it advocates for promoting timber buildings, particularly single-family houses, as an alternative to similar concrete and masonry houses in Luxembourg. Moreover, the study points out the possible environmental gains of reusing timber components.

Acknowledgments

This research has been carried out in collaboration with Kvaadrat SARL, a real estate development company, which maintains impartiality in the study's outcome.

Fundings

This research did not receive any specific grant from funding agencies in the public, commercial, or not-for-profit sectors.

References

- [1] A. Takano, S. Winter, M. Hughes, L. Linkosalmi, Comparison of life cycle assessment databases: A case study on building assessment, *Building and Environment*. 79 (2014) 20–30. <https://doi.org/10.1016/j.buildenv.2014.04.025>.
- [2] Z. Chen, H. Gu, R. Bergman, S. Liang, Comparative Life-Cycle Assessment of a High-Rise Mass Timber Building with an Equivalent Reinforced Concrete Alternative Using the Athena Impact Estimator for Buildings, *Sustainability*. 12 (2020) 4708. <https://doi.org/10.3390/su12114708>.
- [3] C. Chen, L. Bi, Study on spatio-temporal changes and driving factors of carbon emissions at the building operation stage- A case study of China, *Building and Environment*. 219 (2022) 109147. <https://doi.org/10.1016/j.buildenv.2022.109147>.
- [4] J. Knippers, K.G. Nickel, T. Speck, eds., *Biomimetic Research for Architecture and Building Construction*, Springer International Publishing, Cham, 2016. <https://doi.org/10.1007/978-3-319-46374-2>.
- [5] European Commission, Directorate-General for Climate Action, COMMUNICATION FROM THE COMMISSION TO THE EUROPEAN PARLIAMENT, THE COUNCIL, THE EUROPEAN ECONOMIC AND SOCIAL COMMITTEE AND THE COMMITTEE OF THE REGIONS Stepping up Europe's 2030 climate ambition Investing in a climate-neutral future for the benefit of our people, (2020). <https://eur-lex.europa.eu/legal-content/EN/ALL/?uri=CELEX:52020DC0562>.
- [6] J.H. Andersen, N.L. Rasmussen, M.W. Ryberg, Comparative life cycle assessment of cross laminated timber building and concrete building with special focus on biogenic carbon, *Energy and Buildings*. 254 (2022) 111604. <https://doi.org/10.1016/j.enbuild.2021.111604>.
- [7] H. Islam, M. Bhuiyan, Q. Tushar, S. Navaratnam, G. Zhang, Effect of Star Rating Improvement of Residential Buildings on Life Cycle Environmental Impacts and Costs, *Buildings*. 12 (2022) 1605. <https://doi.org/10.3390/buildings12101605>.
- [8] W. Wang, R. Zmeureanu, H. Rivard, Applying multi-objective genetic algorithms in green building design optimization, *Building and Environment*. 40 (2005) 1512–1525. <https://doi.org/10.1016/j.buildenv.2004.11.017>.

- [9] A. Takano, A. Hafner, L. Linkosalmi, S. Ott, M. Hughes, S. Winter, Life cycle assessment of wood construction according to the normative standards, *Eur. J. Wood Prod.* 73 (2015) 299–312. <https://doi.org/10.1007/s00107-015-0890-4>.
- [10] D. D'Agostino, L. Mazzarella, What is a Nearly zero energy building? Overview, implementation and comparison of definitions, *Journal of Building Engineering*. 21 (2019) 200–212. <https://doi.org/10.1016/j.jobe.2018.10.019>.
- [11] A. Vilches, A. Garcia-Martinez, B. Sanchez-Montañes, Life cycle assessment (LCA) of building refurbishment: A literature review, *Energy and Buildings*. 135 (2017) 286–301. <https://doi.org/10.1016/j.enbuild.2016.11.042>.
- [12] J. Bastos, S.A. Batterman, F. Freire, Life-cycle energy and greenhouse gas analysis of three building types in a residential area in Lisbon, *Energy and Buildings*. 69 (2014) 344–353. <https://doi.org/10.1016/j.enbuild.2013.11.010>.
- [13] C. Rodrigues, F. Freire, Integrated life-cycle assessment and thermal dynamic simulation of alternative scenarios for the roof retrofit of a house, *Building and Environment*. 81 (2014) 204–215. <https://doi.org/10.1016/j.buildenv.2014.07.001>.
- [14] K. Allacker, Sustainable building: the development of an evaluation method, *Dissertation Abstracts International*. 71 (2010).
- [15] K. Holschemacher, L. Hoffmann, B. Heiden, ENVIRONMENTAL IMPACT OF TIMBER-CONCRETE COMPOSITE SLABS IN COMPARISON TO OTHER FLOOR SYSTEMS, (n.d.) 6.
- [16] R.M. Andrew, Global CO₂ emissions from cement production, *Earth System Science Data*. 10 (2018) 195–217. <https://doi.org/10.5194/essd-10-195-2018>.
- [17] B. D'Amico, F. Pomponi, J. Hart, Global potential for material substitution in building construction: The case of cross laminated timber, *Journal of Cleaner Production*. 279 (2021) 123487. <https://doi.org/10.1016/j.jclepro.2020.123487>.
- [18] J. Porteous, A. Kermani, Structural timber design to Eurocode 5, Blackwell, Oxford, 2007.
- [19] L. Tupenaite, L. Kanapeckiene, J. Naimaviciene, A. Kaklauskas, T. Gecys, Timber Construction as a Solution to Climate Change: A Systematic Literature Review, *Buildings*. 13 (2023) 976. <https://doi.org/10.3390/buildings13040976>.
- [20] A.B. Robertson, F.C.F. Lam, R.J. Cole, A Comparative Cradle-to-Gate Life Cycle Assessment of Mid-Rise Office Building Construction Alternatives: Laminated Timber or Reinforced Concrete, *Buildings*. 2 (2012) 245–270. <https://doi.org/10.3390/buildings2030245>.
- [21] F. Franzini, R. Toivonen, A. Toppinen, Why Not Wood? Benefits and Barriers of Wood as a Multistory Construction Material: Perceptions of Municipal Civil Servants from Finland, *Buildings*. 8 (2018) 159. <https://doi.org/10.3390/buildings8110159>.
- [22] F. Asdrubali, B. Ferracuti, L. Lombardi, C. Guattari, L. Evangelisti, G. Grazieschi, A review of structural, thermo-physical, acoustical, and environmental properties of wooden materials for building applications, *Building and Environment*. 114 (2017) 307–332. <https://doi.org/10.1016/j.buildenv.2016.12.033>.

- [23] D. Pearce, F.E. Putz, J.K. Vanclay, Sustainable forestry in the tropics: panacea or folly?, *Forest Ecology and Management*. 172 (2003) 229–247. [https://doi.org/10.1016/S0378-1127\(01\)00798-8](https://doi.org/10.1016/S0378-1127(01)00798-8).
- [24] FOREST EUROPE, State of Europe's Forests 2020, (n.d.). https://foresteurope.org/wp-content/uploads/2016/08/SoEF_2020.pdf (accessed May 11, 2023).
- [25] A. Hafner, Aktuell gibt es mehr als genug Holz im Wald, (2020). <https://news.rub.de/wissenschaft/2020-10-05-im-gespraech-aktuell-gibt-es-mehr-als-genug-holz-im-wald> (accessed November 5, 2023).
- [26] R.T. Fauzi, P. Lavoie, A. Tanguy, B. Amor, Life cycle assessment and life cycle costing of multistorey building: Attributional and consequential perspectives, *Building and Environment*. 197 (2021) 107836. <https://doi.org/10.1016/j.buildenv.2021.107836>.
- [27] M. Khasreen, P.F. Banfill, G. Menzies, Life-Cycle Assessment and the Environmental Impact of Buildings: A Review, *Sustainability*. 1 (2009) 674–701. <https://doi.org/10.3390/su1030674>.
- [28] W. Galle, N. De Temmerman, R. De Meyer, Integrating Scenarios into Life Cycle Assessment: Understanding the Value and Financial Feasibility of a Demountable Building, *Buildings*. 7 (2017) 64. <https://doi.org/10.3390/buildings7030064>.
- [29] ISO 14040:2006 Environmental management — Life cycle assessment — Principles and framework, (2006). <https://www.iso.org/standard/37456.html>.
- [30] CEN: Brussels, ILNAS-EN 15978:2011; Sustainability of Construction Works - Assessment of Environmental Performance of Buildings - Calculation Method, (2011).
- [31] G. Rebitzer, K. Buxmann, The role and implementation of LCA within life cycle management at Alcan, *Journal of Cleaner Production*. 13 (2005) 1327–1335. <https://doi.org/10.1016/j.jclepro.2005.05.003>.
- [32] K.P. Shine, The global warming potential—the need for an interdisciplinary retrieval: An editorial comment, *Climatic Change*. 96 (2009) 467–472. <https://doi.org/10.1007/s10584-009-9647-6>.
- [33] L. Gustavsson, A. Joelsson, Life cycle primary energy analysis of residential buildings, *Energy and Buildings*. 42 (2010) 210–220. <https://doi.org/10.1016/j.enbuild.2009.08.017>.
- [34] CEN: Brussels, ILNAS-EN 15804:2012+A2:2019; Sustainability of construction works - Environmental product declarations - Core rules for the product category of construction products, (2012).
- [35] C. Mielecke, T. Mielecke, T. Lützkendorf, Wissenschaftliche Begleitung der Arbeitsgruppe „Modul D“ des Runden Tisches Nachhaltiges Bauen, des Bundesinstituts für Bau-, Stadt- und Raumforschung (BBSR) im Bundesamt für Bauwesen und Raumordnung (BBR), 2017. <https://www.bbsr.bund.de/BBSR/DE/forschung/programme/zb/Auftragsforschung/2NachhaltigesBauenBauqualitaet/2016/runder-tisch-modul-d/01-start.html> (accessed May 15, 2023).
- [36] M. Röck, A. Hollberg, G. Habert, A. Passer, LCA, and BIM: Visualization of environmental potentials in building construction at early design stages, *Building and Environment*. 140 (2018) 153–161. <https://doi.org/10.1016/j.buildenv.2018.05.006>.

- [37] J. Anderson, A. Moncaster, Embodied carbon, embodied energy and renewable energy: a review of environmental product declarations, *Proceedings of the Institution of Civil Engineers - Structures and Buildings*. (2022) 1–12. <https://doi.org/10.1680/jstbu.21.00160>.
- [38] F. Rasmussen, C. Andersen, A. Wittchen, R. Hansen, H. Birgisdóttir, Environmental Product Declarations of Structural Wood: A Review of Impacts and Potential Pitfalls for Practice, *Buildings*. 11 (2021) 362. <https://doi.org/10.3390/buildings11080362>.
- [39] Canadian Wood Council, Sustainability and Life Cycle Analysis for Residential Buildings, (n.d.). https://cwc.ca/wp-content/uploads/2019/03/publications-IBS4_Sustainability_SMC_v2.pdf (accessed May 15, 2023).
- [40] J.L. Skullestad, R.A. Bohne, J. Lohne, High-rise Timber Buildings as a Climate Change Mitigation Measure – A Comparative LCA of Structural System Alternatives, *Energy Procedia*. 96 (2016) 112–123. <https://doi.org/10.1016/j.egypro.2016.09.112>.
- [41] S. Liang, H. Gu, R. Bergman, S.S. Kelley, Comparative life-cycle assessment of a mass timber building and concrete alternative, *WFS*. 52 (2020) 217–229. <https://doi.org/10.22382/wfs-2020-019>.
- [42] C.X. Chen, F. Pierobon, S. Jones, I. Maples, Y. Gong, I. Ganguly, Comparative Life Cycle Assessment of Mass Timber and Concrete Residential Buildings: A Case Study in China, *Sustainability*. 14 (2021) 144. <https://doi.org/10.3390/su14010144>.
- [43] R. Rinne, H.E. Ilgin, M. Karjalainen, Comparative Study on Life-Cycle Assessment and Carbon Footprint of Hybrid, Concrete and Timber Apartment Buildings in Finland, *IJERPH*. 19 (2022) 774. <https://doi.org/10.3390/ijerph19020774>.
- [44] STATEC, The housing situation : residential buildings, households, homeowners and tenants, The Statistics Portal. (2013). <http://statistiques.public.lu/en/actualites/population/population/2013/02/20130213.html> (accessed August 2, 2023).
- [45] J.-M. Hennebert, Y. Lambert, Using wood could speed needed home construction, *Luxembourg-Times-Online*. (2021). <https://www.luxtimes.lu/luxembourg/using-wood-could-speed-needed-home-construction/1331604.html> (accessed August 1, 2023).
- [46] Environmental Product Declaration STEICO flex F flexible wood fibre compartment insulation, (2020). https://www.steico.com/fileadmin/user_upload/importer/downloads/umwelt-produktdeklaration_epd/STEICO_EPD_flex_F_en.pdf (accessed May 15, 2023).
- [47] Environmental Product Declaration STEICOzell wood fibre air-injected insulation, (2020). https://www.steico.com/fileadmin/user_upload/importer/downloads/umwelt-produktdeklaration_epd/STEICOzell_wood_fibre_air-injected_insulation.pdf (accessed May 15, 2023).
- [48] M. Hussain, B. Zheng, H.-L. Chi, S.-C. Hsu, J.-H. Chen, Automated and continuous BIM-based life cycle carbon assessment for infrastructure design projects, *Resources, Conservation and Recycling*. 190 (2023) 106848. <https://doi.org/10.1016/j.resconrec.2022.106848>.
- [49] Le certificat de performance énergétique pour bâtiments | Klima-Agence, (n.d.). <https://www.klima-agence.lu/fr/le-certificat-de-performance-energetique-pour-batiments> (accessed June 5, 2023).

- [50] International Energy Agency IEA Europe Energy Supply, IEA. (n.d.). <https://www.iea.org/regions/europe> (accessed June 7, 2023).
- [51] EPD International AB, Environmental Product Declaration In accordance with ISO 14025 and EN 15804 for: CLT (Cross Laminated Timber) by Stora Enso, (2020). <https://www.storaenso.com/-/media/documents/download-center/certificates/wood-products-approvals-and-certificates/epd/stora-enso-epd-clt-2021.pdf> (accessed May 17, 2023).
- [52] A. Akbarnezhad, J. Xiao, Estimation and Minimization of Embodied Carbon of Buildings: A Review, *Buildings*. 7 (2017) 5. <https://doi.org/10.3390/buildings7010005>.
- [53] ÖKOBAUDAT Sustainable Construction Information Portal, (n.d.). <https://www.oekobaudat.de> (accessed May 15, 2023).
- [54] E. Kridlova Burdova, S. Vilcekova, Analysis of building materials used for the construction of family houses in the boundaries from Cradle to Gate with Options, *IOP Conf. Ser.: Mater. Sci. Eng.* 1252 (2022) 012074. <https://doi.org/10.1088/1757-899X/1252/1/012074>.
- [55] Luxembourg's integrated national energy and climate plan for the period 2021-2030 (PNEC), The Luxembourg Government. (2023). <http://gouvernement.lu/en/dossiers/2023/2023-pnec.html> (accessed August 1, 2023).
- [56] V. Diyamandoglu, L.M. Fortuna, Deconstruction of wood-framed houses: Material recovery and environmental impact, *Resources, Conservation and Recycling*. 100 (2015) 21–30. <https://doi.org/10.1016/j.resconrec.2015.04.006>.
- [57] J. Brol, S. Dawczy, K. Adamczyk, Possibilities of timber structural members reuse, in: *Wroclaw, Poland, 2015*: pp. 9–11.
- [58] A.R. Chini, S.F. Bruening, Deconstruction and materials reuse in the United States, *The Future of Sustainable Construction*. (2003).
- [59] V. Tam, W. Lu, Construction Waste Management Profiles, Practices, and Performance: A Cross-Jurisdictional Analysis in Four Countries, *Sustainability*. 8 (2016) 190. <https://doi.org/10.3390/su8020190>.
- [60] A. Jiménez-Rivero, J. García-Navarro, Best practices for the management of end-of-life gypsum in a circular economy, *Journal of Cleaner Production*. 167 (2017) 1335–1344. <https://doi.org/10.1016/j.jclepro.2017.05.068>.
- [61] M.A. Camilleri, European environment policy for the circular economy: Implications for business and industry stakeholders, *Sustainable Development*. 28 (2020) 1804–1812. <https://doi.org/10.1002/sd.2113>.

3.3 Paper III

The paper “Nonlinear three-dimensional anisotropic material model for failure analysis of timber” [93] was published in *Engineering Failure Analysis* journal. The author of this dissertation served as the first author and his contribution included conceptualization, formal analysis, investigation, the draft preparation, and visualization.

Nonlinear three-dimensional anisotropic material model for failure analysis of timber

Hooman Eslami, Laddu Bhagya Jayasinghe, Daniele Waldmann*

Faculty of Science, Technology and Medicine (FSTM), University of Luxembourg, L-4364
Esch-sur-Alzette, Luxembourg

*Corresponding author: daniele.waldmann@uni.lu (D. Waldmann)

Abstract

In this paper, a constitutive material model is proposed to model the nonlinear mechanical response of timber, as elastoplastic orthotropic material under three-dimensional (3D) stress state. An associated flow rule model based on Hoffmann yield criterion and plastic potential is adopted for describing the plasticity of timber under compression. Isotropic strain hardening during plastic deformation is incorporated into Hoffman yield criterion by assuming that equivalent yield stress is a function of the equivalent plastic strain. A stress-based continuum damage formulation with four independent failure criteria in tension and compression is used. The proposed model is implemented as a user material subroutine UMAT in Abaqus. The results obtained in numerical simulations are evaluated and compared with experimental results. A good agreement has been found between numerical simulations and the experimental results. Therefore, the proposed constitutive model can be used further in numerical simulations of the anisotropic behavior of timber.

Keywords: Constitutive model; Elastoplastic orthotropic material; Numerical finite element simulation in Abaqus; Timber

1. Introduction

In the last years, timber has been increasingly used as a construction material due to high strength to weight ratio while being in parallel reputed to make an essential contribution to a

sustainable future by its positive environmental impact. Since timber products have a good load-bearing capacity under both compression and tension, they can be used for a variety of structural components. Timber is a fully renewable resource as well as it has a low carbon footprint and high carbon storage capacity, and at the end of its life cycle it can be reused or recycled more sustainably compared to other construction materials like steel and concrete [1,2]. Due to its major benefits in sustainability, timber has been noticed rapid development as structural and non-structural components in the construction industry in the last decades, not least as a result of the EU shifts towards environmentally sustainable building practices.

Timber is usually a heterogeneous and orthotropic material that exhibits different constitutive relationship of the material in tension and compression. Although natural imperfections such as knots and resin pockets are not generally considered in numerical modelling, predicting the mechanical behavior of timber is still complicated because of its structure. Timber has unique and independent mechanical properties in three mutually perpendicular axes, defined by the grain direction: longitudinal (parallel to the grain), radial, and tangential [3]. Furthermore, the mechanical properties of timber including strength, modulus of elasticity, shear modulus, and Poisson ratio vary not only by direction but also by the sign of the stress, whether in tension or compression [4]. The behavior in compression parallel to the grain direction is rather linear elastic followed by a ductile failure. In compression perpendicular to the grain, timber shows a plastic behavior with moderate hardening. Under tension, timber shows a linear elastic response followed by a brittle failure in both parallel and perpendicular to the grain direction [4]. Also, it is noticeable that the stiffness and strength properties perpendicular to the grain are much lower than the ones parallel to the grain [5,6].

In order to develop a numerical model of timber structures, it is essential to understand its mechanical behavior. During the last decades, many material models have been developed to define a constitutive law for the complicated behavior of timber, but most of them are only

applicable for 2D finite element (FE) analysis [7-10]. Some earlier efforts to calculate the load-carrying capacity of dowel-type timber joints were done by some researchers [11-14]. They developed material models to simulate the brittle failure of timber by studying the initiation of fracture and its growth based on Linear Elastic Fracture Mechanics (LEFM) and Non-linear Fracture Mechanics (NLFM). These studies mostly considered a 2D constitutive model of timber which was only applicable for timber parts with small thickness. Chen et al. [8] Developed a plane stress nonlinear material model to predict the failure of dowel type joints with a failure criterion consisting of tensile stress perpendicular to the wood grains and shear stress parallel to the wood grains. In another approach to investigate the mechanical performance of dowel-type timber joints, a 3D FE model was developed by Santos et al. [15]. However, the timber material model was limited to an orthotropic elastic constitutive law.

The timber material models which were developed to simulate the non-linear behavior of timber can be categorized into three groups: Elastic-plastic models, elastic-damage models and elastic-plastic in combination with damage models [16,17].

In the first group, some studies considered bilinear [18,19] and trilinear [20] stress-strain curves to describe the non-linear behavior of timber under compression perpendicular to the grain. Several other studies in the first group considered the classical flow theory of plasticity in combination with single-surface isotropic yield criteria such as Hill's criterion [21], Tsai-Wu criterion [22] and Hoffman criterion [23].

Kharouf et al. [9] proposed a 2D orthotropic material model according to Hill's yield criterion associated with anisotropic hardening to model the behavior of timber under compression. However, the model did not consider the brittle failure under tension and shear stresses. Dias et al. [18] presented a model that makes no distinction between the radial and tangential behavior of timber and used orthotropic yield criterion based on Hill's criterion associated with

isotropic hardening to define a linear elastic-plastic behavior for timber with different stress potentials in different directions. However, this model did not realize any difference between the yield strength of timber in compression and tension and assumed linear elastic-perfect plastic behavior for all the stress cases. Oudjene and Khalifa [24] presented an anisotropic elastic-plastic constitutive law with hardening also based on Hill's criterion and without distinction between radial and tangential properties. In this model, the strength difference of timber in compression and tension, the brittle behavior in tension, and densification in compression were applied. Bouchair and Vergne [25] and Clouston and Lam [26] used Tsai-Wu criterion to develop a 2D FE model of timber. Xu et al. [27] use the Hoffman failure criterion associated with the Hill criterion to develop an orthotropic 3D constitutive model for timber based on the elastic-perfect plastic behavior. However, the elastic or elastic-perfect plastic orthotropic material model cannot retrace the load-deformation behavior of timber accurately.

These single-surface yield criteria are not able to effectively predict the different failure modes that occur in materials like timber [28]. To overcome this shortage, researchers [29-32] proposed multi-surface plasticity criteria. In these criteria, different yield surfaces are combined to make the global failure surface considering the mode of failure in timber. Although the multi-surface criteria are more accurate compared to single surface ones in simulating the different failure modes of timber, they have limitations in usage due to complicated constitutive laws and the possibility of numerical instabilities [28,33].

The second group of models [28,33-35] use Continuum Damage Mechanics (CDM) to model the behavior of timber. The CDM method is a simple approach to implement softening and hardening behavior of timber into the model. In comparison to plasticity, damage is much easier to implement in material models. In this method, the material behavior is completely defined by the damage variables which are inserted into fundamental Hooke's equation to

reduce the stiffness matrix. Garib et al. [28] used CDM theory to model stiffness degradation in various stress components and to study the nonlinear behavior under a multi-directional stress state. Sandhaas and Van de Kuilen [34] developed a 3D anisotropic CDM model which is based on eight types of stress-based failure criteria governed by six damage variables. However, no damage interactions were modelled in this model.

The third group of models [36-39] combine the plasticity and different damage models. Most of these models use Hill's criterion as yield surface and damage criteria. Xu et al. [36] developed a timber model includes the anisotropic plasticity coupled with isotropic hardening according to Hill yield criterion to describe the compressive behavior of timber. To describe the brittle behavior in tension and shear, the evolution of damage was modelled by using a reduction of elastic modulus and element removal which is based on modified Hill failure criterion. Khelifa et al. [38] developed a new timber model within the framework of plasticity coupled with CDM which incorporates effects of anisotropic plasticity with isotropic hardening, isotropic damage and large plastic deformations. However, the model uses only one Hill's criterion as plasticity and damage criteria, and does not consider different strength parameters for tension and compression. It is also failed to capture the anisotropic damage developed in timber beams. Later, Sirumbal-Zapata et al. [4] developed a model to represent the cyclic behaviour of timber using the Hofmann criterion for plasticity and the Hill criterion for damage. However, since an isotropic damage was assumed in order to maintain a symmetric stress tensor, the individual failure modes could not be identified. Benvenuti et al. [16] proposed a multi-surface elastic-damaging-plastic constitutive model whereas two plastic activation functions and three damage variables were defined. This constitutive model was found effective in ductile and brittle failure modes [40]. However, to simplify the development of the proposed model, the model was restricted only to plane stress cases.

When performing FE analysis on timber structures, or the constitutive relationship of timber, previous studies have simplified timber material as anisotropic or orthotropic elastic materials [15,41-43]. They also do not distinguish the behaviour under tension and compression. Many of them do not consider material damage [18,19] or simply the damage as isotropic [4,38]. In addition, several studies set the material stiffness when the stress state reaches the strength criterion [27,36]. Based on the characteristics of timber's complex anisotropic materials, this paper attempts to establish a constitutive model that can simulate the complex mechanical properties of wood.

Thus, in this paper, a constitutive relationship is adopted for timber material based on the isotropic hardening elastoplastic model using the Hoffman yield criterion, which is an extension of Hill's criterion. The proposed material model for timber has the characteristics such as: 1) an orthotropic stress-strain relationship is used in the linear phase; 2) an associated flow rule model based on Hoffman yield criterion and plastic potential is used for describing the plasticity under compression; 3) isotropic strain hardening, which is incorporated into the Hoffman yield criterion, is applied using a hardening modulus to incorporate timber plastic flow in the proposed material model under compression; 4) a stress-based continuum damage formulation with four independent failure criteria in tension and compression is used; 5) three different tensile damages in the grain longitudinal, radial and tangential directions are established using the damage factors and fracture energies. Thus, this elastoplastic model is capable of simulating the brittle behaviour of timber in tension and ductile yielding of timber under compression.

The proposed material model can be easily implemented as a user material subroutine (UMAT) in Abaqus [44] commercial FE analysis software. The developed material model is presented in Section 2, and its implementation in Abaqus is described in Section 3. Subsequently, this

material model is validated by comparison of results to some experimental results, and it is presented in Section 4, followed by the conclusion of the study.

2. The constitutive material model

2.1 Orthotropic linear-elastic constitutive behavior

The constitutive relationship reflects the relationship between stress and strain. In the elastic stage, the stress-strain relationship of an orthotropic material can be written as:

$$\sigma = E \varepsilon_e \quad (1)$$

where σ and ε_e are the applied stress and corresponding elastic strain tensors, respectively. E is the orthotropic elastic matrix which is given as:

$$E = \begin{bmatrix} E_{11} & E_{12} & E_{13} & 0 & 0 & 0 \\ E_{21} & E_{22} & E_{23} & 0 & 0 & 0 \\ E_{31} & E_{32} & E_{33} & 0 & 0 & 0 \\ 0 & 0 & 0 & E_{44} & 0 & 0 \\ 0 & 0 & 0 & 0 & E_{55} & 0 \\ 0 & 0 & 0 & 0 & 0 & E_{66} \end{bmatrix} \quad (2)$$

where

$$E_{11} = (E_1/\beta) (1 - \nu_{23}\nu_{32}); \quad E_{12} = (E_1/\beta) (\nu_{21} + \nu_{23}\nu_{31}); \quad E_{13} = (E_1/\beta) (\nu_{31} + \nu_{21}\nu_{32}) \quad (3)$$

$$E_{21} = (E_2/\beta) (\nu_{12} + \nu_{13}\nu_{32}); \quad E_{22} = (E_2/\beta) (1 - \nu_{13}\nu_{31}); \quad E_{23} = (E_2/\beta) (\nu_{32} + \nu_{12}\nu_{13}) \quad (4)$$

$$E_{31} = (E_3/\beta) (\nu_{13} + \nu_{12}\nu_{23}); \quad E_{32} = (E_3/\beta) (\nu_{23} + \nu_{21}\nu_{13}); \quad E_{33} = (E_3/\beta) (1 - \nu_{12}\nu_{21}) \quad (5)$$

$$E_{44} = G_{12}; \quad E_{55} = G_{13}; \quad E_{66} = G_{23} \quad (6)$$

$$\beta = 1 - (\nu_{12}\nu_{21}) - (\nu_{13}\nu_{31}) - (\nu_{23}\nu_{32}) - (\nu_{12}\nu_{23}\nu_{31}) - (\nu_{13}\nu_{21}\nu_{32}) \quad (7)$$

where E_i represent the Young's moduli in the three orthotropic directions, ν_{ij} and G_{ij} are the Poisson's ratio and shear moduli, respectively. Direction 1 is the direction parallel to the grain (longitudinal) and directions 2 and 3 are the radial and tangential directions.

Since the elastic matrix relating the stresses and strains is symmetric, the constants are $\nu_{21} = \nu_{12}(E_2/E_1)$, $\nu_{31} = \nu_{13}(E_3/E_1)$ and $\nu_{32} = \nu_{23}(E_3/E_2)$.

2.2 Elastoplastic constitutive behavior

The behavior of elastoplastic materials can be analyzed by constitutive equations which relate the stress to the incremental formulation of strain and other internal variables. For most materials, under monotonic loading, there is a certain limit stress value σ_e , when the stress is lower than σ_e , the deformation of material will be elastic. When the stress reaches the limit stress value, the material begins to enter the elastoplastic state. If the load is kept increasing, a permanent plastic deformation is observed after the release of the load. If the material deforms at constant stress after the stress reached the limit value σ_e , the material is called ideally elastoplastic. Conversely, if the stress reaches σ_e , while the stress still generally increases with increasing deformation, it is called strain hardening. For a strain-hardening material, the limit stress σ_e is a function of the plastic strain ε_p , which can be expressed in a general form as:

$$\sigma_{ek} = \sigma_e(\varepsilon_p) \quad (8)$$

According to the theory of plasticity, the total strain ε can be divided into an elastic component ε_e and a plastic component ε_p .

$$\varepsilon = \varepsilon_e + \varepsilon_p \quad (9)$$

Since the plastic deformation is related to the deformation history, it is more convenient to give the constitutive relationship reflecting the plastic stress-strain relationship in the form of strain increment. The theory of expressing plastic constitutive relationship in the form of strain increment is called plastic increment theory. Under the condition of proportional deformation, the constitutive relationship of the total quantity theory can be obtained through the constitutive relationship of integral increment theory. When the deviation from the proportional

deformation condition is not much, the calculation result of the total quantity theory is close to the actual risk result.

Yield criterion, hardening rule and plastic flow rule are the three fundamental equations in plastic theory. Under complex stress conditions, yield criterion is useful to accurately determine the yielding of material. For isotropic materials like metals, while many yield criteria are available, the most commonly used yield conditions are the Tresca yield condition and Von Mises condition. However, the yield behavior of anisotropic materials like timber cannot be modelled by these yield criteria. Thus, the Hill anisotropic yield criterion was introduced by Hill in 1948 [21] as an anisotropic extension of the Von Mises criterion. The most of existing models for anisotropic materials are derived based on Hill's criterion which does not distinguish between compressive and tensile strengths. This can result in underestimation of the maximum load that can be applied. Thus, in this paper, a constitutive relationship is adopted for timber material based on the isotropic hardening elastoplastic model using the Hoffman yield criterion [23], which was introduced as an extension of Hill criterion considering the different tensile and compression strengths that could characterize the brittle behavior. The strength difference of timber in tension and compression can be considered for the description of the corresponding yield surface in the Hoffman theory. Compared to the material models based on Hill's criterion, in total nine independent material strength parameters representing three compressive strengths, three tensile strengths and three shear strengths of the material are necessary for the description of yield surface of the proposed material model for timber. In addition, in order to define linear-elastic orthotropic behavior of timber, a total of nine mechanical properties such as three elastic moduli, three shear moduli and three Poisson's ratios are used in the proposed material model.

In this paper, no plastic response is considered for the timber under tension and Hoffman criterion [23] is adopted to consider the plastic deformation of timber under compression. It

means, the timber will show elastic response and will fail in a brittle way when it is subjected to tensile stress. If the timber is subjected to compression, once the stresses reaches the yield criterion, the timber will yield with plastic flow and hardening and will fail in a ductile way. The yield function $f(\sigma)$ used in this elastic-plastic model can be expressed by Eq. (10) [45].

$$f(\sigma) = \alpha_{23}(\sigma_2 - \sigma_3)^2 + \alpha_{13}(\sigma_3 - \sigma_1)^2 + \alpha_{12}(\sigma_1 - \sigma_2)^2 + \alpha_{11}\sigma_1 + \alpha_{22}\sigma_2 + \alpha_{33}\sigma_3 + 3\alpha_{44}\sigma_4^2 + 3\alpha_{55}\sigma_5^2 + 3\alpha_{66}\sigma_6^2 - \sigma_e^2 \quad (10)$$

with

$$\alpha_{12} = \frac{\sigma_e^2}{2} \left(\frac{1}{\sigma_{1c}\sigma_{1t}} + \frac{1}{\sigma_{2c}\sigma_{2t}} - \frac{1}{\sigma_{3c}\sigma_{3t}} \right) \quad (11)$$

$$\alpha_{23} = \frac{\sigma_e^2}{2} \left(-\frac{1}{\sigma_{1c}\sigma_{1t}} + \frac{1}{\sigma_{2c}\sigma_{2t}} + \frac{1}{\sigma_{3c}\sigma_{3t}} \right) \quad (12)$$

$$\alpha_{13} = \frac{\sigma_e^2}{2} \left(\frac{1}{\sigma_{1c}\sigma_{1t}} - \frac{1}{\sigma_{2c}\sigma_{2t}} + \frac{1}{\sigma_{3c}\sigma_{3t}} \right) \quad (13)$$

$$\alpha_{11} = \sigma_e^2 \left(\frac{\sigma_{1c} - \sigma_{1t}}{\sigma_{1c}\sigma_{1t}} \right) \quad (14)$$

$$\alpha_{22} = \sigma_e^2 \left(\frac{\sigma_{2c} - \sigma_{2t}}{\sigma_{2c}\sigma_{2t}} \right) \quad (15)$$

$$\alpha_{33} = \sigma_e^2 \left(\frac{\sigma_{3c} - \sigma_{3t}}{\sigma_{3c}\sigma_{3t}} \right) \quad (16)$$

$$\alpha_{44} = \frac{\sigma_e^2}{3\sigma_{12}^2} \quad (17)$$

$$\alpha_{55} = \frac{\sigma_e^2}{3\sigma_{13}^2} \quad (18)$$

$$\alpha_{66} = \frac{\sigma_e^2}{3\sigma_{23}^2} \quad (19)$$

where σ_1 , σ_2 and σ_3 are the normal stresses in the direction of orthotropic axis 1, 2 and 3, respectively. σ_4 , σ_5 and σ_6 are the shear stresses in the planes 12, 13 and 23, respectively. σ_e is

the equivalent yield stress, σ_{ic} and σ_{it} ($i=1, 2, 3$) are the compressive and tensile strengths in the axes of orthography, respectively. σ_{12} , σ_{13} and σ_{23} are the shear strengths in planes 12 , 13 and 23 , respectively.

The Hoffman yield criterion can be formulated as follows:

$$f(\sigma) = \frac{1}{2} \sigma^T P \sigma + \sigma^T Q - \sigma_e^2 \quad (20)$$

where, σ^T is the stress tensor in a vector form as $\sigma^T = (\sigma_1, \sigma_2, \sigma_3, \sigma_4, \sigma_5, \sigma_6)$. P and Q are the Hoffman mapping matrix and vector, respectively, defined in [45].

$$P = \begin{bmatrix} 2(\alpha_{13} + \alpha_{12}) & -2\alpha_{12} & -2\alpha_{13} & 0 & 0 & 0 \\ -2\alpha_{12} & 2(\alpha_{23} + \alpha_{12}) & -2\alpha_{23} & 0 & 0 & 0 \\ -2\alpha_{13} & -2\alpha_{23} & 2(\alpha_{13} + \alpha_{23}) & 0 & 0 & 0 \\ 0 & 0 & 0 & 6\alpha_{44} & 0 & 0 \\ 0 & 0 & 0 & 0 & 6\alpha_{55} & 0 \\ 0 & 0 & 0 & 0 & 0 & 6\alpha_{66} \end{bmatrix} \quad (21)$$

$$Q^T = (\alpha_{11}, \alpha_{22}, \alpha_{33}, 0, 0, 0) \quad (22)$$

For an ideal elastoplastic material, since there is no strengthening effect, the value of the yield function remains constant during the entire plastic deformation process. For strengthened or softened materials, the yield condition will change with the increase of plastic deformation. The changed yield condition is called the subsequent yield condition. The proposed model considers linear isotropic hardening for timber yield stress under the compression as follows:

$$\sigma_{ek} = \sigma_e + h \cdot k \quad (23)$$

where h is hardening modulus and k is the isotropic hardening variable.

k depends on the equivalent plastic strain obtained by means iterative method (Newton-Raphson) for each load increment. However, h is an input parameter of the proposed model which can be directly obtained from the uniaxial stress-strain diagram. Depending on the chosen value of h , perfect plasticity, slight hardening or softening can be modeled. Simply, the

following equation can be used to calculate the value of h for a particular case of uniaxial plasticity [4].

$$h = \frac{\sigma_e}{\sigma_{2c}} \frac{E_2 T_2}{E_2 - T_2} \quad (24)$$

where T_2 is the plastic tangent modulus in the direction of orthotropic axis 2 (the direction perpendicular to the grain).

In the hardening state, each yield value will change depending on the corresponding hardening parameter k_i ($i = 1, 2, \dots, 9$). Thus, the parameters in the mapping vector Q change also. Isotropic hardening is considered in this paper, because it assumes that the initial yield surface expands uniformly without translation and distortion as plasticity occurs [46]. Thus, all the yield values change in the same order. Consequently, the parameters α_{11} , α_{22} and α_{33} in the mapping vector Q will change depending on the hardening parameter k . Thus, the Hoffman yield function combined with the isotropic hardening can be written in a general form as follows:

$$f(\sigma, k) = \frac{1}{2} \sigma^T P \sigma + \sigma^T Q(k) - \sigma_{ek}^2 \quad (25)$$

The stress point must remain on the yield surface to obtain plastic deformations. The yield condition is the condition that each combination of stress components should satisfy. Mathematically speaking, the yield function must be less than zero for elastic deformations and it must remain zero for a short period for material yielding so that plastic flow can occur.

$$f(\sigma, k) < 0 \quad \text{for elastic} \quad (26)$$

$$f(\sigma, k) = 0 \quad \text{yield condition} \quad (27)$$

When the stress reaches the strength criterion of Eq. (27), the elastoplastic radial mapping algorithm is used to constrain stress point on the yield surface. According to the theory of

plasticity, the total strain increment $\Delta\varepsilon$ can be divided into elastic component $\Delta\varepsilon^e$ and plastic component $\Delta\varepsilon^p$ as:

$$\Delta\varepsilon = \Delta\varepsilon^e + \Delta\varepsilon^p \quad (28)$$

In this study, the associated flow rule was used to determine the plastic strain and is given as:

$$\Delta\varepsilon^p = \Delta\lambda \left(\frac{\partial f}{\partial \sigma} \right) \quad (29)$$

where $\Delta\lambda$ denotes the plastic multiplier and $\frac{\partial f}{\partial \sigma}$ is the gradient vector of the plastic potential energy function of $f(\sigma, k)$ which can be written as:

$$\left(\frac{\partial f}{\partial \sigma} \right) = \begin{pmatrix} 2(\alpha_{13} + \alpha_{12})\sigma_1 - 2\alpha_{12}\sigma_2 - 2\alpha_{13}\sigma_3 + \alpha_{11} \\ -2\alpha_{12}\sigma_1 + 2(\alpha_{23} + \alpha_{12})\sigma_2 - 2\alpha_{23}\sigma_3 + \alpha_{22} \\ -2\alpha_{13}\sigma_1 - 2\alpha_{23}\sigma_2 + 2(\alpha_{13} + \alpha_{23})\sigma_3 + \alpha_{33} \\ 6\alpha_{44}\sigma_4 \\ 6\alpha_{55}\sigma_5 \\ 6\alpha_{66}\sigma_6 \end{pmatrix} \quad (30)$$

2.3 Damage evolution equations

A damage model is needed to characterise the different responses of timber in tension and compression. The damage in any direction of the timber causes a gradual degradation of its stiffness. The effective stress concept has been successfully used in the most damage mechanics models recently. The effective stress is the stress acting on the undamaged material. According to the continuum damage mechanics, the hypothesis of strain equivalence states that the strain associated with the Cauchy stress in the damaged state is equivalent to the strain associated with the effective stress in the undamaged state [47]. Therefore, the relationship of the Cauchy stress, that is the stress tensor associated with the damaged state, σ , and the effective stress tensor associated with the undamaged state, $\bar{\sigma}$, can be described by the following equation:

$$\sigma = M(d) \bar{\sigma} \quad (31)$$

where $M(d)$ is a fourth-order tensor which characterise the state of damage.

Accordingly, the constitutive relationships of undamaged and damaged states of timber, respectively, are given as

$$\bar{\sigma} = E \varepsilon_e \quad (32)$$

$$\sigma = E_d \varepsilon_e \quad (33)$$

where E_d is the damaged stiffness matrix.

In this study, anisotropic damage with non-uniform distribution of micro cracks and voids in all directions of the timber matrix is considered. To consider the anisotropic damage, three different damage factors must be introduced. The reduction of the elastic stiffness matrix is simulated here as a function of damage evolution in three orthogonal directions. Therefore, the damaged stiffness matrix with the damage factors can be written as [48]

$$E_d = \begin{bmatrix} (1-d_1)E_{11} & (1-d_1)(1-d_2)E_{12} & (1-d_1)(1-d_3)E_{13} & 0 & 0 & 0 \\ (1-d_1)(1-d_2)E_{12} & (1-d_2)E_{22} & (1-d_2)(1-d_3)E_{23} & 0 & 0 & 0 \\ (1-d_1)(1-d_3)E_{13} & (1-d_2)(1-d_3)E_{23} & (1-d_3)E_{33} & 0 & 0 & 0 \\ 0 & 0 & 0 & (1-d_1)(1-d_2)E_{44} & 0 & 0 \\ 0 & 0 & 0 & 0 & (1-d_1)(1-d_3)E_{55} & 0 \\ 0 & 0 & 0 & 0 & 0 & (1-d_2)(1-d_3)E_{66} \end{bmatrix} \quad (34)$$

where d_1 , d_2 and d_3 are the damage factors defined in the longitudinal, radial and tangential directions, respectively. The damage factor, d_i ($i=1,2,3$), increases from 0 to 1 as damage grows from threshold value to its ultimate value.

Since the timber has different damage evolution for tensile and compression failures, the damage models proposed by Wang et al. [49] are used to define the tensile and compression damage evolutions. In this study, different tensile damages in three orthogonal directions and compressive damage in only longitudinal direction were considered as shown in Eqs. (35) and (36).

$$d_{it} = 1 - \frac{1}{F_{it}} e^{\left((1-F_{it}) \frac{L_c \sigma_{it}^2}{E_i G_{it}^f} \right)} \quad (i = 1,2,3) \quad (35)$$

$$d_{1c} = 1 - \frac{1}{F_{1c}} (1 - A) - A e^{B(1-F_{1c})} \quad (36)$$

where d_{it} , and G_{it}^f are the tensile damage factor and fracture energy under tension in the i -th direction of the timber, respectively. d_{lc} is the compression damage factor in the longitudinal direction of the timber. L_c is the element characteristic length. F_{it} and F_{lc} are the variables defined in Eqs. (35) to (38). A and B are the material constants.

The stress-based continuum damage formulation with different failure criteria in tension and compression is used in this study. It means, damage starts to accumulate as soon as the stresses satisfy the failure criterion. The failure criterion proposed by Sandhaas and Van de Kuilen [34] is used in this study due to successful applications in combining ductile and brittle failures within on model, which is described as

$$\text{If } \sigma_1 < 0; \quad F_{1c} = \frac{-\sigma_1}{\sigma_{1c}} \leq 1 \quad (37)$$

$$\text{If } \sigma_1 > 0; \quad F_{1t} = \frac{\sigma_1}{\sigma_{1t}} \leq 1 \quad (38)$$

$$\text{If } \sigma_2 > 0; \quad F_{2t} = \left(\frac{\sigma_2}{\sigma_{2t}} \right)^2 + \left(\frac{\sigma_4}{\sigma_{12}} \right)^2 + \left(\frac{\sigma_6}{\sigma_{23}} \right)^2 \leq 1 \quad (39)$$

$$\text{If } \sigma_3 > 0; \quad F_{3t} = \left(\frac{\sigma_3}{\sigma_{3t}} \right)^2 + \left(\frac{\sigma_5}{\sigma_{13}} \right)^2 + \left(\frac{\sigma_6}{\sigma_{23}} \right)^2 \leq 1 \quad (40)$$

Damage models can encounter convergence problems in static analysis. In order to improve the convergence, viscous regularisation method [50,51] is used to define the model. In the viscous regularisation, the response of damaged material is evaluated using a viscous regularized damage variable d^v which is defined as

$$\dot{d}^v = \frac{1}{\eta} (d - d^v) \quad (41)$$

where η is the viscous parameter. A small value of the viscous parameter usually helps to improve the convergence rate of the model without significantly influencing the results. Thus, the value of viscous parameter is chosen to be equal to 0.0001, in this study.

By the introduction of Δt , that is the increment of time, into Eq. (41), the regularised damage variable at the $(n+1)^{\text{th}}$ load increment can be derived as

$$d_{n+1}^v = \frac{\eta}{\eta + \Delta t} d_n^v + \frac{\Delta t}{\eta + \Delta t} d_{n+1} \quad (42)$$

where d_n^v and d_{n+1}^v are the regularised damage variables of the n^{th} and $(n+1)^{\text{th}}$ steps, respectively. d_{n+1} is the non-regularised damage variable of the $(n+1)^{\text{th}}$ step.

2.4 Numerical integration

In the numerical algorithm, nonlinear plastic response of timber, as elastoplastic orthotropic material under three-dimensional (3D) stress state, is solved by the use of strain increment-based method. The numerical integration steps are presented in this section.

At the moment t_{n+1} , the state variables ε_n , ε_n^e , ε_n^p , $\Delta\varepsilon_{n+1}$, σ_n , $\sigma_{ek,n}$, and $d_{i,n}$ are known. The current value of the total strain ε_{n+1} can be expressed as

$$\varepsilon_{n+1} = \varepsilon_n + \Delta\varepsilon_{n+1} \quad (43)$$

The effective stress at the end of the load increment $n+1$, $\bar{\sigma}_{n+1}$, can be calculated as a summation of the effective stress at the beginning of the load increment $\bar{\sigma}_n$ and the stress increment $\Delta\bar{\sigma}_{n+1}$.

$$\bar{\sigma}_{n+1} = \bar{\sigma}_n + \Delta\bar{\sigma}_{n+1} \quad (44)$$

Substitution of Eq. (33) into Eq. (44) and rearranging gives

$$\bar{\sigma}_{n+1} = \bar{\sigma}_n + E \Delta\varepsilon_{n+1}^e \quad (45)$$

According to the theory of plasticity, for the finite load increment $n+1$, the increment of total strain $\Delta\varepsilon_{n+1}$ can be divided into an elastic component $\Delta\varepsilon_{n+1}^e$ and a plastic component $\Delta\varepsilon_{n+1}^p$.

$$\Delta\varepsilon_{n+1} = \Delta\varepsilon_{n+1}^e + \Delta\varepsilon_{n+1}^p \quad (46)$$

Therefore, subsequent substitution of Eq. (46) into Eq. (45) and rearranging gives

$$\bar{\sigma}_{n+1} = \bar{\sigma}_n + E (\Delta\varepsilon_{n+1} - \Delta\varepsilon_{n+1}^p) \quad (47)$$

In the developed algorithm, an elastic predictor step is carried out to predict the trial elastic stress $\bar{\sigma}_{n+1}^{trial}$ considering no plastic strain increment in the $n+1$ load increment as

$$\bar{\sigma}_{n+1}^{trial} = \bar{\sigma}_n + E \Delta\varepsilon_{n+1} \quad (48)$$

Then, by the substitution of Eq. (44) into Eq. (43), the plastic corrector of the effective stress in the $n+1$ load increment can be derived as

$$\bar{\sigma}_{n+1} = \bar{\sigma}_{n+1}^{trial} - E \Delta\varepsilon_{n+1}^p \quad (49)$$

The incremental plastic strain $\Delta\varepsilon_{n+1}^p$ can be written as the product of a plastic multiplier $\Delta\lambda$ and the derivative of $f(\bar{\sigma}, k)$ with respect to $\bar{\sigma}$.

$$\Delta\varepsilon_{n+1}^p = \Delta\lambda_{n+1} \left(\frac{\partial f}{\partial \bar{\sigma}} \right)_{n+1} \quad (50)$$

where

$$\left(\frac{\partial f}{\partial \bar{\sigma}} \right)_{n+1} = \begin{pmatrix} 2(\alpha_{13} + \alpha_{12})\sigma_1 - 2\alpha_{12}\sigma_2 - 2\alpha_{13}\sigma_3 + \alpha_{11} \\ -2\alpha_{12}\sigma_1 + 2(\alpha_{23} + \alpha_{12})\sigma_2 - 2\alpha_{23}\sigma_3 + \alpha_{22} \\ -2\alpha_{13}\sigma_1 - 2\alpha_{23}\sigma_2 + 2(\alpha_{13} + \alpha_{23})\sigma_3 + \alpha_{33} \\ 6\alpha_{44}\sigma_4 \\ 6\alpha_{55}\sigma_5 \\ 6\alpha_{66}\sigma_6 \end{pmatrix}_{n+1} \quad (51)$$

It can also be written as

$$\left(\frac{\partial f}{\partial \bar{\sigma}} \right)_{n+1} = P \bar{\sigma}_{n+1} + Q_{n+1} \quad (52)$$

Subsequent substitution of Eqs. (50) and (52) Eq. (49) and rearranging gives

$$\bar{\sigma}_{n+1} = \bar{\sigma}_{n+1}^{trial} - E \Delta\lambda_{n+1} (P \bar{\sigma}_{n+1} + Q_{n+1}) \quad (53)$$

According to Owen and Hinton [52], the incremental equivalent plastic strain $\Delta\bar{\varepsilon}^p$ can be defined as,

$$\Delta\bar{\varepsilon}^p = \sqrt{\frac{2}{3} (\Delta\varepsilon^p)^T Z \Delta\varepsilon^p} \quad (54)$$

with

$$Z = \begin{bmatrix} 1 & 0 & 0 & 0 & 0 & 0 \\ 0 & 1 & 0 & 0 & 0 & 0 \\ 0 & 0 & 1 & 0 & 0 & 0 \\ 0 & 0 & 0 & 0.5 & 0 & 0 \\ 0 & 0 & 0 & 0 & 0.5 & 0 \\ 0 & 0 & 0 & 0 & 0 & 0.5 \end{bmatrix} \quad (55)$$

Now Eq. (54) can be rewritten with the aid of Eqs. (50) and (52) as follows:

$$\Delta\bar{\varepsilon}^p_{n+1} = \Delta\lambda_{n+1} \sqrt{\frac{2}{3} \left(\frac{\partial f}{\partial \bar{\sigma}} \right)_{n+1}^T Z \left(\frac{\partial f}{\partial \bar{\sigma}} \right)_{n+1}} \quad (56)$$

$$\Delta\bar{\varepsilon}^p_{n+1} = \Delta\lambda_{n+1} \sqrt{\frac{2}{3} (P \bar{\sigma}_{n+1} + Q_{n+1})^T Z (P \bar{\sigma}_{n+1} + Q_{n+1})} \quad (57)$$

$$\bar{\varepsilon}^p_{n+1} = \bar{\varepsilon}^p_n + \Delta\lambda_{n+1} \sqrt{\frac{2}{3} (P \bar{\sigma}_{n+1} + Q_{n+1})^T Z (P \bar{\sigma}_{n+1} + Q_{n+1})} \quad (58)$$

where $\bar{\varepsilon}^p_n$ and $\bar{\varepsilon}^p_{n+1}$ are the equivalent plastic strain at the beginning and at the end of the load step increment, respectively.

According to the Eqs. (53) and (58), the updated effective stress $\bar{\sigma}_{n+1}$ and equivalent plastic strain $\bar{\varepsilon}^p_{n+1}$ are a function of $\Delta\lambda$. The Newton-Raphson method is used to obtain the unknown parameter $\Delta\lambda_{n+1}$. At the end of $n+1$ load increment, the updated stresses and effective accumulated plastic strain must also satisfy the yield criterion condition. Then, Eq. (25) gives:

$$f_{n+1} = \frac{1}{2} \bar{\sigma}_{n+1}^T P \bar{\sigma}_{n+1} + \bar{\sigma}_{n+1}^T Q_{n+1} - (\sigma_{ek}^2)_{n+1} = 0 \quad (59)$$

In the Newton-Raphson method, if $\Delta\lambda$ has approximate expression $f(\Delta\lambda) = 0$ is not true, there are residual values. In fact, in specific calculations, when $f(\Delta\lambda) \neq 0$, but extremely small (less than 10^{-9}), then it is considered that f is close to the true value and the iteration is stopped. In this method, the k^{th} iteration of the $\Delta\lambda$ is obtained as,

$$\Delta\lambda^k = \Delta\lambda^{k-1} + \delta\Delta\lambda^k \quad (60)$$

If the k^{th} iteration is a true solution, it can be expanded according to the Taylor series as,

$$f(\Delta\lambda)^k = f(\Delta\lambda)^{k-1} + \left(\frac{df(\Delta\lambda)}{d\Delta\lambda} \right)^{k-1} \delta\Delta\lambda^k = 0 \quad (61)$$

Then,

$$\delta\Delta\lambda^k = \frac{-f(\Delta\lambda)^{k-1}}{\left(\frac{df(\Delta\lambda)}{d\Delta\lambda} \right)^{k-1}} \quad (62)$$

The derivative of f is given by

$$\frac{df(\Delta\lambda)}{d\Delta\lambda} = (P\bar{\sigma} + Q) \frac{d\bar{\sigma}}{d\Delta\lambda} - 2\sigma_e \frac{d\bar{\sigma}}{d\bar{\epsilon}^p} \frac{d\bar{\epsilon}^p}{d\Delta\lambda} \quad (63)$$

When $\Delta\lambda$ is computed, the new stress $\bar{\sigma}_{n+1}$ and equivalent plastic strain $\bar{\epsilon}_{n+1}^p$ can be computed using Eqs. (53) and (58), respectively. Subsequently, plastic strain ϵ_{n+1}^p and elastic strain ϵ_{n+1}^e will be updated. Then, the damage factors and damaged stiffness matrix are computed using Eqs. (34) to (36). Accordingly, the final stress σ_{n+1} at the end of load increment $n+1$ can be updated using Eq. (33).

3. UMAT implementation in Abaqus

Today vast number of Finite Element (FE) codes are available that are capable of analyzing challenging engineering problems. Among many finite element analysis software, researchers

are keen to use Abaqus because it provides users with powerful, easy-to-use secondary development tools and interfaces, allowing users to easily carry out FE modelling, analysis and post-processing to meet the needs of specific engineering problems. Through the user material subroutine interface, the user can define any supplementary material model.

This research work aims to develop a user subroutine for the timber material model. As described in the previous chapter, the constitutive relationship adopted in this paper is the isotropic hardening elastoplastic model coupled with the Hoffman yield criterion and anisotropic damage. The implicit integration algorithm formulas for calculating the problem are derived from the Newton-Raphson method. The Abaqus/Standard FE software was used to conduct numerical simulations via a Fortran UMAT user subroutine. The flow diagram of the developed timber material subroutine is shown in Figure 1.

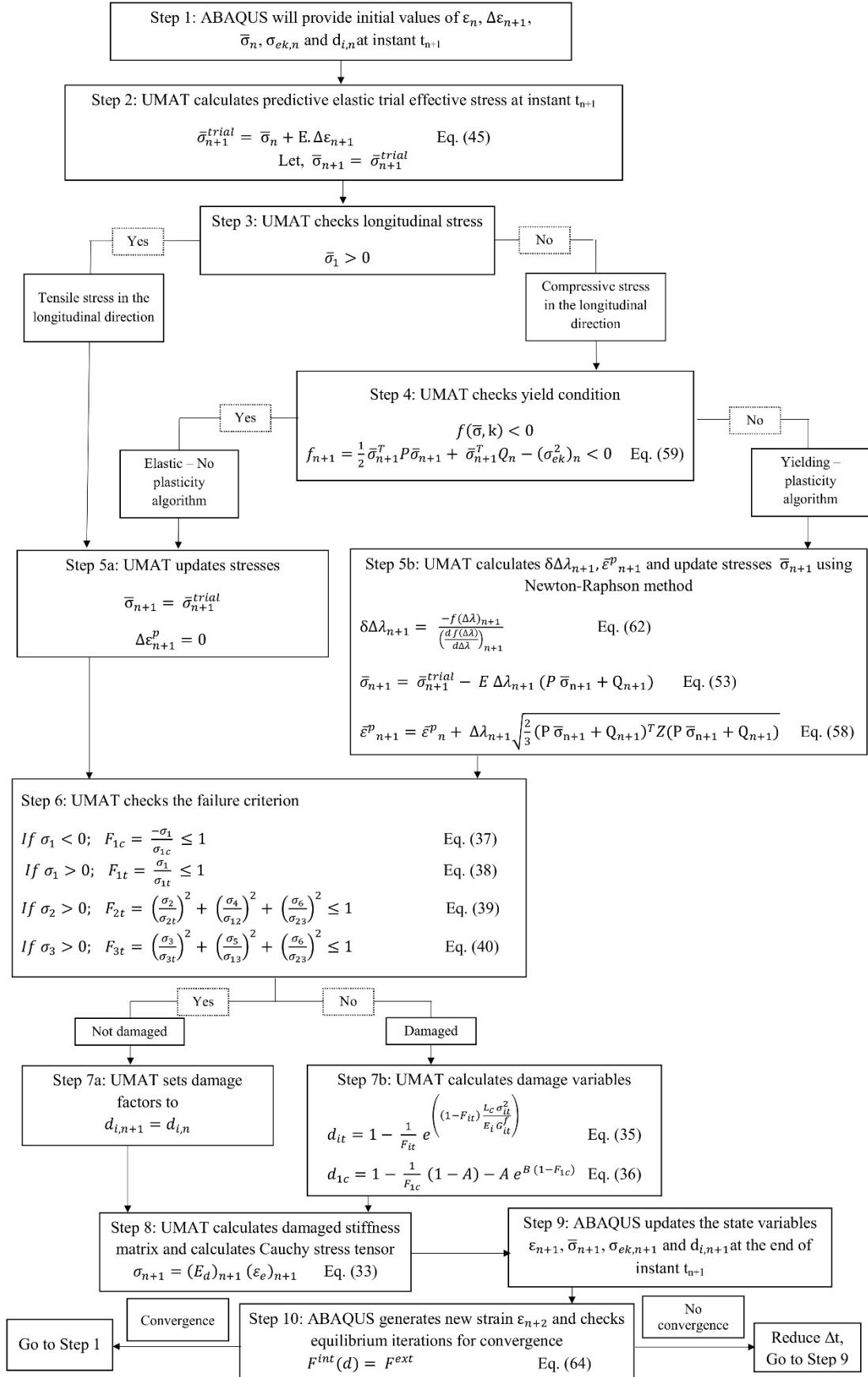


Figure 1. Flow chart for analysis of timber material in UMAT.

To implement the previously described material law a user-defined material model (UMAT) was implemented as a subroutine in Abaqus. Regarding the writing format of UMAT, the variables commonly used in UMAT are defined at the beginning of the file. As described in the previous chapter, in addition to the typical nine orthotropic elasticity parameters, the proposed material model requires three compressive strengths, three tensile strengths and three shear strengths parameters as well as two strain hardening parameters, which leads to a total of twenty input parameters.

In the code, for a given strain increment $\Delta\epsilon_{n+1}$ (DSTRAN), the results of the previous time step t_n , that is stress σ_n and strain ϵ_n , are used to calculate and update the Jacobian matrix (DDSDDE), stress tensor (STRESS) and solution-dependent state variables (STATEV) at the current time step t_{n+1} . First, the trial stress is calculated using the elastic stiffness matrix. Then, if the longitudinal stress is compressive, it is evaluated in order to determine if there is strain-hardening or not. In the next step, the compression stress is evaluated into the flow criterion is derived from Hoffman yield function coupled with the strain hardening is described by the effective plastic strain to transfer the yield surface. In the case of plasticity, the value of plastic multiplier $\Delta\lambda_{n+1}$ and the equivalent plastic strain $\bar{\epsilon}_{n+1}^p$ are obtained by solving the equations above according to the Newton-Raphson method. In the next step, the effective stress tensor and the stiffness matrix are updated. In the case of no plasticity, the effective stress tensor is updated with the trial stress. Then, the conditions of the failure criterion is evaluated and the damage variables are calculated. Following, the effective stress tensor and the Jacobian matrix are updated. At the end of UMAT, the updated value of the variable will be returned to the Abaqus solver through the interface and convergence conditions must be satisfied.

In Abaqus implicit analysis, the displacement of the node (and thus the strain) is calculated, so that the balance of internal force and external force is as follows:

$$F^{int}(d) = F^{ext} \quad (64)$$

where d is the vector of displacement of nodes, and F^{int} and F^{ext} are the internal force vector and external force vector, respectively. Except for small deformation and linear elasticity problems, Eq. (64) is non-functional, and an iterative method should be used to solve the discretized equilibrium equation for the FE model as follows:

$$F_{n+1}^{ext} - F^{int}(d_{n+1}^i) = K_T \Delta d \quad (65)$$

$$d_{n+1}^{i+1} = d_{n+1}^i + \Delta d \quad (66)$$

where K_T is the global tangent stiffness matrix, i represents the i^{th} iteration within an incremental step, and n represents the n^{th} incremental step.

Iterations are repeated in each time increment until convergence is achieved. To converge quickly, the displacement increment should change along the direction of the gradient. No matter how fast the convergence is, the Eq. (64) for force equilibrium which is attained at every node, is the only criterion for judging the accuracy of the results.

4. Results and Discussion

In this section, the performance and accuracy of the developed model are verified against an experimental test and some examples obtained by other researchers. A timber specimen under 4-point bending is simulated in the first simulation to validate the timber model introduced in this paper in predicting the flexural behavior of timber. Compressive tests for parallel to grain and perpendicular to grain which are conducted by Kargiannis et al. [53] and Oudejene and Khelifa [24] are simulated in the second example to validate the proposed material model in compression. In the third example, the tensile test results presented in ref. [37] are used to validate the timber model in tension.

4.1 Example 1: Compression test

Several authors have described that timber depicts a compressive failure with softening parallel to grain while the loading in the perpendicular direction to the grain exhibits a plateau region due to the plastic yielding and the damage evolution, after the linear elastic response [3,24,28,53,54]. Hence, in this example, the developed material model for timber is examined for the compression and verified against the available test data in refs. [24,53]. The compressive strength of a material is the capacity of a material to withstand loads tending to reduce size. The compressive strengths of the timber vary along the grain and against the grain. Thus, the compression behavior of timber with loads acting parallel and perpendicular to the grain are studied in this example. Karagiannis et al. [53] conducted a series of compression and shear load tests using Scandinavian spruce specimens with a mean density of 430 kg/m^3 and a moisture content of approximately 10%, according to European standards EN408. In order to validate the developed material model under uniaxial compressive loadings, compressive test results from Karagiannis et al. [53] was chosen in this study. For the compression tests, they have used a total of eight wood cubes of $45 \text{ mm} \times 45 \text{ mm} \times 45 \text{ mm}$ and nine wood cuboids of $45 \text{ mm} \times 70 \text{ mm} \times 90 \text{ mm}$ under compression parallel and perpendicular to the grain direction, respectively. The axial load was incrementally increased at a rate of 1 mm/min . Figure 2 shows the obtained curves of the stress versus the strain for the compressions tests [53].

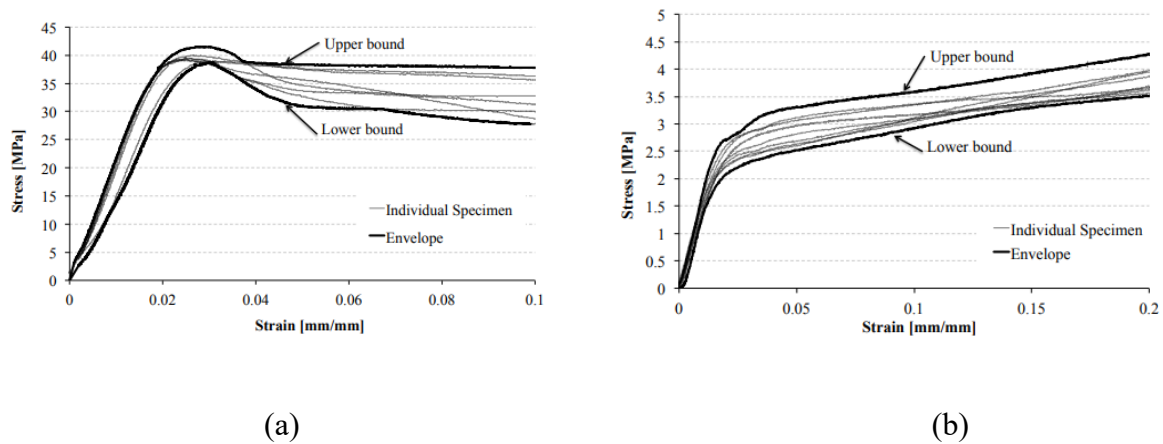


Figure 2. Stress-strain relationships from compression tests (a) parallel (b) perpendicular to the grain [53].

Figure 3 shows the FE models used for the numerical simulations to adequately reproduce the uniaxial compression tests carried out on these real specimens of Karagiannis et al. [53]. Eight-node 3D elements (C3D8R) were used to discretize the timber cube and cuboid. The bottom of the wood specimens was assumed to be fixed in all directions. The simulations were carried out by applying a downward load acting on the top surface of the specimens. The material properties adopted for wood are listed in Table 1.

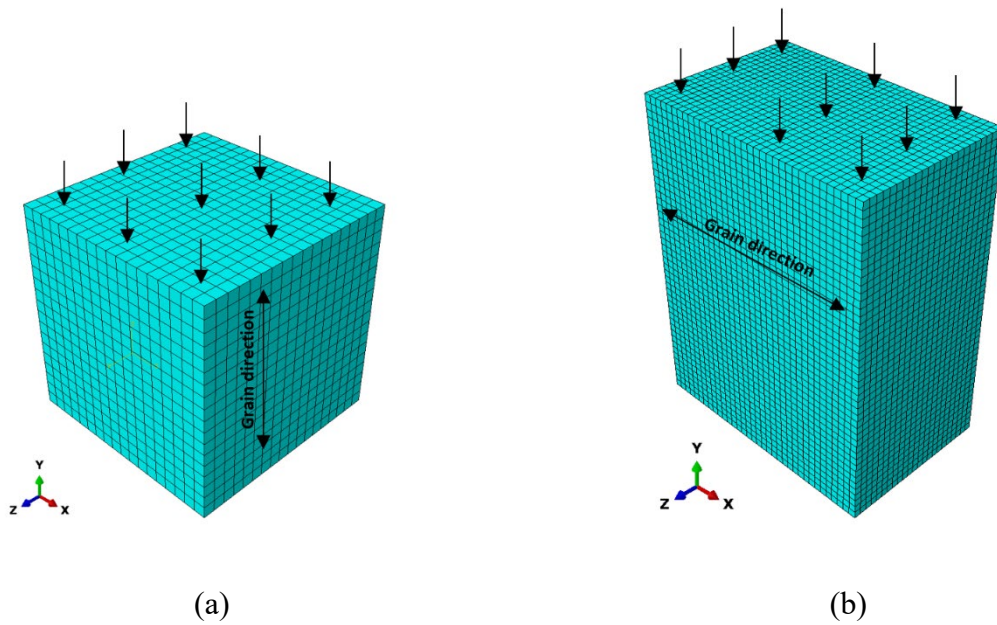


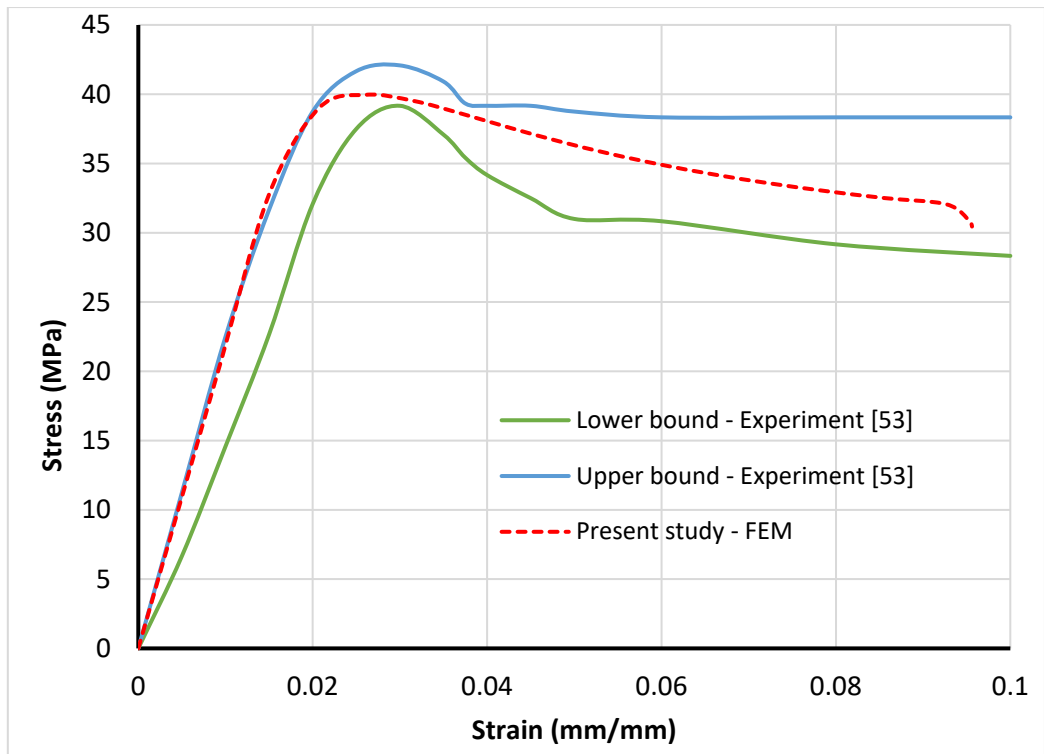
Figure 3. FE models for uniaxial compression tests (a) parallel (b) perpendicular to the grain.

Table 1. Material properties of wood for FE modelling of compression tests.

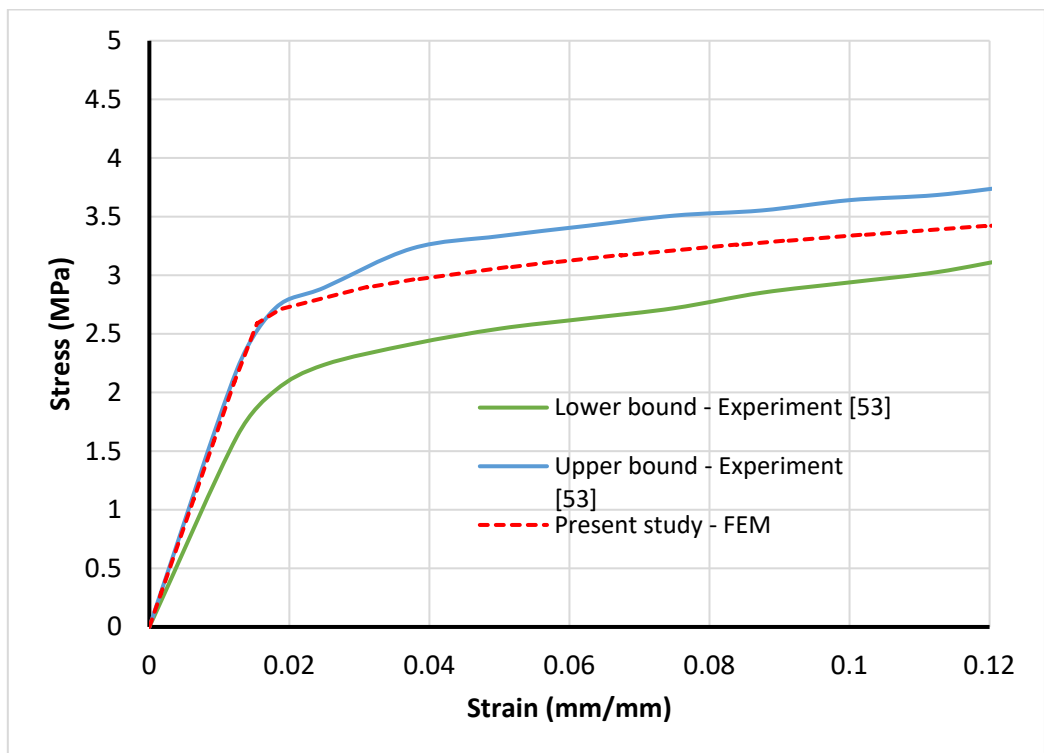
Elasticity parameters					
E_1 (MPa)	$E_2 = E_3$ (MPa)	G_{23} (MPa)	$G_{12} = G_{13}$ (MPa)	ν_{23}	$\nu_{12} = \nu_{13}$
2050.8	172.1	68	145.2	0.5	0.45
Strength components					
σ_{1c} (MPa)	$\sigma_{2c} = \sigma_{3c}$ (MPa)	σ_{1t} (MPa)	$\sigma_{2t} = \sigma_{3t}$ (MPa)	σ_{23} (MPa)	$\sigma_{12} = \sigma_{13}$ (MPa)
35	2.5	20	0.7	0.5	5
Hardening parameters					
h (MPa)					
1200					
Fracture energies					
$G_{1t,f}$ (N/mm)	$G_{2t,f}$ (N/mm)	$G_{3t,f}$ (N/mm)			
60	0.5	0.5			

The stress-strain curves obtained from the numerical analyses are selected to compare the numerical results with the experimental results. Figure 4(a) illustrates the obtained stress-strain curve from the numerical analysis until the failure under loading parallel to the grain. It can be seen that under compression parallel to the grain, the timber cube shows an almost linear elastic behavior until the compression strength of timber, and then shows a plastic behavior as observed by Karagiannis et al. [53]. As the predicted stress-strain curve ranges between the upper and lower bound of the experimental results, it can be stated that the FE model predicts the stress-strain curve with good agreement compared to experimental results [53].

The results obtained under loading perpendicular to the grain are shown in Figure 4(b). It is also observed that the predicted stress-strain curve has a good correlation with the experimental curve as again the numerical results range between the upper and lower bound of the experimental results. Although the results of the experiment varies, the trends of the graphs are similar. Timber shows a linear elastic behavior and plastic hardening under the compression perpendicular to the grain. A good level of agreement between the numerically predicted stress-strain curve and their corresponding experimental results under both compression tests, the tests parallel and perpendicular to the grain, demonstrate that the proposed material model adequately simulates the non-linear response of the timber element in compression.



(a)



(b)

Figure 4. Stress versus strain curves for uniaxial compression tests (a) parallel (b) perpendicular to the grain.

4.2 Example 2: Tensile test

In this part, the developed material model for timber is validated under tensile stress in comparison to the available experimental data [37] found in literature. Khennane et al. [37] developed a numerical model for the failure of timber under bending and tension parallel to the grain direction and compared the result of the material model to experimental results. In this example, the results of uniaxial tensile modelling is compared to the results from Khennane et al. [37].

Khennane et al. [37] conducted the tensile tests using 40mm long x 10mm wide x 2mm thick pine wood specimen with the density of 460 kg/m³. The tensile test parallel to the gain direction was carried out and the axial load was incrementally increased at a rate of 1 mm/min. A rectangular cuboid timber specimen with the dimensions of 40 mm x 10 mm x 2 mm was modeled with the material model developed in this study under the uniaxial tensile test as depicted in Figure 5. Since strain hardening is not considered for timber under tension, the hardening modulus is not important for the analysis. The same modelling procedure that has been used in two previous examples is used here as well. The properties of the timber that were used as the inputs of the UMAT are shown in Table 2. The specimen was meshed using the C3D8R element available in Abaqus/Standard library. Fixed boundary conditions were applied at the two ends of the specimen and the loading was implemented by displacement in the Y-direction parallel to the grain.

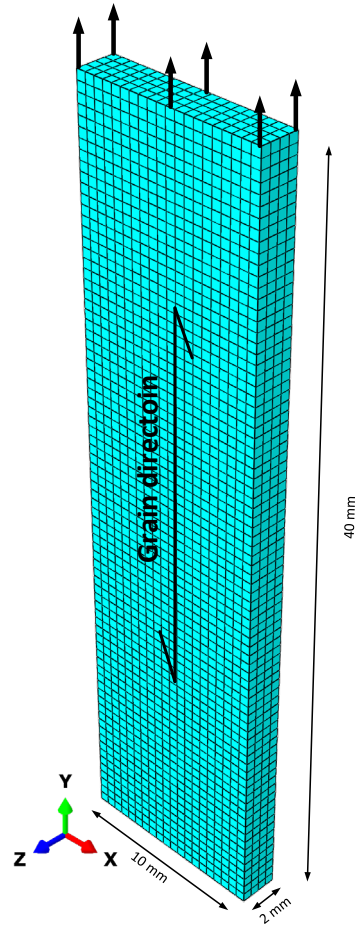


Figure 5. FE model for uniaxial tensile test.

Table 2. Material properties of timber for FE modelling.

Elasticity parameters					
E ₁ (MPa)	E ₂ = E ₃ (MPa)	G ₂₃ (MPa)	G ₁₂ = G ₁₃ (MPa)	ν ₂₃	ν ₁₂ = ν ₁₃
13010	870	340	980	0.02	0.29
Strength components					
σ _{1c} (MPa)	σ _{2c} = σ _{3c} (MPa)	σ _{1t} (MPa)	σ _{2t} = σ _{3t} (MPa)	σ ₂₃ (MPa)	σ ₁₂ = σ ₁₃ (MPa)
50	4.5	43.1	0.7	0.5	6.9
Fracture energies					
G _{1t,f} (N/mm)	G _{2t,f} (N/mm)	G _{3t,f} (N/mm)			
5	0.7	0.7			

The FE model mesh size influences significantly on the behavior of the model when the material exhibits softening. This is due to the energy dissipation decreases with the mesh

refinement. Therefore, a mesh sensitivity study was carried out with 780, 1560, 1950, 2340, 2730, 3120, 3510 and 6240 elements. The load-displacement curves of the numerical results for each case are shown in Figure 6. It is evident that the softening stage of material is strongly dependent on the mesh size. However, it is also clear that the models with finer meshes have considerably similar softening behaviour of the material.

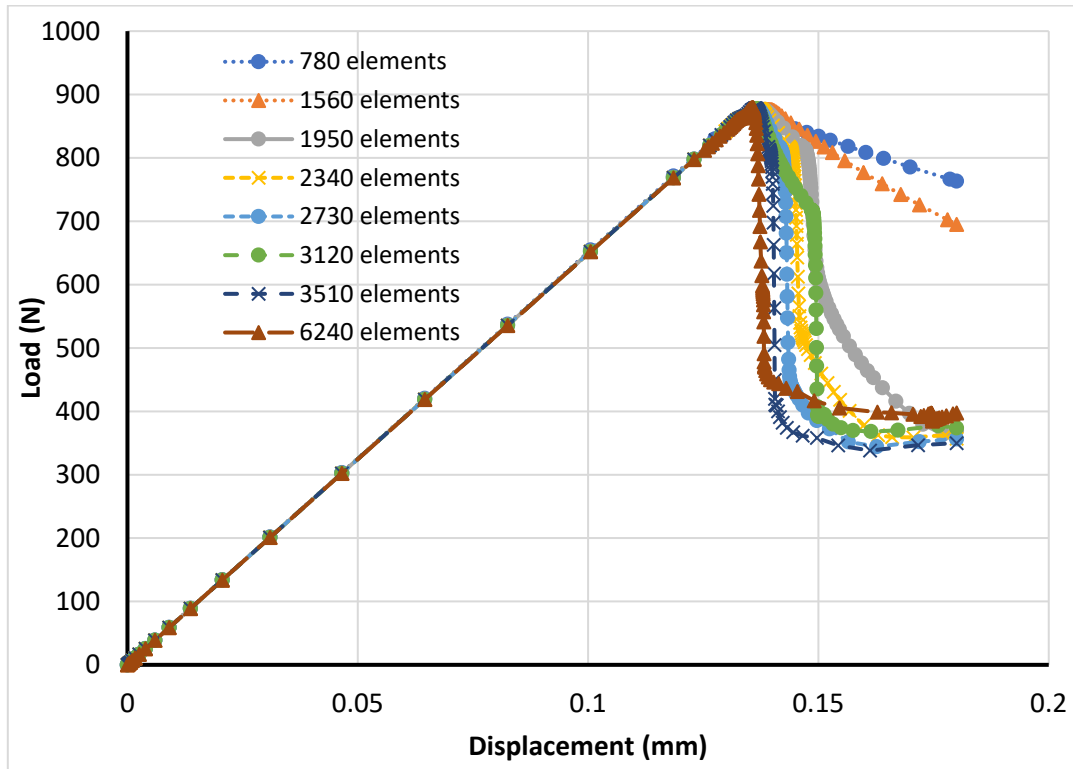


Figure 6. Load-displacement from numerical study with different mesh sizes.

To validate the model, the load-displacement diagram of the numerical and the experimental results are compared in Figure 7. The results from the load-displacement curve of the FE model show satisfactory compatibility with the experimental results from Khennane et al. [37]. It can be seen that the specimen starts to deform linearly before reaching the yield strength and the model accurately predicts the brittle failure of timber specimen under tension. Even though the failure strain was underestimated, the model predicts the characteristic tensile strength of timber and failure mode precisely. As mentioned above, the differences in results are caused

by the differences in actual timber specimens and material properties used in the numerical model.

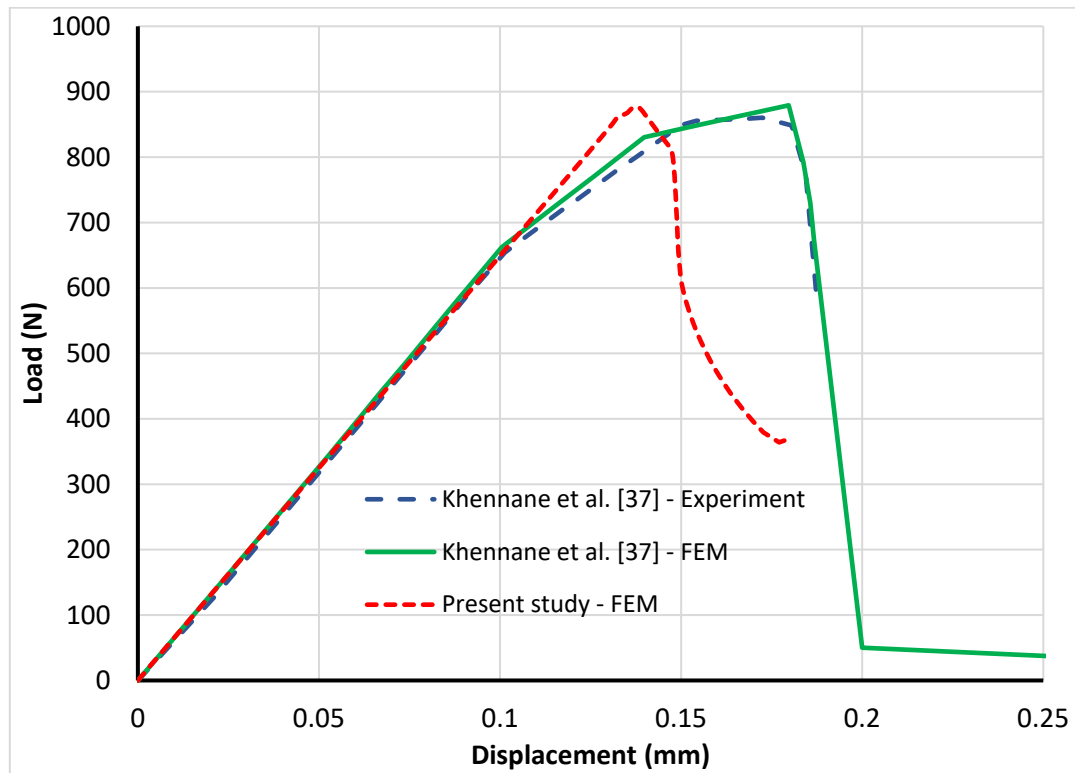


Figure 7. Load-displacement curves of timber under uniaxial tension force.

4.3 Example 3: Bending test

In this section, to validate the constitutive timber model under bending two models have been developed. In both models, timber is modelled as elastoplastic orthotropic material according to Hoffman yield criterion coupled with isotropic hardening. However, the anisotropic damage evolution combined with the failure criterion is not used in first model (Model 1). In second model (Model 2), the damage evolution combined with the failure criterion proposed by Sandhaas and Van de Kuilen [34], discussed in Section 2.3, is associated with Hoffmann yield criterion is adopted to model the timber.

To validate the model, the experimental test program carried out by the authors at the laboratory of Solid Structures of the University of Luxembourg is used. Three timber boards manufactured

from KVH-Si timber material of strength class C24 were tested under four-point bending tests. The specimens of length 1 m had a cross section of 30 mm x 170 mm. All the timber boards were simply supported over 0.8 m span and they were subjected to two-point loading through two 30 mm diameter steel rods which were positioned at a distance of 0.37 m from the ends of the timber board, as shown in Figure 8. The loads were applied at a loading rate of 0.1 kN/s. During the experiment, mid-span deflection of the timber board was measured a LVDT (Linear Variable Displacement Transducer) mounted on the top face of the specimen.

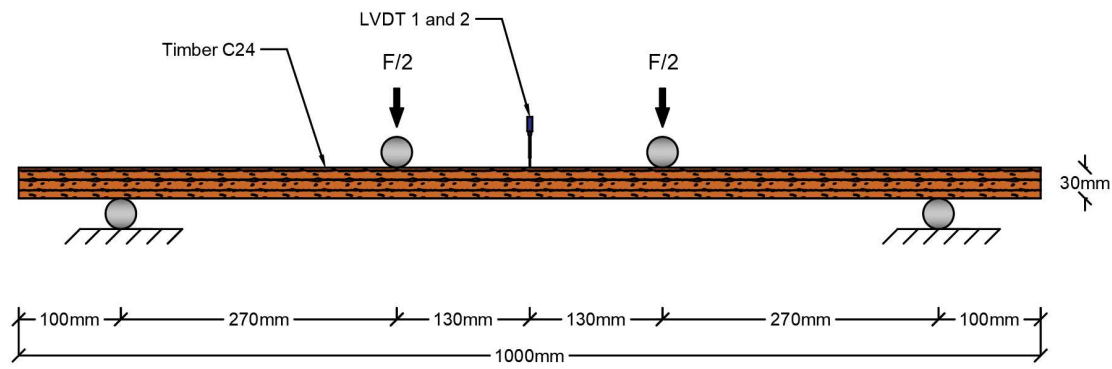


Figure 8. Experimental Setup.

The mid-span deformation of the timber specimens versus the load is shown in Figure 9. It was observed that all the specimens presented a brittle failure at mid-span and that the ultimate load resisting capacity is in the range of 8.2-12.1 kN. Such variations are apparent since the timber products are heterogeneous and some natural growth variations and defects exist in the specimens.

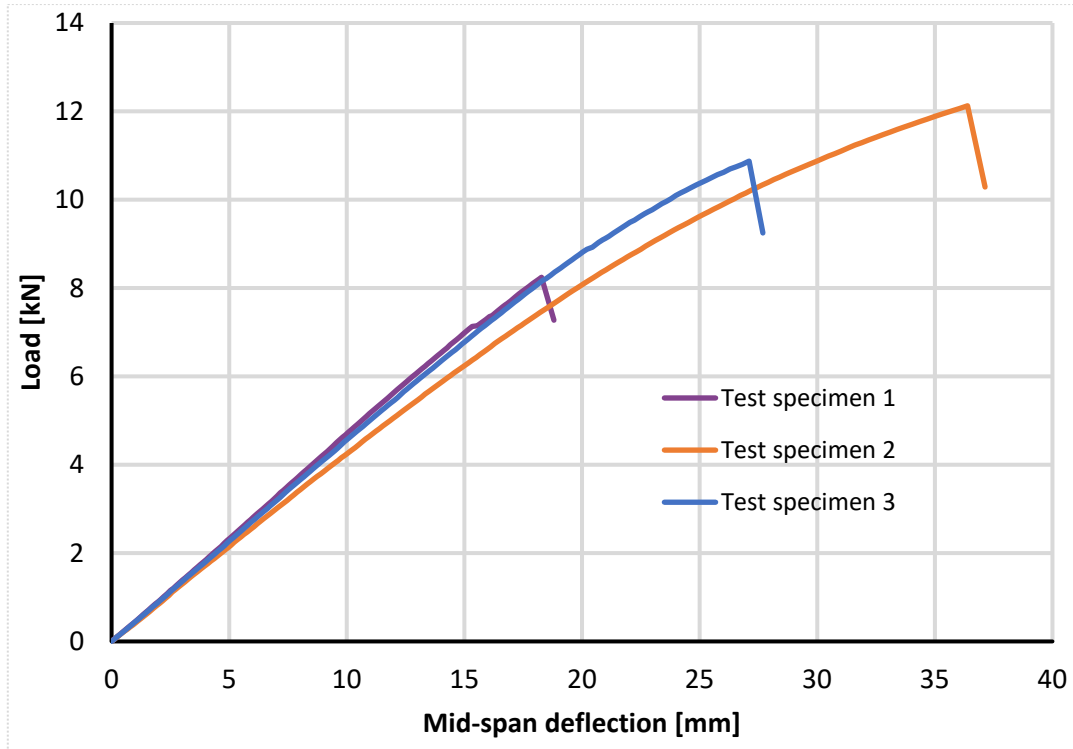


Figure 9. Load-deformation curves of the test specimens.

The software package Abaqus was used to develop the finite element (FE) models for the timber boards. Figure 10 shows a schematic view of the FE model utilized in the study. Taking advantage of symmetry, only a quarter of the specimen was modelled with the material properties of C24 timber material [34] given in Table 3. The FE model consists of a three-dimensional timber specimen as well as one cylindrical support and one cylindrical loading rod, which are modelled as analytical rigid surfaces. The timber specimen has the same dimensions as those used in the experimental tests.

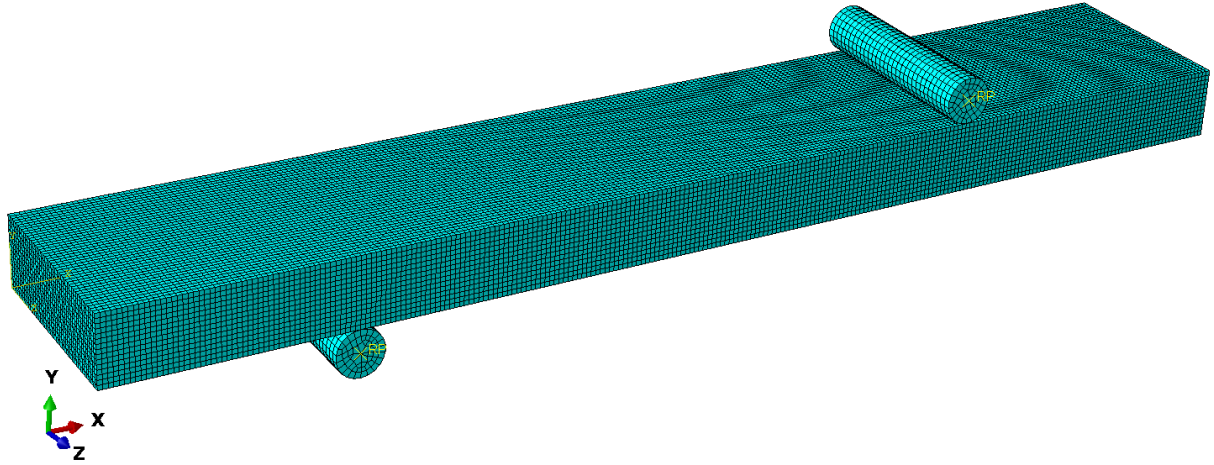


Figure 10. Quarter of FE model of a four-point bending test.

Table 3. Material properties of timber for FE modelling.

Elasticity parameters					
E_1 (MPa)	$E_2 = E_3$ (MPa)	G_{23} (MPa)	$G_{12} = G_{13}$ (MPa)	ν_{23}	$\nu_{12} = \nu_{13}$
11000	370	60	690	0.5	0.45
Strength components					
σ_{1c} (MPa)	$\sigma_{2c} = \sigma_{3c}$ (MPa)	σ_{1t} (MPa)	$\sigma_{2t} = \sigma_{3t}$ (MPa)	σ_{23} (MPa)	$\sigma_{12} = \sigma_{13}$ (MPa)
36	4.6	24	0.7	0.5	6.9
Hardening parameters					
h (MPa)					
6436					
Fracture energies					
$G_{1t,f}$ (N/mm)	$G_{2t,f}$ (N/mm)	$G_{3t,f}$ (N/mm)			
6	0.5	0.5			

Linear hexahedral elements (C3D8R) of Abaqus with reduced integration were employed to discretize the timber board and the average mesh size was first set to 15 mm. The boundary conditions were modelled using the cylindrical support constrained in all degrees of freedom. The loads were applied as a constant displacement in the vertical direction using the cylindrical rigid body acting on the timber board. The contact between the timber specimen and the cylindrical rigid bodies was defined in both normal and transverse directions with the

consideration of Pressure-overclosure “Hard” contact, and the static coefficient of friction equaled to 0.4, respectively. In addition, a relevant symmetric boundary condition was assigned at the symmetric plane.

In Model 1, mesh sensitivity was considered with a convergence study. Since the thickness of the timber element is significantly smaller than its length and width, the thickness was assigned with a minimum number of four elements. Thus, in a first approach, a model with a mesh size of 15 mm was analyzed leading to at least four elements over the thickness of the timber board. Then, the mesh size was subsequently reduced to 2 mm in five different scenarios.

To find a proper mesh size configuration, the results were compared by comparing the deflection accuracy and computing time. Figure 11 plots the mid-span deflection of the timber board for various mesh sizes. It can be seen that the mesh size affects the analysis to approach the solution that governs the exact response. It can be seen that the coarse mesh gives less accurate deflections at the mid-span of the timber board. However, the fine meshes (2, 3 and 5 mm mesh size) show a very similar pattern for the load-deflection curve and little change in the solution. Thus, 5mm mesh size is assumed to have converged.

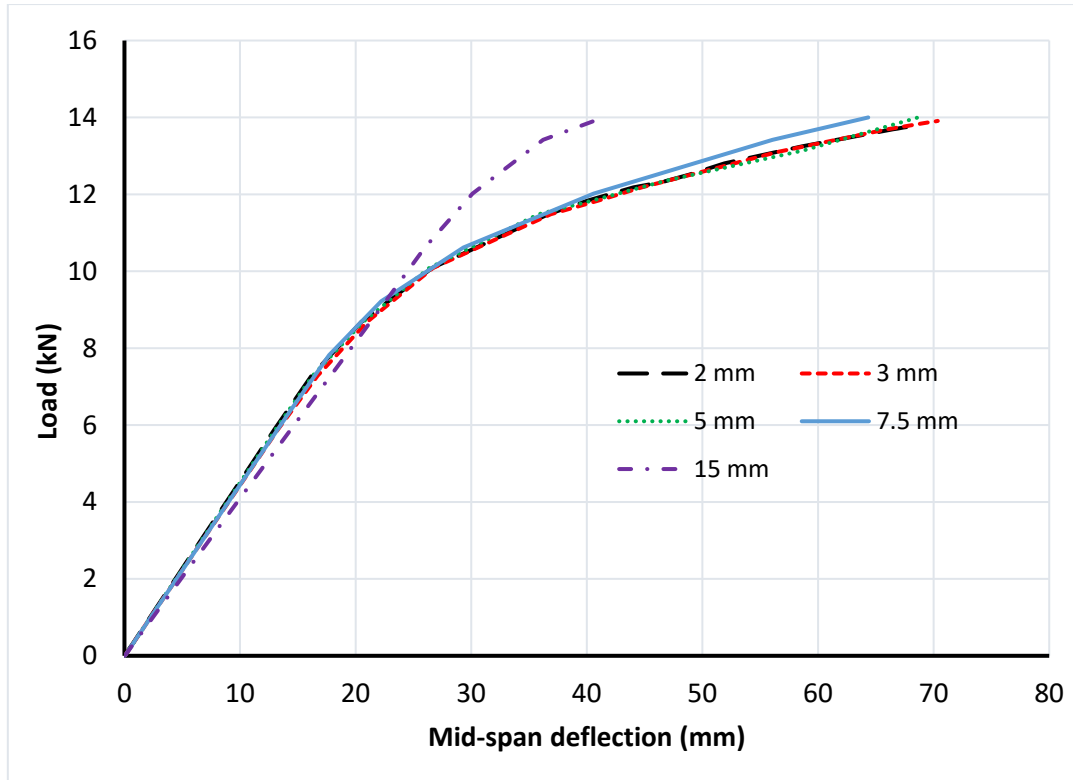


Figure 11. Load vs mid-span deflection for various meshing size.

The computing time and the number of finite elements of each mesh scenario are shown in Figure 12. When the meshing size decreases, the number of element in the model increases. As a result of decreasing meshing size, the solution procedure uses an excessive number of increments and iteration, and hence the computing time also increases. As a summary of the convergence study, the 5 mm mesh size is almost accurate as of the 2 mm and reduces the computation time by almost 88 percent.

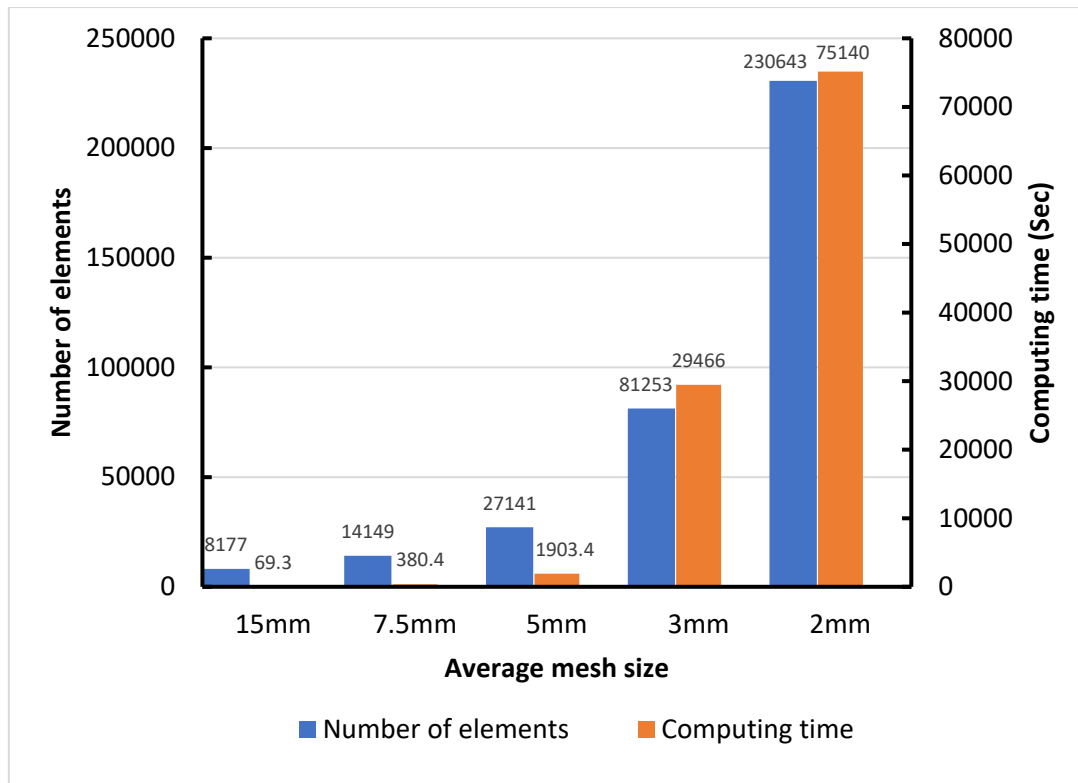


Figure 12. Computing time vs number of elements for various mesh size.

The load-displacement curves obtained from the numerical analysis is illustrated in Figure 13 and compared with the experimental test results. The stiffness of the FE model is in line with the experimental results in the elastic zone. Overall, a reasonably good correlation between the numerical and experimental results is observable. In Model 1, timber depicts a plateau region due to the plastic yielding, and it grows continuously because of no failure criterion is introduced. It can be seen that the predicted response of Model 2 is in good agreement with the experiment because local failure of timber specimen is defined. Therefore, it demonstrates that the proposed material model adequately simulates the non-linear response of the timber element in bending.

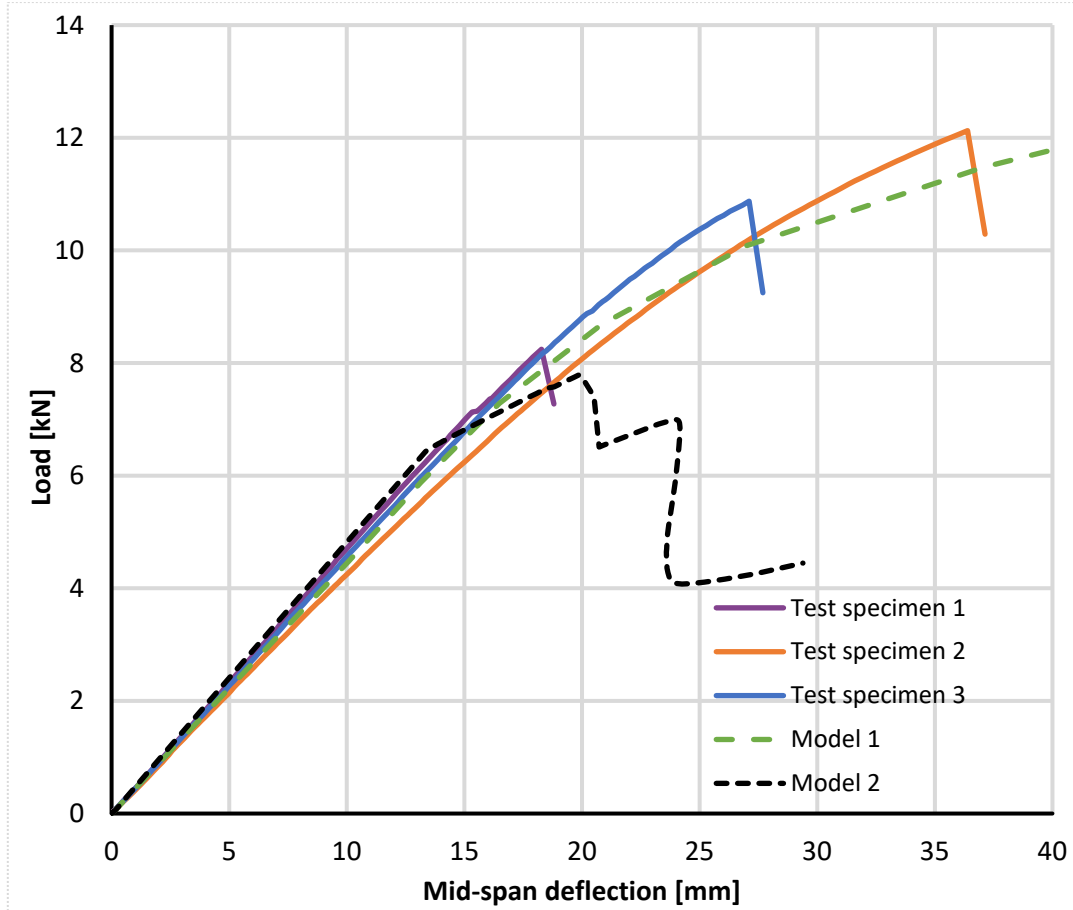


Figure 13. Comparison between experimental and numerical load-deflection responses.

Figure 14 shows the maximum principal stress distribution of the timber specimen in Model 1. It can be seen that the highest stress values are at mid-span which are almost equal to the defined strength of the timber. Therefore, it is clear that the failure in the FE model occurs at mid-span and starts about the same load as in the test results.

Figure 15 shows the damage evolution in the timber in Model 2. It is clearly seen that first damage occurs in the vicinity of the loading rod. The damaged zone increases with the load increases. Subsequently, the failure occurs at mid-span deflection of 20.2 mm due the fact that damage is highly localized in the vicinity to the loading rod. The predicted failure of the model is in good agreement with the observed rupture in the experiment as shown in Figure 16. Hence, Model 2 can accurately predict the localized damage in the timber element.

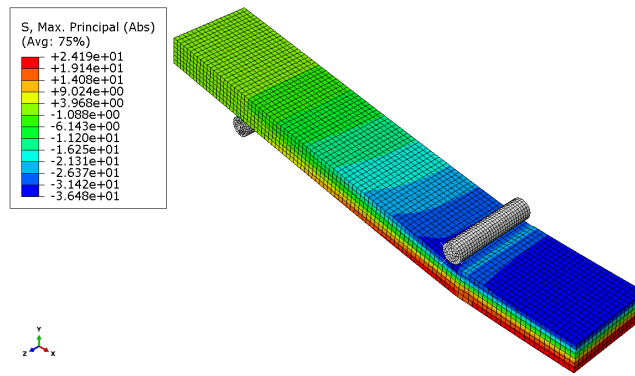


Figure 14. Stress distribution of timber model at failure load (values in MPa).

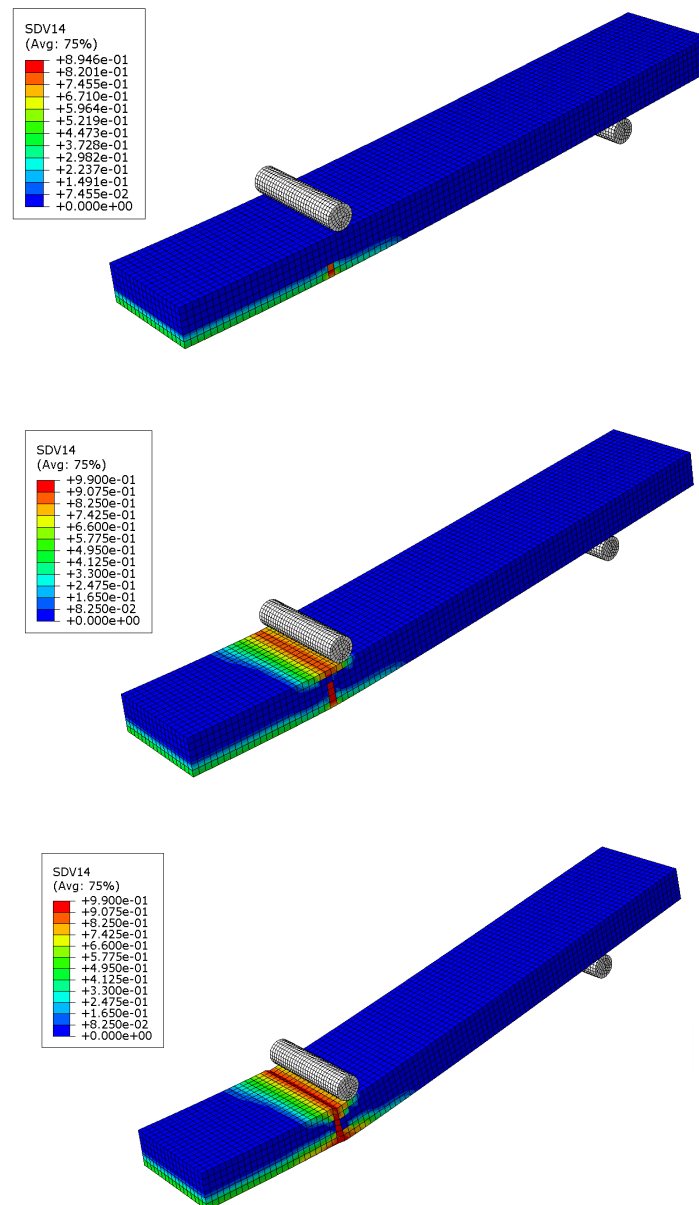


Figure 15. Damage evolution in the timber model.

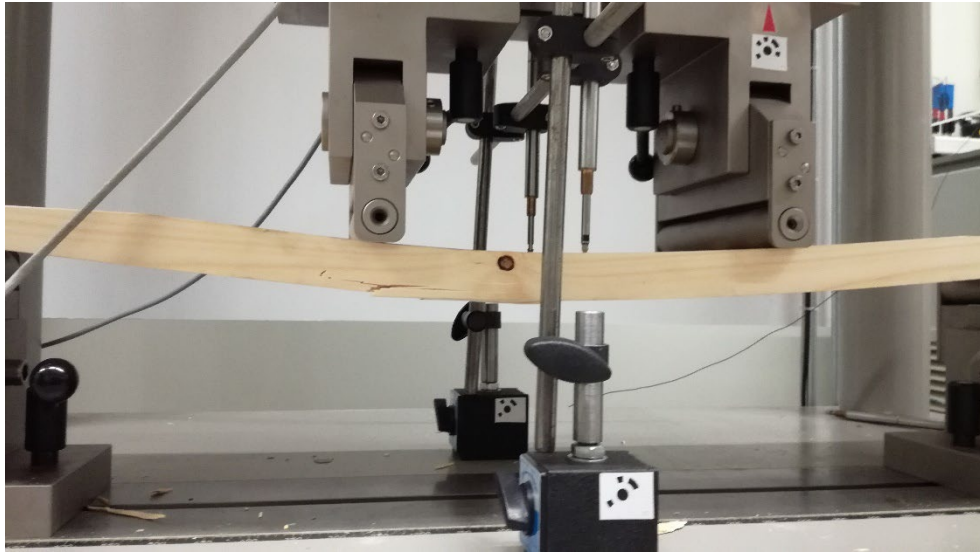


Figure 16. Failure in timber specimen obtained in bending test experiment.

5. Conclusions

Timber is a heterogeneous and orthotropic material. In structural engineering applications, the nonlinear response of timber is typically predicted by phenomenological models and 2D analysis. In this study, a new 3D constitutive model was developed to model nonlinear mechanical response of timber, as elastoplastic orthotropic material. Since there are only a few 3D FE models representing timber behavior available in the literature, the proposed model makes an important addition to the structural timber engineering.

An isotropic hardening elastoplastic model that is combined with Hoffman yield criterion, which defines the anisotropic yield of materials, and combined with anisotropic damage effect in failure criterion was developed and implemented as a user material subroutine UMAT in Abaqus FE code. The strain hardening of the timber was introduced into the Hoffman criterion using the strength of the material is a function of the equivalent plastic strain. An associated flow rule model based on Hoffman yield criterion and plastic potential was used for the development of the plasticity when the timber under compression. A stress-based continuum damage formulation with four independent failure criteria in tension and compression was used

to distinguish the timber response under tension and compression. Three tensile damages in the grain longitudinal, radial and tangential directions was established using the damage factors and fracture energies. Abaqus provides the development function for users to develop their own material model to complete various material analyses. The FORTRAN syntax was used to program the UMAT which includes the integration procedures using vector formed state variables. The algorithm formulas for calculating the problem were derived from the Newton-Raphson method.

Three timber specimens were tested in bending in order to study their structural behavior. Finite element simulations of timber elements with hardening behavior were carried out and the analysis is validated by comparing with the experimental test results. In addition, the material model developed in this study was validated in the context of uniaxial compressive and tensile loadings by comparing it to the experimental results available in literature. The validation of the developed constitutive model was confirmed.

Acknowledgements

This research is in the framework of the project Eco-construction for Sustainable Developments (ECON4SD), supported by the program “*Investissement pour la croissance et l’emploi*”—European Regional Development Fund (2014–2020) (Grant agreement: 2017-02-015-15).

References

- [1] J. Porteous and A. Kermani, "Timber as a structural material," in *Structural Timber Design to Eurocode 5*, Blackwell, 2007.
- [2] A. Padilla-Rivera, B. Amor and P. Blanchet, "Evaluating the link between low carbon reductions strategies and its performance in the context of climate change: A carbon footprint of a wood-frame residential building in Quebec, Canada," *Sustainability*, vol. 10, no. 2715, 2018.

- [3] A. Reiterer and S. E. Stanzl-Tschegg, "Compressive behaviour of softwood under uniaxial loading at different orientations to the grain," *Mechanics of Materials*, vol. 33, no. 12, pp. 705-715, 2001.
- [4] L. F. Sirumbal-Zapata, C. Malaga-Chuquitaype and A. Y. Elghazouli, "A three-dimensional plasticity-damage constitutive model for timber under cyclic loads," *Computers and Structures*, vol. 195, pp. 47-63, 2018.
- [5] E. Borgström, Design of timber structures - Structural aspects of timber construction, Stockholm: Swedish Forest Industries Federation, 2016.
- [6] A. Harte, "Introduction to timber as an engineering material," *ICE Manual of Construction Materials*, vol. 2, pp. 707-715, 2009.
- [7] L. Daudeville, "Fracture in spruce: Experiment and numerical analysis by linear and non linear fracture mechanics," *Holz als Roh- und Werkstoff*, vol. 57, no. 6, pp. 425-432, 1999.
- [8] C. J. Chen, T. L. Lee and D. S. Jeng, "Finite element modelling for the mechanical behavior of dowel-type timber joints," *Computers and Structures*, vol. 81, pp. 2731-2738, 2003.
- [9] N. Kharouf, G. McClure and I. Smith, "Elasto-plastic modelling of wood bolted connections," *Computers and Structures*, vol. 81, pp. 747-754, 2003.
- [10] K. Sawata and M. Yasamura, "Estimation of yield and ultimate strengths of bolted timber joints by nonlinear analysis and yield theory," *Journal of Wood Science*, vol. 49, pp. 383-391, 2003.
- [11] L. Daudeville, L. Davenne and M. Yasumura, "Prediction of the load carrying capacity of bolted timber joints," *Wood Science and Technology*, vol. 33, pp. 15-29, 1999.
- [12] E. Serrano, "Glued-in rods for timber structures — a 3D model and finite element parameter studies," *International Journal of Adhesion and Adhesives*, vol. 21, no. 2, pp. 115-127, 2001.
- [13] I. Smith and S. Vasic, "Fracture behaviour of softwood," *Mechanics of Materials*, vol. 35, pp. 803-815, 2003.
- [14] S. Vasic, I. Smith and E. N. Landis, "Finite element techniques and models for wood fracture mechanics," *Wood Science and Technology*, vol. 39, pp. 3-17, 2005.
- [15] C. L. Santos, A. M. P. De Jesus, J. J. L. Morais and J. L. P. C. Lousada, "Quasi-static mechanical behaviour of a double-shear single dowel wood connection," *Construction and Building Materials*, vol. 23, pp. 171-182, 2009.
- [16] E. Benvenuti, N. Orlando, C. Gebhardt and M. Kaliske, "An orthotropic multi-surface damage-plasticity FE-formulation for wood: Part I – Constitutive model," <https://www.sciencedirect.com/science/journal/00457949>, vol. 240, p. 106350, 2020.
- [17] F. Nouri and H. R. Valipour, "Moment-rotation model for steel-timber composite connections with slab continuity steel rods," *Journal of Constructional Steel Research*, vol. 173, p. 106257, 2020.

- [18] A. Dias, J. V. D. Kuilen, S. Lopes and H. Cruz, "A non-linear 3D FEM model to simulate timber-concrete joints," *Advances in Engineering Software*, vol. 38, pp. 522-530, 2007.
- [19] D. M. Moses and H. G. L. Prion, "Stress and failure analysis of wood composites: a new model," *Composites Part B: Engineering*, vol. 35, no. 3, pp. 251-261, 2004.
- [20] M. Patton-Mallory, S. M. Cramer, F. W. Smith and P. J. Pellicane, "Nonlinear material model for analysis of bolted wood connections," *Journal of Structural Engineering*, vol. 123, no. 8, pp. 1063-1070, 1997.
- [21] R. Hill, "A theory of the yielding and plastic flow of anisotropic metals," *Proceedings of the Royal Society of London. Series A*, vol. 193, pp. 281-297, 1948.
- [22] S. W. Tsai and E. M. Wu, "A general theory of strength for anisotropic materials," *Journal of Composite Materials*, vol. 5, no. 1, pp. 58-80, 1971.
- [23] O. Hoffman, "The brittle strength of orthotropic materials," *Journal of Composite*, vol. 1, pp. 200-206, 1967.
- [24] M. Oudjene and M. Khalifa, "Elasto-plastic constitutive law for wood behavior under compressive loadings," *Construction and Building Materials*, vol. 23, pp. 3359-3366, 2009.
- [25] A. Bouchair and A. Vergne, "An application of the Tsai criterion as a plastic law for timber bolted joint modelling," *Wood Science and Technology*, vol. 30, pp. 3-19, 1995.
- [26] P. L. Clouston and F. Lam, "Computational modeling of strand-based wood composites," *Journal of Engineering Mechanics*, vol. 127, no. 8, pp. 844-851, 2001.
- [27] B. H. Xu, M. Taazount, A. Bouchair and P. Rancher, "Numerical 3D finite element modelling and experimental tests for dowel-type timber joints," *Construction and Building Materials*, vol. 23, pp. 3043-3052, 2009.
- [28] M. Gharib, A. Hassanieh, H. Valipour and M. A. Bradford, "Three-dimensional constitutive modelling of arbitrarily orientated timber based on continuum damage mechanics," *Finite Elements in Analysis and Design*, vol. 135, pp. 79-90, 2017.
- [29] M. Lukacevic, W. Lederer and J. Füssl, "A microstructure-based multisurface failure criterion for the description of brittle and ductile failure mechanisms of clear-wood," *Engineering Fracture Mechanics*, vol. 176, pp. 83-99, 2017.
- [30] P. Mackenzie-Helnwein, H. W. Müllner, J. Eberhardsteiner and H. A. Mang, "Analysis of layered wooden shells using an orthotropic elasto-plastic model for multi-axial loading of clear spruce wood," *Computer Methods in Applied Mechanics and Engineering*, vol. 194, no. 21-24, pp. 2661-2685, 2005.
- [31] P. Mackenzie-Helnwein, J. Eberhardsteiner and H. A. Mang, "A multi-surface plasticity model for clear wood and its application to the finite element analysis of structural details," *Computational Mechanics*, vol. 31, pp. 204-218, 2003.
- [32] J. Schmidt and M. Kaliske, "Models for numerical failure analysis of wooden structures," *Engineering Structures*, vol. 31, no. 2, pp. 571-579, 2009.

- [33] C. Sandhaas, J.-W. Van de Kuilen and H. J. Blass, "Constitutive model for wood based on continuum damage mechanics," in *12th World Conference on Timber Engineering*, Auckland, 2012.
- [34] C. Sandhaas and J. Van de Kuilen, "Material model for wood," *Heron*, vol. 58, pp. 173-194, 2013.
- [35] N. Orlando, Y. Taddia, E. Benvenuti, B. Pizzo and C. Alessandri, "End-repair of timber beams with laterally-loaded glued-in rods: Experimental trials and failure prediction through modelling," *Construction and Building Materials*, vol. 195, pp. 623-637, 2019.
- [36] B.-H. Xu, A. Bouchaïr and P. Racher, "Appropriate Wood Constitutive Law for Simulation of Nonlinear Behavior of Timber Joints," *Journal of Materials in Civil Engineering*, vol. 26, no. 6, p. 04014004, 2014.
- [37] A. Khennane, M. Khelifa, L. Bleron and J. Viguier, "Numerical modelling of ductile damage evolution in tensile and bending tests of timber structures," *Mechanics of Materials*, vol. 68, pp. 228-236, 2014.
- [38] M. Khelifa, A. Khennane, M. El Ganaoui and A. Celzard, "Numerical damage prediction in dowel connections of wooden structures," *Materials and Structures*, vol. 49, pp. 1829-1840, 2016.
- [39] T.-T. Tran, V.-D. Thi, M. Khelifa, M. Oudjene and Y. Rogaume, "A constitutive numerical modelling of hybrid-based timber beams with partial composite action," *Construction and Building Materials*, vol. 178, pp. 462-472, 2018.
- [40] E. Benvenuti, N. Orlando, C. Gebhardt and M. Kaliske, "An orthotropic multi-surface damage-plasticity FE-formulation for wood: Part II – Numerical applications," *Computers and Structures*, vol. 240, p. 106351, 2020.
- [41] N. T. Mascia and F. A. R. Lahr, "Remarks on orthotropic elastic models applied to wood," *Materials Research*, vol. 9, no. 3, pp. 301-310, 2006.
- [42] N. T. Mascia and L. Vanalli, "Evaluation of the coefficients of mutual influence of wood through off-axis compression tests," *Construction and Building Materials*, vol. 30, pp. 522-528, 2012.
- [43] N. Khorsandnia, H. R. Valipour and K. Crews, "Nonlinear finite element analysis of timber beams and joints using the layered approach and hypoelastic constitutive law," *Engineering Structures*, vol. 46, pp. 606-614, 2013.
- [44] Abaqus, "Theory manual, version 6.14," Dassault Systèmes Simulia Corp., 2018.
- [45] J. C. J. Schellekens and R. De Borst, "The use of the Hoffman yield criterion in finite element analysis of anisotropic composites," *Computers and Structures*, vol. 37, no. 6, pp. 1087-1096, 1990.
- [46] J.-Y. Lee, J.-W. Lee, M.-G. Lee and F. Barlat, "An application of homogeneous anisotropic hardening to springback prediction in pre-strained U-draw/bending," *International Journal of Solids and Structures*, vol. 49, no. 25, pp. 3562-3572, 2012.

- [47] J. C. Simo and J. W. Ju, "Strain- and stress-based continuum damage models-I. formulation," *International Journal of Solids and Structures*, vol. 23, no. 7, pp. 821-840, 1987.
- [48] A. Shigang, F. Daining, H. Rujie and P. Yongmao, "Effect of manufacturing defects on mechanical properties and failure features of 3D orthogonal woven C/C composites," *Composites Part B: Engineering*, vol. 71, pp. 113-121, 2015.
- [49] M. Wang, X. Song and X. Gu, "Three-Dimensional combined elastic-plastic and damage model for nonlinear analysis of wood," *Journal of Structural Engineering*, vol. 144, no. 8, p. 04018103, 2018.
- [50] J. L. Chaboche, F. Feyel and Y. Monerie, "Interface debonding models: a viscous regularization with a limited rate dependency," *International Journal of Solids and Structures*, vol. 38, no. 18, pp. 3127-3160, 2001.
- [51] I. Lapczyk and J. A. Hurtado, "Progressive damage modeling in fiber-reinforced materials," *Composites Part A: Applied Science and Manufacturing*, vol. 38, no. 11, pp. 2333-2341, 2007.
- [52] D. R. J. Owen and E. Hinton, *Finite elements in plasticity, Theory and practice*, Swansea: Pineridge Press, 1980.
- [53] V. Karagiannis, C. Malaga-Chuquitaype and A. Y. Elghazouli, "Modified foundation modelling of dowel embedment in glulam connections," *Construction and Building Materials*, vol. 102, pp. 1168-1179, 2016.
- [54] S. Maiti, L. Gibson and M. Ashby, "Deformation and energy absorption diagrams for cellular solids," *Acta Metallurgica*, vol. 32, no. 11, pp. 1963-1975, 1984.

3.4 Paper IV

The paper “Experimental and numerical investigation of a novel demountable timber–concrete composite floor” [94] was published in *Buildings* journal. the author of the dissertation served as the first author contributing to conceptualization, methodology, formal analysis, investigation, resources, data curation, writing—original draft preparation and visualization of the paper.

Experimental and Numerical Investigation of a Novel Demountable Timber–Concrete Composite Floor

Hooman Eslami¹, Laddu Bhagya Jayasinghe² and Daniele Waldmann^{3,*}

¹ Faculty of Science, Technology and Medicine (FSTM), University of Luxembourg, L-4365 Esch-sur-Alzette, Luxembourg; hooman.eslami@uni.lu

² Department of Earth and Environmental Sciences, Ludwig-Maximilians-Universität München, Theresien Str. 41, 80333 Munich, Germany; bhagya.jayasinghe@lmu.de

³ Institute for Solid Structures, Technical University of Darmstadt, Karolinenplatz 5, 64289 Darmstadt, Germany

* Correspondence: waldmann@massivbau.tu-darmstadt.de

Abstract: In recent years, there has been an increasing interest in timber–concrete composite (TCC) floors as a sustainable structural solution. Until now, only a few studies have investigated the demounting of TCC floors, which is essential to increase sustainability and improve the end-of-life environmental benefits of a floor system. This study investigates an innovative and straightforward demountable TCC slab that has notched and bolted connections. Six downscaled slabs are tested under four-point bending. The results show that the slab system has high composite action with an efficiency of 0.73. A three-dimensional finite element model is developed and calibrated with the experimental result. The model is used to study the influence of several parameters, such as the shape and dimensions of the notch as well as the bolt location on the load-bearing capacity and the load-deflection behavior of the slab. The results show that the failure tends to be more ductile when a birdsmouth-shaped notch is used, and the bolt is placed within the notch. Moreover, the load-bearing capacity of the shear connection increases by increasing the distance of the notch to the end of the slab and using a triangular notch.

Keywords: timber–concrete composite floors; demountable shear connection; notched shear connection; design for deconstruction; demountable structures

1. Introduction

The building industry is responsible for significant energy and natural resource consumption and greenhouse gas emission. Construction and demolition wastes have a substantial share in waste generation. For example, in Europe, this goes up to more than one-third of all waste production [1]. To develop new structural solutions, it is critical to consider two key factors. The first factor is the promotion of the use of more sustainable construction materials, while the second factor is the incorporation of de-sign for deconstruction (DfD) [2] principles into the development of structural elements. DfD encourages the design of structural elements with reflection on their end-of-life scenario in addition to their load-bearing capacity and durability [3]. DfD elements can be demounted, reused, or recycled with limited energy, time, and resource consumption. Regarding sustainable construction materials, in the last few years, the focus on timber and engineered wood products as the appropriate solutions has increased, as they are renewable, have a low carbon footprint, and have high carbon storage capacity. However, when considering timber structural elements, such as slabs and beams, some unfavorable features, such as springiness, vibration, and poor sound insulation, have to be considered, mostly in the serviceability stage. These drawbacks can be improved by using timber as hybrid solutions such as timber–concrete composite (TCC) [4,5].

TCC structural systems have been extensively studied and employed as different structural elements in both new construction and rehabilitation applications since the early decades of the last century [6,7]. TCC slabs are typically designed with the concrete slab on the top predominantly subjected to compression, while all or most of the timber section at the bottom bears tensile stresses. If the system is effectively developed, it can exhibit a three to five times higher load-bearing capacity compared to conventional timber or concrete systems [8]. In addition, a proper shear connector system is used to effectively transfer the shear between the timber and the concrete components. The shear connection between the two materials is a

critical component in the performance of TCC slabs [9]. It directly impacts the composite behavior, stress distribution, deformations, and the design of the slab. In the last two decades, new shear connections were developed using different methods, such as nails [10], screws [11], adhesives [12], perforated plates [13], and notches [14], to connect concrete and timber. Figure 1 illustrates some of these connection techniques. These studies investigated the mechanical properties of shear connections like stiffness and strength through push-out and bending tests. Among all, notched shear connections offer an exceptional combination of mechanical performance and simplicity since they are easy to construct and present high stiffness and strength [6]. Moreover, notched connections are suitable for DfD as no permanent bond is needed for their fabrication. However, the failure mode in the notched connection is brittle [15,16]; therefore, it is usually accompanied by steel fasteners that are embedded in the concrete to improve the post-failure performance [17,18].

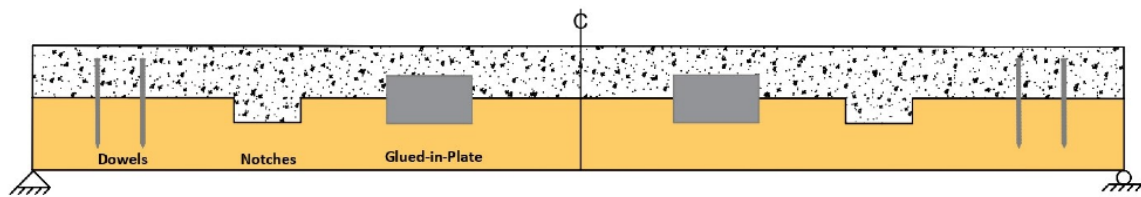


Figure 1. Longitudinal cross-section of a TCC beam with 3 different shear connections: dowels, notches, and glued-in-plate. Figure from Mirdad et al. [19].

Most of the existing shear connections permanently bond timber to concrete. Consequently, the slabs in which they are used cannot easily be prefabricated, de-mounted, overhauled, or reused. Thus, the sustainability of these slabs is diminished. Several researchers attempted to address the prefabrication in TCC floors by proposing wet-dry [20–23] and dry-dry systems [24–30]. In the wet-dry system, the concrete is cast directly on the timber component, while the shear connection is implemented on the timber part. In the dry-dry system, the concrete part is precast, and the shear connection is embedded within the concrete. Subsequently, it is fastened to the timber component using screws and bolts. Although certain dry-dry systems

may have the potential for disassembly, the demounting of these connections was not studied. While many researchers have investigated demountable shear connectors for steel–concrete composite floors [31–34], only a few studies investigated the deconstruction of TCC slabs. Khorsandnia et al. [35,36] developed and tested six different types of demountable connections using screws, bolts, and steel sections. The researchers addressed that the accuracy required for fabrication and assembly and the labor required for fabrication and installation are among the most crucial characteristics of deconstruction. Derikvand and Fink [37,38] introduced a demountable TCC shear connection using a self-tapping screw. The shear and bending tests showed that the connection was al-most as good as a similar non-demountable one. However, the screw connection inherently showed a low stiffness and strength compared to other types of connections.

In this paper, a novel modular prefabricated TCC floor system is proposed, which is fully demountable. The novelty of this floor system corresponds to its demountable shear connection that upgrades the sustainability of the floor system since it facilitates its reusing and recycling. Also, this modular system is designed to be prefabricated in the wet–dry system so that the concrete is cast on the timber part, which is a fast process that is not labor-intensive, and overcomes the construction and assembly challenges that exist in similar floor systems. The TCC module can then be transferred to the building site and put in place in a dry–dry process. The shear connection is de-signed to have high stiffness and strength to achieve a high level of shear connection. This paper presents an experimental study on a downscaled model of the floor where the structural performance and fabrication process are investigated. Later, analytical and numerical studies on the floor system are presented, and a parametrical study is performed on the shear connection.

2. Experimental Study

2.1. The Demountable TCC Floor System

The TCC floor system consists of a concrete layer on a timber layer that is connected via a demountable shear connection. The timber part can be in the form of joists or a timber slab, which is made from a suitable type of timber or engineered wood products as presented in Figure 2. The shear connection includes a triangular notch that transfers the shear force between the two layers. The notched connection is chosen as the shear connection because notches transfer the shear force through the direct contact of the two materials without a permanent bond. Notched connections show relatively high strength and stiffness compared to other non-binding connections [39]. The shear connection is associated with a vertical bolt instead of the commonly embedded steel fasteners in notched connections, which keeps the two layers together and avoids the uplift of the concrete. The bolt is placed in a slotted hole so that it does not resist any shear but only the uplift forces caused by the eccentric forces at the connection. The bolt is designed to perform in the elastic zone so that it does not undertake permanent deformation in favor of deconstruction and reuse.

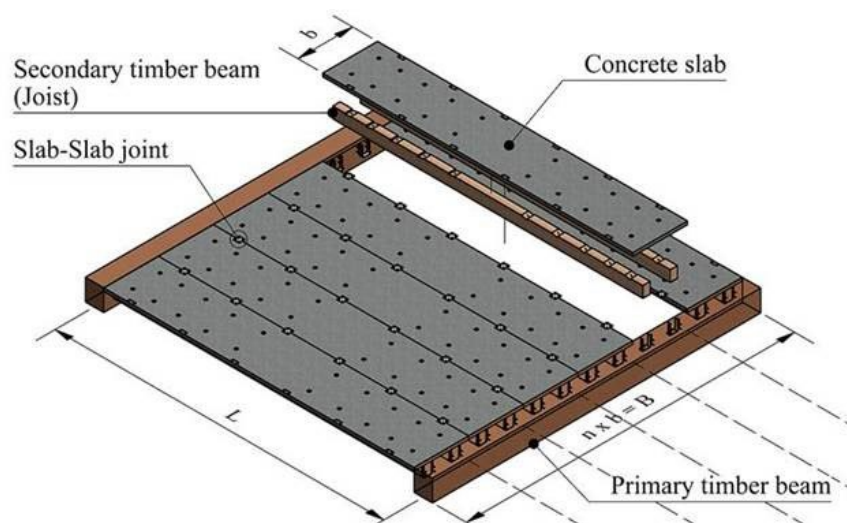


Figure 2. Conceptual design of the novel demountable timber–concrete composite floor system.

2.2. Fabrication

Before casting the concrete, the notches and the holes for the bolt in the timber are cut, and the formworks for the bolts in the concrete are placed. The wet–dry system is used for the fabrication of the floor modules, which means that the concrete layer is directly cast against the timber part. Therefore, there is no need to consider assembly tolerances between the concrete and timber. When the concrete is hardened, the bolt formwork is removed, the bolt is installed, and the TCC module is completed. Then, the modules are transferred to the construction site and installed on the main frame of the structure as depicted in Figure 2. The TCC modules are connected to the primary beams with a simple supported connection. The dimensions of the grids of the building dictate the length (L), width (b), and number (n) of the modules. This paper investigates the fabrication and demounting possibility and the flexural behavior of one module.

2.3. Downscaled Model

To investigate the proposed floor with the available resources and facilities, a downscaled model of the TCC slab was designed, which is presented in Figure 3. One shear connection is placed on each side of the slab. Based on the design, the concrete mixture was developed, and the timber was cut and prepared for fabrication.

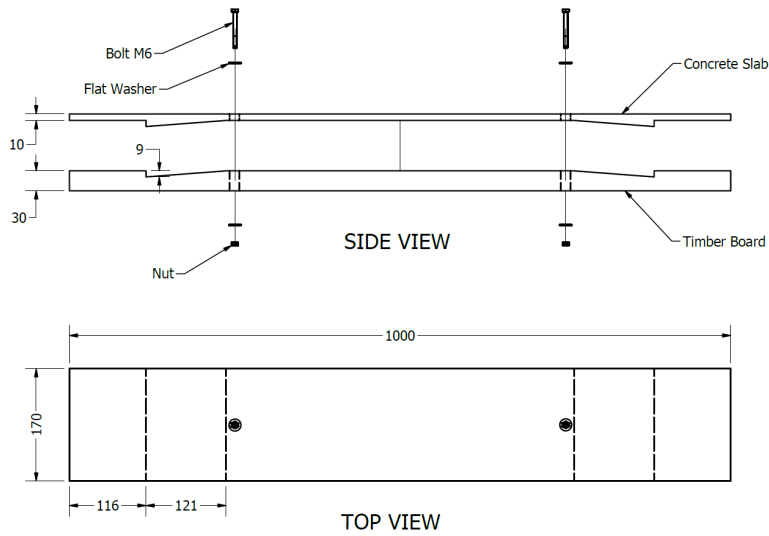


Figure 3. Design of the downscaled novel TCC slab (Dimensions are in mm).

2.3.1. Concrete

The concrete layer in the downscaled model of the slab has a thickness of only 10 mm, which is not deep enough for concrete with conventional aggregate sizes. Accordingly, the placement of steel reinforcement in the concrete layer is impossible; therefore, the tensile stresses due to shrinkage and loading must be borne by the concrete itself. Moreover, the concrete must fill the notched geometry without air voids. Hence, a special self-compacting mixture with fine aggregates and high tensile strength was developed. A mixture of water, high-performance binder [40], CEN standard sand [41], and superplasticizer [42] was used to develop the special mixture for the concrete layer of the downscaled element. To find the best mixture with appropriate self-compacting properties while avoiding segregation effects, five different mixtures with water–binder ratios from 0.15 to 0.29 and superplasticizer–binder ratios from 0.3% to 2.0% were batched and tested under compression according to the DIN EN 196-1 [41]. In addition, the vertical section of the samples was visually checked for segregation.

The compression strengths of the mixtures are compared in Figure 4 in the function of the water–binder ratio and the superplasticizer–binder ratio. As expected, the strength of the

mixtures improved by reducing the water–binder ratio. On the other hand, the superplasticizer dosage must be adjusted separately for each water–binder ratio to achieve self-compacting properties without segregation effects. The mixture with the water–binder ratio of 0.15 was chosen based on the self-compacting behavior, lack of aggregate segregation, and compression strength. Details of the chosen mixture are shown in Table 1.

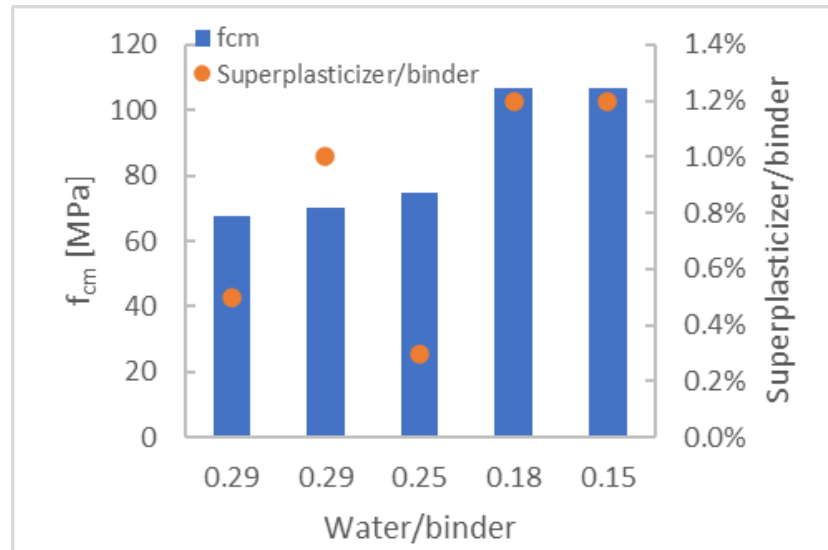


Figure 4. Comparison of the strength of the different concrete mixtures.

Table 1. Chosen mixture specifications.

Item	Amount [kg/m ³]
Sand	1108
Binder	1108
Water	169
Superplasticizer	13.4
Total	2399

Table 2 presents the mechanical properties of the concrete used for producing the TCC slab on 28-day-old specimens. The properties include the E-Modulus under compression, strength under compression, and tensile splitting strength of the concrete. It is important to consider

that, due to the thin thickness of the concrete similar to thin-walled sections, the mechanical properties may differ from standard test results [43].

Table 2. Mechanical properties of the special mixture for 28-day-old specimens.

	Compression Strength [MPa]	Modulus of Elasticity [GPa]	Tensile Splitting Strength [MPa]
Range	105.5–113.1	43.9–46.0	6.9–7.8
Average	109.1	45.0	7.5
SD	2.8	1.1	0.5
COV [%]	2.6	2.3	6.7

2.3.2. Timber

The timber board was from the C24 strength class. The strength and stiffness of the timber material are depicted in Table 3 according to EN 338:2009 [44].

Table 3. Timber C24 characteristic values according to EN 338:2009.

Strength Properties [MPa]	
Bending	24
Tension parallel	14
Tension perpendicular	0.4
Compression parallel	21
Compression perpendicular	2.5
Shear	4
Stiffness Properties [MPa]	
Mean Modulus of Elasticity parallel to grain direction	11,000
Mean Modulus of Elasticity perpendicular to grain direction	370
Mean Shear Modulus	690
Mean density [kg/m ³]	420

2.4. Experimental Setup

The experiment program was carried out at the Laboratory of Solid Structures at the University of Luxembourg. Six downscaled slabs were tested under a four-point bending experiment. All specimens were simply supported at a distance of 100 mm from the end of the slab and spanned a distance of 800 mm. The timber grain orientation for all specimens was aligned parallel to the span length. The loading was applied at a rate of 0.1 kN/s until the failure of the specimens. The experimental setup is shown in Figure 5. Linear Variable Displacement Transducers (LVDT) were used to measure the mid-span deflection and the slip between the concrete and timber (Figure 6). The absolute deflection of the slab w was calculated by the average of the two LVDT sensors at mid-span.

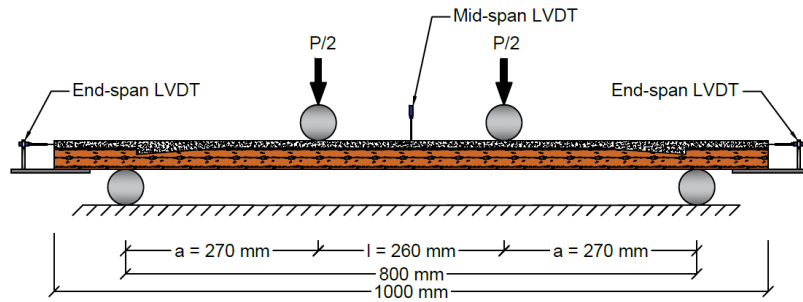


Figure 5. Experimental setup.



(a)



(b)

Figure 6. LVDT displacement sensors for (a) slip measurement at end-span and (b) deflection measurement at mid-span.

2.5. Experimental Results

Figure 7a illustrates the results of mid-span deflection versus loading for the TCC specimens. The ultimate load of the specimens primarily varies due to variations in timber properties. To address this, Figure 7b presents the normalized load-deflection graphs. The load-deflection behavior is quasi-linear at the beginning of the loading for all the specimens, and later, the slab starts to deflect nonlinearly before a brittle failure occurs. The two failure modes observed in the specimens are the shear failure in timber, which occurred from notch to end-span (Figure 8a), and the bending failure, which occurred around mid-span (Figure 8b). After the failure, the timber and concrete are still easily detachable. No permanent deformation was observed in the bolt.

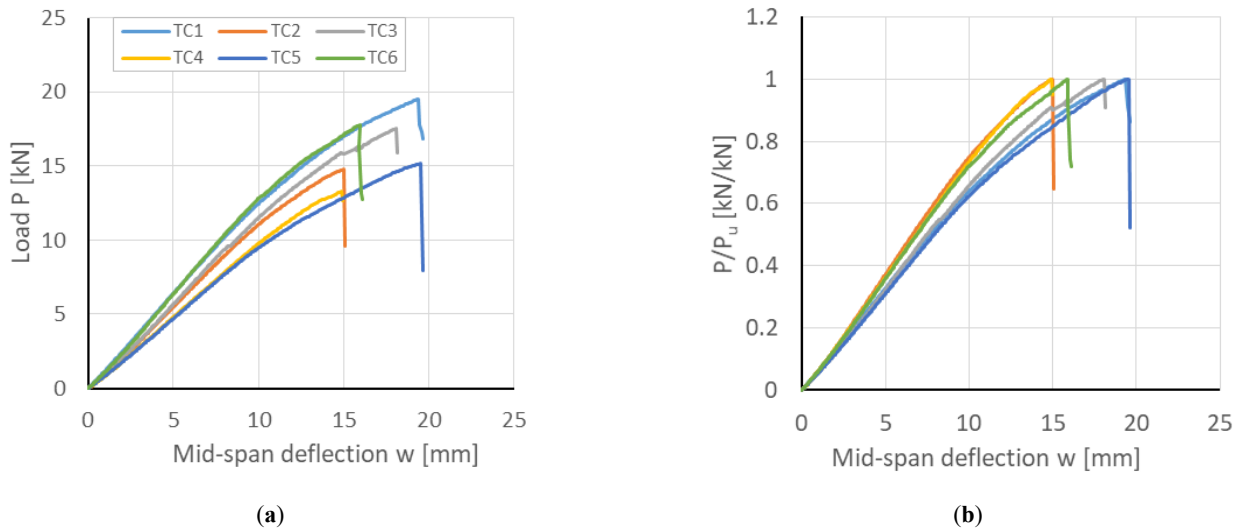
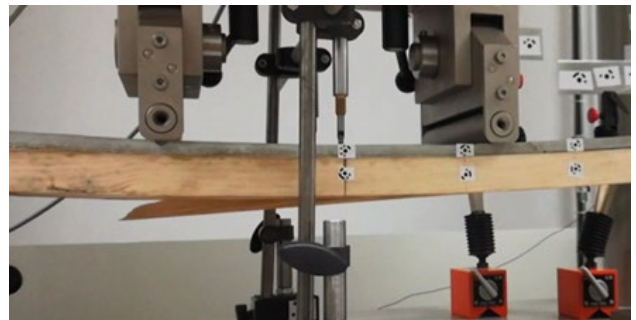


Figure 7. Results from the experiment: (a) Load-deflection; (b) Normalized load-deflection.



(a)



(b)

Figure 8. Failure modes in timber: (a) Horizontal shear failure at the notch; (b) Bending failure at mid-span.

The load-deflection measurements from the test results are used to calculate the bending stiffness and the effective flexural rigidity of the composite slab in different loading stages. In Table 4, the mid-span deflection and the bending stiffness at ultimate load P_u are presented as w_u and k_u , respectively. Accordingly, the deflection and the bending stiffness for the linear deformation part are calculated at 30% of the ultimate load $P_{0.3}$ and presented as $w_{0.3}$ and $k_{0.3}$, respectively. The effective flexural rigidity is calculated at $P_{0.3}$ with the following formula [45]:

$$(EI)_{eff} = P_{0.3}a(3L^2 - 4a^2)/48w_{0.3} \quad (1)$$

which corresponds to a four-point bending loading setup. The ultimate load and the bending stiffness vary among the specimens, which is expected due to the inherent variation in the wood properties.

Table 4. Summary of the experimental results.

Specimens No.	At Ultimate Load			At 30% of the Ultimate Load		Effective Rigidity	
	P_u [kN]	w_u [mm]	k_u [kN/mm]	$P_{0.3}$ [kN]	$w_{0.3}$ [mm]	$k_{0.3}$ [kN/mm]	$(EI)_{eff}$ [kN.m ²]
T1	19.5	19.4	1.01	5.9	4.6	1.29	11.8
T2	14.8	15.0	0.99	4.4	4.1	1.09	10.0
T3	17.5	18.0	0.97	5.3	4.6	1.13	10.4
T4	13.3	14.9	0.89	4.0	4.2	0.95	8.7
T5	15.2	19.5	0.78	4.6	4.8	0.94	8.6
T6	17.8	15.9	1.12	5.3	4.2	1.26	11.5
Average	16.3	17.1	0.96	4.9	4.4	1.11	10.2
SD	2.10	1.95	0.10	0.63	0.27	0.13	1.22
CV%	12.9%	11.4%	10.8%	12.9%	6.2%	12.0%	12.0%

2.6. Analytical Analysis

The method that is commonly used to design TCC slabs is a linear–elastic method proposed by Ceccotti [46] based on the method known as the γ -method in annex B of Eurocode 5 [47]. This method assumes that the slab is simply supported where the two individual parts, here concrete and timber, are connected through shear connections with a slip modulus of K . In this method, effective flexural rigidity is defined as:

$$(EI)_{eff} = E_c I_c + \gamma_c E_c A_c a_c^2 + E_t I_t + \gamma_t E_t A_t a_t^2 \quad (2)$$

and

$$\gamma_c = \frac{1}{1 + \frac{\pi^2 E_c A_c s^2}{K l^2}}, \quad (3)$$

$$\gamma_t = 1 \quad (4)$$

where the subscripts c and t refer to the concrete and timber, and E , I , A , and a indicate Young's modulus, the second moment of area, the area, and the distance from the centroid of the element to the neutral axis of the composite section, respectively. In the formula of γ_c , s is the space between the shear connectors, and l is the beam span. γ_c can vary between zero, which means no composite connection, and one, which means a full composite connection between the two layers. The slip modulus of the shear connections K and the space between them s is decisive in determining the value of γ_c . Based on the above formulas and the experimental results, the effective flexural rigidity of the current slab for the extension of no composite to full composite is shown in Table 5. For analytical analysis, only the linear part of the experimental results at 30% of the ultimate load is considered.

Table 5. Composite action of the slab.

Composite Connection	γ_c	γ_t	$(EI)_{\text{eff}}$ [kN.m ²]
No composite	0	1	4.8
Experimented connection	0.23	1	10.2
Full composite	1	1	17.8

Considering the results, the efficiency of the composite slab can be calculated with the method proposed by Gutkowski et al. [48]:

$$EFF = \frac{\Delta_N - \Delta_I}{\Delta_N - \Delta_C} \quad (5)$$

where Δ_N , Δ_I , and Δ_C represent the theoretical deflection of no composite system, the measured deflection, and the theoretical deflection of the completely composite system, respectively. According to the experimental results and the analytical calculations, the load-deflection graphs for these three cases are depicted in Figure 9. By substituting the values of Δ_N , Δ_I , and Δ_C in Equation (5) (where at $P/P_u = 0.15$, these values are 4.67, 2.20, and 1.27, respectively, as depicted in Figure 9), the efficiency of the current slab can be calculated as 0.73.

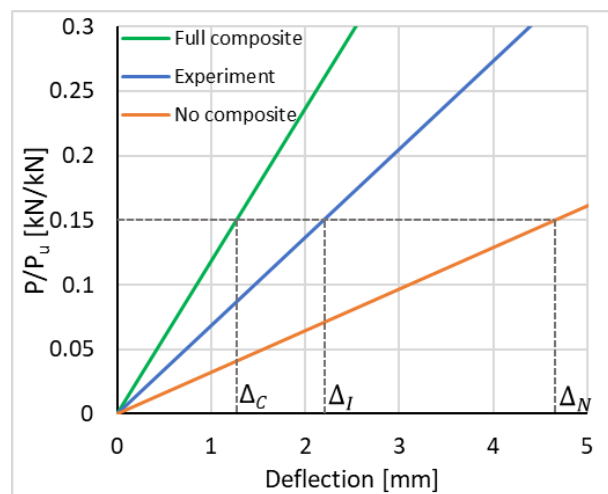


Figure 9. Analytical load-deflection graphs for no composite, full composite, and experimental composite action.

3. Numerical Study

In this section, a numerical model is presented for the investigation of the structural performance of the slabs under quasi-static loading conditions during a four-point bending test. A three-dimensional finite element (FE) model was developed using the Abaqus software package. The developed FE model was validated using the experimental results, which were described in the previous section.

The geometry of the slab has two symmetric planes. For the benefit of saving computation costs, only one-quarter of the geometry was modeled, and symmetric boundary conditions were assigned at the symmetry planes. A linear hexahedral element type with reduced integration (C3D8R) was used. The loading and support parts were modeled as a 3D analytic rigid shell. All dimensions were identical to the experimental ones. The loading was applied by displacement of the rigid loading profile in the Y-direction at a constant rate. The support was applied by constraining all the degrees of freedom of the support profile. The geometry of the model is shown in Figure 10.

The interaction between the parts was characterized by pressure-overclosure “Hard” contact in the normal and static coefficient of friction in the tangential directions. The static coefficient of friction was defined as 0.57 between timber–concrete [49] and concrete–steel [50], 0.4 between timber–steel [51], and 0.15 for all other contact pairs.

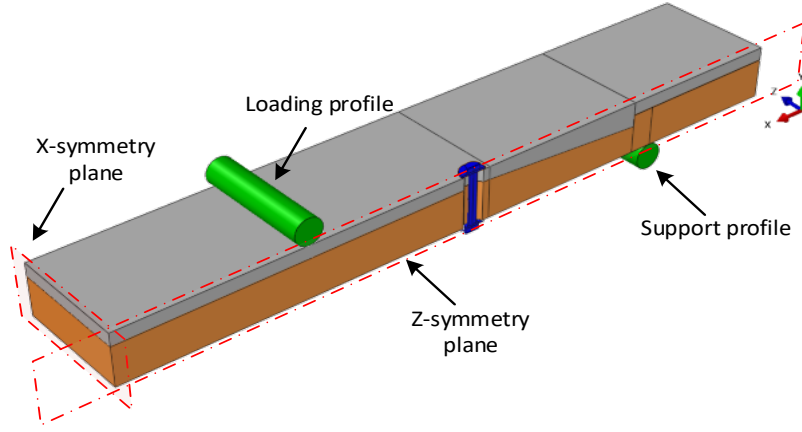


Figure 10. The geometry of the modeled bending experiment in Abaqus.

3.1. Material Modeling

3.1.1. Concrete

The Concrete Damage Plasticity (CDP) model was used for modeling the concrete. The CDP model assumes that the main two failure mechanisms are tensile cracking and compressive crushing of the concrete material [52]. In the CDP model, the total strain tensor is as $\varepsilon = \varepsilon^{el} + \varepsilon^{pl}$, where ε^{el} and ε^{pl} are the elastic and plastic parts of the strain, respectively. The stress–strain relations in both compression and tension are governed by scalar damaged elasticity as [52]:

$$\sigma = (1 - d)D_0^{el} : (\varepsilon - \varepsilon^{pl}) \quad (6)$$

where d is the scalar stiffness degradation variable that can be in a range of 0 for undamaged material to 1 for fully damaged material, D_0^{el} is the undamaged elastic stiffness of the material, ε is the total strain, and ε^{pl} is the plastic part of the strain. The evolution of the degradation variable is defined by $d = d(\bar{\sigma}, \varepsilon^{pl})$, where $\bar{\sigma}$ is the effective stress that is defined as [52]:

$$\bar{\sigma} \stackrel{\text{def}}{=} D_0^{el} : (\varepsilon - \varepsilon^{pl}) \quad (7)$$

and ε^{pl} is the hardening variable. The damaged states in tension and compression are individually considered by two hardening variables, ε_t^{pl} and ε_c^{pl} , which refer to equivalent plastic strain in tension and compression, respectively. Accordingly, the Cauchy stress can be represented as:

$$\sigma = (1 - d)\bar{\sigma} \quad (8)$$

In this model, the states of failure or damage are determined with the yield function as $F(\bar{\sigma}, \varepsilon^{pl})$. The yield function represents a surface in the effective stress space, which is controlled by the hardening variables. Conveniently, uniaxial loading conditions in compression and tension are considered for formulating the evolution of the hardening variables, and later, it is extended to multiaxial conditions. The uniaxial behavior is considered differently under tension and compression. Under uniaxial tension, the stress–strain behavior is considered a linear elastic response until the failure stress σ_{t0} . After the failure, a softening stress–strain response represents the formation of micro-cracks. Under uniaxial compression, the response is linear until the value of the initial yield, σ_{c0} , followed by a stress hardening until the ultimate stress, σ_{cu} . Beyond that, the response is characterized by stress softening. In both tension and compression stresses, in the softening response region, the unloading response of the concrete specimen is weakened by the degrading (damage) variables d_t and d_c , standing for tensile and compressive damage, respectively [52].

To define the stress–strain behavior of the concrete for numerical calculations, the behavior should be extracted either from test results or from mathematical constitutive models. The concrete in this study was high-strength concrete. The stress–strain response of high-strength concrete in compression is different from conventional concrete. With an increase in the strength of concrete, the initial trend of the stress–strain response tends to become mostly

linear, and the linear portion of the ascending part of the graph extends [53]. Moreover, to some extent, the strain at maximum strength becomes greater, and the descending part of the stress–strain response becomes steeper [54]. Considering the behavior of high-strength concrete and the test results, the response curve was based on the model from Carreira and Chu [55], which is as follows:

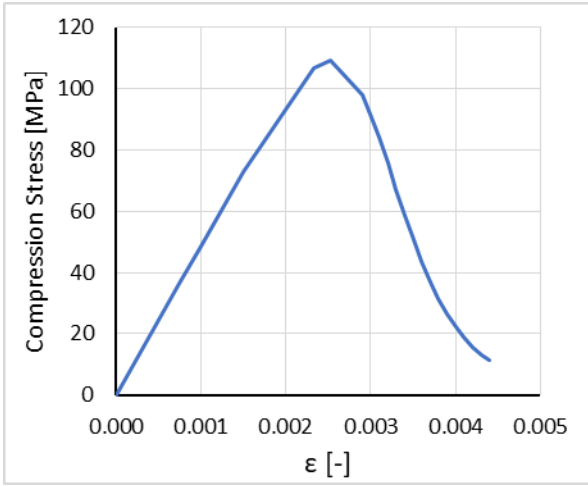
$$\sigma = f_{cm} \frac{\beta \left(\frac{\varepsilon}{\varepsilon_u} \right)}{\beta - 1 + \left(\frac{\varepsilon}{\varepsilon_u} \right)^\beta} \quad (9)$$

and

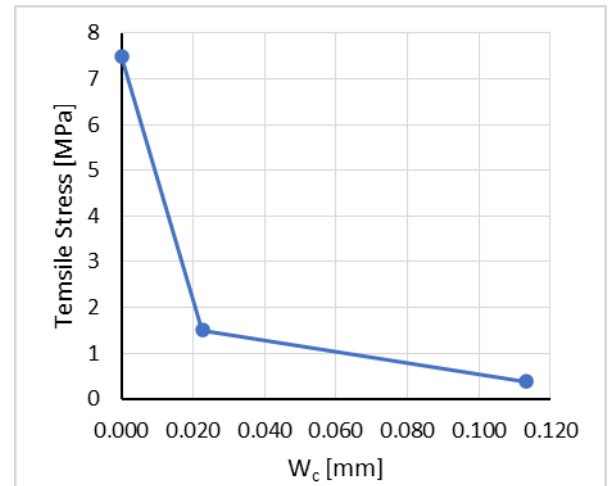
$$\beta = \frac{1}{1 - \frac{f_{cm}}{\varepsilon_u E_{it}}} \quad (10)$$

where f_{cm} is the concrete maximum stress, ε_u is the strain at maximum stress, and E_{it} is the initial tangent modulus of elasticity. Considering the above formulas and the results from the tests on the concrete mixture presented in Section 2, the stress–strain response in Figure 11a was used as input for the CDP model.

The post-failure behavior of concrete in tension, i.e., the strain-softening for cracked concrete, can be defined by tension stiffening in the CDP model, which can be defined either by the stress–strain relation or by applying a fracture energy cracking criterion. When no reinforcement exists in the region, the latter method is preferable to avoid mesh sensitivity in the results [52]. Therefore, in this model, the post-failure behavior under tension was defined by a bilinear stress-crack opening (W_c) response as demonstrated in Figure 11b, which was calculated based on the fracture energy of concrete [56].



(a)



(b)

Figure 11. (a) Stress–strain response of the concrete in compression; (b) Post-failure crack opening response of the concrete under tensile stress.

3.1.2. Timber

Timber is an orthotropic material that shows different mechanical behavior in three mutually perpendicular axes and has different strengths under compression, tension, and shear. Therefore, three mutually perpendicular planes needed to be defined for the timber-board part so that the mechanical properties of longitudinal, radial, and tangential axes were assigned in the right orientations. Directions 1, 2, and 3 were assigned to the X, Y, and Z axes, respectively, where direction 1 was parallel to the grain, and directions 2 and 3 were in the tangential and radial directions, respectively.

There is no predefined material model in Abaqus to model the orthotropic nonlinear behavior of timber. The material model used in this model was developed by Eslami et al. [57], which is a nonlinear anisotropic elastoplastic three-dimensional material model with failure analysis capacity that was implemented as a UMAT subroutine for Abaqus. The model associates Hoffman's [58] yield criterion with isotropic hardening to model the plastic strain hardening behavior of timber under compression. Also, four failure criteria are defined to trigger the damage propagation under both compression and tension. Hoffman's criterion, which is an

extension of Hill's [59] criterion, is considered for this material model because it distinguishes between the compression and tension strengths. Some timber mechanical properties, such as elasticity, strength and hardening parameters, and fracture energies, that are needed as the inputs of the material model vary for different timber types. The timber material properties that were used in the material model are shown in Table 6. These properties were calibrated based on the test results reported on the same batch of timber by Eslami et al. [57]. For further detail about the material model, its implementation, and validation and also the tests on timber material, please see reference [57].

Table 6. Material properties of timber for FE modeling.

Elasticity Parameters					
E_1 [MPa]	$E_2 = E_3$ [MPa]	G_{23} [MPa]	$G_{12} = G_{13}$ [MPa]	ν_{23}	$\nu_{12} = \nu_{13}$
11,000	370	60	690	0.5	0.45
Strength parameters					
σ_{1c} [MPa]	$\sigma_{2c} = \sigma_{3c}$ [MPa]	σ_{1t} [MPa]	$\sigma_{2t} = \sigma_{3t}$ [MPa]	σ_{23} [MPa]	$\sigma_{12} = \sigma_{13}$ [MPa]
54	6.9	36	0.7	0.5	3.5
Hardening parameters					
h [MPa]					
6436					
Fracture energies					
$G_{1t, f}$ [N/mm]	$G_{2t, f}$ [N/mm]	$G_{3t, f}$ [N/mm]			
10	0.2	0.2			

3.2. Results and Discussion

The load-deflection curve obtained from the FE model is illustrated in Figure 12 and compared with an average graph of the load displacement of the experimental results. The stiffness of the FE model is in line with the experimental results. Overall, a reasonably good correlation

between the numerical and experimental results is observed. Also, the brittle failure is simulated with the numerical model.

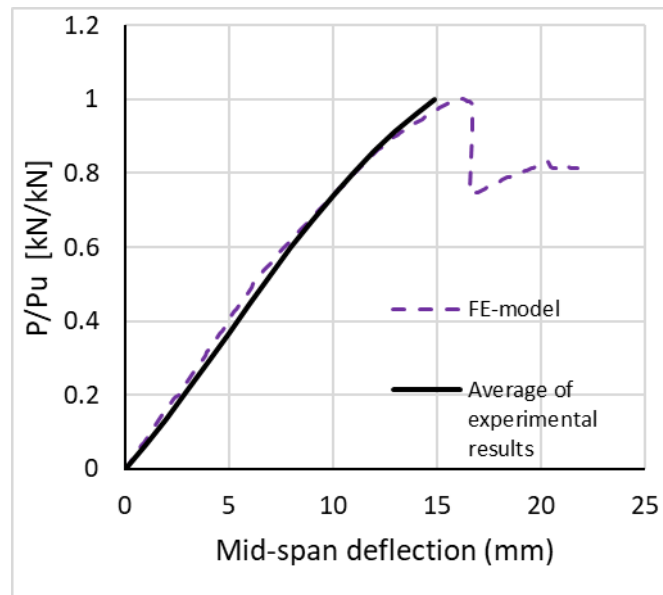


Figure 12. Load-deflection result from the FE model compared to the experimental results.

Figure 13 illustrates the maximum principal stress distribution in the concrete and timber parts. The maximum compression stress happened at mid-span in the concrete part close to the loading zone. For the tensile stress, the concentration was in the timber part at mid-span as well as at the notched corner, which is in correlation with the damage evolution in the timber presented in Figure 14. The figure shows the damage evolution with the increase in the load. It can be observed that the first damage occurred in the vicinity of the notch. The damaged zone increased with the increase in load and propagated toward the end of the slab in the longitudinal direction. The failure occurred later when the damage was initiated and distributed between the loading part and the mid-span. The predicted failure of the model is in good agreement with the observed rupture in the timber part during the experiment, as shown in Figure 8.

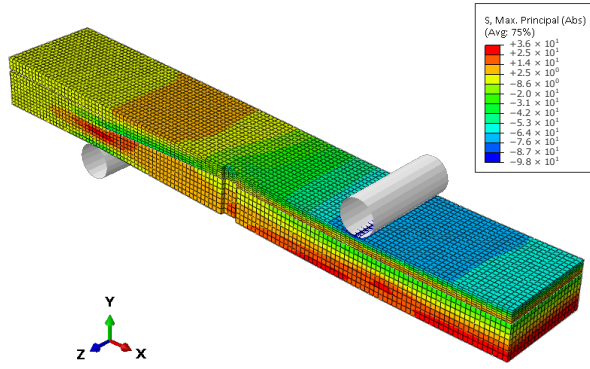


Figure 13. Stress distribution of the composite slab at failure load (values in MPa).

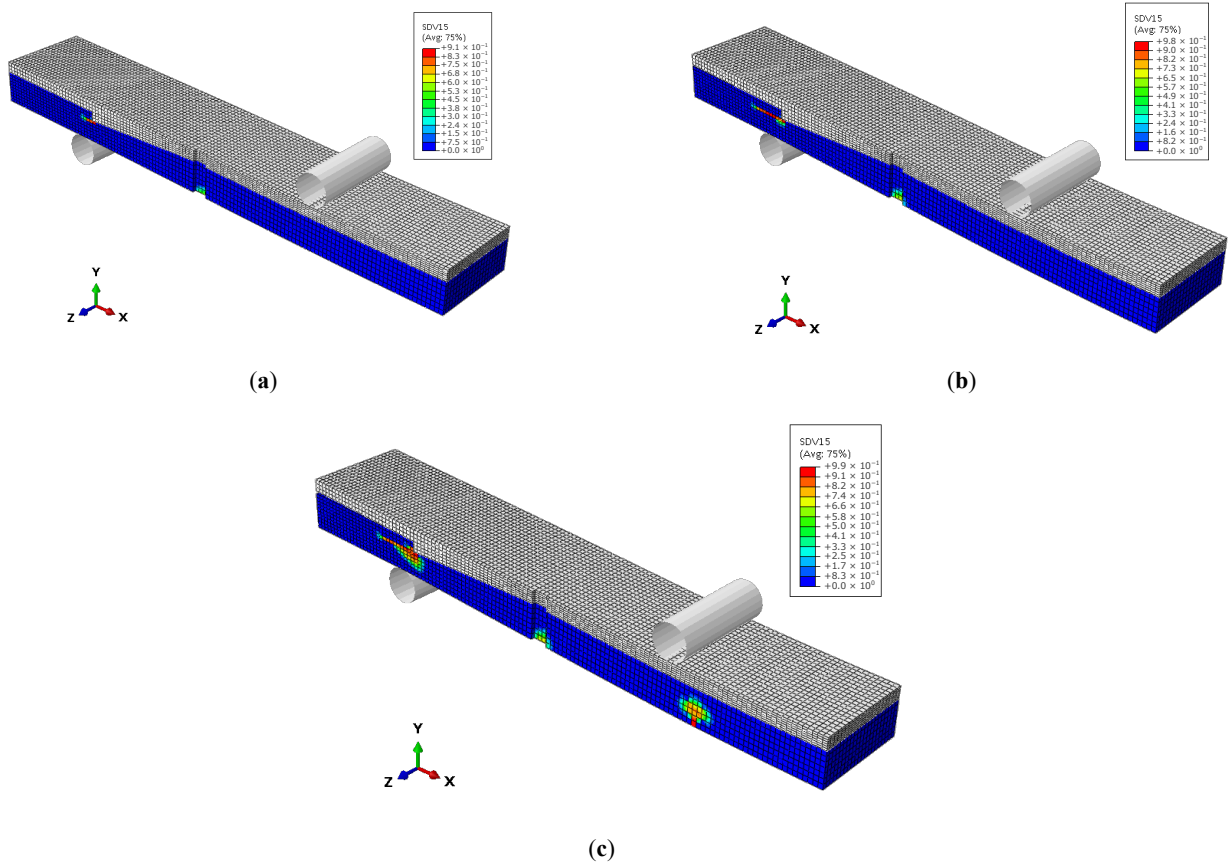


Figure 14. Damage evolution in the timber part at (a) $P/P_u = 0.67$; (b) $P/P_u = 0.95$; (c) $P = P_u$.

4. Parametric Study

The FE model is used to perform a parametric study on the TCC slab. The models and their varying parameters are presented in Table 7. For each parameter, the primary model is

compared to two or three other models. The parameters that are considered are notch depth (ND), notch length (NL), and timber length in front of the notch (NH) in addition to the shape of the notch (NS) and the bolt's position (BP). The parameters are depicted in Figure 15. For the shape of the notch, triangular, rectangular, and birdsmouth shapes are considered. The bolt location, which in the original design is between the notch and mid-span (BN), is studied as well when located in the notch (IN) and between the notch and the end span (AN).

Table 7. Parameters in the parametric models.

Model	Notch Depth [mm]	Notch Length [mm]	Notch Head [mm]	Notch Shape	Bolt Position
ND—06	6	121	116	Triangular	BN
ND—09	9	121	116	Triangular	BN
ND—11	11	121	116	Triangular	BN
ND—12	12	121	116	Triangular	BN
NL—100	9	100	116	Triangular	BN
NL—115	9	115	116	Triangular	BN
NL—121	9	121	116	Triangular	BN
NL—140	9	140	116	Triangular	BN
NH—100	9	121	100	Triangular	BN
NH—108	9	121	108	Triangular	BN
NH—116	9	121	116	Triangular	BN
NH—140	9	121	140	Triangular	BN
NS—B	9	121	116	Birdsmouth	BN
NS—T	9	121	116	Triangular	BN
NS—R	9	121	116	Rectangular	BN
BP—IN	9	121	116	Triangular	IN
BP—BN	9	121	116	Triangular	BN
BP—AN	9	121	116	Triangular	AN

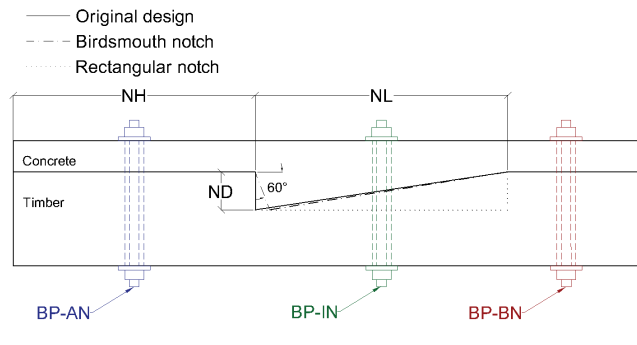


Figure 15. Parameters of the shear connection considered in the parametric study.

The ultimate load and the deflection at the ultimate load for each model are presented in Figure 16. The highest and lowest ultimate load belong to models NH-140 and BP-AN, respectively. The largest deflection at the ultimate load occurs in model NS-B. Accordingly, the bolt position has the most influence on the strength of the slab, while for the deflection at the failure, the shape of the notch is the most influential parameter.

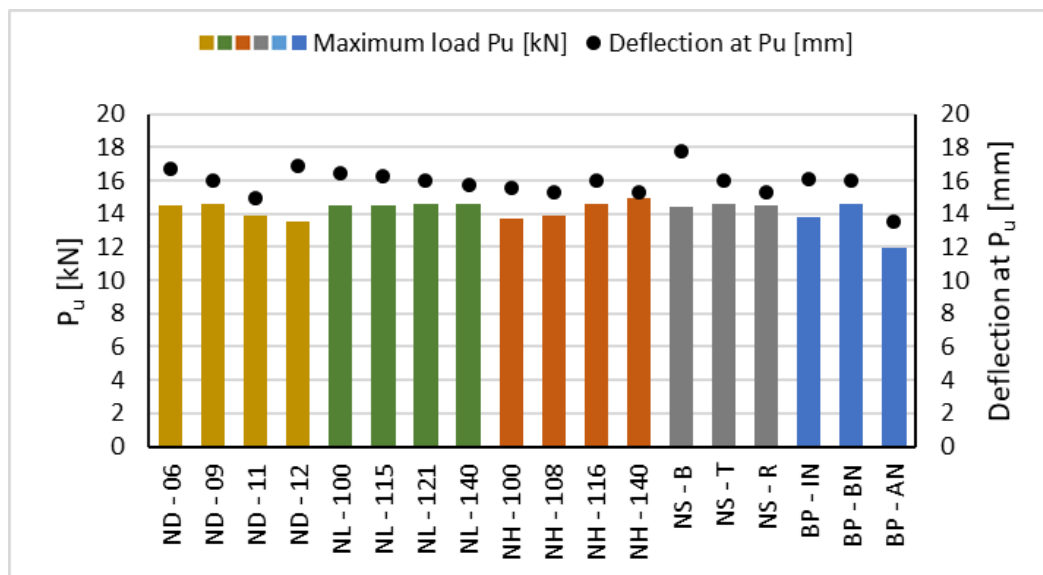


Figure 16. Results of the parametrical study.

Figures 17–21 depict the load-deflection curves and damage propagation at the failure load in the timber part for each varied parameter. The results show that the studied parameters have no noticeable influence on the stiffness of the slab, especially in the first one-third of the loading

stage. However, the impact is more noticeable in the strength and the maximum deflection before the failure of the slab. Figure 17 shows that the shape of the notch does not have a significant influence on the strength and bending stiffness of the slab, while the slab with the birdsmouth notch shows the best ductility at failure. Figure 18 shows that the bolt positions in BN and IN are not significantly different in strength and bending stiffness but having the bolt in the AN position causes the separation of concrete and timber parts between the notch and loading part and decreases the strength of the slab by approximately 20%. Figure 19 shows that the notch length does not have a noticeable effect on the bending behavior of the slab within the modeled lengths. As Figure 20 depicts, increasing the depth of the notch from 6 mm to 9 mm does not change the load-bearing capacity. However, when increasing the depth by 12 mm, the load-bearing capacity of the slab decreases by approximately 7% since the effective cross-section of the timber is reduced considerably because of the notch cut. Lastly, Figure 21 illustrates that an increase in timber length in front of the notch (the distance between the notch and the end of the slab), which concurrently increases the distance of the notch from the support, increases the strength and stiffness of the slab.

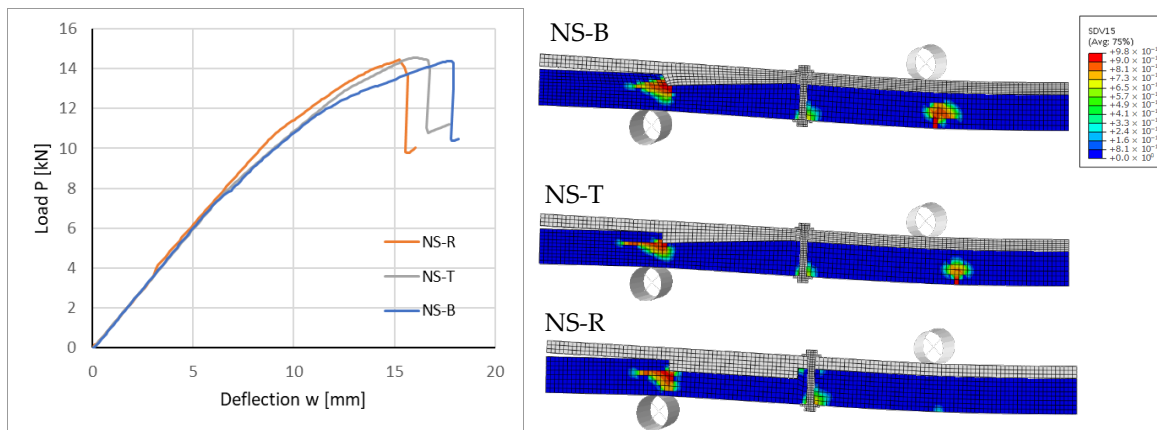


Figure 17. Influence of the shape of the notch on load deflection and failure of the TCC slab.

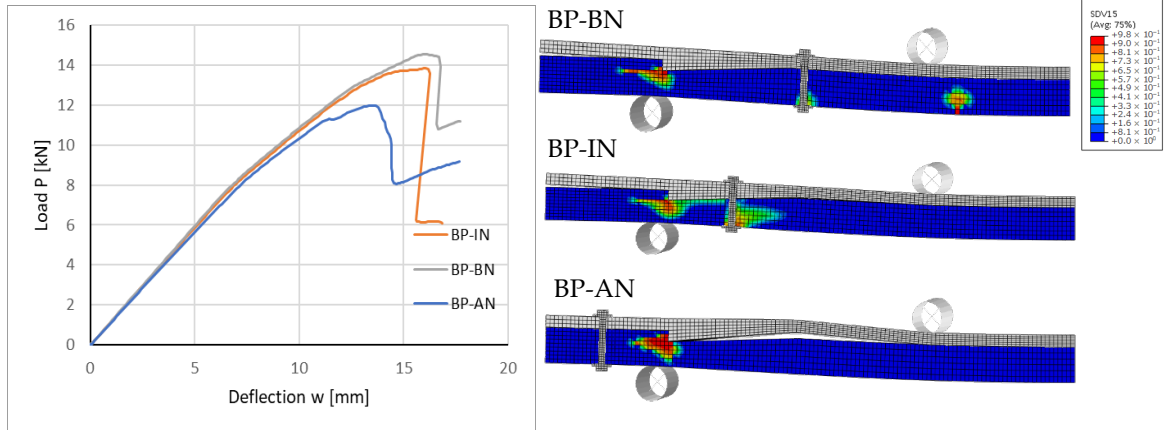


Figure 18. Influence of the position of the bolt on load deflection and failure of the TCC slab.

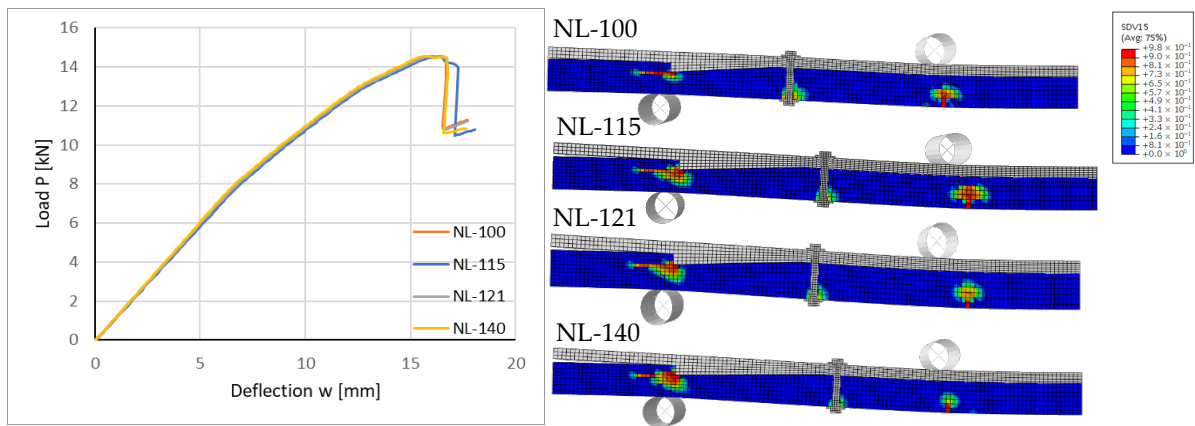


Figure 19. Influence of the length of the notch on load deflection and failure of the TCC slab.

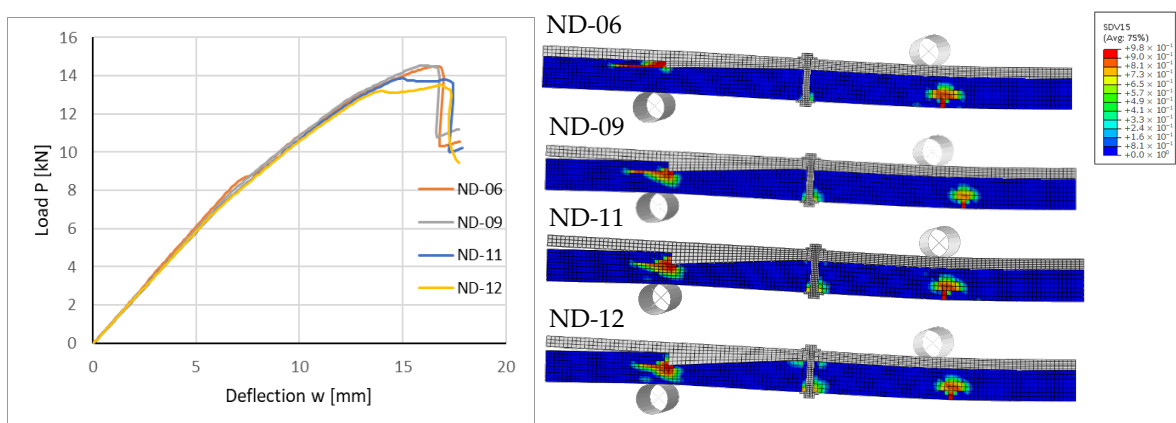


Figure 20. Influence of the depth of the notch on load deflection and failure of the TCC slab.

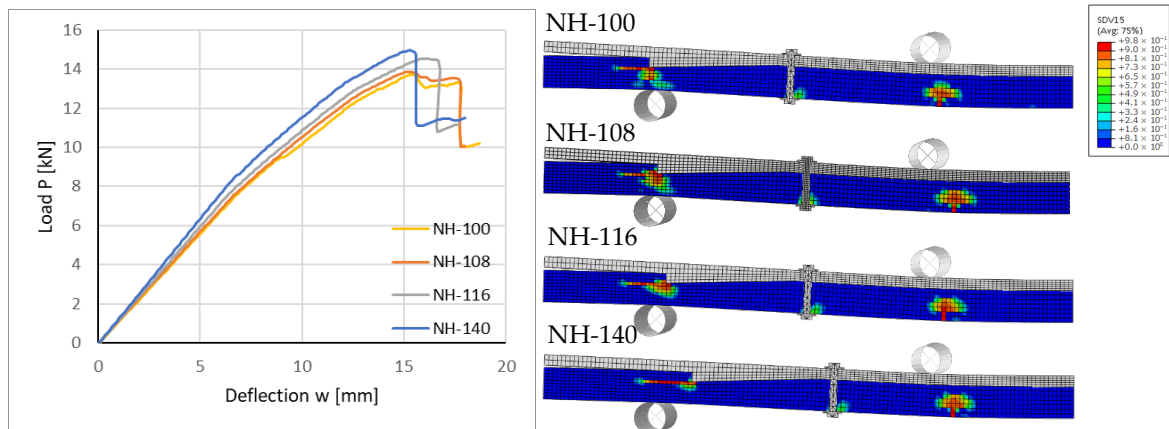


Figure 21. Influence of the timber length in front of the notch on load deflection and failure of the TCC slab.

5. Conclusions

In this study, the aim was to present and examine a novel prefabricated modular TCC floor that facilitates the construction process and can be demounted at the end of the service life. This study proposed a modular demountable slab with a notched shear connection, which can be prefabricated with a wet–dry system. The production of the downscaled specimens showed that the slab is fully demountable, and the modular wet–dry prefabrication design facilitates the fabrication process. The four-point bending experimental results showed a profound load-bearing behavior of the proposed slab. A FE model was developed, a parametric study was carried out, and variations of different parameters were studied. In brief, this study shows the following:

- The floor system is fully demountable before and after failure;
- The proposed construction method of the floor system facilitates the prefabrication and installation of the slab;
- The slab has a noticeable efficiency of 0.73 of the composite action;
- The studied parameters mostly affect the load-bearing capacity and the deflection at the failure of the slab rather than its stiffness;

- The birdsmouth notch increases the ductility of the slab compared to rectangular and triangular notches;
- The position of the bolt can vary the load-bearing capacity up to 20%;
- The length of the notch does not have a significant influence on the strength of the slab;
- An increase in the timber length in front of the notch increases the bearing capacity of the shear connection;
- An excessive increase in the notch's depth decreases the bending capacity of the slab;

This study contributes to the research field of DfD in TCC floors by featuring a straightforward, demountable shear connection with remarkable load-bearing behavior. Since the study was performed based on a downscaled model and limited specimens, more work is required to determine the load-bearing behavior, the influence of the frequency of notches and bolts, and the fabrication and deconstruction process in real-scale flexural and push-out tests. Also, since the used concrete in this study can vary from the conventional concrete, the impact of the concrete mixture must be investigated in future studies.

Author Contributions: Conceptualization, H.E., L.B.J., and D.W.; methodology, H.E. and L.B.J.; software, L.B.J.; validation, L.B.J. and D.W.; formal analysis, H.E. and L.B.J.; investigation, H.E., L.B.J., and D.W.; resources, H.E. and D.W.; data curation, H.E. and L.B.J.; writing—original draft preparation, H.E. and L.B.J.; writing—review and editing, D.W.; visualization, H.E.; supervision, D.W.; project administration, D.W.; funding acquisition, D.W. All authors have read and agreed to the published version of the manuscript.

Funding: This research is in the framework of the project Eco-Construction for Sustainable Developments (ECON4SD), supported by the program “Investissement pour la croissance et l’emploi”—European Regional Development Fund (2014–2020) (Grant agreement: 2017-02-015-15).

Data Availability Statement:

The data presented in this study are available on request from the corresponding author. The data are not publicly available due to ongoing research project.

Conflicts of Interest: The authors declare no conflicts of interest.

References

1. Gálvez-Martos, J.-L.; Styles, D.; Schoenberger, H.; Zeschmar-Lahl, B. Construction and Demolition Waste Best Management Practice in Europe. *Resour. Conserv. Recycl.* **2018**, *136*, 166–178. <https://doi.org/10.1016/j.resconrec.2018.04.016>.
2. Kanters, J. Design for Deconstruction in the Design Process: State of the Art. *Buildings* **2018**, *8*, 150. <https://doi.org/10.3390/buildings8110150>.
3. Allam, A.S.; Nik-Bakht, M. From Demolition to Deconstruction of the Built Environment: A Synthesis of the Literature. *J. Build. Eng.* **2023**, *64*, 105679. <https://doi.org/10.1016/j.jobbe.2022.105679>.
4. Zhou, H.; Lu, W.; Lu, B.; Wang, L.; Bao, Y.; Zhang, J.; Chen, Z. Experimental and Numerical Analyses on the Fire Resistance of Timber–Concrete Composite Boards Using an Innovative Form of Partial Protection. *Buildings* **2023**, *13*, 725. <https://doi.org/10.3390/buildings13030725>.
5. Ceccotti, A. Timber-Concrete Composite Structures. *Timber Eng.–STEP* **1995**, *2*, E13.
6. Dias, A.; Schänzlin, J.; Dietsch, P. Design of Timber-Concrete Composite Structures. In *A State-of-the-Art Report by COST Action FP1402/WG*; Shaker: Aachen, Germany, 2018; Volume 4.
7. Monteiro, S.; Dias, A.; Lopes, S. Distribution of Concentrated Loads in Timber-Concrete Composite Floors: Simplified Approach. *Buildings* **2020**, *10*, 32. <https://doi.org/10.3390/buildings10020032>.
8. Siddika, A.; Mamun, Md.A.A.; Aslani, F.; Zhuge, Y.; Alyousef, R.; Hajimohammadi, A. Cross-Laminated Timber–Concrete Composite Structural Floor System: A State-of-the-Art Review. *Eng. Fail. Anal.* **2021**, *130*, 105766. <https://doi.org/10.1016/j.engfailanal.2021.105766>.
9. De Santis, Y.; Sciomenta, M.; Spera, L.; Rinaldi, V.; Fragiocomo, M.; Bedon, C. Effect of Interlayer and Inclined Screw Arrangements on the Load-Bearing Capacity of Timber-Concrete Composite Connections. *Buildings* **2022**, *12*, 2076. <https://doi.org/10.3390/buildings12122076>.
10. Steinberg, E.; Selle, R.; Faust, T. Connectors for Timber–Lightweight Concrete Composite Structures. *J. Struct. Eng.* **2003**, *129*, 1538–1545. [https://doi.org/10.1061/\(ASCE\)0733-9445\(2003\)129:11\(1538\)](https://doi.org/10.1061/(ASCE)0733-9445(2003)129:11(1538)).
11. Bao, Y.; Lu, W.; Yue, K.; Zhou, H.; Lu, B.; Chen, Z. Structural Performance of Cross-Laminated Timber-Concrete Composite Floors with Inclined Self-Tapping Screws

- Bearing Unidirectional Tension-Shear Loads. *J. Build. Eng.* **2022**, *55*, 104653. <https://doi.org/10.1016/j.jobbe.2022.104653>.
12. Negrão, J.H.J. de O.; Maia de Oliveira, F.M.; Leitão de Oliveira, C.A.; Cachim, P.B. Glued Composite Timber-Concrete Beams.II: Analysis and Tests of Beam Specimens. *J. Struct. Eng.* **2010**, *136*, 1246–1254. [https://doi.org/10.1061/\(ASCE\)ST.1943-541X.0000251](https://doi.org/10.1061/(ASCE)ST.1943-541X.0000251).
 13. Clouston, P.; Civjan, S.; Bathon, L. Experimental Behavior of a Continuous Metal Connector for a Wood-Concrete Composite System. *For. Prod. J.* **2004**, *54*, 10.
 14. Xu, Q.; Wang, M.; Chen, L.; Harries, K.A.; Song, X.; Wang, Z. Mechanical Performance of Notched Shear Connections in CLT-Concrete Composite Floor. *J. Build. Eng.* **2023**, *70*, 106364. <https://doi.org/10.1016/j.jobbe.2023.106364>.
 15. Zhang, L.; Chui, Y.H.; Tomlinson, D. Experimental Investigation on the Shear Properties of Notched Connections in Mass Timber Panel-Concrete Composite Floors. *Constr. Build. Mater.* **2020**, *234*, 117375. <https://doi.org/10.1016/j.conbuildmat.2019.117375>.
 16. Boccadoro, L.; Zweidler, S.; Steiger, R.; Frangi, A. Bending Tests on Timber-Concrete Composite Members Made of Beech Laminated Veneer Lumber with Notched Connection. *Eng. Struct.* **2017**, *132*, 14–28. <https://doi.org/10.1016/j.engstruct.2016.11.029>.
 17. Van Thai, M.; Ménard, S.; Elachachi, S.M.; Galimard, P. Performance of Notched Connectors for CLT-Concrete Composite Floors. *Buildings* **2020**, *10*, 122. <https://doi.org/10.3390/buildings10070122>.
 18. Yeoh, D.; Fragiaco, M.; De Franceschi, M.; Buchanan, A.H. Experimental Tests of Notched and Plate Connectors for LVL-Concrete Composite Beams. *J. Struct. Eng.* **2011**, *137*, 261–269. [https://doi.org/10.1061/\(ASCE\)ST.1943-541X.0000288](https://doi.org/10.1061/(ASCE)ST.1943-541X.0000288).
 19. Mirdad, M.A.H.; Khan, R.; Chui, Y.H. Analytical Procedure for Timber-Concrete Composite (TCC) System with Mechanical Connectors. *Buildings* **2022**, *12*, 885. <https://doi.org/10.3390/buildings12070885>.
 20. Kuklík, P.; Nechanický, P.; Kuklíková, A. Development of Prefabricated Timber-Concrete Composite Floors. In *Materials and Joints in Timber Structures*; Aicher, S., Reinhardt, H.-W., Garrecht, H., Eds.; Springer: Dordrecht, The Netherlands, 2014; pp. 463–470. ISBN 978-94-007-7810-8.
 21. Yilmaz, S.; Demir, S.; Vural, N. Experimental Investigation of a Prefabricated Timber-Concrete Composite Floor Structure: Notched-Slab Approach. *Adv. Concr. Constr.* **2021**, *12*, 13–23. <https://doi.org/10.12989/ACC.2021.12.1.013>.
 22. Yeoh, D.; Fragiaco, M. The Design of a Semi-Prefabricated LVL-Concrete Composite Floor. *Adv. Civ. Eng.* **2012**, *2012*, 626592. <https://doi.org/10.1155/2012/626592>.
 23. Sebastian, W.; Webb, S.; Nagree, H.S. Orthogonal Distribution and Dynamic Amplification Characteristics of Partially Prefabricated Timber-Concrete Composites. *Eng. Struct.* **2020**, *219*, 110693. <https://doi.org/10.1016/j.engstruct.2020.110693>.
 24. Crocetti, R.; Sartori, T.; Tomasi, R. Innovative Timber-Concrete Composite Structures with Prefabricated FRC Slabs. *J. Struct. Eng.* **2015**, *141*, 04014224. [https://doi.org/10.1061/\(ASCE\)ST.1943-541X.0001203](https://doi.org/10.1061/(ASCE)ST.1943-541X.0001203).

25. Crocetti, R.; Sartori, T.; Flansbjerg, M. Timber-Concrete Composite Structures with Prefabricated FRC Slab. In Proceedings of the 11th World Conference on Timber Engineering, Trentino, Italy, 20-24 June 2010; Vol. 1, pp. 121–130.
26. Sartori, T.; Crocetti, R. Prefabricated Timber-Concrete Composite Floors. *Eur. J. Wood Wood Prod.* **2016**, *74*, 483–485. <https://doi.org/10.1007/s00107-016-1007-4>.
27. Lukaszewska, E.; Johnsson, H.; Fragiocomo, M. Performance of Connections for Prefabricated Timber–Concrete Composite Floors. *Mater. Struct.* **2008**, *41*, 1533–1550. <https://doi.org/10.1617/s11527-007-9346-6>.
28. Lukaszewska, E.; Fragiocomo, M.; Johnsson, H. Laboratory Tests and Numerical Analyses of Prefabricated Timber-Concrete Composite Floors. *J. Struct. Eng.* **2010**, *136*, 46–55. [https://doi.org/10.1061/\(ASCE\)ST.1943-541X.0000080](https://doi.org/10.1061/(ASCE)ST.1943-541X.0000080).
29. Shi, B.; Zhu, W.; Yang, H.; Liu, W.; Tao, H.; Ling, Z. Experimental and Theoretical Investigation of Prefabricated Timber-Concrete Composite Beams with and without Prestress. *Eng. Struct.* **2020**, *204*, 109901. <https://doi.org/10.1016/j.engstruct.2019.109901>.
30. Shi, B.; Liu, W.; Yang, H. Experimental Investigation on the Long-Term Behaviour of Prefabricated Timber-Concrete Composite Beams with Steel Plate Connections. *Constr. Build. Mater.* **2021**, *266*, 120892. <https://doi.org/10.1016/j.conbuildmat.2020.120892>.
31. Ataei, A.; Bradford, M.A.; Valipour, H. Sustainable Design of Deconstructable Steel-Concrete Composite Structures. *Procedia Eng.* **2016**, *145*, 1153–1160.
32. Hosseini, S.M.; Mashiri, F.; Mirza, O. Research and Developments on Strength and Durability Prediction of Composite Beams Utilising Bolted Shear Connectors (Review). *Eng. Fail. Anal.* **2020**, *117*, 104790. <https://doi.org/10.1016/j.engfailanal.2020.104790>.
33. He, J.; Feng, S.; Vasdravellis, G.; Xin, H.; Correia, J.A.F.O.; Berto, F. Behaviour of the Lockbolt Demountable Shear Connector under Combined Shear and Tension Loading. *Eng. Fail. Anal.* **2022**, *141*, 106712. <https://doi.org/10.1016/j.engfailanal.2022.106712>.
34. Shamel Fahmy, A.; Mostafa Swelem, S.; Kamal Abdelaziz, M. Behavior of High-Strength Demountable Bolted Shear Connectors in Steel-Concrete Girders with Prefabricated Slabs. *Alex. Eng. J.* **2023**, *70*, 247–260. <https://doi.org/10.1016/j.aej.2023.02.041>.
35. Khorsandnia, N.; Valipour, H.; Schänzlin, J.; Crews, K. Experimental Investigations of Deconstructable Timber–Concrete Composite Beams. *J. Struct. Eng.* **2016**, *142*, 04016130. [https://doi.org/10.1061/\(ASCE\)ST.1943-541X.0001607](https://doi.org/10.1061/(ASCE)ST.1943-541X.0001607).
36. Khorsandnia, N.; Valipour, H.; Bradford, M. Deconstructable Timber-Concrete Composite Beams with Panelised Slabs: Finite Element Analysis. *Constr. Build. Mater.* **2018**, *163*, 798–811. <https://doi.org/10.1016/j.conbuildmat.2017.12.169>.
37. Derikvand, M.; Fink, G. Deconstructable Connector for TCC Floors Using Self-Tapping Screws. *J. Build. Eng.* **2021**, *42*, 102495. <https://doi.org/10.1016/j.jobe.2021.102495>.
38. Derikvand, M.; Fink, G. Bending Properties of Deconstructable Cross-Laminated Timber-Concrete Composite Floor Elements. *Wood Mater. Sci. Eng.* **2022**, *17*, 253–260. <https://doi.org/10.1080/17480272.2022.2077658>.

39. Dias, A.M.P.G.; Martins, A.R.D.; Simões, L.M.C.; Providência, P.M.; Andrade, A.A.M. Statistical Analysis of Timber–Concrete Connections—Mechanical Properties. *Comput. Struct.* **2015**, *155*, 67–84. <https://doi.org/10.1016/j.compstruc.2015.02.036>.
40. Premiumzemente. Available online: <https://www.dyckerhoff.com/premiumzemente> (accessed on 4 June 2023).
41. DIN EN 196-1:1995-05, Prüfverfahren für Zement Teil 1: Bestimmung der Festigkeit 2005.
42. MasterGlenium ACE 456. Available online: <https://mbcc.sika.com/en-ae/products/masterglenium/masterglenium-ace-456> (accessed on 4 June 2023).
43. Flaga, K.; Derkowski, W.; Surma, M. Concrete Strength and Elasticity of Precast Thin-Walled Elements. *Cem. Wapno Beton* **2016**, *2016*, 310–317.
44. Comité européen de normalisation; *ILNAS-EN 338: 2016—Structural Timber—Strength Classes*. 2016.
45. Šubic, B.; Fajdiga, G.; Lopatič, J. Bending Stiffness, Load-Bearing Capacity and Flexural Rigidity of Slender Hybrid Wood-Based Beams. *Forests* **2018**, *9*, 703. <https://doi.org/10.3390/f9110703>.
46. Ceccotti, A. Composite Concrete-Timber Structures. *Prog. Struct. Eng. Mater.* **2002**, *4*, 264–275. <https://doi.org/10.1002/pse.126>.
47. Comité européen de normalisation; *ILNAS-EN 1995-1-1:2004*; Eurocode 5: Design of Timber Structures—Part 1-1: General—Common Rules and Rules for Buildings. 2004.
48. Gutkowski, R.M.; Goodman, J.R.; Pault, J.D.; Bodig, J. *Tests and Analysis for Composite Action in Glulam Bridge Systems*; The Engineering Foundation for Grant Rc-A-74-6; Colorado State University: Fort Collins, CO, USA, 1977; p. 49.
49. Dias, A.M.P.G.; Helena, C.; Lopes, S.; Kuilen, J.W.G. Experimental Shear–Friction Tests on Dowel-Type Fastener Timber–Concrete Joints. In Proceedings of the 8th World Conference on Timber Engineering, Lahti, Finland, 14–17 June 2004.
50. Rabbat, B.G.; Russell, H.G. Friction Coefficient of Steel on Concrete or Grout. *J. Struct. Eng.* **1985**, *111*, 505–515. [https://doi.org/10.1061/\(ASCE\)0733-9445\(1985\)111:3\(505\)](https://doi.org/10.1061/(ASCE)0733-9445(1985)111:3(505)).
51. Koubek, R.; Dedicova, K. *Friction of Wood on Steel*; Linnaeus University, Faculty of Technology: Växjö, Sweden, 2014.
52. SIMULIA; *Abaqus 6.11 Theory Manual*; Dassault Systèmes: Vélizy-Villacoublay, France, 2011; Chapter 4.
53. Wee, T.H.; Chin, M.S.; Mansur, M.A. Stress-Strain Relationship of High-Strength Concrete in Compression. *J. Mater. Civ. Eng.* **1996**, *8*, 70–76. [https://doi.org/10.1061/\(ASCE\)0899-1561\(1996\)8:2\(70\)](https://doi.org/10.1061/(ASCE)0899-1561(1996)8:2(70)).
54. Olsen, N.H.; Krenchel, H.; Shah, S.P. Mechanical Properties of High Strength Concrete. *IABSE Rep.* **1987**, *55*, 395–400. <https://doi.org/10.5169/SEALS-42754>.
55. Carreira, D.J.; Chu, K.-H. Stress-Strain Relationship for Plain Concrete in Compression. *ACI J. Proc.* **1985**, *82*, 797–804. <https://doi.org/10.14359/10390>.

56. Federation internationale du beton; Beverly, P. *Fib Model Code for Concrete Structures 2010*; Ernst & Sohn: Berlin, Germany, 2013; ISBN 978-3-433-60421-2.
57. Eslami, H.; Jayasinghe, L.B.; Waldmann, D. Nonlinear Three-Dimensional Anisotropic Material Model for Failure Analysis of Timber. *Eng. Fail. Anal.* **2021**, *130*, 105764. <https://doi.org/10.1016/j.engfailanal.2021.105764>.
58. Hoffman, O. The Brittle Strength of Orthotropic Materials. *J. Compos. Mater.* **1967**, *1*, 200–206. <https://doi.org/10.1177/002199836700100210>.
59. Hill, R. A Theory of the Yielding and Plastic Flow of Anisotropic Metals. *Proc. R. Soc. Lond. Ser. A Math. Phys. Sci.* **1948**, *193*, 281–297. <https://doi.org/10.1098/rspa.1948.0045>.

Disclaimer/Publisher’s Note: The statements, opinions and data contained in all publications are solely those of the individual author(s) and contributor(s) and not of MDPI and/or the editor(s). MDPI and/or the editor(s) disclaim responsibility for any injury to people or property resulting from any ideas, methods, instructions or products referred to in the content.

3.5 Paper V

The paper “Experimental and numerical study on shear behavior of a demountable CLT-concrete composite shear connection” [95] was published in *Construction and Building Materials* journal. The author of the dissertation served as the first author and his contribution was conceptualization, methodology, formal analysis, investigation, resources, data curation, writing—original draft preparation and visualization of the paper.

Experimental and numerical study on shear behavior of a demountable CLT-concrete composite shear connection

Hooman Eslami^a, Laddu Bhagya Jayasinghe^b, Daniele Waldmann^{c*}

^a Faculty of Science, Technology, and Medicine (FSTM), University of Luxembourg, Luxembourg

^b Department of Earth and Environmental Sciences, Ludwig-Maximilians-Universität München, Germany

^c Institute for Solid Structures, Technical University of Darmstadt, Germany

*Corresponding author: waldmann@massivbau.tu-darmstadt.de, Franziska-Braun Str. 3, 64287 Darmstadt, Germany

Abstract

Recently, there has been a growing interest in using Cross-Laminated Timber (CLT) in the construction industry, particularly as slabs and walls. This heightened interest is attributed to CLT's favorable mechanical properties, ease of prefabrication, and environmental advantages. Consequently, CLT-Concrete Composite (CCC) floor systems have gained more attention for their application in mid- and high-rise buildings. These CCC systems offer substantial advantages over standalone CLT slabs, including enhanced bending stiffness, increased load-bearing capacity, and improved dynamic performance. However, a notable research gap exists when it comes to the deconstruction of CCC slabs, a crucial aspect for enhancing sustainability and reducing the environmental impacts of these structural elements. This study investigates innovative demountable shear connections designed for a reusable prefabricated CCC floor system. A series of push-out tests were conducted on six different shear connectors to obtain the shear properties of the connection. The demountable shear connections exhibited a load-bearing capacity similar to conventional permanent connections. Moreover, these connections demonstrated a significantly higher stiffness than existing options. One specimen was examined in a reuse scenario test to evaluate its reusability, which revealed a notable increase in stiffness during its second use. A three-dimensional finite element model of the push-out

test was validated and calibrated with the experimental results. This model was utilized to study the load-bearing behavior of the notched connections.

Keywords: Timber-concrete composite; CLT-concrete composite; Demountable shear connection; Design for Deconstruction; Push-out test

1. Introduction

The building industry is responsible for significant natural resource consumption and waste production [1,2]. The manufacturing processes of conventional construction materials such as steel and concrete are energy-consuming and contribute significantly to carbon dioxide emissions [3]. Consequently, in the last decades, substantial attention has been devoted to fostering the usage of timber and engineered wood products (EWPs) [4]. They are more sustainable due to their low embodied energy, high carbon storage, and renewability [5]. Other characteristics of timber, such as its high strength-to-density ratio, desirable aesthetic, and low thermal conductivity, made it a good solution for substituting steel and concrete in structural elements [6–8].

However, when considering timber solutions such as slabs and beams, some unfavorable features such as springiness, vibration, and poor sound insulation are challenging for designers [9,10]. These defaults led to an increased usage of timber as a hybrid structure with concrete [11]. Timber-concrete composite (TCC) floors consist of a concrete slab on top of the timber part as a joist or slab connected through a shear connection [12]. The shear connection determines the level of composite action between the two components under bending [13]. The concrete component resists the compression dominantly and the timber component undertakes the tension [14]. A well-developed TCC system can enhance the bending capacity of a conventional timber floor by a factor of 3 to 5 [15]. This method reduces the amount of concrete used, which causes a decrease in self-weight and carbon dioxide emissions. Research findings

show that TCC slabs can exhibit a 30% [16] to 70% [17] reduction in global warming potential compared to concrete slabs of equivalent flexural properties. As a result, many researchers focused on developing new TCC slabs and shear connections [18,19]. In TCC slabs, the timber component can comprise joists or a panel-type EWP. Panel-type EWPs became substitutes for conventional timber joists as the demand for prefabrication and rapid on-site assembly grew [20].

Cross Laminated Timber (CLT) is a panel-type EWP with substantial appeal in the construction industry. It offers benefits such as orthogonal rigidity, sound and thermal insulation properties, and efficient prefabrication [21,22]. CLT has rapidly found its way into TCC floor systems as a prominent panel-type EWP. CLT-Concrete Composite (CCC) floor has all the benefits of a TCC floor system. The adoption of CCC floor systems in mid- and high-rise buildings, as opposed to traditional timber joist TCC slabs, can lead to a decrease of up to 30 cm in the overall thickness of the slab per floor [23]. Although contingent on factors like span length and joist separation, this reduction potentially translates to gaining an extra floor in a 10-story building for a predetermined total height.

Accordingly, many investigations have been done on CCC floor systems in recent years. Mai et al. studied the shear [24] and bending [25] behavior of CCC shear connections made of mechanical fasteners with various connection types, angles and spacing. The results showed that the inclined fasteners outperformed orthogonal connectors in terms of stiffness. The study compared the performance of a CLT panel to another CLT panel with the same thickness but with an additional 100mm concrete topping. The findings revealed improvements in vibration behavior by up to 25% and an enhancement in bending capacity from 3 to 5 times. Wang et al. [26] investigated the shear performance of the self-tapping screw shear connection between CLT and concrete. The results showed that the screw configuration, inclination angle, and thread type are the main affective factors in the stiffness of the connection. The maximum load

of the connection was most significantly influenced by factors such as screw configuration, inclination angle, and penetration length into CLT. Although mechanical fasteners are cheap and easy to install, they show a lower stiffness and strength compared to other types of shear connections.

Gerber and Tannert [27] tested TCC floors with three panel-type EWPs, including CLT, Laminated Veneer Lumber (LVL), and Laminated Strand Lumber (LSL). These EWPs were fastened using screws and adhesive-bonded steel mesh as the shear connection. Higgins et al. [28] carried out short-term and long-term tests on a full-scale CCC floor. They found that the HBV system has superior performance, providing close to the full composite action. The HBV system comprises a perforated steel plate, with its lower section glued within a groove in timber, while its upper segment is embedded within concrete [29]. In another study, Tannert et al. [30] did short- and long-term tests on CCC with self-tapping screws, HBV and epoxy adhesive. In the long-term study of about 2.5 years, the effective bending stiffness and the load-bearing capacity of the tested TCC panels degraded on average by 16% and 5%, respectively. During the same time, the vibration performance did not change noticeably.

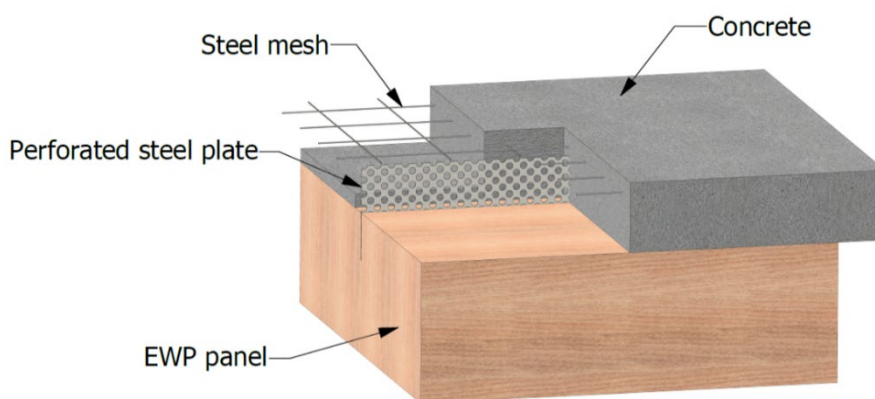


Figure 1 HBV system as a timber-concrete composite shear connection. The figure is rebuilt based on [29].

An alternative method to achieving a rigid connection between timber and concrete involves gluing the two materials using adhesives [31]. While this approach yields a high degree of shear connection, when wet glue is used to bond the wet concrete to the CLT panel, the deflection due to shrinkage can consist of about 60% of the total deflection after 125 days [32,33]. Bajzecerova et al. [33] tried to overcome this deflection by prestressing the CLT panel before casting the concrete. The CLT panel was precambered about 0.01 of the span length. The results of the long-term loading showed that the precambered was enough to eliminate the deflection from shrinkage. In addition, they estimated that prestressing a CCC slab would increase the load-bearing capacity by about 20%.

Notch shear connections are another suitable connection type used in CCC slabs because of their reliability, strength, stiffness, and cost-effectiveness [34]. The parametric experimental study of Thai et al. [23] showed that the notch's depth and heel length (timber length ahead of the notch) significantly impact the connection's stiffness and maximum load, unlike concrete thickness and length of the screw, which did not demonstrate significant influence. In addition, they found that the notched connection with removable screws has the potential for disassembly. The bending test results by Lamothe et al. [35] on a CCC slab employing high-performance concrete and ultra-high-performance fiber-reinforced concrete demonstrated the feasibility of achieving a ductile floor system with a notch connection. As the moisture from concrete can cause delamination between the laminae of the CLT panel, it is vital to limit the moisture transfer between concrete and timber by separation layers [36]. However, an experiment conducted [35] on slabs with notch connections revealed that using a separation layer between the concrete and timber reduced the stiffness of the slabs as it diminished the interaction of the two materials at the notch. Xu et al. [37] found that adding glue or self-tapping screws to a notch connection can reinforce the shear capacity of a notch CCC system. Shear connections with steel kerf plates, examined by Shahnewaz et al. [38] in a 10-story mass

timber building, proved highly efficient and provided exceptional stiffness and strength to the floor system. The authors recommended maintaining an embedment depth not exceeding the thickness of the first layer in the CLT panel to prevent the timber's rolling shear strength from governing the slab's failure.

Furthermore, the shear connection impacts the mechanical performance of the TCC slab and influences its construction method. The fabrication methods of TCC floors can be divided into two categories: wet-dry and dry-dry. In the wet-dry process [39–41], the timber part is generally put in place on the construction site and the cast-in-situ concrete is poured on the timber part. In this method, the shear connection is usually installed on the timber part before pouring the concrete and then embedded in it. Therefore, the wet-dry shear connectors usually generate a permanent bond between the two materials. In the dry-dry method [42–44], the concrete is prefabricated with the shear connection embedded inside and bolted or glued to timber. The advantage of the dry-dry method is that it allows the prefabrication of the TCC slab, resulting in various benefits, including reduced waste, material consumption, and labor costs. Simultaneously, it enhances the construction process's safety, speed, and precision [45–47]. Several studies developed prefabricated TCC floor systems in the last two decades. Lukaszewska [48] investigated the feasibility of prefabrication by embedded connection in a precast concrete slab, which will later be installed on-site on the timber joist. Yeoh et al. [49] explored semi-prefabricated LVL joists and plywood sheets with preassembled connections and cast-in-situ concrete on top. Researchers performed different experiments to develop prefabricated TCC floors, such as shear tests [50], short-term [51] and long-term [52] 4-point bending tests. The results showed that the prefabricated TCC slabs are feasible, reliable, and beneficial.

Although prefabricated TCC floors were studied, not much effort has been put into the possibility of deconstruction and reusability of this kind of slab. Concerning the quest for more

sustainable construction, design for deconstruction (DfD) [53] is essential in reducing the use of material and construction and demolition waste. DfD elements can be demounted, reused, repaired, and recycled with minimum energy, time, and resource consumption [54]. Although some of the prefabricated TCC floors can be deconstructed, only a few researchers attempted to investigate this issue in TCC floors. Khorsandinia et al. [55] investigated the bending performance of several demountable TCC beams manufactured from LVL joists and concrete segments. The construction and deconstruction processes were successfully performed. A 1D and 2D finite element models were developed to simulate the nonlinear behavior of these beams [56]. Wacker et al. [57] performed static, cyclic and fatigue push-out and bending tests on a reusable TCC system for bridge decks. The results showed while the load capacity was slightly decreased, the stiffness was increased under cyclic and fatigue loading. Derikvand and Fink [58] studied the shear behavior of demountable connections using self-tapping screws. The demountable connections performed similar shear behavior and properties to the permanent ones. The Authors investigated the shear connection under bending on a CCC slab [59]. Once again, the results confirmed the similar static and dynamic behavior between the demountable CCC slab and a comparable non-detachable one. Pang et al. [60] developed and tested separable CCC floors with round-notch shape shear connections. They employed a high-sulfated calcium silicate cement-infused concrete, limiting energy demands during cement production. Despite push-out test outcomes indicating a lower slip modulus than similar notched connections, the researchers discovered that the composite slab outperformed a pure CLT slab. Specifically, the composite design allowed for 1.9 and 1.5 times longer spans, aligning with load bearing and deflection limits.

The practical application of demountable TCC floors is constrained by limited research and challenges, including the absence of adaptable connection systems and higher initial costs than existing systems [61]. Accordingly, in a previous study [62], the authors of this paper addressed

these gaps in the field by proposing a modular prefabricated TCC floor system with a demountable shear connection. As illustrated in Figure 2, the concept was designed to offer a straightforward prefabricated TCC modular slab, facilitating reuse at the module level. Subsequently, upon reaching the end of its lifecycle, the demountable shear connection enables the effortless separation of the two materials for separate recycling or reuse purposes.

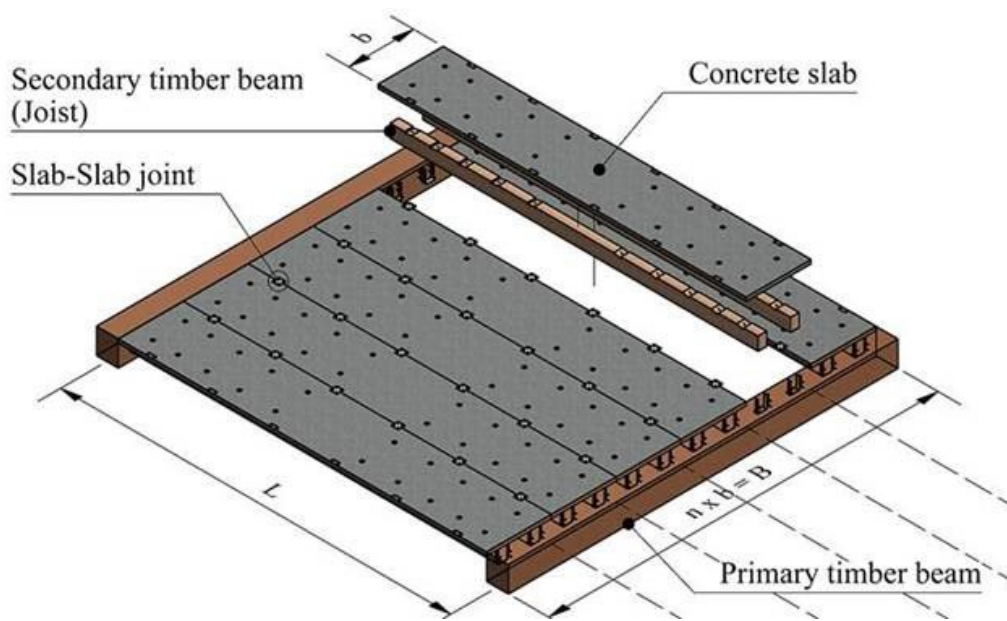


Figure 2 Conceptual design of the demountable TCC floor system with the demountable shear connection. Figure from Eslami et al.[62].

Building upon the findings of the downscaled study [62], which highlighted the significant potential of the proposed concept, this paper presents the results of a real-scaled parametric investigation for a demountable CCC floor system. Six connection variations were tested under push-out tests, wherein their shear performance, maximum strength, and failure modes were investigated. A three-dimensional nonlinear finite element (FE) model was developed and validated with the experimental results. Subsequently, the FE model was applied to study the load-bearing behavior of the connections.

2. Experimental study

2.1 Materials and setup

The experiment setup contains a CLT panel with a thickness of 280 mm comprised of 7 layers with varying thicknesses of 60 mm, 40 mm, 20 mm, 40 mm, 20 mm, 40 mm, and 60 mm. The CLT panel is positioned between and being pushed against two concrete layers with a thickness of 100 mm. As shown in Figure 3 (left), a notch in the CLT on each side linked the two materials with the company of a fastened rod to overcome the uplift caused by the eccentric force at the shear connection. The CLT panel and the concrete layers, including the notch, have an identical width of 300 mm. Six samples of the shear connection were designed, and four specimens were cast for each sample. The variables between the samples were the notch's shape and heel length. The drawings for all samples are shown in Figure 4.

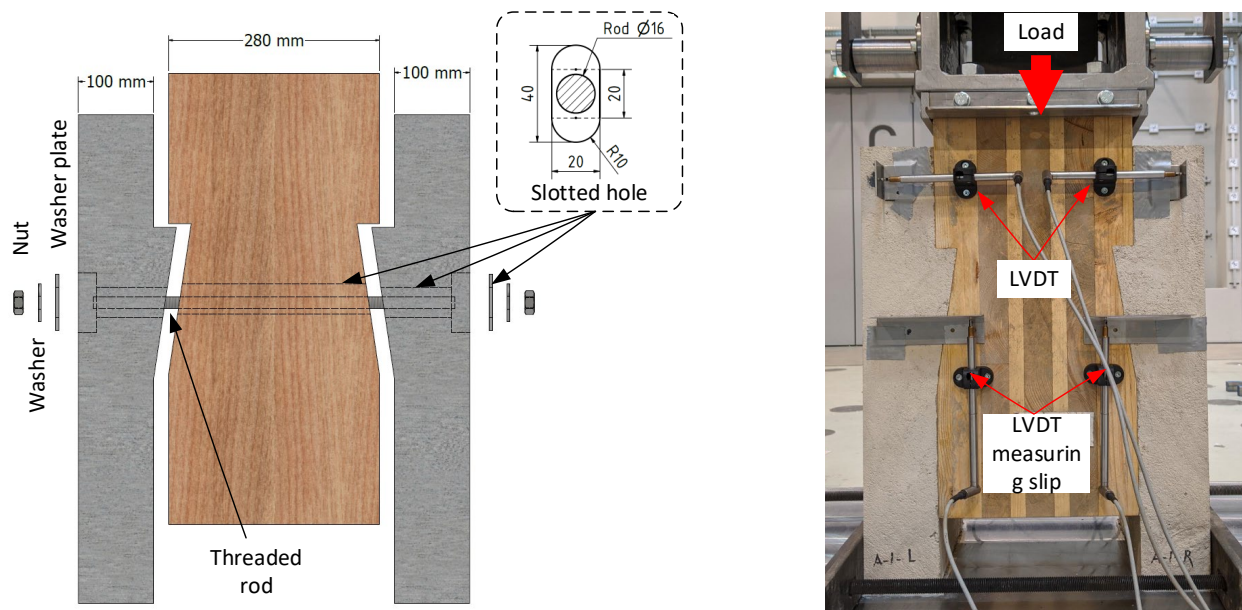


Figure 3 Assembly of the specimens (left) and the experiment setup (right).

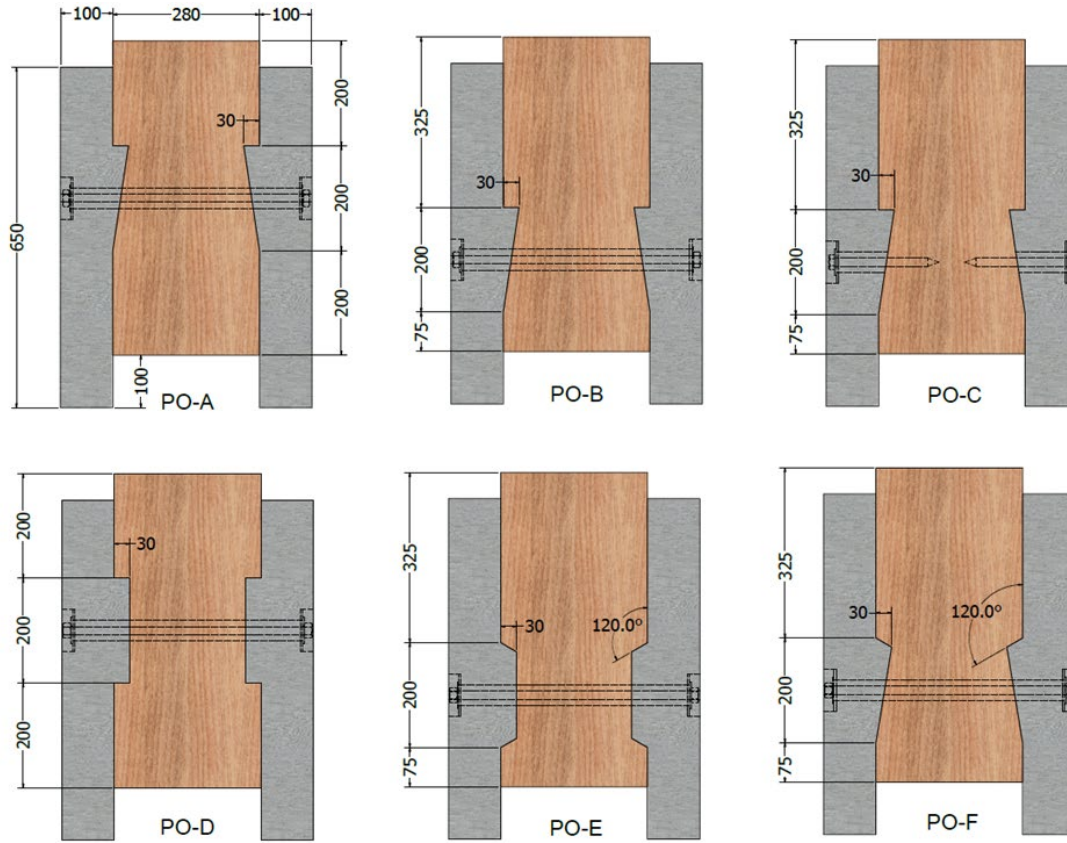


Figure 4 Drawing of all push-out samples. Dimensions are in mm.

The CLT parts were cut with the notches and holes for the rod. Then, the required formworks were used to cast the concrete directly on CLT (Figure 5). The hole for the rod was considered as a slotted hole as illustrated in Figure 3 (left) in both CLT and concrete to allow the rod to keep the two materials together without undertaking direct shear. Only in sample C M16 lag screws were used instead of the rod. For this sample, the same hole was precast in concrete, but in the CLT part, holes with a diameter of 12 mm were predrilled to avoid splitting the timber when installing the lag screw. When the concrete was hardened, the formworks were removed. Then the rods and nuts or screws attached the concrete layers to the CLT panel. The properties of all the used fasteners can be found in Table1.

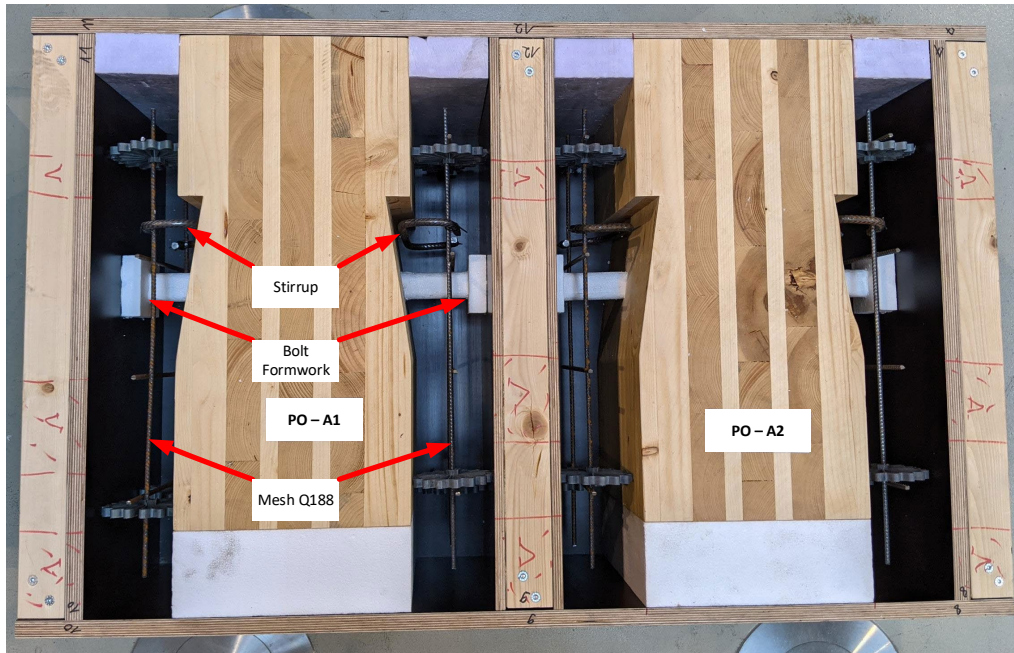






Figure 5 Push-out specimens ready for concreting.

Table 1 List of fasteners used in the experiment and their properties.

Part	Image	Standard	Nominal diameter [mm]	Source of image and property details
Threaded rod		DIN 976-1	16	[63]
Lag screw		DIN 571	16	[64]
Washer		DIN 9021	17	[65]
Nut		DIN 934	16	[66]

The experiment was undertaken in the Laboratory of Solid Structures at the University of Luxembourg. The mechanical properties of the concrete were tested to determine the compression strength, modulus of elasticity and tensile strength, which were, on average, 50.6 MPa, 38.8 GPa and 4.0 MPa [67–69]. The CLT panel comprised C24 timber boards

manufactured based on ETA-06/0009 [70]. The material properties for C24 timber based on EN 338:2009 [71] are shown in Table 2. Additional shear tests were performed on the timber parts cut out of the CLT panel near the failure area after the push-out test. The push-out test was performed in a symmetric setup, as shown in Figure 3 (right). Four LVDT displacement sensors (two on each side) measured the horizontal gap, and four others measured the vertical slip between concrete and timber. The final slip was calculated as average of the four vertical LVDTs. No significant disparity was observed between the measurements of the sensors.

Table 2: Timber C24 characteristic values according to EN 338:2009[71].

Strength properties [N/mm ²]	C24
Bending	24
Tension parallel	14
Tension perpendicular	0.4
Compression parallel	21
Compression perpendicular	2.5
Shear	4
Shear (test)	4.14
Stiffness properties [N/mm ²]	
Mean modulus of elasticity parallel	11000
Mean modulus of elasticity perpendicular	370
Mean shear modulus	690
Mean density [kg/m ³]	420

2.2 Loading configuration

The loading was performed according to EN26891 [72], originally used for timber joints made with mechanical fasteners. However, it has also been used for push-out tests on TCC shear connections. The estimated maximum load F_{est} was initially calculated through analytical design for each sample. If the disparity between the maximum load F_{max} derived from tests and F_{est} exceeded 20%, F_{est} was recalculated for the rest of the specimens based on the previously measured F_{max} . As shown in Figure 6, the loading procedure started with an initial increase of up to 40% of F_{est} . Once this load was reached, the specimen was unloaded to 10% F_{est} . Then,

the loading continued until the specimen failed or the connection slip exceeded 15mm, whichever came first.

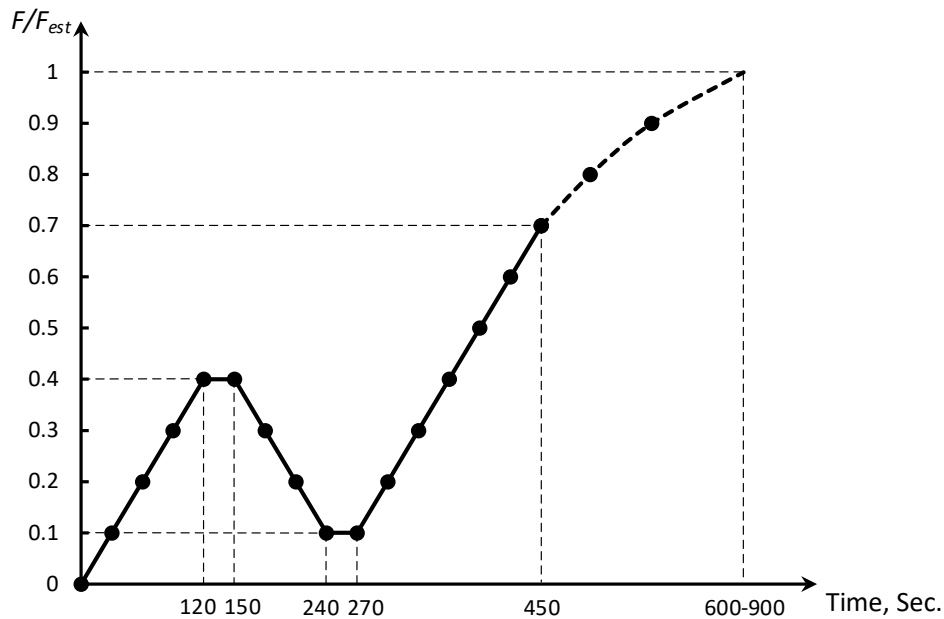


Figure 6 Loading procedure according to EN 26891 [72].

Two different loading configurations were tested and compared on sample A. In the first loading configuration tested on specimens A1 and A2, the load was implemented on the entire section of the CLT panel. This loading configuration did not allow the shear failure in timber since the CLT was confined to the loading plate. On the other hand, in the second loading configuration implemented on specimens A3 and A4, the loading plate implemented the load partially on the CLT section at a distance from the edge of the CLT panel to allow the shear failure. The second loading configuration imitates the last notch toward the end span of a TCC slab. In contrast, the first loading configuration represents the other notches toward the mid-span of the slab. The two loading configurations and the corresponding load-slip results are shown in Figure 7. A shear failure in timber occurred for both specimens with the second load configuration. In comparison, ductile compression failure in timber (specimen A1) and shear failure in concrete (specimen A2) happened for the specimens with the first load configuration.

The results show that the stiffness and strength of the connections loaded with the first load configuration are about 20% higher than those with the second. As the second loading configuration feature is more critical, it seemed more appropriate for testing the notch connection between timber and concrete. Therefore, this loading configuration was used for the rest of the experiment.

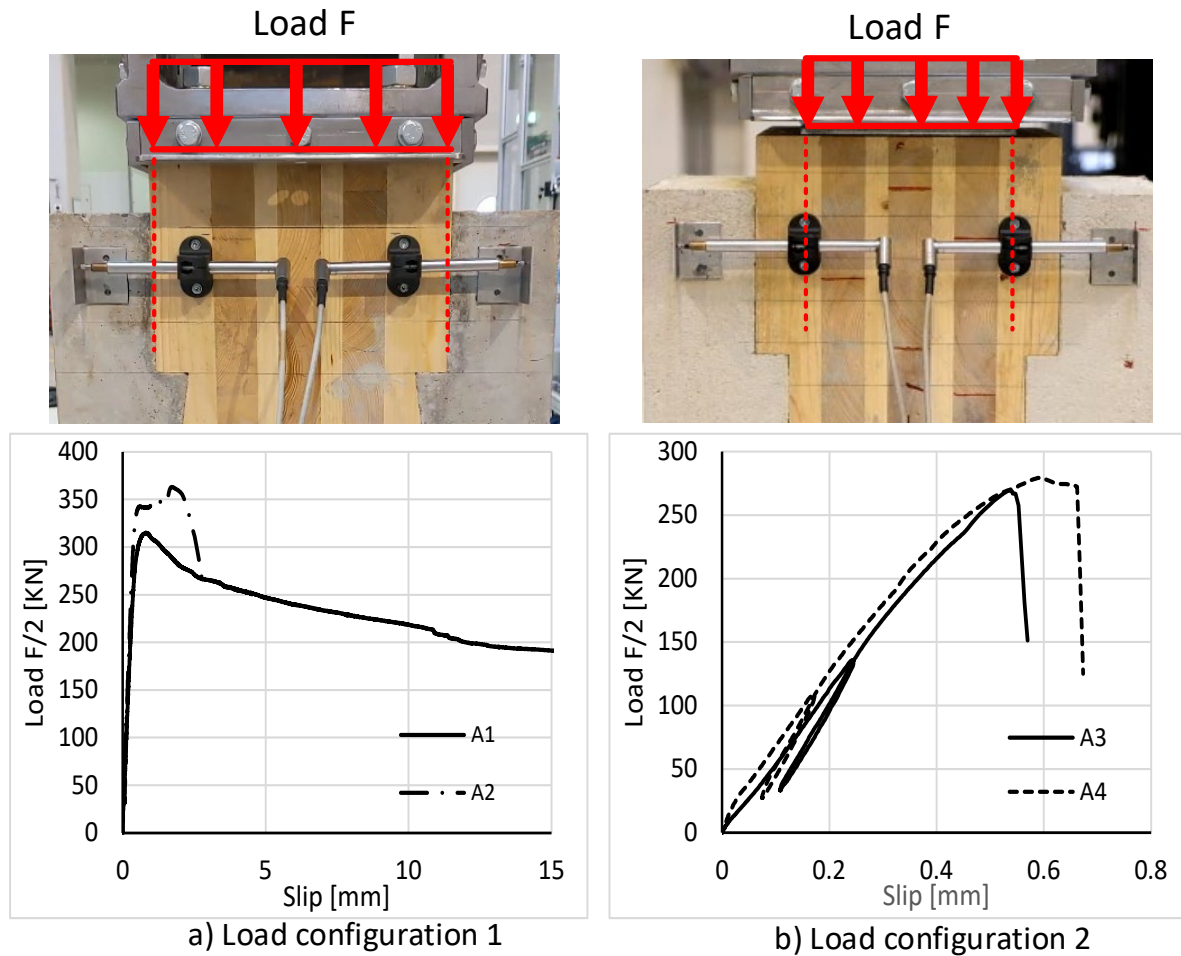


Figure 7 Comparison of the results and setup of different load configurations of the push-out test with loading a) entire and b) partial surface of the CLT section.

2.3 Failure modes

Figure 8 illustrates the observed failures during the test. The rod and screw, explicitly designed to avoid direct shear forces, showed no signs of failure or permanent deformation. In all specimens, as the load increased, a crack initiated and propagated in the concrete, originating

from the notch and extending toward the concrete's surface (Figure 8a). Specimen A2 exhibited shear failure in concrete at the notch due to the extensive opening of this crack, as depicted in Figure 8b. Moreover, concrete crushing under compression was observed in some specimens (Figure 8c). The observed failures in the CLT panel involved both compression-induced crushing and longitudinal shear failure of the timber, as depicted in Figure 8d and Figure 8e, respectively. Furthermore, as shown in Figure 8f, rolling shear failure was observed in the second layer of the CLT panel in specimen C4, attributed to the embedment of the screw in the second and third layers of the CLT panel. While the shear failure in concrete and timber resulted in a brittle failure, the compression crushing in both timber and concrete was ductile. The failure modes that occurred for each specimen are noted in Table 3.

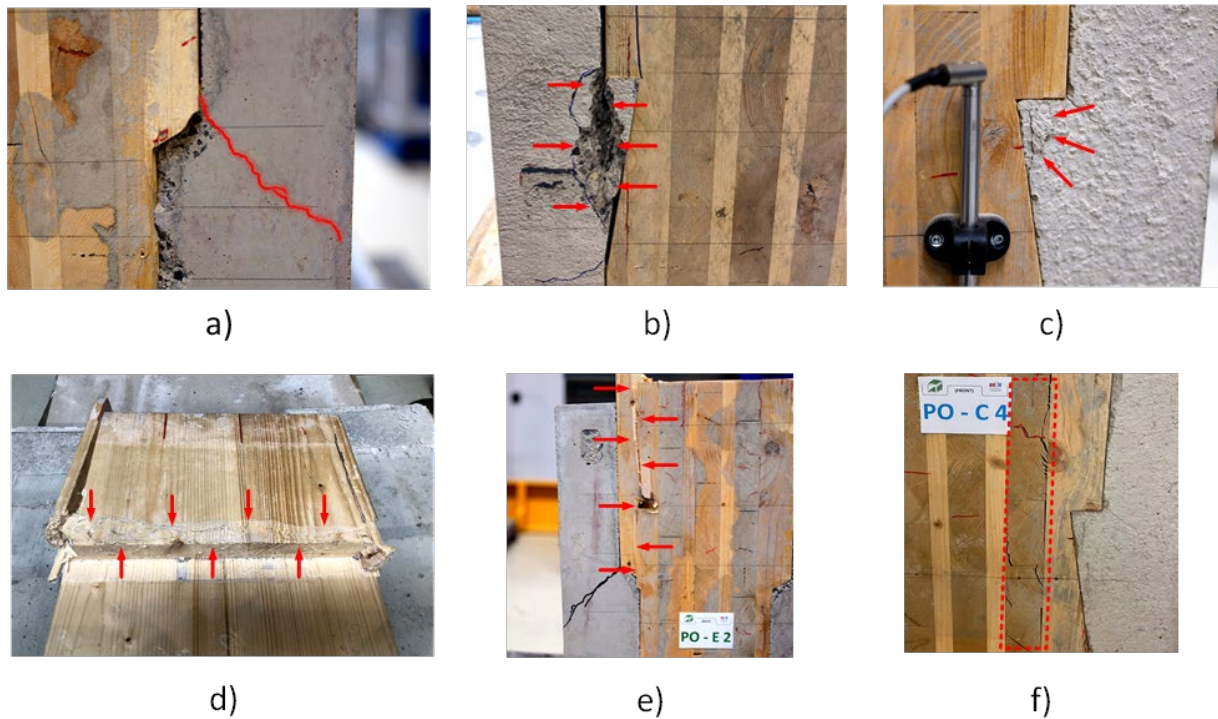


Figure 8 Failure modes of the notched connection: a) crack in concrete; b) shear failure at the notch; c) crushing of concrete; d) compression failure in timber at the face of the notch; e) shear failure in timber; f) rolling shear failure in CLT.

Table 3 Calculated F_{est} and failure modes occurred for all specimens according to the modes presented in Figure 8.

Specimen	F_{est}	Failure mode					
		a	b	c	d	e	f
A3	340	X				X	
A4	270	X				X	
B1	320	X		X		X	
B2	285	X	X	X		X	
B3	285	X		X		X	
B4	285	X	X	X	X	X	
C1	260	X		X		X	
C3	325	X				X	
C4	325					X	X
D1	225	X				X	
D3	270	X				X	
D4	270					X	
E1	345	X		X	X		
E2	345	X		X		X	
E4	320	X			X	X	
F1	280			X		X	
F2	275	X		X	X		
F3	265	X		X	X		
F4	275	X		X	X	X	

2.4 Results and discussion

The load-slip results of all specimens are shown in Figure 9. In these curves, the slip is the average of the 4 vertical LVDTs, and the load is the measured load on the specimens divided by two to represent the load on each shear connection. As the load-slip diagrams depict, minor settlements were evident in the subsequent initial loading and unloading stage, ranging from 0.08 mm for sample D to 0.3 mm for sample F. Further loading led to a gradual linear increase in slip for all specimens, reaching approximately 80% of the maximum load. After the linear stage, a softening in the shear connection stiffness can be observed until reaching the maximum load. Upon reaching the maximum load, two distinct behaviors became evident. The first behavior was a brittle failure in most specimens without further deformation, attributed to timber's brittle shear failure. The second behavior involved more deformation after the

maximum load. Specimens B4 and F4 showed a plastic deformation after the maximum load and then a brittle failure, while specimens E1, F2 and F3 showed a plastic slip until the test finished at the slip of 15 mm without a brittle failure.

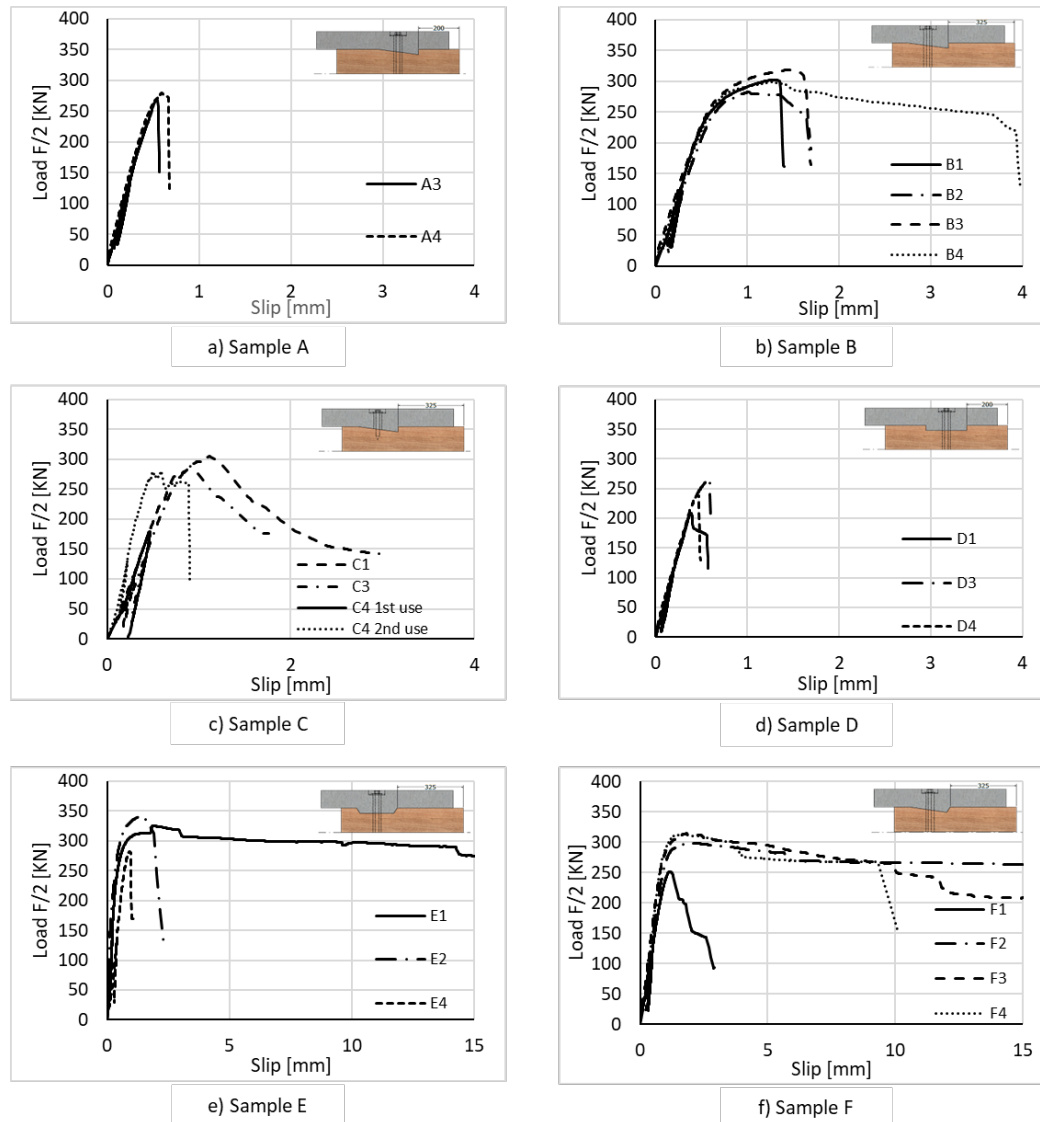


Figure 9 Load-slip results of all the push-out specimens.

The results from the experiment, including maximum load F_{\max} , slip at the maximum load v_{\max} , and slip modulus from different load stages, are presented in Table 4. Sample D has the minimum average strength, while sample E has the highest. Figure 10 shows that longer notch heel lengths (samples B, C, E, and F) are associated with higher F_{\max} , indicating a correlation between connection strength and heel length. Samples E and F exhibited increased v_{\max} ,

suggesting more significant deformation in these connections than in others. This trend is visually noticeable in the load-slip diagrams in Figure 9. The percentage coefficient of variation (CV%) for F_{\max} ranges from 2.6% (sample A) to 11.9% (sample D), while for v_{\max} , CV% varies from 14.5% (sample B) to 46.2% (sample A). The increased variability in slip at the maximum load can be attributed to the sophisticated behavior of the connection, influenced by variations in material properties and inherent imperfections in fabrication.

Table 4 Results from the experiment.

Series		A	B	C	D	E	F
No. of specimens		2	4	3	3	3	4
F_{\max} [kN]	Average	274.4	300.3	291.2	237.4	316.1	294.0
	SD ^a	7.1	14.7	12.7	28.3	30.4	29.3
	CV% ^b	2.6%	4.9%	4.4%	11.9%	9.6%	10.0%
v_{\max} [mm]	Average	0.6	1.3	0.9	0.5	1.4	1.7
	SD	0.04	0.18	0.22	0.11	0.47	0.40
	CV%	6.7%	14.5%	24.7%	22.2%	33.8%	24.0%
K_i [kN/mm]	Average	604.4	465.2	393.7	589.6	493.6	289.6
	SD	59.6	42.5	78.6	25.3	228.3	33.8
	CV%	9.9%	9.1%	20.0%	4.3%	46.3%	11.7%
K_s [kN/mm]	Average	786.3	757.9	901.9	769.3	1019.9	741.7
	SD	56.4	99.9	238.0	95.2	146.4	148.9
	CV%	7.2%	13.2%	26.4%	12.4%	14.4%	20.1%
$K_{0.6}$ [kN/mm]	Average	719.2	628.7	748.7	721.8	861.9	533.0
	SD	3.8	74.3	192.3	67.5	89.5	55.1
	CV%	0.5%	11.8%	25.7%	9.4%	10.4%	10.3%
$K_{0.8}$ [kN/mm]	Average	641.9	525.1	639.7	649.3	638.1	432.5
	SD	0.9	35.7	162.4	39.3	34.1	45.3
	CV%	0.1%	6.8%	25.4%	6.1%	5.3%	10.5%

^a Standard deviation; ^b Percentage coefficient of variation

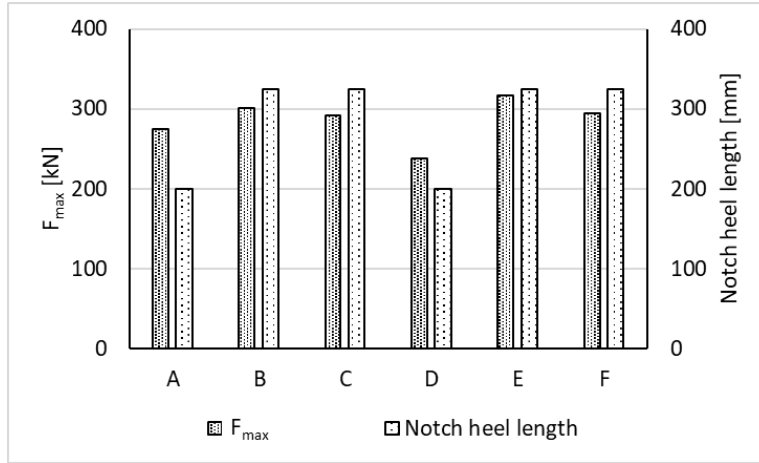


Figure 10 Comparison of the experiment results for the maximum load and the length of the notch heel.

The slip moduli were calculated based on the slope of the lines shown in Figure 11. As demonstrated, the initial slip modulus K_i is calculated at the first loading cycle. The serviceability slip modulus K_s is calculated in the second loading cycle at 40% F_{est} . $K_{0.6}$ and $K_{0.8}$ represent the slip moduli at 60% and 80% of F_{est} , respectively, marking the ultimate and close-to-failure load states. As illustrated, the initial settlement is not considered in the K_s , $K_{0.6}$, and $K_{0.8}$ calculations. The average slip modulus results for each connection sample are presented in Table 4. For all samples, the highest slip modulus is at K_s , and the slip modulus decreases with the load increase. Samples E and C have the highest slip modulus, while the values for the rest do not differentiate noticeably. The CV% of the results for K_s ranges from 7.20% (sample A) to 26.40% (sample C). The disparity of the results decreases for $K_{0.6}$ and $K_{0.8}$.

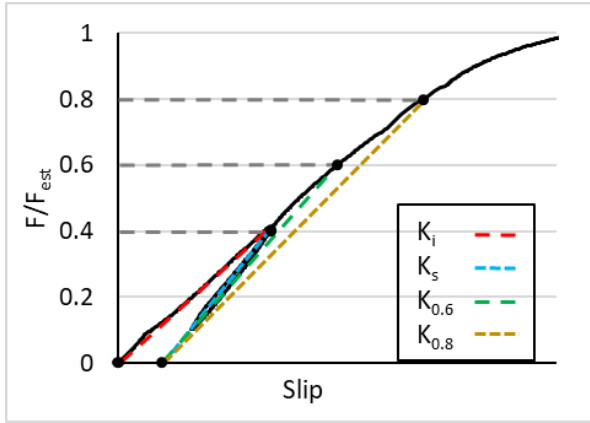


Figure 11 Demonstration of calculated slip modulus as the slope of the demonstrated lines for initial (K_i), serviceability state (K_s), ultimate state ($K_{0.6}$), and close to failure ($K_{0.8}$) slip modulus

Given the diverse post-failure behaviors of the samples, a comparison of their ductility μ was conducted. According to [73] μ can be formulated as:

$$\mu = \frac{v_u - v_{\max}}{v_{\max}} \quad (1)$$

where v_u is the slip at the ultimate load F_u . F_u is defined as the 80% of F_{\max} load at the softening side of the load-slip curve or the load at the end of the experiment (at 15 mm slip), whichever occurred earlier. If failure occurred before either of these conditions, then F_u is the load just before the failure initiation. Figure 12 illustrates the determination of F_{\max} , F_u , v_{\max} and v_u on the load-slip curve.

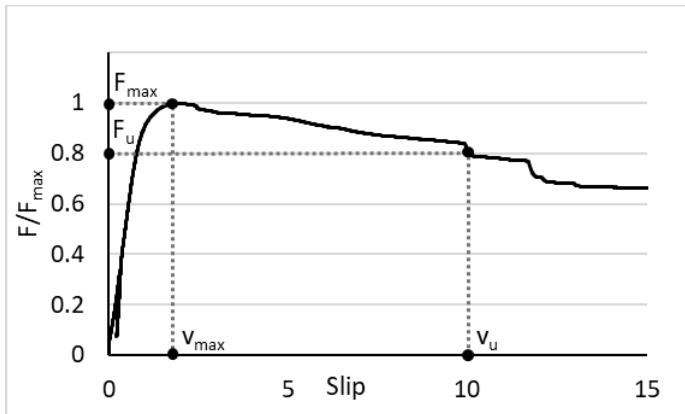


Figure 12 The determination of the maximum load (F_{\max}) and ultimate load (F_u), along with their corresponding slips (v_{\max} and v_u).

The average ductility for each connection sample is presented in Figure 13. Specimens E1 and F1 were excluded from this average calculation due to their distinctive failure modes compared to the other specimens in their respective samples, as well as their significantly different levels of ductility. Samples A and D demonstrate the lowest ductility, likely due to the length of the notch heel and the brittle nature of the failure mode. Sample F has the highest ductility, which can be attributed to the inclined shape of the notch.

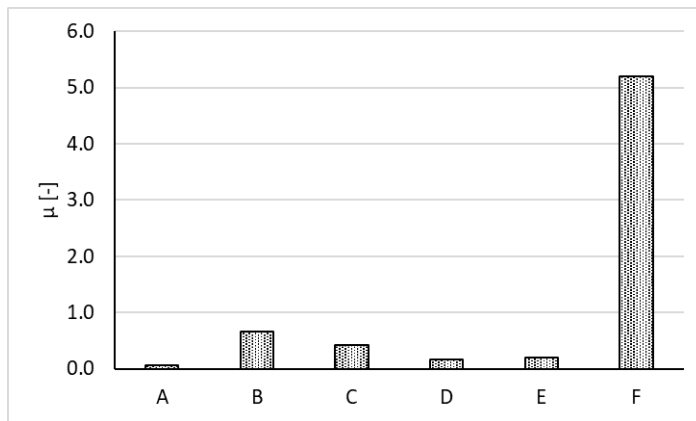


Figure 13 Ductility μ for each connection sample.

2.5 Overall comparison of connection samples

Three categories were considered to compare the connection samples: strength (F_{\max}), stiffness (K_s), and ductility (μ). A scoring system was defined, assigning a score based on a scale of 1 for each category, where 0 represents the worst score and 1 is the best. The maximum achievable score for each sample was 3. The score was calculated for each category by dividing their values by the maximum value in that category. The results are presented in Figure 14. Overall, sample F emerges as the top connection with a score of 2.7, followed by sample E with a score of 2.0. While sample F exhibits notable ductility, sample E excels in strength and stiffness.

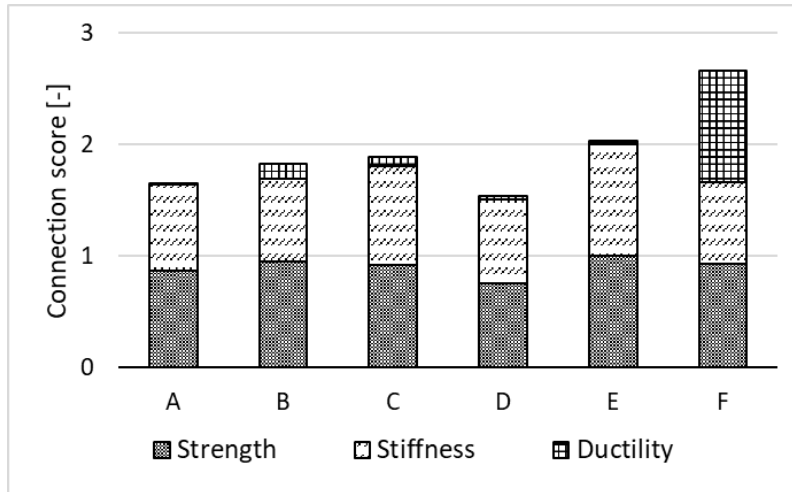


Figure 14 Overall comparison of the connection samples.

Although deconstruction was feasible for all samples, some proved easier to disassemble than others. To compare the ease of deconstruction of the samples, a qualitative grading system was employed, consisting of three levels: Attainable, Simple, and Effortless, ordered with increasing degrees of ease. Sample D received a score of Attainable due to the rectangular notch shape, which made its deconstruction more time and effort-consuming compared to other samples. Samples E and F, characterized by inclined notch faces, were graded as Effortless, denoting the simplest assembly and deconstruction process. The inclined faces of the notch facilitated easy assembly, as they were self-adjusting while tightening the bolts, and simplified demounting procedures. Samples A, B, and C received a score of simple, reflecting deconstruction that was not as complex as sample D but not as straightforward as samples E and F.

2.6 Comparison to results from the literature

Generally, TCC shear connections with notches show higher load-bearing capacity and stiffness than those using self-tapping screws but lower than connections with adhesives or glued-in steel plates like the HBV system [19,23,38,74]. Here, only experimental results from the literature focusing on notched shear connections for CCC systems were considered for

comparison with the results of this study. Table 5 displays some of the notch connections for the CCC system existing in the literature, which are distinguished by a number from 1 to 8. The presented notches have different geometries: rectangular, triangular, trapezoidal, inverted trapezoidal (dovetail), and circular. Apart from connection no. 2, no. 4 and no. 5, the rest of the connections from the literature lack separability between timber and concrete and, as a result, are not suitable for DfD. This lack of separability often arises from factors such as embedded screws in concrete, the use of adhesives, and the shape of the notch. The concrete strength under compression (f_c) is presented in the table, ranging from 23.6 to 60 MPa. These values are derived from tests on cylindrical specimens or converted accordingly.

Table 5 Details of similar CCC notch connections from the literature compared to the experimental results of this study.

No.	Ref.	DfD	Connection system	Notch shape and dimensions (length*width*depth [mm])	Concrete f_c [MPa]
1	[34]	No	notch + 2 lag screws + stirrup	Rectangular (200*450*25)	36.8 ^a
2	[23]	Yes	notch + 2 screws	Rectangular (200*200*20-35)	36.8 ^a
3	[75]	No	notch + 2 screws	Triangular (250*200*20)	60
4	[60]	Yes	Notch	Circular (100*20 ^b)	36.2
5		Yes	Notch	Circular (200*20 ^b)	36.2
6	[37].	No	Notch + adhesive	Trapezoidal (250*200*25)	23.6 ^a
7		No	Notch + 2 inclined screws	Rectangular (200*200*20-30)	23.6 ^a
8	[76]	No	Reinforced notch	Inverted trapezoidal (150*400*50)	34.4

^a = Cube results converted to cylinder by formula from [77]

^b = Diameter*depth

The maximum load and the slip modulus of the shear connections from the literature are compared to those tested in this study in Figure 15. The strength and stiffness of a notch connection vary directly with the width of the notch. Thus, the results are presented per one mm width to compare notches with different widths. Consequently, the maximum load and the slip modulus are expressed in kN/mm and kN/mm². Connection E exhibits the highest load-bearing capacity per width at 1.05 kN/mm. Connection no. 2, a demountable connection with

a load-bearing capacity of 0.90 kN/mm, is slightly weaker than all connections in this study except for sample D. Other demountable connections, no. 4 and no. 5, display significantly lower strength, measuring at 0.31 and 0.44 kN/mm, respectively.

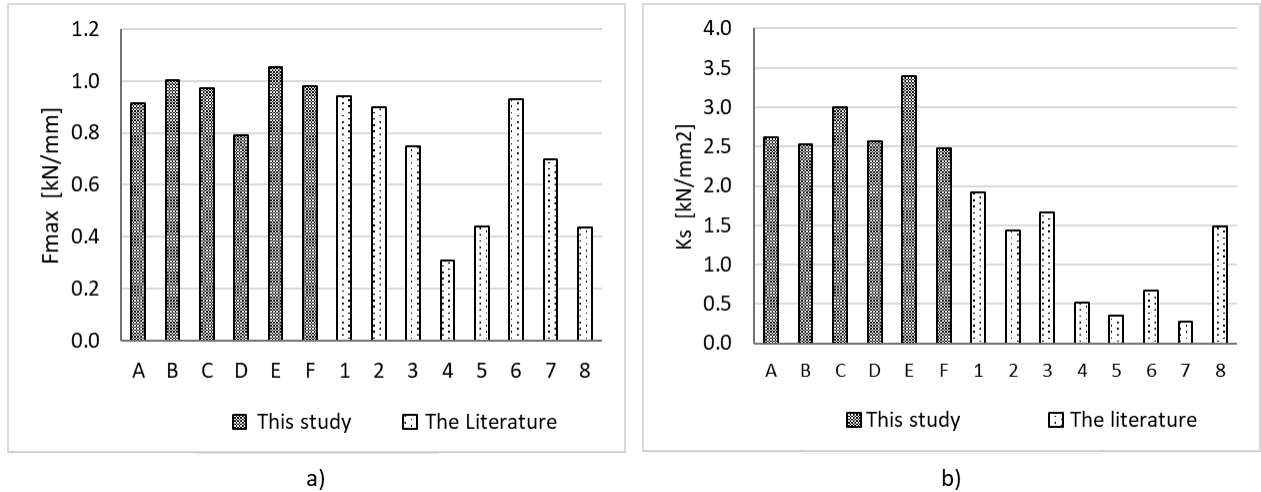


Figure 15 Comparison of the experimental results of this study with similar notch connections from the literature: a) the maximum load per mm width of the notch; b) the slip serviceability slip modulus per mm width of the notch.

Overall, the connections tested in this study demonstrated significantly higher stiffness per unit width compared to the connections presented in Figure 15. The stiffest connection in the literature, connection no. 1, exhibits a stiffness of 1.92 kN/mm², approximately 29% lower than the least stiff connection (sample F) from this study. This highlights the superiority of the connections introduced in this study compared to other demountable and conventional permanent connections in strength and stiffness.

Except for connections 4 and 5, all literature results are derived from experiments with a loading setup covering the CLT panel's entire loading/supporting face. As discussed in Section 2.2, this confinement of the timber leads to an increase in both strength and stiffness. Given this, the results from this study are even more significant than those presented in Figure 15 from the literature.

2.7 Reuse scenario of the connection

Specimen C4 was used to investigate the reuse of the connection concerning fabrication and mechanical performance. For the first use stage, the specimen was fabricated, assembled, loaded up to 60% of the estimated load, and unloaded. Then, for the second use stage, the specimen was unassembled, re-assembled, and loaded according to the loading procedure. The load-slip results of the two stages are shown Figure 16. When comparing the initial slip modulus, an increase from 375 kN/mm to 461 kN/mm is observed from the first use to the second one. However, it is important to note that the residual deformations are not factored into the calculation of the second-use slip modulus. The observed increase in the initial slip modulus can be attributed to the elimination of the existing gap between the concrete and timber faces at the notch, along with the stiffening effect induced by compression on the timber face. While this observation indicates an increase in stiffness through the reuse of the shear connection, it is crucial to emphasize that further experimental studies are required before any conclusion can be made. On the other hand, no difficulty was observed during the fabrication and reassembly of the connection since no permanent deformation or bond was noticed.

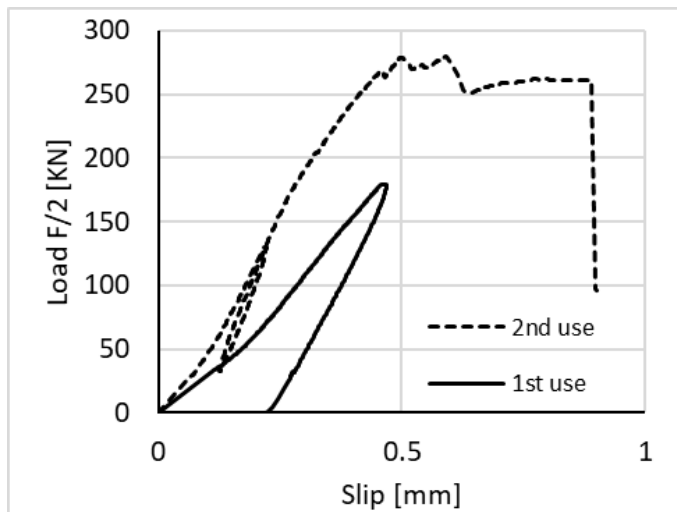


Figure 16 Load-slip results of specimen C4 for a reuse scenario.

3. Numerical study

This section presents numerical models developed to simulate the shear behavior of the connections under push-out test conditions. Three-dimensional FE models were developed using the Abaqus software package. The models were validated against the experimental results presented in Section 2. The validated models were subsequently employed to examine the shear behavior of each connection sample.

3.1 *Geometry and contact*

The geometry of the push-out test specimens has 2 symmetry planes. Therefore, only one-quarter of the specimen was modeled to save computation costs, and Symmetric boundary conditions were applied to the symmetric planes. The modeled geometry is depicted in Figure 17. All dimensions are identical to the experimental ones. A linear hexahedral element type with reduced integration (C3D8R) with hourglass control was used for timber and concrete. A ten-node tetrahedral element (C3D10) was used to mesh the bolt as it facilitated the meshing of its geometry. A 2-node linear 3-D truss (T3D2) element type was used for the steel mesh and stirrup, which is suitable for parts that take only axial stress. The support was provided by translational boundary conditions implemented at the bottom plane of the concrete part. The loading was implemented by displacement of an analytical rigid shell in the Y-direction with a constant rate at the top plane of the timber part, simulating the loading plate.

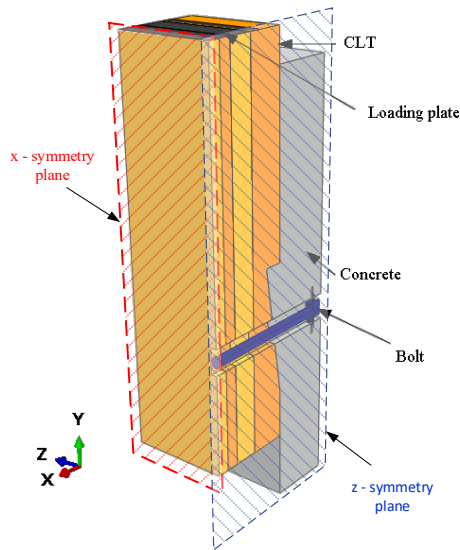


Figure 17 Geometry of the push-out FE model in Abaqus

The interaction between the parts in the normal direction was characterized by pressure-overclosure “Hard” contact type, preventing penetration and separating the contacting surfaces. In the tangential direction, the static coefficient of friction was set as 0.57 for timber-concrete [78] and concrete-steel [79] pairs. This value was set at 0.4 [75] for the timber-steel pair, and for the loading part pairs a value of 0.15 was applied. Contact pairs are specified for the surfaces where two adjoining parts come into contact.

3.2 Material modeling

The concrete was modeled using the Concrete Damage Plasticity (CDP) material model, which considers tensile cracking and compressive crushing as two main failure mechanisms. More details about the CDP material model can be found in a previous paper by the authors of this paper [62] and in [80]. The stress-strain behavior of concrete was defined based on the formulas from Eurocode 2 [81] as:

$$\sigma_c = f_{cm} \frac{k(\frac{\varepsilon}{\varepsilon_u}) - (\frac{\varepsilon}{\varepsilon_u})^2}{1 + (k - 2)(\frac{\varepsilon}{\varepsilon_u})} \quad (2)$$

and

$$k = 1.05 E_{cm} \times \frac{\varepsilon_u}{f_{cm}} \quad (3)$$

where f_{cm} is the strength of concrete, ε_u is the strain at maximum stress and E_{cm} is the modulus of elasticity as the secant value between $\sigma_c = 0$ and $0.4f_{cm}$. Considering the above formulas and the results from the tests on the concrete mixture presented in Section 2, the stress-strain response in Figure 18a was used as input for the CDP model. The post-failure behavior under tension was defined by a bilinear stress-crack opening W_c response, as demonstrated in Figure 18b, which was calculated based on the fracture energy of concrete [82].

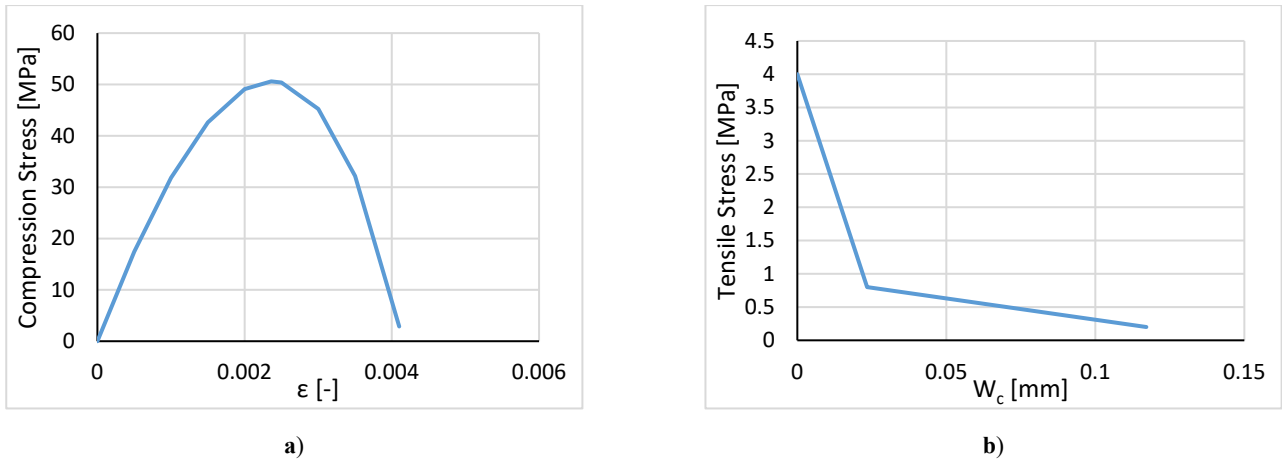


Figure 18 a) Stress-strain response of the concrete in compression; b) post-failure crack opening response of the concrete under tensile stress.

The timber material model used in this study is a three-dimensional nonlinear anisotropic elastoplastic material model with failure analysis capacity developed by Eslami et al. [83] and implemented as a UMAT subroutine for Abaqus. Hoffman's yield criterion [84], an extension of Hill's criterion [85], was used in this material model due to its ability to distinguish the strength of timber under compression and tension. The yield criterion was coupled with

isotropic hardening to represent timber's plastic strain hardening behavior under compression. Additionally, four failure criteria trigger damage propagation under both compression and tension. Further details about the material model, its implementation and validation can be found in [83]. The input parameters of the timber material model are demonstrated in Table 6.

Table 6 Timber properties for FE material model

Elasticity Parameters					
E ₁ [MPa]	E ₂ = E ₃ [MPa]	G ₂₃ [MPa]	G ₁₂ = G ₁₃ [MPa]	ν ₂₃	ν ₁₂ = ν ₁₃
11,000	370	60	690	0.5	0.45
Strength parameters					
σ _{1c} [MPa]	σ _{2c} = σ _{3c} [MPa]	σ _{1t} [MPa]	σ _{2t} = σ _{3t} [MPa]	σ ₂₃ [MPa]	σ ₁₂ = σ ₁₃ [MPa]
24.8	3.3	16.5	0.5	1.0	3.0
Hardening parameters					
h [MPa]					
6436					
Fracture energies					
G _{1t, f} [N/mm]	G _{2t, f} [N/mm]	G _{3t, f} [N/mm]			
60	0.2	0.2			

For the steel parts, including the bolt and the reinforcements, an isotropic elastic fully plastic material behavior was defined with Young's Modulus of 210 GPa and yield stress of 420 MPa.

3.3 Mesh size

The behavior of a model is significantly impacted by the mesh size when the material undergoes softening, owing to a reduction in energy dissipation with increased mesh refinement [83]. Hence, it became essential to undertake a mesh sensitivity study. Sample B was studied with various mesh sizes to determine the appropriate one. Given that the depth of the notch is markedly smaller than other dimensions in the model, a minimum of 3 elements in the depth direction was assigned in all models. Figure 19 depicts the load-slip diagram and the

correlation between the number of elements and computing time for six models with different mesh sizes ranging from 30 mm to 11 mm.

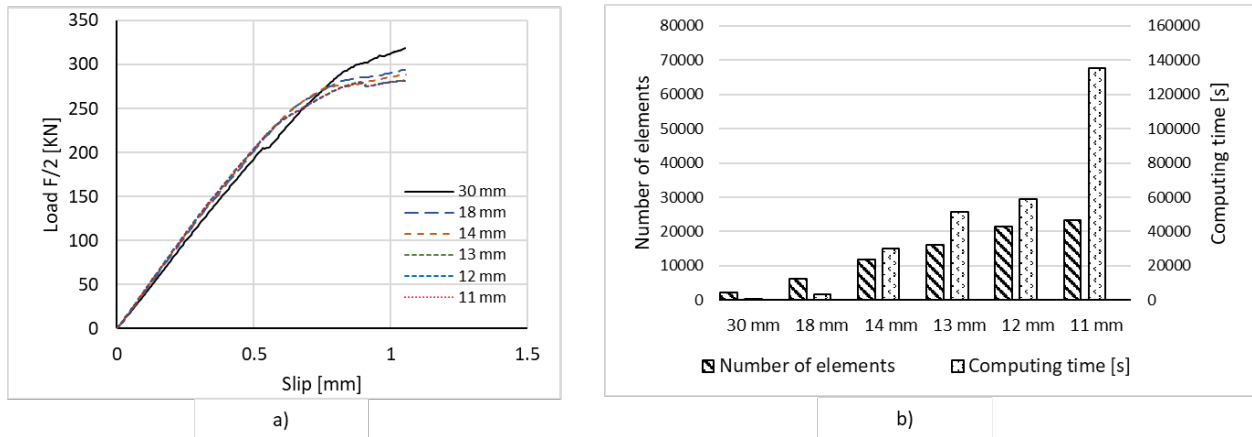


Figure 19 Various meshing size finite element analysis results for sample B: a) load-slip diagram; b) number of elements vs. computing time.

The mesh size noticeably influences the analysis in approaching a solution that accurately represents the system's response. Specifically, a coarse mesh yields less accurate load-slip results, while finer meshes exhibit similar load-slip curves with minimal solution variance. Notably, the 12mm and 11mm mesh sizes demonstrate a compatibility of 99%. Consequently, the model with a 12mm mesh size was deemed to have converged. Figure 19b illustrates that reducing mesh dimensions increases the number of elements, resulting in longer computation times. Opting for the model with a 12mm mesh dimension over 11mm resulted in a significant 66% reduction in computing time while maintaining an acceptable level of accuracy.

3.4 Results and discussion

The results from the FE analysis of samples A to F are shown in Figure 20 to Figure 25. The load-slip response derived from the FE model and corresponding experimental results are demonstrated for each sample. The comparison reveals that the model replicates the linear stage of the responses with comparable stiffness to the experimental results. Furthermore, the model accurately reproduces the specimen's stiffness softening and eventual failure, standing well

with the experimental data. This agreement between the model and experimental results validates its accuracy and suitability for simulating the behavior of the specimens under the given loading conditions.

Additionally, the damage propagation in concrete and timber and the principal stress distribution in the whole model at the maximum load are depicted for each sample. In Figure 20, the crack initiation in concrete is observable in sample A. The shear failure of the connection is evident in the timber damage. The stress distribution illustrates a concentration of compression stress in both materials at the notch face. Furthermore, the bolt undertakes tension, resulting from the tendency of separation between the CLT and concrete components. In Figure 23, sample D demonstrates results closely resembling sample A with similar damage and stress patterns, differing only in reduced crack propagation in concrete. In Figure 21, sample B reveals more tensile crack openings in the concrete due to higher loading. Compression failure is observed in the timber at the notch face, also beginning beneath the loading plate in the first CLT panel layer. While high compression stresses exist in the concrete at the notch face, the bolt experiences minimal forces. The stresses in the bolt become more prominent following the failure of the connection.

Similar to sample B, sample F in Figure 25 exhibits a comparable behavior, with the difference being lower stress concentrations. Concrete compression stress drops from around 59 MPa to about 40 MPa, and timber tensile stress reduces from approximately 16 MPa to 11 MPa. Sample E in Figure 24 shows a stress distribution similar to sample F. The notch shape in sample F facilitates a smoother transition of the load in concrete from the notch to the support compared to sample E. This can be attributed to the higher ductility of sample F compared to sample E. In Figure 19, sample C displays damage in the timber at the screw embedment in the second and third CLT layers. High principal stress, reaching up to 150 MPa, is noticeable in

the screw. The damage in concrete and timber failure at the notch face resembles those observed in samples B, E, and F.

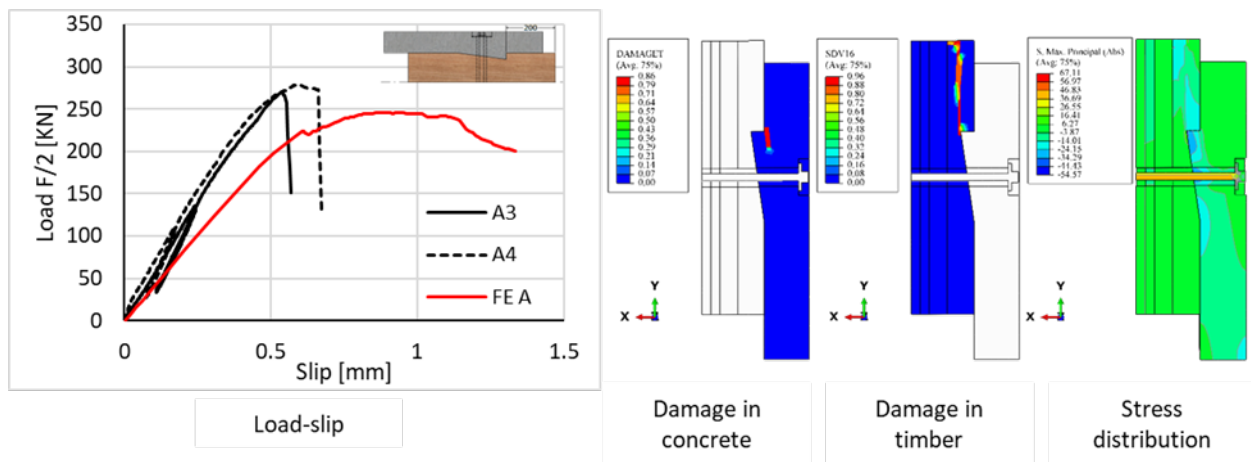


Figure 20 Sample A finite element analysis results. Crack opening in concrete and shear failure in timber can be observed.

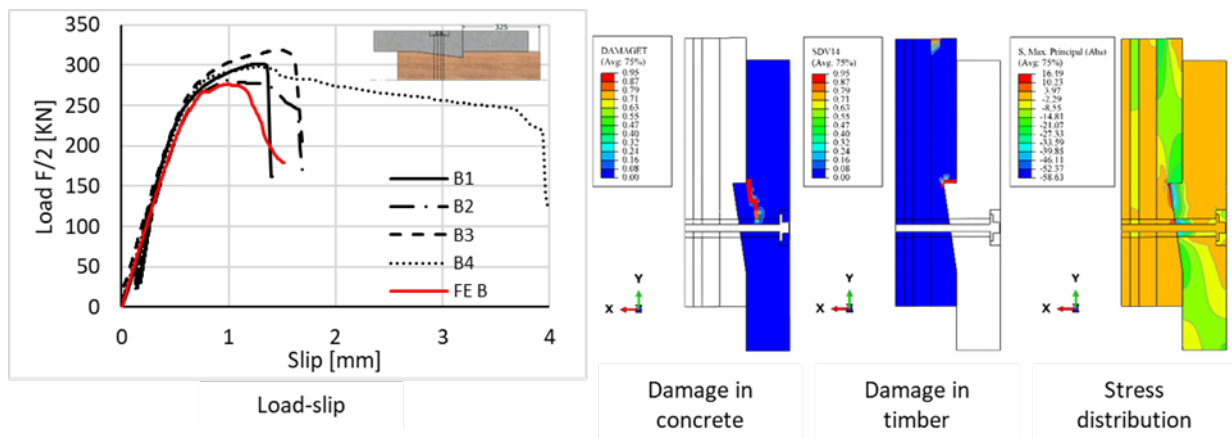


Figure 21 Sample B finite element analysis results. Crack opening in concrete and compression failure in timber can be observed.

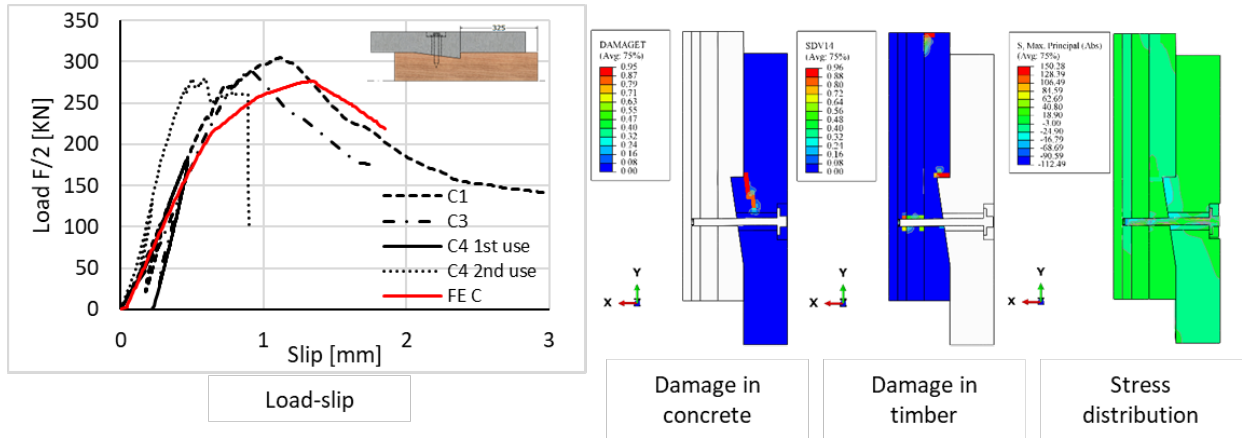


Figure 22 Sample C finite element analysis results. Crack opening in concrete and compression failure in timber can be observed.

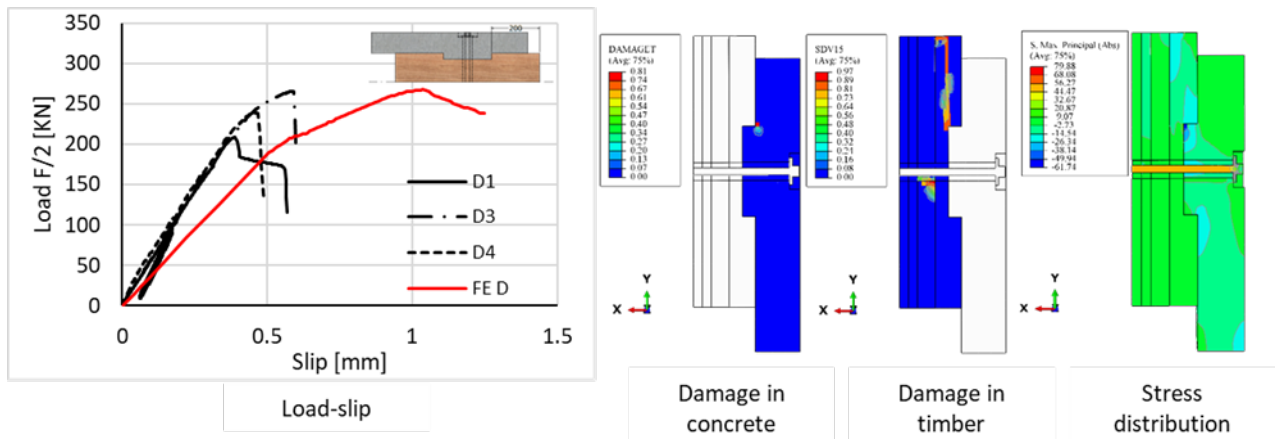


Figure 23 Sample D finite element analysis results. Small crack opening in concrete and shear failure in timber can be observed.

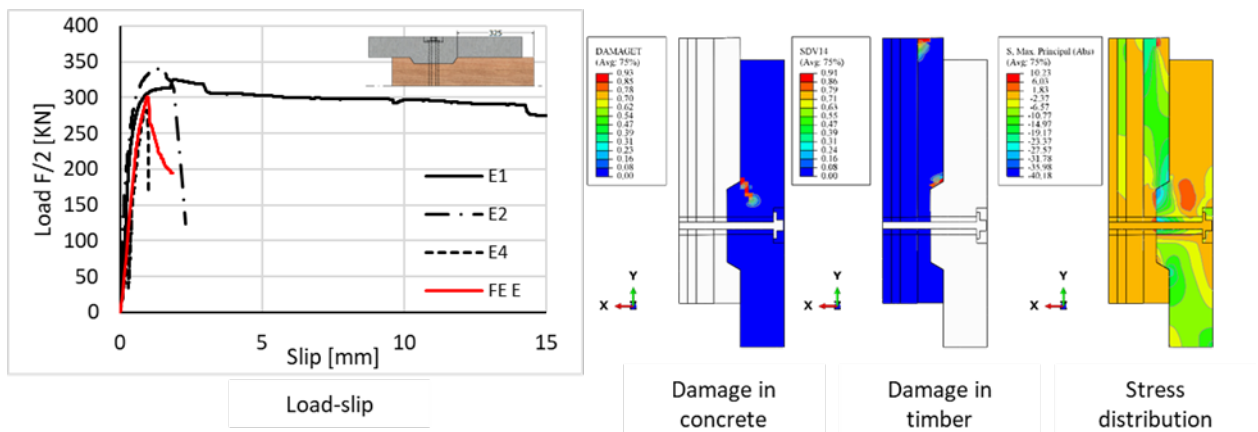


Figure 24 Sample E finite element analysis results. Crack opening in concrete and compression failure in timber can be observed.

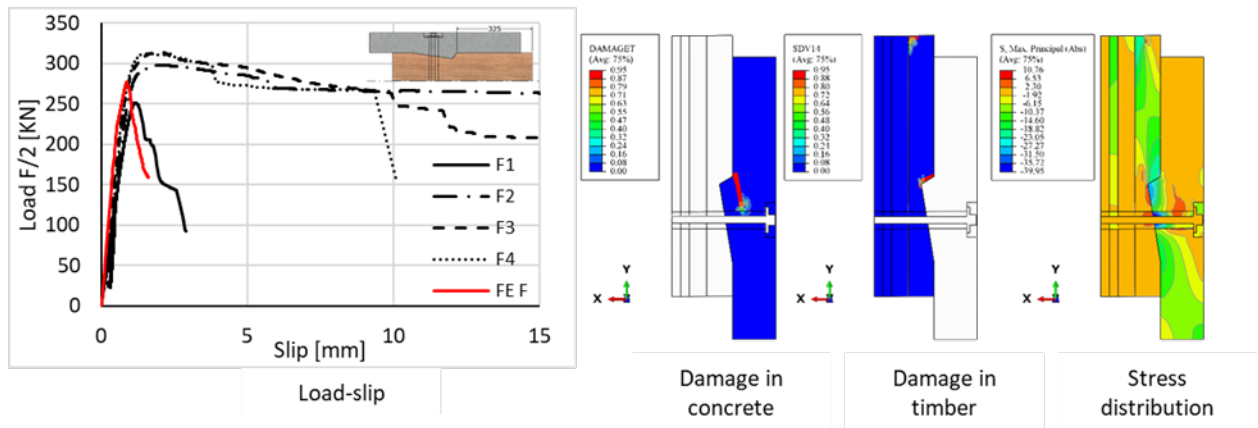


Figure 25 Sample F finite element analysis results. Crack opening in concrete and compression failure in timber can be observed.

4. Conclusion

This study used push-out tests to test six demountable notch shear connections for a modular prefabricated CLT-concrete composite floor system. The study examined the influence of two loading configurations and a reuse scenario. The experimental findings revealed the following outcomes:

- The loading configuration for a notch shear connection in an experimental test must allow the evolution of the horizontal shear failure in the timber.
- The strength of the shear connection increases as the heel length of the notch in timber increases. Notched connections with inclined faces show greater ductility than those with perpendicular faces.
- The proposed shear connections have load-bearing capacity comparable to conventional permanent shear connections and surpass existing demountable ones for CCC slabs, with the average results of the proposed connections being up to three times higher.
- The stiffness of the proposed connections is noticeably higher than that of existing connections for CCC slabs, with the average results being up to seven times higher than those of existing connections in the literature.

- The shear connections are fully demountable and reusable without any fabrication or reassembly issues, remaining demountable even after loading up to 60% of the estimated strength.

While the results are promising for the demountable modular prefabricated CCC floor system, further work is necessary. This includes expanding the number of push-out tests and conducting short-term and long-term bending tests to advance the development of the system.

Acknowledgments

This research is in the framework of the project Eco-Construction for Sustainable Development (ECON4SD). The experimental studies were conducted with the support of the Laboratory of Solid Structures personnel at the University of Luxembourg.

Funding

This work was supported by the program “Investissement pour la croissance et l’emploi”—European Regional Development Fund (2014–2020) (Grant agreement: 2017-02-015-15).

References

- [1] M. Sandanayake, W. Lokuge, G. Zhang, S. Setunge, Q. Thushar, Greenhouse gas emissions during timber and concrete building construction—A scenario based comparative case study, *Sustainable Cities and Society* 38 (2018) 91–97.
- [2] A. Hafner, Contribution of timber buildings on sustainability issues, *Proceedings of the World Sustainable Building* (2014).
- [3] B. D’Amico, F. Pomponi, J. Hart, Global potential for material substitution in building construction: The case of cross laminated timber, *Journal of Cleaner Production* 279 (2021) 123487. <https://doi.org/10.1016/j.jclepro.2020.123487>.
- [4] Z. Chen, H. Gu, R. Bergman, S. Liang, Comparative Life-Cycle Assessment of a High-Rise Mass Timber Building with an Equivalent Reinforced Concrete Alternative Using the Athena Impact Estimator for Buildings, *Sustainability* 12 (2020) 4708. <https://doi.org/10.3390/su12114708>.
- [5] L. Tupenaite, L. Kanapeckiene, J. Naimaviciene, A. Kaklauskas, T. Gecys, Timber Construction as a Solution to Climate Change: A Systematic Literature Review, *Buildings* 13 (2023) 976. <https://doi.org/10.3390/buildings13040976>.
- [6] F. Franzini, R. Toivonen, A. Toppinen, Why Not Wood? Benefits and Barriers of Wood as a Multistory Construction Material: Perceptions of Municipal Civil Servants from Finland, *Buildings* 8 (2018) 159. <https://doi.org/10.3390/buildings8110159>.

- [7] F. Asdrubali, B. Ferracuti, L. Lombardi, C. Guattari, L. Evangelisti, G. Grazieschi, A review of structural, thermo-physical, acoustical, and environmental properties of wooden materials for building applications, *Building and Environment* 114 (2017) 307–332. <https://doi.org/10.1016/j.buildenv.2016.12.033>.
- [8] A.B. Robertson, F.C.F. Lam, R.J. Cole, A Comparative Cradle-to-Gate Life Cycle Assessment of Mid-Rise Office Building Construction Alternatives: Laminated Timber or Reinforced Concrete, *Buildings* 2 (2012) 245–270. <https://doi.org/10.3390/buildings2030245>.
- [9] E.S. Bernard, Dynamic Serviceability in Lightweight Engineered Timber Floors, *J. Struct. Eng.* 134 (2008) 258–268. [https://doi.org/10.1061/\(ASCE\)0733-9445\(2008\)134:2\(258\)](https://doi.org/10.1061/(ASCE)0733-9445(2008)134:2(258)).
- [10] L.J. Hu, Y.H. Chui, D.M. Onysko, Vibration serviceability of timber floors in residential construction, *Prog. Struct. Engng Mater.* 3 (2001) 228–237. <https://doi.org/10.1002/pse.69>.
- [11] H. Zhou, W. Lu, B. Lu, L. Wang, Y. Bao, J. Zhang, Z. Chen, Experimental and Numerical Analyses on the Fire Resistance of Timber–Concrete Composite Boards Using an Innovative Form of Partial Protection, *Buildings* 13 (2023) 725. <https://doi.org/10.3390/buildings13030725>.
- [12] A. Ceccotti, Timber-concrete composite structures, *Timber Engineering–STEP 2* (1995) E13.
- [13] A.M.P.G. Dias, Mechanical behaviour of timber-concrete joints, Universidade de Coimbra, 2005.
- [14] D. Yeoh, M. Fragiaco, M. De Franceschi, K. Heng Boon, State of the Art on Timber-Concrete Composite Structures: Literature Review, *J. Struct. Eng.* 137 (2011) 1085–1095. [https://doi.org/10.1061/\(ASCE\)ST.1943-541X.0000353](https://doi.org/10.1061/(ASCE)ST.1943-541X.0000353).
- [15] A. Siddika, Md.A.A. Mamun, F. Aslani, Y. Zhuge, R. Alyousef, A. Hajimohammadi, Cross-laminated timber–concrete composite structural floor system: A state-of-the-art review, *Engineering Failure Analysis* 130 (2021) 105766. <https://doi.org/10.1016/j.engfailanal.2021.105766>.
- [16] K. Holschemacher, L. Hoffmann, B. Heiden, Environmental impact of timber-concrete composite slabs in comparison to other floor systems, in: Santiago, Chile, 2021: p. 6.
- [17] H. Eslami, A. Yaghma, L. Bhagya Jayasinghe, D. Waldmann, INFLUENCE OF DIFFERENT END-OF-LIFE CYCLE SCENARIOS ON THE ENVIRONMENTAL IMPACTS OF TIMBER-CONCRETE COMPOSITE FLOOR SYSTEMS, in: *World Conference on Timber Engineering (WCTE 2023)*, World Conference on Timber Engineering (WCTE 2023), Oslo, Norway, 2023: pp. 982–988. <https://doi.org/10.52202/069179-0134>.
- [18] S. Monteiro, A. Dias, S. Lopes, Distribution of Concentrated Loads in Timber-Concrete Composite Floors: Simplified Approach, *Buildings* 10 (2020) 32. <https://doi.org/10.3390/buildings10020032>.
- [19] A. Dias, J. Schänzlin, P. Dietsch, Design of timber-concrete composite structures, A State-of-the-Art Report by COST Action FP1402/WG (2018).
- [20] T. Tannert, A. Gerber, T. Vallee, Hybrid adhesively bonded timber-concrete-composite floors, *International Journal of Adhesion and Adhesives* 97 (2020) 102490. <https://doi.org/10.1016/j.ijadhadh.2019.102490>.
- [21] K. Jones, J. Stegemann, J. Sykes, P. Winslow, Adoption of unconventional approaches in construction: The case of cross-laminated timber, *Construction and Building Materials* 125 (2016) 690–702. <https://doi.org/10.1016/j.conbuildmat.2016.08.088>.
- [22] A. Di Bella, M. Mitrovic, Acoustic Characteristics of Cross-Laminated Timber Systems, *Sustainability* 12 (2020) 5612. <https://doi.org/10.3390/su12145612>.

- [23] M.V. Thai, S. Ménard, S.M. Elachachi, P. Galimard, Performance of Notched Connectors for CLT-Concrete Composite Floors, *Buildings* 10 (2020) 122. <https://doi.org/10.3390/buildings10070122>.
- [24] K.Q. Mai, A. Park, K. Lee, Experimental and numerical performance of shear connections in CLT-concrete composite floor, *Mater Struct* 51 (2018) 84. <https://doi.org/10.1617/s11527-018-1202-3>.
- [25] K. Quang Mai, A. Park, K.T. Nguyen, K. Lee, Full-scale static and dynamic experiments of hybrid CLT-concrete composite floor, *Construction and Building Materials* 170 (2018) 55–65. <https://doi.org/10.1016/j.conbuildmat.2018.03.042>.
- [26] M. Wang, Q. Xu, K.A. Harries, L. Chen, Z. Wang, X. Chen, Experimental study on mechanical performance of shear connections in CLT-concrete composite floor, *Engineering Structures* 269 (2022) 114842. <https://doi.org/10.1016/j.engstruct.2022.114842>.
- [27] A. Gerber, T. Tannert, Timber-Concrete Composites Using Flat-Plate Engineered Wood Products, in: *Structures Congress 2015*, American Society of Civil Engineers, Portland, Oregon, 2015: pp. 2314–2325. <https://doi.org/10.1061/9780784479117.201>.
- [28] C. Higgins, C. Blank, A.R. Barbosa, *Structural Tests of Concrete Composite-Cross-Laminated Timber Floors*, 2017.
- [29] DOPS, HBV-Ceilings, TiComTec GmbH (n.d.). <https://ticomtec.de/en/hbv-systems/hbv-ceilings/> (accessed August 17, 2023).
- [30] T. Tannert, M.M. Ebadi, A. Gerber, Serviceability Performance of Timber Concrete Composite Floors, *Mocs* (2019) 206–212. <https://doi.org/10.29173/mocs95>.
- [31] A. Nemati Giv, Q. Fu, L. Yan, B. Kasal, Interfacial bond strength of epoxy and PUR adhesively bonded timber-concrete composite joints manufactured in dry and wet processes, *Construction and Building Materials* 311 (2021) 125356. <https://doi.org/10.1016/j.conbuildmat.2021.125356>.
- [32] J. Kanócz, V. Bajzecerová, Š. Šteller, Timber-concrete composite elements with various composite connections. Part 3: Adhesive connection, *Wood Res* 60 (2015) 939–952.
- [33] V. Bajzecerová, J. Kanócz, M. Rovňák, M. Kováč, Prestressed CLT-concrete composite panels with adhesive shear connection, *Journal of Building Engineering* 56 (2022) 104785. <https://doi.org/10.1016/j.jobe.2022.104785>.
- [34] Y. Jiang, R. Crocetti, CLT-concrete composite floors with notched shear connectors, *Construction and Building Materials* 195 (2019) 127–139. <https://doi.org/10.1016/j.conbuildmat.2018.11.066>.
- [35] S. Lamothe, L. Sorelli, P. Blanchet, P. Galimard, Lightweight and slender timber-concrete composite floors made of CLT-HPC and CLT-UHPC with ductile notch connectors, *Engineering Structures* 243 (2021) 112409. <https://doi.org/10.1016/j.engstruct.2021.112409>.
- [36] Y.-J. Song, S.-Y. Baek, I.-H. Lee, S.-I. Hong, Variations of moisture content in manufacturing CLT-concrete composite slab using wet construction method, *BioRes* 16 (2020) 372–386. <https://doi.org/10.15376/biores.16.1.372-386>.
- [37] Q. Xu, M. Wang, L. Chen, K.A. Harries, X. Song, Z. Wang, Mechanical performance of notched shear connections in CLT-concrete composite floor, *Journal of Building Engineering* 70 (2023) 106364. <https://doi.org/10.1016/j.jobe.2023.106364>.
- [38] M. Shahnewaz, R. Jackson, T. Tannert, CLT concrete composite floors with steel kerf plate connectors, *Construction and Building Materials* 319 (2022) 126092. <https://doi.org/10.1016/j.conbuildmat.2021.126092>.
- [39] P. Kuklík, P. Nechanický, A. Kuklíková, Development of Prefabricated Timber-Concrete Composite Floors, in: S. Aicher, H.-W. Reinhardt, H. Garrecht (Eds.), *Materials and*

- Joints in Timber Structures, Springer Netherlands, Dordrecht, 2014: pp. 463–470. https://doi.org/10.1007/978-94-007-7811-5_42.
- [40] S. Yilmaz, S. Demir, N. Vural, Experimental investigation of a prefabricated timber-concrete composite floor structure: Notched-slab approach, *Advances in Concrete Construction* 12 (2021) 13–23. <https://doi.org/10.12989/ACC.2021.12.1.013>.
 - [41] W. Sebastian, S. Webb, H.S. Nagree, Orthogonal distribution and dynamic amplification characteristics of partially prefabricated timber-concrete composites, *Engineering Structures* 219 (2020) 110693. <https://doi.org/10.1016/j.engstruct.2020.110693>.
 - [42] R. Crocetti, T. Sartori, M. Flansbjer, Timber-Concrete Composite Structures with Prefabricated FRC Slab, in: 11th World Conference on Timber Engineering 2010, Curran Associates, Inc., Trentino, Italy, 2010: pp. 121–130.
 - [43] T. Sartori, R. Crocetti, Prefabricated timber-concrete composite floors, *Eur. J. Wood Prod.* 74 (2016) 483–485. <https://doi.org/10.1007/s00107-016-1007-4>.
 - [44] B. Shi, W. Zhu, H. Yang, W. Liu, H. Tao, Z. Ling, Experimental and theoretical investigation of prefabricated timber-concrete composite beams with and without prestress, *Engineering Structures* 204 (2020). <https://doi.org/10.1016/j.engstruct.2019.109901>.
 - [45] M. Fragiaco, E. Lukaszewska, Development of prefabricated timber–concrete composite floor systems, *Proceedings of the Institution of Civil Engineers - Structures and Buildings* 164 (2011) 117–129. <https://doi.org/10.1680/stbu.10.00010>.
 - [46] V.W.Y. Tam, C.M. Tam, S.X. Zeng, W.C.Y. Ng, Towards adoption of prefabrication in construction, *Building and Environment* 42 (2007) 3642–3654. <https://doi.org/10.1016/j.buildenv.2006.10.003>.
 - [47] D. Yeoh, M. Fragiaco, A. Buchanan, C. Gerber, Preliminary Research Towards A Semi-Prefabricated LVL–Concrete Composite Floor System for the Australasian Market, *Australian Journal of Structural Engineering* 9 (2009) 225–240. <https://doi.org/10.1080/13287982.2009.11465025>.
 - [48] E. Lukaszewska, Development of prefabricated timber-concrete composite floors, Division of Structural Engineering, Luleå University of Technology, 2009.
 - [49] D. Yeoh, M. Fragiaco, The Design of a Semi-Prefabricated LVL-Concrete Composite Floor, *Advances in Civil Engineering* 2012 (2012) 1–19. <https://doi.org/10.1155/2012/626592>.
 - [50] E. Lukaszewska, H. Johnsson, M. Fragiaco, Performance of connections for prefabricated timber–concrete composite floors, *Mater Struct* 41 (2008) 1533–1550. <https://doi.org/10.1617/s11527-007-9346-6>.
 - [51] R. Crocetti, T. Sartori, R. Tomasi, Innovative Timber-Concrete Composite Structures with Prefabricated FRC Slabs, *J. Struct. Eng.* 141 (2015) 04014224. [https://doi.org/10.1061/\(ASCE\)ST.1943-541X.0001203](https://doi.org/10.1061/(ASCE)ST.1943-541X.0001203).
 - [52] B. Shi, W. Liu, H. Yang, Experimental investigation on the long-term behaviour of prefabricated timber-concrete composite beams with steel plate connections, *Construction and Building Materials* 266 (2021) 120892. <https://doi.org/10.1016/j.conbuildmat.2020.120892>.
 - [53] J. Kanters, Design for Deconstruction in the Design Process: State of the Art, *Buildings* 8 (2018) 150. <https://doi.org/10.3390/buildings8110150>.
 - [54] A.S. Allam, M. Nik-Bakht, From demolition to deconstruction of the built environment: A synthesis of the literature, *Journal of Building Engineering* 64 (2023) 105679. <https://doi.org/10.1016/j.jobe.2022.105679>.
 - [55] N. Khorsandnia, H. Valipour, J. Schänzlin, K. Crews, Experimental Investigations of Deconstructable Timber–Concrete Composite Beams, *J. Struct. Eng.* 142 (2016). [https://doi.org/10.1061/\(ASCE\)ST.1943-541X.0001607](https://doi.org/10.1061/(ASCE)ST.1943-541X.0001607).

- [56] N. Khorsandnia, H. Valipour, M. Bradford, Deconstructable timber-concrete composite beams with panelised slabs: Finite element analysis, *Construction and Building Materials* 163 (2018) 798–811. <https://doi.org/10.1016/j.conbuildmat.2017.12.169>.
- [57] J.P. Wacker, J.A. Campos, A.M. Dias, Development of a Reusable Timber-Concrete-Composite System for Bridge Decks, in: Santiago, Chile, 2021.
- [58] M. Derikvand, G. Fink, Deconstructable connector for TCC floors using self-tapping screws, *Journal of Building Engineering* 42 (2021) 102495. <https://doi.org/10.1016/j.jobbe.2021.102495>.
- [59] M. Derikvand, G. Fink, Bending properties of deconstructable cross-laminated timber-concrete composite floor elements, *Wood Material Science & Engineering* (2022) 1–8. <https://doi.org/10.1080/17480272.2022.2077658>.
- [60] S.-J. Pang, K.-S. Ahn, S. Jeong, G.-C. Lee, H.S. Kim, J.-K. Oh, Prediction of bending performance for a separable CLT-concrete composite slab connected by notch connectors, *Journal of Building Engineering* 49 (2022) 103900. <https://doi.org/10.1016/j.jobbe.2021.103900>.
- [61] M. Derikvand, G. Fink, Design for Deconstruction: Benefits, Challenges, and Outlook for Timber–Concrete Composite Floors, *Buildings* 13 (2023) 1754. <https://doi.org/10.3390/buildings13071754>.
- [62] H. Eslami, L.B. Jayasinghe, D. Waldmann, Experimental and Numerical Investigation of a Novel Demountable Timber–Concrete Composite Floor, *Buildings* 13 (2023) 1763. <https://doi.org/10.3390/buildings13071763>.
- [63] Würth Belux, Threaded rod DIN 976-1 (shape A) with standard metric ISO thread, zinc-plated steel 8.8, blue passivated (A2K) (0959016), (n.d.). <https://eshop.wurth.be/Threaded-rod-DIN-976-1-shape-A-with-standard-metric-ISO-thread-zinc-plated-steel-88-blue-passivated-A2K-THRROD-DIN976-A-88-A2K-M16X1000/0959016.sku/en/US/EUR/> (accessed February 24, 2024).
- [64] Würth Belux, Wood screw Hexagon head DIN 571, steel zinc-plated blue (019216 200), (n.d.). <https://eshop.wurth.be/Wood-screw-Hexagon-head-DIN-571-steel-zinc-plated-blue-SCR-HEX-DIN571-WO-WS24-A2K-16X200/019216%20200.sku/en/US/EUR/> (accessed February 24, 2024).
- [65] Würth Belux, Washer with large outside diameter DIN 9021, steel, plain (041716), (n.d.). <https://eshop.wurth.be/Washer-with-large-outside-diameter-DIN-9021-steel-plain-WSH-DIN9021-140HV-D170/041716.sku/en/US/EUR/> (accessed February 24, 2024).
- [66] Würth Belux, Hexagon nut DIN 934, steel I6I/I8I, zinc-plated, blue passivated (A2K) (031716), (n.d.). <https://eshop.wurth.be/Hexagon-nut-DIN-934-steel-I6I-I8I-zinc-plated-blue-passivated-A2K-NUT-HEX-DIN934-I8I-WS24-A2K-M16/031716.sku/en/US/EUR/> (accessed February 24, 2024).
- [67] CEN: Brussels, ILNAS-EN 12390-3:2019 Testing hardened concrete - Part3: Compressive strength of test specimens, (2019).
- [68] CEN: Brussels, ILNAS-EN 12390-6:2009 Testing hardened concrete - Part 6: Tensile splitting strength of test specimens, (2009).
- [69] CEN: Brussels, ILNAS-EN 12390-13:2013 Testing hardened concrete - Part 13: Determination of secant modulus of elasticity in compression, (2013).
- [70] European Technical Assessment ETA-06/0009, (2017). https://www.dibt.de/pdf_storage/2017/ETA-06%210009%288.03.04-37%2116%29e.pdf (accessed August 17, 2023).
- [71] EN 338:2009 - Structural timber - Strength classes, (2009).
- [72] European Committee for Standardization, ILNAS-EN 26891:1991 Timber structures - Joints made with mechanical fasteners - General principles for the determination of strength and deformation, (n.d.).

- [73] L.-M. Ottenhaus, R. Jockwer, D. van Drimmelen, K. Crews, Designing timber connections for ductility – A review and discussion, *Construction and Building Materials* 304 (2021) 124621. <https://doi.org/10.1016/j.conbuildmat.2021.124621>.
- [74] A. Ceccotti, Composite concrete-timber structures, *Prog. Struct. Engng Mater.* 4 (2002) 264–275. <https://doi.org/10.1002/pse.126>.
- [75] S. Lamothe, L. Sorelli, P. Blanchet, P. Galimard, Engineering ductile notch connections for composite floors made of laminated timber and high or ultra-high performance fiber reinforced concrete, *Engineering Structures* 211 (2020) 110415. <https://doi.org/10.1016/j.engstruct.2020.110415>.
- [76] V. Ouch, P. Heng, Q.-H. Nguyen, H. Somja, T. Soquet, An experimental investigation on the dovetail notched connection for cross-laminated-timber-concrete composite slabs, *European Journal of Environmental and Civil Engineering* 0 (2023) 1–31. <https://doi.org/10.1080/19648189.2023.2194351>.
- [77] M.A. Mansur, M.M. Islam, Interpretation of Concrete Strength for Nonstandard Specimens, *J. Mater. Civ. Eng.* 14 (2002) 151–155. [https://doi.org/10.1061/\(ASCE\)0899-1561\(2002\)14:2\(151\)](https://doi.org/10.1061/(ASCE)0899-1561(2002)14:2(151)).
- [78] A.M.P.G. Dias, C. Helena, S. Lopes, J.W.G. Kuilen, Experimental shear–friction tests on dowel-type fastener timber–concrete joints, in: Lahti, Finland, 2004.
- [79] B.G. Rabbat, H.G. Russell, Friction Coefficient of Steel on Concrete or Grout, *Journal of Structural Engineering* 111 (1985) 505–515. [https://doi.org/10.1061/\(ASCE\)0733-9445\(1985\)111:3\(505\)](https://doi.org/10.1061/(ASCE)0733-9445(1985)111:3(505)).
- [80] SIMULIA, Abaqus 6.11 Theory Manual, Dassault Systèmes, 2011.
- [81] CEN: Brussels, Eurocode 2: Design of concrete structures - Part 1-1: General rules and rules for buildings, (2004).
- [82] Federation Internationale du Beton, P. Beverly, Fib Model Code for Concrete Structures 2010, Ernst & Sohn, Berlin, Germany, 2013. <https://books.google.lu/books?id=wEUqnwEACAAJ>.
- [83] H. Eslami, L.B. Jayasinghe, D. Waldmann, Nonlinear three-dimensional anisotropic material model for failure analysis of timber, *Engineering Failure Analysis* 130 (2021) 105764. <https://doi.org/10.1016/j.engfailanal.2021.105764>.
- [84] O. Hoffman, The Brittle Strength of Orthotropic Materials, *Journal of Composite Materials* 1 (1967) 200–206. <https://doi.org/10.1177/002199836700100210>.
- [85] R. Hill, A theory of the yielding and plastic flow of anisotropic metals, *Proc. R. Soc. Lond. A* 193 (1948) 281–297. <https://doi.org/10.1098/rspa.1948.0045>.

4 CCC slab under bending

In Paper IV, a modular and prefabricated TCC concept for a demountable floor system was developed. Paper V's experiments presented the strength and stiffness of different shear connections proposed for a demountable and reusable CCC slab. The experimental results showed that connection sample F, featuring a birdsmouth-shaped notch, achieved the highest overall score. Consequently, this connection was chosen to design a modular slab for Building Prototype 3, as detailed in Paper I. A CCC slab was designed for a 10-meter span, connected by 10 shear connections. Figure 22 illustrates the designed CCC slab, which is 10.6 meters long, comprising a 280 mm deep CLT plate and a 100 mm concrete layer. The first notched connection is 600 mm from the slab edge, with subsequent connections spaced 500 mm apart. The notch design and reinforcements align with those presented in Paper V for connection sample F, while the stirrup setup was modified for easier installation. The slabs in Paper I were presented with a width of 1800 mm. However, practical laboratory limits led to a reduction to a width of 700 mm for this experiment. All materials, including CLT, concrete, and bolts, have the same material properties as presented in Paper V.

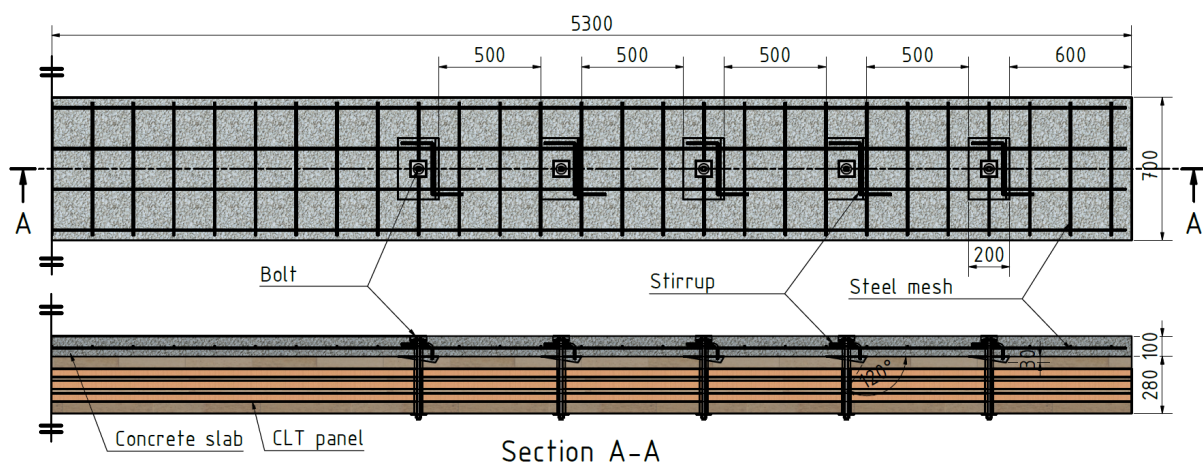


Figure 22. The CCC slab designed for the bending experiment. Dimensions are in millimeters.

The experiment was done in the laboratory of solid materials at the Technical University of Darmstadt. Three CCC slabs B1, B2 and B3 were fabricated for this test. The CLT plates were initially cut to form the notched shapes and holes for the bolts. Formworks for the concrete slab and bolts were installed, and reinforcement was placed. The concrete was then cast directly onto the CLT slab. Figure 23 shows the slabs prepared for concreting. The bolts were installed after the concrete had completed its curing time.

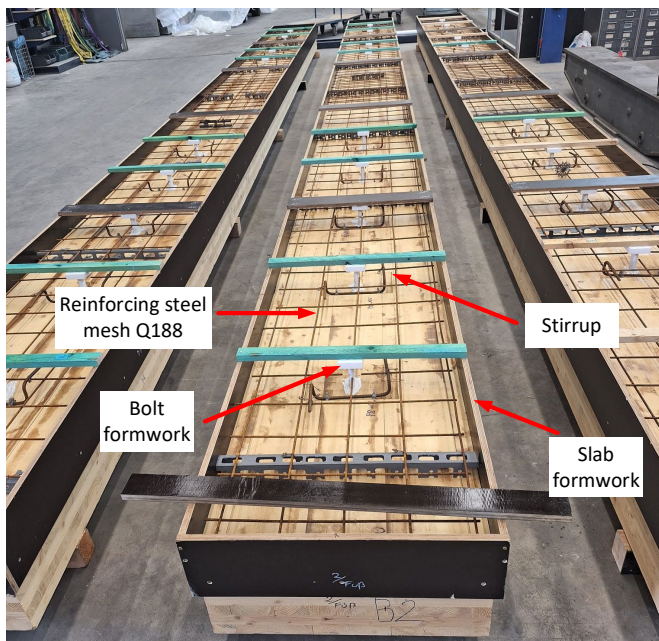


Figure 23. Slabs before casting concrete.

Figure 24 illustrates the experimental setup for the six-point bending test, depicting the positions of loading, support, and displacement sensors. Sensors h1 to h14 measured the slip between CLT and concrete, with h1 to h12 on the front side and h13 and h14 on the opposite side as control points. Sensors w1 to w4 gauged the vertical deflection, and sensors v1 and v2 measured the vertical separation between the concrete layer and CLT at the mid-span. The displacement sensors are shown in Figure 25. The load was recorded as the total load implied on the slab. The average displacement measured by sensors w2 and w3 was considered the mid-span deflection.

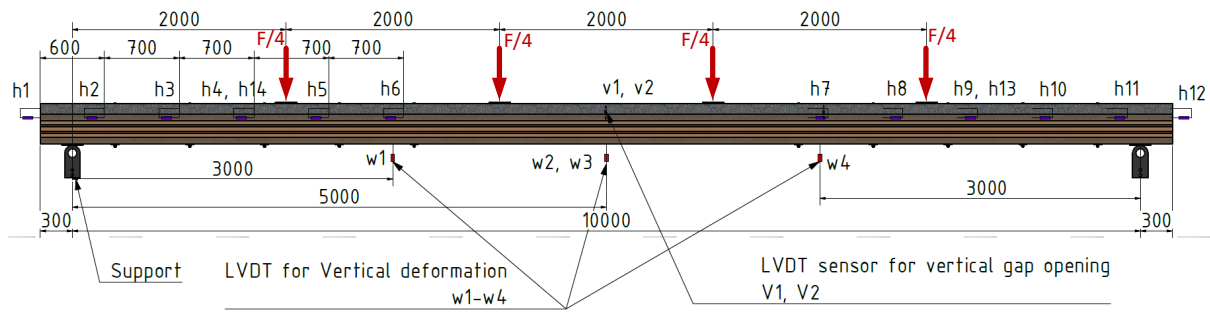
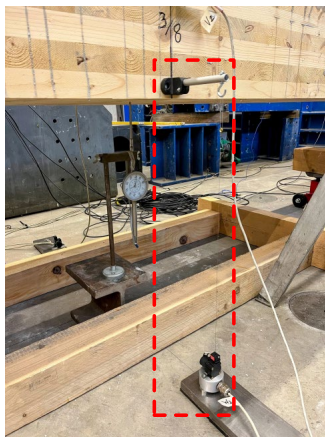


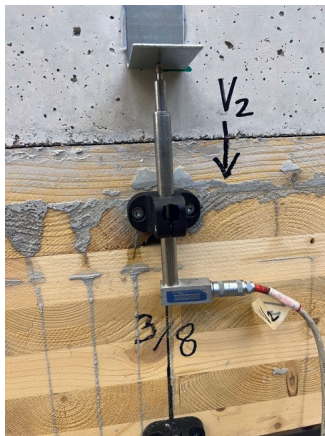
Figure 24. Six-point bending experiment setup. Dimensions are in millimeters.



a)



b)



c)



d)

Figure 25. Displacement sensors in the bending experiment used for 1) vertical deflection ($w1-w4$), b) end-span slip ($h1$ and $h12$), c) separation of the concrete and timber at the mid-span ($v1$ and $v2$), and d) slip at each notched connection ($h2-h11$, $h13$ and $h14$).

The loading procedure for all specimens is depicted in Figure 26. CCC-B1 was loaded up to 70 kN, then unloaded and demounted, and the concrete slab was removed for separate testing of the CLT panel (CLT-B1). CLT-B1 was then loaded until failure with the setup depicted in

Figure 24 but without the sensors for measuring the horizontal slip (h1-h14) and vertical gap (v1 and v2). CCC-B2 underwent loading and unloading for 3 cycles before being loaded until failure. CCC-B3 experienced loading and unloading for 4 cycles, followed by loading until failure. For all specimens, load control mode was used with a rate of 0.5 kN/s, except during loading until failure, where displacement control with a rate of 0.3 mm/s was applied. The load was kept constant for 60 seconds between each loading and unloading.

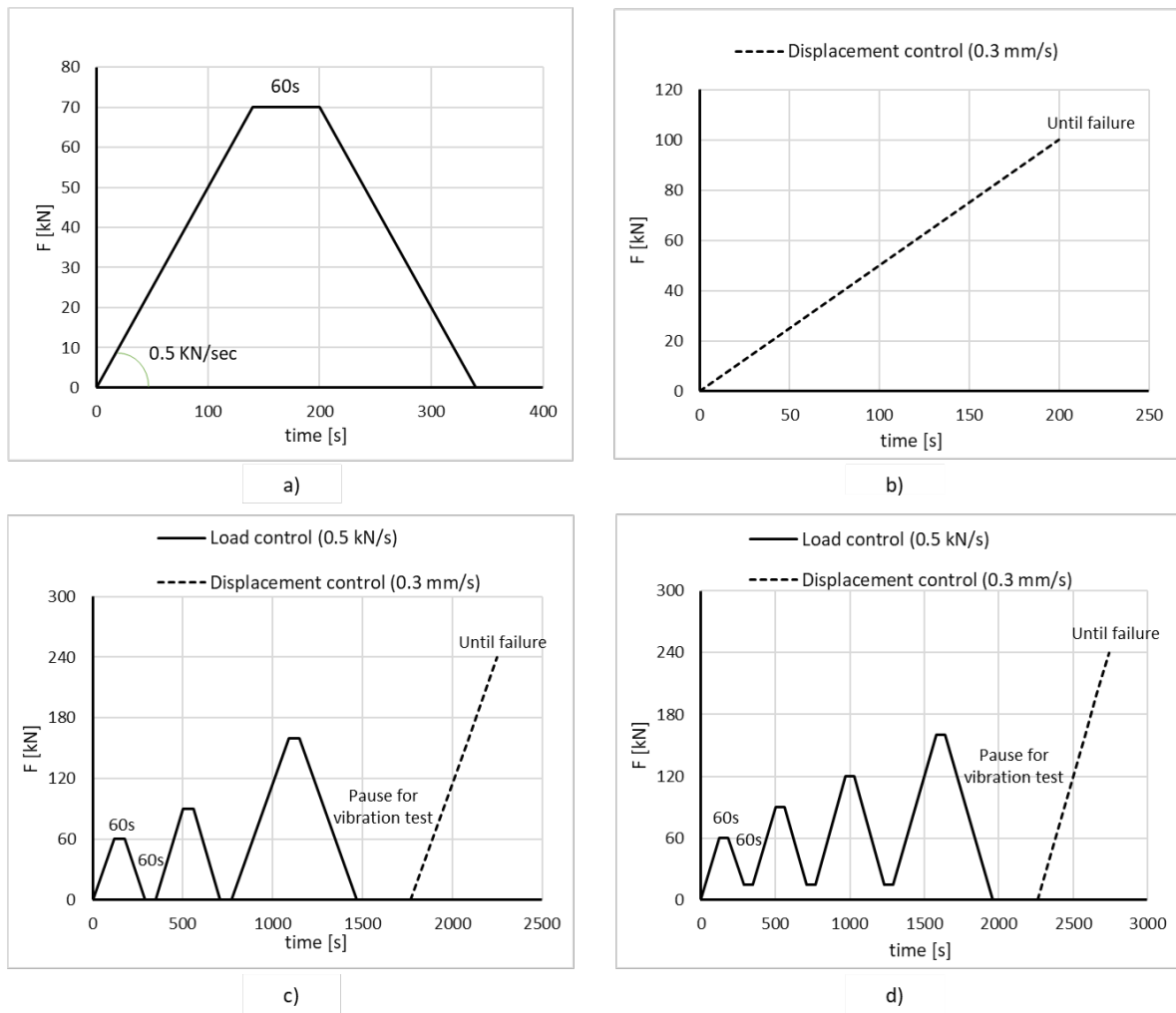


Figure 26. Loading procedure of the bending experiment for a) CCC B1, b) CLT B1, c) CCC B2, and d) CCC B3.

Figure 27 illustrates both the global and local failure modes of the specimens. Global failure in all cases resulted from brittle flexural failure of the CLT panels. CLT-B1 and CCC-B2 experienced this failure near the mid-span, while CCC-B3 encountered it closer to the loading

point. Flexural failure originated from the failure of finger joint connections or tensile splintering of timber boards on the lower layer of CLT panels. Additionally, local failures were observed at notched shear connections, involving compression crushing and shear crack opening in timber and concrete.

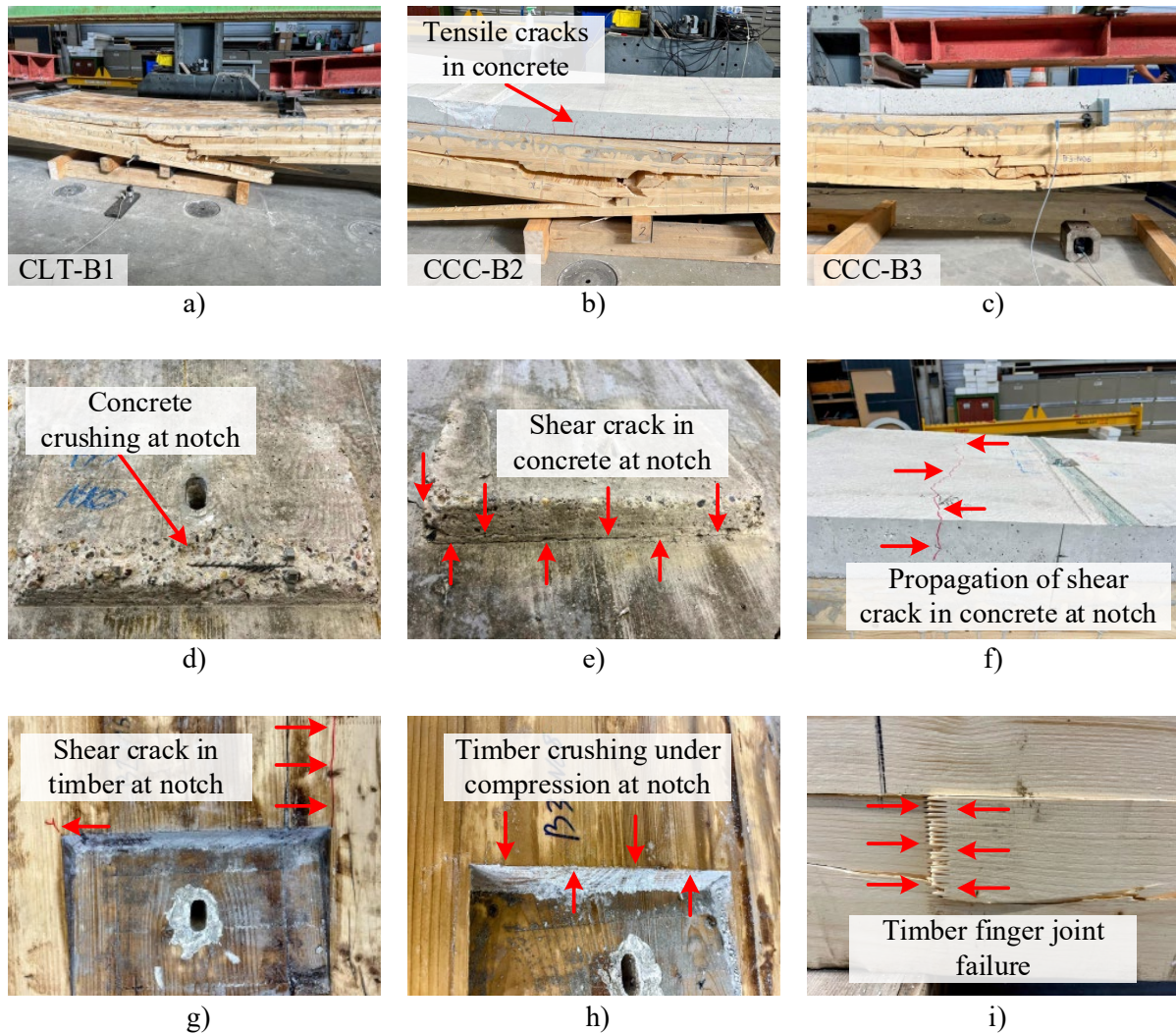


Figure 27. Failure modes of the specimens: a) flexural failure of the CLT panel in CLT-B1, b) flexural failure of the CLT panel and tensile crack opening in concrete in CCC B2, c) flexural failure of the CLT panel in CCC-B3, d) concrete crushing under compression at the notch, e) shear crack opening in concrete at notch, f) shear crack propagation at the concrete from notch to concrete surface, g) shear cracks in timber at notch, h) timber crushing under compression at notch, i) finger joint failure in the tensile zone under bending at the midspan.

The load-deflection results from the bending experiments are depicted in Figure 28. For CCC-B1, a linear deflection was recorded with the load increase. The unloaded slab had about 8 mm of settlement. CLT-B1 deflected linearly up to close to the failure load. Before the failure, the stiffness drop due to the failure of some timber laminated boards and finger joints can be observed. CCC-B2 and CCC-B3 also performed linearly until the brittle failure. After loading and unloading cycles, an accumulation of permanent settlements can be observed.

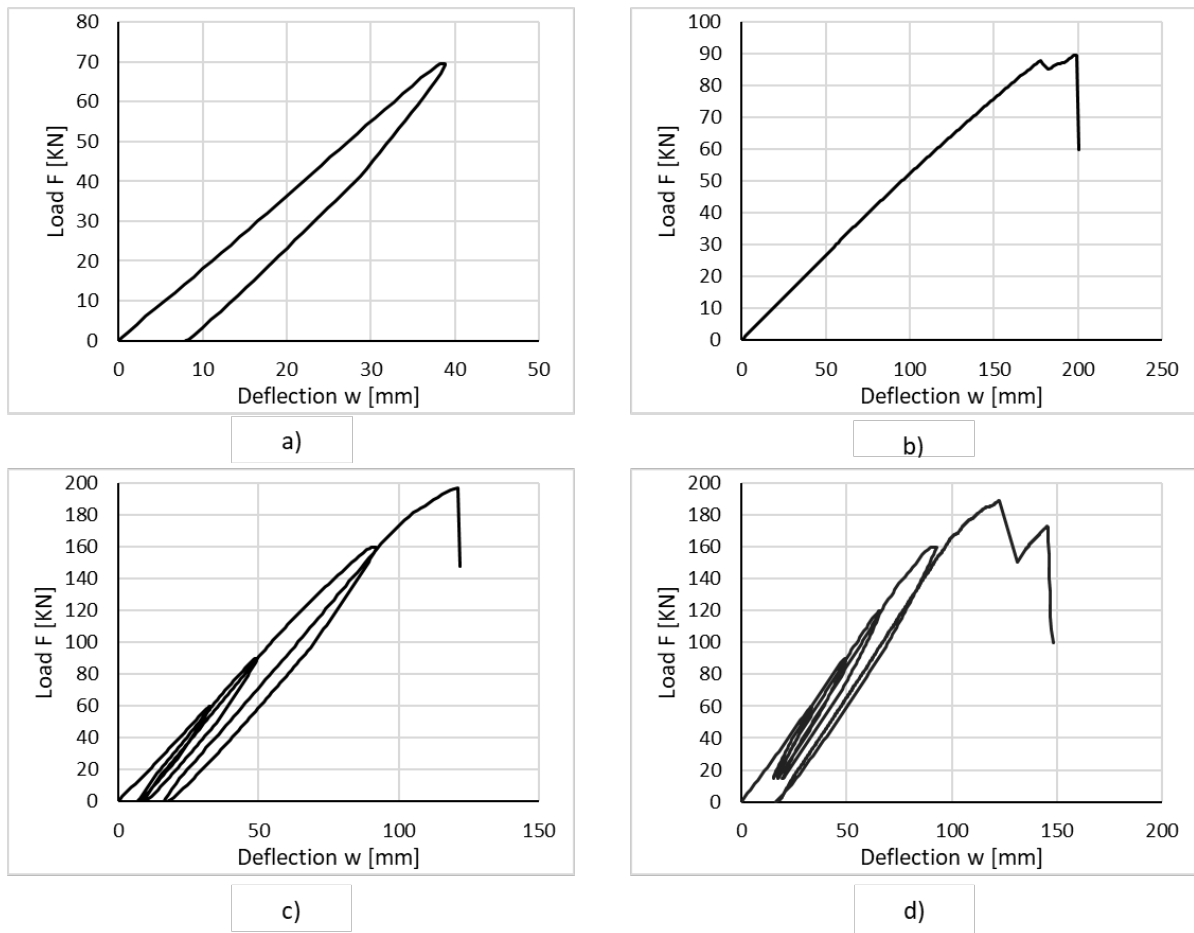


Figure 28. Load-deflection results of the bending experiment for a) CCC-B1, b) CLT-B1, c) CCC-B2, and d) CCC-B3.

Figure 29 depicts the end-span slip of each slab as recorded by sensors h1 and h2. The results are similar for all the slabs. A hardening in the slip curve can be observed during the initial loading cycle. This can be attributed to the gap closures between the concrete and timber at the notched connections. With the load increase in later cycles, the slip increases more linearly.

Stiffness softening in the 3rd and 4th loading cycles can be observed in CCC-B2 and CCC-B3, respectively. This softening becomes more significant in the last loading cycle, specifically before the failure of the slab.

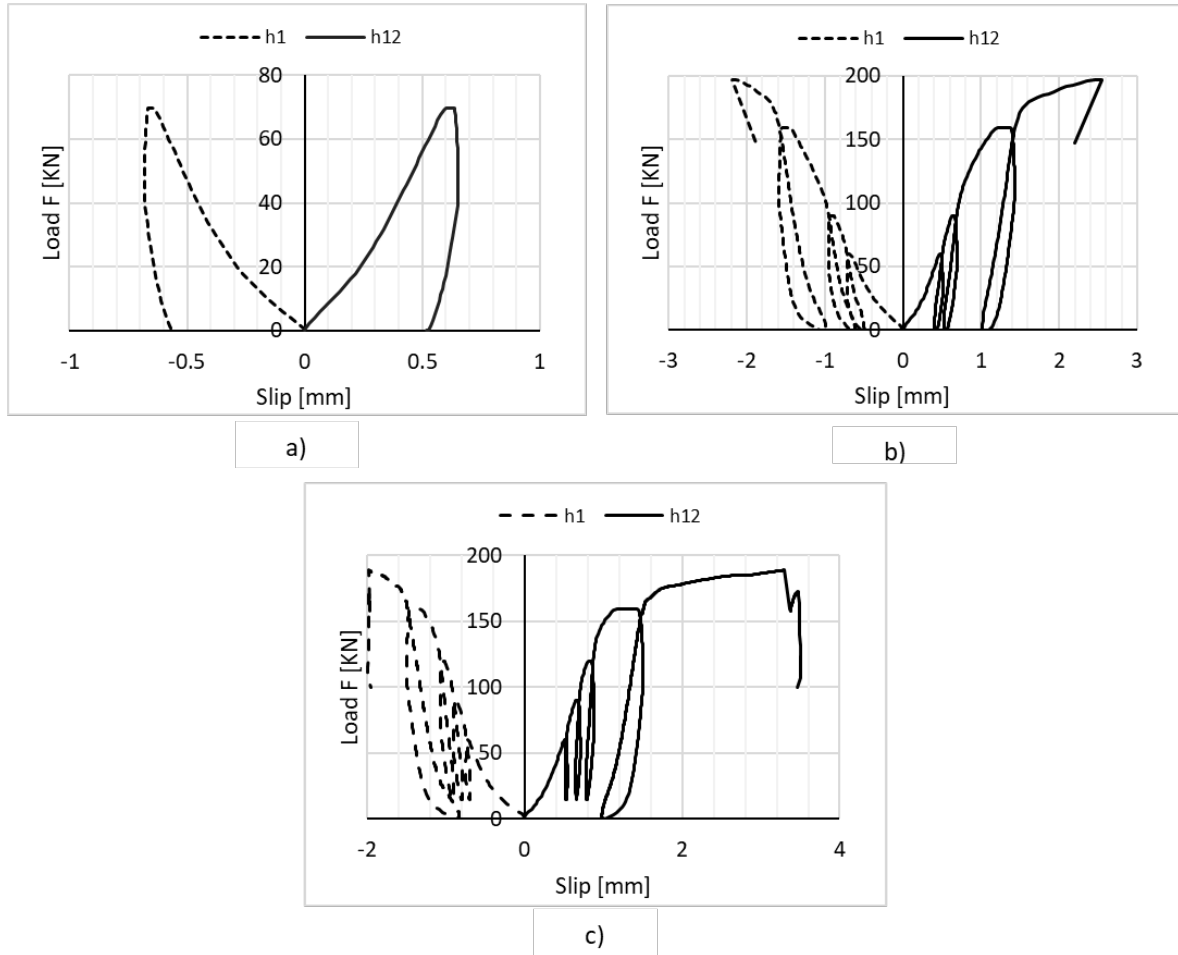


Figure 29. End-span slip of a) CCC-B1, b) CCC-B2 and c) CCC-B3.

Table 1 presents results from bending stiffness and the effective flexural rigidity of the composite slab at the ultimate load and service load stages. The ultimate load F_u , mid-span deflection at the ultimate load Δw_u , and the bending stiffness at ultimate load k_u are extracted from the last loading cycle of the load-deflection curves. Accordingly, the first loading cycle was used to calculate the service load F_{ser} , deflection at service load w_{ser} , and bending stiffness at service load k_{ser} . The effective flexural rigidity is calculated at F_{ser} with the following formula from structural mechanics:

$$(EI)_{eff} = 3F_{ser}a(L^2 - 4a^2)/32w_{ser} \quad (9)$$

corresponding to a six-point bending loading setup. The flexural rigidity of the three CCC slabs is similar, averaging 28.91 MN.m² with a %CV of 0.67%. The average strength of the CCC slabs is 193.10 kN with a %CV of 2.13%. The results indicate that the composite slab exhibits 2.2 and 3.4 times higher strength and stiffness, respectively, compared to the CLT panel.

Table 1. The results from the six-point bending experiment.

Specimens No.	At the ultimate load cycle			At service load (first load cycle)			Flexural rigidity
	F _u [kN]	Δw _u [mm]	k _u [kN/mm]	F _{ser} [kN]	w _{ser} [mm]	k _{ser} [kN/mm]	(EI) _{eff} [MN.m ²]
CCC B1	-	-	-	60.0	32.8	1.83	28.82
CCC B2	197.2	104.9	1.88	59.4	32.1	1.85	29.17
CCC B3	189.0	106.5	1.77	59.6	32.7	1.82	28.74
CLT B1	89.4	199.0	0.45	26.7	49.7	0.54	8.45

Figure 30 shows the CCC-B2 slab demounted after failure. After opening the bolts, the concrete slab was easily separated from the CLT panel.



Figure 30. Demounted CCC-B2 slab after failure.

The demounting of concrete from the CLT panel in specimen CCC-B1 after the first loading cycle is depicted in Figure 31. The figure shows that the concrete slab was cut into smaller

pieces and easily removed. This demounting represents the ease of deconstruction in the proposed floor system.



Figure 31. Demounting concrete slab from CCC-B1 after the first loading cycle.

5 Discussion

In this chapter, the results from the five papers included in this dissertation are discussed. For each paper, the highlights, relevance to the dissertation topic, limitations, and connections to other papers in this dissertation are examined. Furthermore, considering that there may be a time gap between the publication of the papers and the writing of this dissertation, any possible updates and relevant studies in the literature during this gap are presented.

5.1 Paper I

To examine the implications of various materials utilized in a floor system, this paper conducted a comparative analysis of the environmental impacts associated with a TCC floor system in contrast to RC and SCC systems, all designed for identical loading conditions and span lengths. The results showed that the TCC floor system has slight advantages compared to the SCC system. However, compared to an RC floor system, the impacts were reduced by the TCC system to one-third. The result demonstrated the importance of this dissertation in exploring new shear connections for TCC floor systems.

In the latter part of the paper, a comparison was drawn between various EoL scenarios for the timber component within a TCC floor system. Upon reaching the end of the lifecycle of a TCC floor system, the paper suggested that the concrete undergoes downcycling, while the steel parts were recycled. Subsequently, different scenarios were proposed for the timber component, as a CLT panel, with reuse emerging as the most sustainable solution, given its lowest GWP and required PE. Moreover, the environmental advantages of the reuse scenario were deemed more sustainable, taking into account both GWP and PE metrics. The outcome highlighted the importance of developing demountable shear connections for TCC systems to enable the reuse of timber while minimizing time and energy expenses.

While the paper underscored the benefits of TCC floor systems and demountable shear connections, it is important to note that the analysis only encompassed data pertinent to Luxembourg and its surrounding regions. Additionally, the range of alternative floor systems considered in the study was limited, indicating a need for further research to comprehensively address the environmental impacts of the floor systems. Expanding the scope to include a broader array of solutions would provide a broader understanding of different materials and methods within this context.

Since the publication of Paper I, other studies have delved into the same topic. In a similar study [96] researchers compared the greenhouse gas emissions of CLT, TCC, and RC slabs designed for equivalent structural performance. The findings revealed that CLT slabs emitted 75% less carbon dioxide compared to RC slabs under all conditions. Similarly, TCC slabs exhibited a reduction in emissions ranging from 50% to 70%, depending on the span length of the slab. The study identified span length as the most crucial structural design factor, rather than material strength or live load. These outcomes are consistent with those presented in Paper I, despite the absence of consideration for the EoL stage. Additionally, this study highlights the significant role of timber components in mitigating the carbon footprint of buildings. Furthermore, it demonstrates that TCC slabs become more beneficial in longer spans.

Another study [97] compared the environmental impacts of various CLT-hybrid walls and insulation types with conventional RC walls in tall residential buildings using LCA. The findings showed that when factoring in insulation, the environmental impacts of CLT walls are about 35% lower compared to traditional ones.

5.2 Paper II

Continuing with the same objective, Paper II extended the LCA study from the component level, as done in Paper I, to the building level. This paper presented a real case study comparing

the environmental impacts of two functionally identical buildings in Luxembourg constructed with different structural materials: masonry reinforced concrete and light-frame timber.

BIM models of the buildings were developed based on 2D drawings, enabling the extraction of material quantities for environmental impact assessment. The findings indicated that the timber building surpasses the concrete structure, with a 43.5% lower global warming potential. Conversely, the concrete building exhibited a 15.6% reduction in primary energy demand.

In assessing benefits and loads beyond the system's boundaries, the timber building showcased substantial advantages over the reinforced concrete masonry counterpart. Specifically, it delivered 3.6 times greater benefits in global warming potential and 4 times greater benefits in primary energy.

Moreover, the study delved into the impact of reusing floors within the timber building. According to the LCA, reusing timber slabs enhanced the building's global warming potential by 2.4% and its primary energy by 1.2%. However, when considering benefits and loads beyond the system's boundaries, reusing the floor system demonstrated a significant 38.9% increase in global warming advantages, albeit at the expense of a 28.1% reduction in primary energy benefits. These findings underscored at the level of building analysis, the necessity of promoting timber construction and reusable elements which aligns closely with the goal of this thesis.

The study holds significant value as it compares two real buildings constructed on the same site by the same company. This provided a realistic basis for conducting the comparative LCA, as factors such as design conditions, transportation methods and distances, and climate conditions were consistent between the buildings. Despite its importance, the study is constrained by the fact that it focuses on single-family houses, limiting its applicability to larger structures. Additionally, both buildings were constructed with identical basements and

foundations, which diminishes the potential benefits for the timber building, as timber typically requires less strong foundations.

Given the recent publication of Paper II, there are few new scientific publications in the literature. For instance, a study [98] comparing 48 non-residential buildings also underscores the advantages of timber as a structural material. Likewise, another study investigates the environmental performance of prefabricated construction compared to traditional methods, employing LCA and focusing on an office building case study in Sri Lanka. The findings of this research demonstrate an approximate 8% reduction in greenhouse gas emissions and overall impact savings across various impact categories for the prefabricated building. Once more, these findings underscore the significance of timber structures and prefabrication in mitigating the environmental footprint of buildings.

5.3 Paper III

Timber exhibits a complex mechanical behavior when subjected to loading. As an orthotropic material, it demonstrates linear elastic characteristics with a brittle failure mode under tension, whereas under compression, it displays elastic-plastic behavior with strain softening and ductile failure. To conduct numerical studies on timber structural components effectively, it is crucial to utilize an accurate three-dimensional material model that can simulate timber's behavior, including its damage and failure mechanisms.

The extended literature review of Paper III demonstrated that timber material models designed to replicate the non-linear behavior of timber can be classified into three main groups: elastic-plastic models, elastic-damage models, and a combination of elastic-plastic and damage models. Although different models exist in the literature, this paper proposes a model as an elastoplastic orthotropic material under a 3D stress state. A flow rule model associated with the Hoffmann yield criterion and plastic potential is utilized to characterize the plastic behavior

of timber under compression. Isotropic strain hardening during plastic deformation is integrated into the Hoffmann yield criterion by considering the equivalent yield stress as a function of the equivalent plastic strain. The Hoffman criterion was chosen as it differentiates between the strength under compression and tension, unlike other models. As of the present date of writing this thesis, to the knowledge of the author, no other material model has been proposed in the literature for timber since the proposal of this particular model.

The paper facilitated the numerical studies on the demountable TCC floor system proposed in this thesis. The material model is used in Paper IV and Paper V for the simulation of the downscaled TCC slab and the shear connection, respectively.

5.4 Paper IV

Recognizing the significance of timber structures and reusability for sustainability in construction, Paper IV aimed to explore the design of a modular TCC system that optimizes processes related to prefabrication, transportation, installation, maintenance, disassembly, modular reuse, deconstruction, and material recycling. The paper proposed a novel TCC modular floor system capable of prefabrication, modular reuse, demounting, and recycling at the end of its lifecycle using demountable shear connections.

The paper conducted a downscaled experimental and numerical study on the proposed floor system. Subsequently, it carried out a parametric numerical investigation to identify the key parameters influencing the mechanical behavior of such a slab under bending. To accomplish this, the paper utilized the timber material model proposed in Paper III. The findings indicated that the system exhibits a high level of composite action, along with suitable stiffness and strength, rendering the floor system reliable for its intended purpose.

Demonstrating the feasibility and, more importantly, the reliability of the system, Paper IV paved the way for the real-scaled study on the demountable shear connection, as implemented

in Paper V. Any gaps identified between the literature review of Paper IV and the most current literature were subsequently addressed in Paper V.

5.5 Paper V

Continuing the exploration of the novel demountable floor system proposed in Paper IV, Paper V explored the key parameters that influence the design of the system and ensured its reliability and adaptability considering the stiffness, strength, and load-bearing behavior.

Six different shear connections for a CLT-concrete composite floor system were designed and fabricated for testing, with various parameters examined against their stiffness, strength, and failure modes. The experimental test outcomes were subsequently utilized to develop numerical models, employing the material model introduced in Paper III.

The results from this paper were essential in determining the reusability of the connection and the essential parameters required for designing and analyzing the real-scaled floor system, as explored in Chapter 4 of this thesis. Since the paper was published recently, to the author's knowledge, no gaps exist between the literature review of the paper and the most updated literature.

6 Conclusion and outlook

The challenges in the modern construction industry demand contemporary solutions. Over the past few decades, the construction sector has focused on reducing energy consumption and carbon footprint. Initially, efforts were concentrated on minimizing energy demand during the use stage of a building's life cycle, resulting in the development of passive houses as the new standard in construction. The outcomes have been significant, with about a 30% decrease in the carbon footprint during the use stage (Paper II). However, it's crucial to recognize that the use stage does not solely determine the environmental impact of buildings. The production, construction, and end-of-life stages also contribute significantly to resource consumption and emission production. To mitigate the environmental impacts of these stages, a concentrated effort on the construction materials used in buildings is essential.

As a structural material, timber has gained significant attention for its potential to reduce the environmental impact of buildings. This reduction can be as much as 77.1% in GWP in a single-family house compared to a concrete masonry structure (Paper II). The arrival of EWPs has expanded the possibilities of using timber not only in low-rise buildings but also in mid- and high-rise constructions. The advantages of timber extend beyond its environmental benefits as it offers construction advantages such as rapid erection and ease of prefabrication. On the other hand, timber has certain drawbacks, like springiness, vibration, and poor sound insulation. These issues must be addressed, particularly during serviceability design.

The application of TCC floor systems emerged as a solution to harness the hybrid benefits of timber and concrete. A TCC slab, while exposing about one-third of the GWP compared to a conventional concrete slab (Paper I), can achieve a flexural stiffness approximately 3.4 times higher than a plain timber slab (Chapter 4). Consequently, TCC floor systems have garnered significant attention for sustainable construction. Prefabrication, with its associated advantages

like waste reduction, decreased labor hours, and shorter construction time leading to environmental benefits, has been studied in several studies. However, limited research has focused on the possibilities of reusing and deconstructing TCC floor systems. Deconstructing and reusing a TCC slab can double its EoL benefits, particularly regarding GWP (Paper I). Therefore, the primary focus of this study was to incorporate the DfD concept in a TCC floor system.

Four key topics were explored to address this study's primary focus. The first topic involved determining the potential environmental benefits of timber and TCC structures. This investigation was undertaken in Papers I and II through a series of LCA studies, comparing timber and TCC solutions to conventional ones. Additionally, various EoL scenarios for timber were examined.

The second topic involved finding a material model to simulate the behavior of timber as a construction material, as discussed in Paper III. This task was challenging due to timber's anisotropic nature and differing behaviors under compression and tension stresses. An orthotropic material constitution law was developed based on Hoffman's yield criterion. The material model accurately simulated the strain-hardening behavior of timber under compression and the brittle failure under tension. It was also valid for simulating timber's behavior and failure in bending. Moreover, the material model could address the propagation of the damage in timber. This material model facilitated the development of numerical studies used in developing the TCC shear connection.

The third topic focused on the conceptual design of a modular and prefabricated slab that could be reused and easily demounted for material separation and recycling. The concept involved prefabricated reusable modules of TCC slabs with demountable shear connections. This approach allowed the TCC slab to be reused as a module and, at the end of its life, easily

demounted to separate timber and concrete for new applications or recycling with minimal effort, time, and energy. The concept was detailed in Paper IV, and a downscaled slab sample was fabricated and tested. Additionally, a parametric numerical study was conducted to explore the behavior of different shapes of the notched shear connection.

The fourth topic involved a real-scaled investigation of the shear connection and the floor system. The focus was on the shear behavior of the shear connection through a push-out experiment campaign, as presented in Paper V, and the bending performance of the real-scaled slab detailed in Chapter 4. CLT was chosen as the timber component in the TCC slab due to its orthogonal rigidity, sound and thermal insulation properties, efficient prefabrication, and high strength and stiffness with lower variability in mechanical properties compared to solid timber.

The push-out experiments assessed the stiffness, strength, and shear behavior of 6 samples of the demountable shear connection, complemented by the study of numerical models for these connection samples. Based on the shear behavior results, shear connection sample F was selected for the bending test. A six-point bending setup with a span length of 10 meters was prepared, and 3 CCC slabs were designed and tested. One CCC slab was loaded up to the service load, then demounted, and the concrete layer was removed, allowing separate testing of the CLT under the same bending setup. This experiment also provided insights into the feasibility of demounting and reusing the slab.

Overall, the findings of this study can be highlighted as follows.

1. Comparative Environmental Impact Analysis:

- TCC floor system exhibits one-third of GWP and half of the PE demand compared to the RC floor.
- TCC floor system shows significantly higher environmental benefits in stage D of LCA.
- Full CLT reuse is the most sustainable EoL scenario, with the lowest GWP and PE.

2. GWP Comparison between Masonry Concrete and Timber Buildings:

- The concrete building emits 77.1% higher GWP than the timber building.
- Structural components are primarily responsible for GWP in the concrete building (61.4%).
- For the timber building, insulation and finishing parts contribute significantly (59.3%).

3. PE Comparison between Masonry Concrete and Timber Buildings:

- The timber building has an overall PE of approximately 15.6% higher than the concrete building.
- Finishing components in the timber building require 211% more PE than in the concrete building.

4. Proposed shear connection and CCC slab Analysis:

- Notch length does not significantly influence slab strength.
- Excessive increase in notch depth decreases the bending capacity of the slab.
- The proposed construction method facilitates prefabrication and installation.
- The slab could exhibit a noticeable efficiency of 73% in composite action.
- The push-out test configuration for testing notched shear connections must allow horizontal shear failure in timber.
- The strength of the shear connection increases with the timber length in front of the notch (notch heel length).
- Inclined face notches enhance the ductility of the shear connection.
- Proposed shear connections by this study match or surpass conventional permanent and deconstructable ones.
- Proposed connections by this study exhibit noticeably higher stiffness than existing CCC connections.
- Reuse increases the stiffness of the proposed shear connections.

- The proposed floor system is fully demountable before and after failure.

The outlook of the thesis suggests a need for extensive experimental studies to discover various aspects of the proposed shear connection and the demountable modular CCC floor system. A key area for exploration is the behavior of the shear connection under cyclic and long-term loading with varying environmental conditions. This will contribute to a comprehensive understanding of the connection's performance over time.

Moreover, the bending behavior of the CCC slab demands further investigation. Dynamic behavior studies for both individual modules and interconnected series are essential. This involves exploring the influence of varying numbers of shear connections in both the length and width of the slab and studying the bending behavior of several CCC modules connected together. Understanding the long-term deformations of such slabs is crucial, as it can significantly affect reuse potential and bending stiffness.

7 Bibliography

1. Gálvez-Martos, J.-L.; Styles, D.; Schoenberger, H.; Zeschmar-Lahl, B. Construction and Demolition Waste Best Management Practice in Europe. *Resources, Conservation and Recycling* **2018**, *136*, 166–178, doi:10.1016/j.resconrec.2018.04.016.
2. Takano, A.; Winter, S.; Hughes, M.; Linkosalmi, L. Comparison of Life Cycle Assessment Databases: A Case Study on Building Assessment. *Building and Environment* **2014**, *79*, 20–30, doi:10.1016/j.buildenv.2014.04.025.
3. Chen, C.; Bi, L. Study on Spatio-Temporal Changes and Driving Factors of Carbon Emissions at the Building Operation Stage- A Case Study of China. *Building and Environment* **2022**, *219*, 109147, doi:10.1016/j.buildenv.2022.109147.
4. *Biomimetic Research for Architecture and Building Construction*; Knippers, J., Nickel, K.G., Speck, T., Eds.; Biologically-Inspired Systems; Springer International Publishing: Cham, 2016; Vol. 8; ISBN 978-3-319-46372-8.
5. European Commission, Directorate-General for Climate Action COMMUNICATION FROM THE COMMISSION TO THE EUROPEAN PARLIAMENT, THE COUNCIL, THE EUROPEAN ECONOMIC AND SOCIAL COMMITTEE AND THE COMMITTEE OF THE REGIONS Stepping up Europe's 2030 Climate Ambition Investing in a Climate-Neutral Future for the Benefit of Our People 2020.
6. Anderson, J.; Moncaster, A. Embodied Carbon, Embodied Energy and Renewable Energy: A Review of Environmental Product Declarations. *Proceedings of the Institution of Civil Engineers - Structures and Buildings* **2022**, 1–12, doi:10.1680/jstbu.21.00160.
7. Eco-Construction for Sustainable Development (ECON4SD) – Just Another UL Multisite Site.
8. Islam, H.; Bhuiyan, M.; Tushar, Q.; Navaratnam, S.; Zhang, G. Effect of Star Rating Improvement of Residential Buildings on Life Cycle Environmental Impacts and Costs. *Buildings* **2022**, *12*, 1605, doi:10.3390/buildings12101605.
9. Takano, A.; Hafner, A.; Linkosalmi, L.; Ott, S.; Hughes, M.; Winter, S. Life Cycle Assessment of Wood Construction According to the Normative Standards. *Eur. J. Wood Prod.* **2015**, *73*, 299–312, doi:10.1007/s00107-015-0890-4.
10. D'Agostino, D.; Mazzarella, L. What Is a Nearly Zero Energy Building? Overview, Implementation and Comparison of Definitions. *Journal of Building Engineering* **2019**, *21*, 200–212, doi:10.1016/j.jobe.2018.10.019.
11. Vilches, A.; Garcia-Martinez, A.; Sanchez-Montañes, B. Life Cycle Assessment (LCA) of Building Refurbishment: A Literature Review. *Energy and Buildings* **2017**, *135*, 286–301, doi:10.1016/j.enbuild.2016.11.042.
12. Rodrigues, C.; Freire, F. Integrated Life-Cycle Assessment and Thermal Dynamic Simulation of Alternative Scenarios for the Roof Retrofit of a House. *Building and Environment* **2014**, *81*, 204–215, doi:10.1016/j.buildenv.2014.07.001.
13. Allacker, K. Sustainable Building: The Development of an Evaluation Method. *Dissertation Abstracts International* **2010**, *71*.
14. D'Amico, B.; Pomponi, F.; Hart, J. Global Potential for Material Substitution in Building Construction: The Case of Cross Laminated Timber. *Journal of Cleaner Production* **2021**, *279*, 123487, doi:10.1016/j.jclepro.2020.123487.
15. Chen, Z.; Gu, H.; Bergman, R.; Liang, S. Comparative Life-Cycle Assessment of a High-Rise Mass Timber Building with an Equivalent Reinforced Concrete Alternative Using the Athena Impact Estimator for Buildings. *Sustainability* **2020**, *12*, 4708, doi:10.3390/su12114708.

16. Tupenaite, L.; Kanapeckiene, L.; Naimaviciene, J.; Kaklauskas, A.; Gecys, T. Timber Construction as a Solution to Climate Change: A Systematic Literature Review. *Buildings* **2023**, *13*, 976, doi:10.3390/buildings13040976.
17. Franzini, F.; Toivonen, R.; Toppinen, A. Why Not Wood? Benefits and Barriers of Wood as a Multistory Construction Material: Perceptions of Municipal Civil Servants from Finland. *Buildings* **2018**, *8*, 159, doi:10.3390/buildings8110159.
18. Asdrubali, F.; Ferracuti, B.; Lombardi, L.; Guattari, C.; Evangelisti, L.; Grazieschi, G. A Review of Structural, Thermo-Physical, Acoustical, and Environmental Properties of Wooden Materials for Building Applications. *Building and Environment* **2017**, *114*, 307–332, doi:10.1016/j.buildenv.2016.12.033.
19. Robertson, A.B.; Lam, F.C.F.; Cole, R.J. A Comparative Cradle-to-Gate Life Cycle Assessment of Mid-Rise Office Building Construction Alternatives: Laminated Timber or Reinforced Concrete. *Buildings* **2012**, *2*, 245–270, doi:10.3390/buildings2030245.
20. Bernard, E.S. Dynamic Serviceability in Lightweight Engineered Timber Floors. *J. Struct. Eng.* **2008**, *134*, 258–268, doi:10.1061/(ASCE)0733-9445(2008)134:2(258).
21. Hu, L.J.; Chui, Y.H.; Onysko, D.M. Vibration Serviceability of Timber Floors in Residential Construction. *Prog. Struct. Engng Mater.* **2001**, *3*, 228–237, doi:10.1002/pse.69.
22. Zhou, H.; Lu, W.; Lu, B.; Wang, L.; Bao, Y.; Zhang, J.; Chen, Z. Experimental and Numerical Analyses on the Fire Resistance of Timber–Concrete Composite Boards Using an Innovative Form of Partial Protection. *Buildings* **2023**, *13*, 725, doi:10.3390/buildings13030725.
23. Ceccotti, A. Timber-Concrete Composite Structures. *Timber engineering–STEP* **1995**, *2*, E13.
24. Dias, A.M.P.G. Mechanical Behaviour of Timber-Concrete Joints, Universidade de Coimbra: Portugal, 2005.
25. Siddika, A.; Mamun, Md.A.A.; Aslani, F.; Zhuge, Y.; Alyousef, R.; Hajimohammadi, A. Cross-Laminated Timber–Concrete Composite Structural Floor System: A State-of-the-Art Review. *Engineering Failure Analysis* **2021**, *130*, 105766, doi:10.1016/j.engfailanal.2021.105766.
26. Holschemacher, K.; Hoffmann, L.; Heiden, B. Environmental Impact of Timber-Concrete Composite Slabs in Comparison to Other Floor Systems.; Santiago, Chile, August 9 2021; p. 6.
27. Eslami, H.; Yaghma, A.; Bhagya Jayasinghe, L.; Waldmann, D. INFLUENCE OF DIFFERENT END-OF-LIFE CYCLE SCENARIOS ON THE ENVIRONMENTAL IMPACTS OF TIMBER-CONCRETE COMPOSITE FLOOR SYSTEMS. In Proceedings of the World Conference on Timber Engineering (WCTE 2023); World Conference on Timber Engineering (WCTE 2023): Oslo, Norway, 2023; pp. 982–988.
28. Monteiro, S.; Dias, A.; Lopes, S. Distribution of Concentrated Loads in Timber-Concrete Composite Floors: Simplified Approach. *Buildings* **2020**, *10*, 32, doi:10.3390/buildings10020032.
29. Dias, A.; Schänzlin, J.; Dietsch, P. Design of Timber-Concrete Composite Structures. *A State-of-the-Art Report by COST Action FPI402/WG* **2018**.
30. Tannert, T.; Gerber, A.; Vallee, T. Hybrid Adhesively Bonded Timber-Concrete-Composite Floors. *International Journal of Adhesion and Adhesives* **2020**, *97*, 102490, doi:10.1016/j.ijadhadh.2019.102490.
31. Pieragostini, C.; Mussati, M.C.; Aguirre, P. On Process Optimization Considering LCA Methodology. *Journal of Environmental Management* **2012**, *96*, 43–54, doi:10.1016/j.jenvman.2011.10.014.

32. Hollberg, A.; Kiss, B.; Röck, M.; Soust-Verdaguer, B.; Wiberg, A.H.; Lasvaux, S.; Galimshina, A.; Habert, G. Review of Visualising LCA Results in the Design Process of Buildings. *Building and Environment* **2021**, *190*, 107530, doi:10.1016/j.buildenv.2020.107530.
33. Réglementation environnementale RE2020 Available online: <https://www.ecologie.gouv.fr/reglementation-environnementale-re2020> (accessed on 12 September 2023).
34. Fish, L.A. Managerial Best Practices to Promote Sustainable Supply Chain Management & New Product Development. In *Applications of Contemporary Management Approaches in Supply Chains*; Tozan, H., Ertürk, A., Eds.; InTech, 2015 ISBN 978-953-51-2045-2.
35. ISO 14040:2006 Environmental Management — Life Cycle Assessment — Principles and Framework 2006.
36. *Life Cycle Assessment: Theory and Practice*; Hauschild, M.Z., Rosenbaum, R.K., Olsen, S.I., Eds.; Springer International Publishing: Cham, 2018; ISBN 978-3-319-56474-6.
37. Dixit, M.K.; Culp, C.H.; Fernández-Solís, J.L. System Boundary for Embodied Energy in Buildings: A Conceptual Model for Definition. *Renewable and Sustainable Energy Reviews* **2013**, *21*, 153–164, doi:10.1016/j.rser.2012.12.037.
38. Guinée, J.B. Selection of Impact Categories and Classification of LCI Results to Impact Categories. In *Life Cycle Impact Assessment*; Hauschild, M.Z., Huijbregts, M.A.J., Eds.; LCA Compendium – The Complete World of Life Cycle Assessment; Springer Netherlands: Dordrecht, 2015; pp. 17–37 ISBN 978-94-017-9744-3.
39. CEN: Brussels ILNAS-EN 15978:2011; Sustainability of Construction Works - Assessment of Environmental Performance of Buildings - Calculation Method 2011.
40. Mielecke, C.; Mielecke, T.; Lützkendorf, T. *Wissenschaftliche Begleitung der Arbeitsgruppe „Modul D“ des Runden Tisches Nachhaltiges Bauen*; Forschungsinitiative „Zukunft Bau“; des Bundesinstituts für Bau-, Stadt- und Raumforschung (BBSR) im Bundesamt für Bauwesen und Raumordnung (BBR), 2017;
41. Kanters, J. Design for Deconstruction in the Design Process: State of the Art. *Buildings* **2018**, *8*, 150, doi:10.3390/buildings8110150.
42. Crawford, R. *Life Cycle Assessment in the Built Environment*; Taylor & Francis, 2011; ISBN 978-1-135-24509-2.
43. Architects, W.T. Murray Grove | Waugh Thistleton Architects Available online: <http://waughthistleton.com/murray-grove/> (accessed on 10 August 2023).
44. Multi Residential Architecture Available online: <https://www.architectureanddesign.com.au/projects/multi-residential/forte-by-lend-lease> (accessed on 13 September 2023).
45. Malo, K.A.; Abrahamsen, R.B.; Bjertnæs, M.A. Some Structural Design Issues of the 14-Storey Timber Framed Building “Treet” in Norway. *Eur. J. Wood Prod.* **2016**, *74*, 407–424, doi:10.1007/s00107-016-1022-5.
46. Inside Vancouver’s Brock Commons, the World’s Tallest Mass Timber Building Available online: <https://www.archdaily.com/879625/inside-vancouvers-brock-commons-the-worlds-tallest-timber-structured-building> (accessed on 13 September 2023).
47. Building Available online: <https://hautamsterdam.nl/en/> (accessed on 13 September 2023).
48. Reiterer, A.; Stanzl-Tschegg, S.E. Compressive Behaviour of Softwood under Uniaxial Loading at Different Orientations to the Grain. *Mechanics of Materials* **2001**, *33*, 705–715, doi:10.1016/S0167-6636(01)00086-2.

49. Daudeville, L.; Davenne, L.; Yasumura, M. Prediction of the Load Carrying Capacity of Bolted Timber Joints. *Wood Science and Technology* **1999**, *33*, 15–29, doi:10.1007/s002260050095.
50. Serrano, E. Glued-in Rods for Timber Structures - a 3D Model and Finite Element Parameter Studies. **2001**, 13.
51. Smith, I.; Vasic, S. Fracture Behaviour of Softwood. *Mechanics of Materials* **2003**, *35*, 803–815, doi:10.1016/S0167-6636(02)00208-9.
52. Vasic, S.; Smith, I.; Landis, E. Finite Element Techniques and Models for Wood Fracture Mechanics. *Wood Sci Technol* **2005**, *39*, 3–17, doi:10.1007/s00226-004-0255-3.
53. Benvenuti, E.; Orlando, N.; Gebhardt, C.; Kaliske, M. An Orthotropic Multi-Surface Damage-Plasticity FE-Formulation for Wood: Part I – Constitutive Model. *Computers & Structures* **2020**, *240*, 106350, doi:10.1016/j.compstruc.2020.106350.
54. Nouri, F.; Valipour, H.R. Moment-Rotation Model for Steel-Timber Composite Connections with Slab Continuity Steel Rods. *Journal of Constructional Steel Research* **2020**, *173*, 106257, doi:10.1016/j.jcsr.2020.106257.
55. Dias, A.M.P.G.; Van de Kuilen, J.W.; Lopes, S.; Cruz, H. A Non-Linear 3D FEM Model to Simulate Timber–Concrete Joints. *Advances in Engineering Software* **2007**, *38*, 522–530, doi:10.1016/j.advengsoft.2006.08.024.
56. Moses, D.M.; Prion, H.G.L. Stress and Failure Analysis of Wood Composites: A New Model. *Composites Part B: Engineering* **2004**, *35*, 251–261, doi:10.1016/j.compositesb.2003.10.002.
57. Patton-Mallory, M.; Cramer, S.M.; Smith, F.W.; Pellicane, P.J. Nonlinear Material Models for Analysis of Bolted Wood Connections. *Journal of Structural Engineering* **1997**, *123*, 1063–1070, doi:10.1061/(ASCE)0733-9445(1997)123:8(1063).
58. Kharouf, N.; McClure, G.; Smith, I. Elasto-Plastic Modeling of Wood Bolted Connections. *Computers & Structures* **2003**, *81*, 747–754, doi:10.1016/S0045-7949(02)00482-0.
59. Hill, R. A Theory of the Yielding and Plastic Flow of Anisotropic Metals. *Proc. R. Soc. Lond. A* **1948**, *193*, 281–297, doi:10.1098/rspa.1948.0045.
60. Oudjene, M.; Khelifa, M. Elasto-Plastic Constitutive Law for Wood Behaviour under Compressive Loadings. *Construction and Building Materials* **2009**, *23*, 3359–3366, doi:10.1016/j.conbuildmat.2009.06.034.
61. Bouchair, A.; Vergne, A. An Application of the Tsai Criterion as a Plastic Flow Law for Timber Bolted Joint Modelling. *Wood Science and Technology* **1995**, *30*, 17.
62. Clouston, P.L.; Lam, F. Computational Modeling of Strand-Based Wood Composites. *J. Eng. Mech.* **2001**, *127*, 844–851, doi:10.1061/(ASCE)0733-9399(2001)127:8(844).
63. Tsai, S.W.; Wu, E.M. A General Theory of Strength for Anisotropic Materials. *Journal of Composite Materials* **1971**, *5*, 58–80, doi:10.1177/002199837100500106.
64. Srinivasan, V.S.; Saxena, A. 5.08 - Creep Resistance in Nonferritic Metals. In *Comprehensive Structural Integrity*; Milne, I., Ritchie, R.O., Karihaloo, B., Eds.; Pergamon: Oxford, 2007; pp. 374–403 ISBN 978-0-08-043749-1.
65. Rémy, L. 5.03 - Thermal–Mechanical Fatigue (Including Thermal Shock). In *Comprehensive Structural Integrity*; Milne, I., Ritchie, R.O., Karihaloo, B., Eds.; Pergamon: Oxford, 2003; pp. 113–199 ISBN 978-0-08-043749-1.
66. Shojaei, A.K.; Voyiadjis, G.Z. 11 - Dynamic Fracture Mechanics in Rocks with Application to Drilling and Perforation. In *Porous Rock Fracture Mechanics*; Shojaei, A.K., Shao, J., Eds.; Woodhead Publishing, 2017; pp. 233–256 ISBN 978-0-08-100781-5.
67. Kachanov, L.M. *Introduction to Continuum Damage Mechanics*; Mechanics of Elastic Stability; Springer Netherlands: Dordrecht, 1986; Vol. 10; ISBN 978-90-481-8296-1.

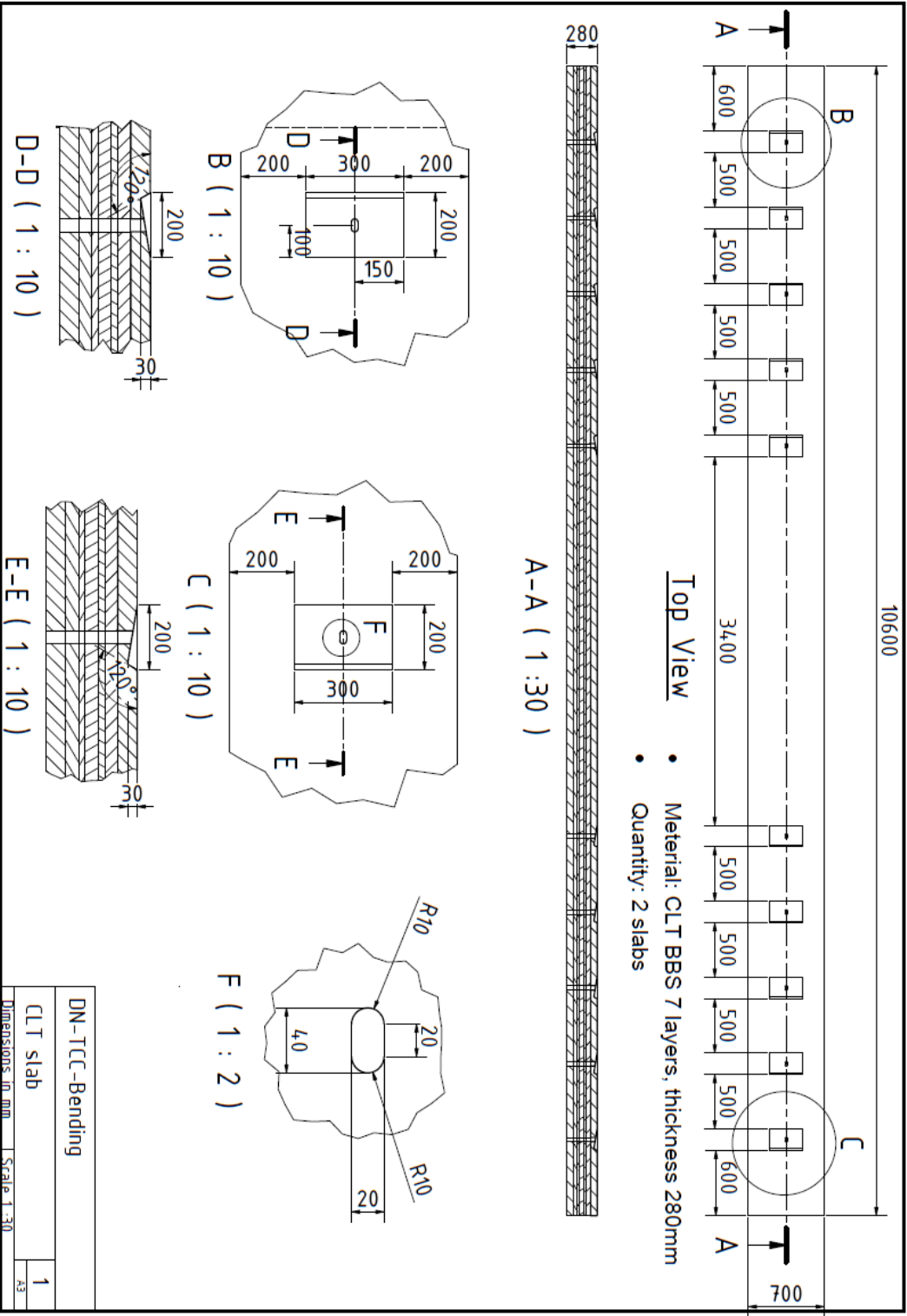
68. Chaboche, J.L.; Lesne, P.M. A Non-Linear Continuous Fatigue Damage Model. *Fatigue & Fracture of Engineering Materials & Structures* **1988**, *11*, 1–17, doi:10.1111/j.1460-2695.1988.tb01216.x.
69. Cui, W.C. 5 - Fatigue Cracking in Aged Structures. In *Condition Assessment of Aged Structures*; Paik, J.K., Melchers, R.E., Eds.; Woodhead Publishing Series in Civil and Structural Engineering; Woodhead Publishing, 2008; pp. 107–148 ISBN 978-1-84569-334-3.
70. Saanouni, K.; Chaboche, J.L. 3.06 - Computational Damage Mechanics: Application to Metal Forming Simulation. In *Comprehensive Structural Integrity*; Milne, I., Ritchie, R.O., Karihaloo, B., Eds.; Pergamon: Oxford, 2003; pp. 321–376 ISBN 978-0-08-043749-1.
71. Gharib, M.; Hassanieh, A.; Valipour, H.; Bradford, M.A. Three-Dimensional Constitutive Modelling of Arbitrarily Orientated Timber Based on Continuum Damage Mechanics. *Finite Elements in Analysis and Design* **2017**, *135*, 79–90, doi:10.1016/j.finel.2017.07.008.
72. Sandhaas, C.; Van De Kuilen, J.-W.G.; Blass, H.J. Constitutive Model for Wood Based on Continuum Damage Mechanics.; Auckland New Zealand, 2012.
73. Orlando, N.; Taddia, Y.; Benvenuti, E.; Pizzo, B.; Alessandri, C. End-Repair of Timber Beams with Laterally-Loaded Glued-in Rods: Experimental Trials and Failure Prediction through Modelling. *Construction and Building Materials* **2019**, *195*, 623–637, doi:10.1016/j.conbuildmat.2018.11.045.
74. Khennane, A.; Khelifa, M.; Bleron, L.; Viguiier, J. Numerical Modelling of Ductile Damage Evolution in Tensile and Bending Tests of Timber Structures. *Mechanics of Materials* **2014**, *68*, 228–236, doi:10.1016/j.mechmat.2013.09.004.
75. Tran, T.-T.; Thi, V.-D.; Khelifa, M.; Oudjene, M.; Rogaume, Y. A Constitutive Numerical Modelling of Hybrid-Based Timber Beams with Partial Composite Action. *Construction and Building Materials* **2018**, *178*, 462–472, doi:10.1016/j.conbuildmat.2018.05.080.
76. Xu, B.-H.; Bouchair, A.; Racher, P. Appropriate Wood Constitutive Law for Simulation of Nonlinear Behavior of Timber Joints. *J. Mater. Civ. Eng.* **2014**, *26*, 04014004, doi:10.1061/(ASCE)MT.1943-5533.0000905.
77. Khelifa, M.; Khennane, A.; El Ganaoui, M.; Celzard, A. Numerical Damage Prediction in Dowel Connections of Wooden Structures. *Mater Struct* **2016**, *49*, 1829–1840, doi:10.1617/s11527-015-0615-5.
78. Sirumbal-Zapata, L.F.; Málaga-Chuquitaype, C.; Elghazouli, A.Y. A Three-Dimensional Plasticity-Damage Constitutive Model for Timber under Cyclic Loads. *Computers & Structures* **2018**, *195*, 47–63, doi:10.1016/j.compstruc.2017.09.010.
79. Ceccotti, A. Composite Concrete-Timber Structures. *Prog. Struct. Engng Mater.* **2002**, *4*, 264–275, doi:10.1002/pse.126.
80. Gutkowski, R.M.; Goodman, J.R.; Pault, J.D.; Bodig, J. *TESTS AND ANALYSIS FOR COMPOSITE ACTION IN GLULAM BRIDGE SYSTEMS*; the ENGINEERING FOUNDATION for Grant RC-A-74-6; Colorado State University: Fort Collins, Colorado, 1977; p. 49;.
81. Piazza, M.; Ballerini, M. Experimental and Numerical Results on Timber-Concrete Composite Floors with Different Connection Systems.; University of British Columbia, 2000.
82. EN 1995-1-1 (2004) (English): Eurocode 5: Design of Timber Structures - Part 1-1: General - Common Rules and Rules for Buildings.

83. Vasiljevs, R.; Serdjuks, D.; Gerasimova, J.; Buka-Vaivade, K.; Erüz, A.O. Behaviour of Timber-Concrete Joints in Hybrid Members Subjected to Flexure. *IOP Conf. Ser.: Mater. Sci. Eng.* **2019**, *660*, 012050, doi:10.1088/1757-899X/660/1/012050.
84. Du, H.; Hu, X.; Xie, Z.; Wang, H. Study on Shear Behavior of Inclined Cross Lag Screws for Glulam-Concrete Composite Beams. *Construction and Building Materials* **2019**, *224*, 132–143, doi:10.1016/j.conbuildmat.2019.07.035.
85. Deam, B.L.; Fragiaco, M.; Buchanan, A.H. Connections for Composite Concrete Slab and LVL Flooring Systems. *Mater Struct* **2008**, *41*, 495–507, doi:10.1617/s11527-007-9261-x.
86. Lukaszewska, E.; Johnsson, H.; Fragiaco, M. Performance of Connections for Prefabricated Timber–Concrete Composite Floors. *Mater Struct* **2008**, *41*, 1533–1550, doi:10.1617/s11527-007-9346-6.
87. Shi, B.; Zhu, W.; Yang, H.; Liu, W.; Tao, H.; Ling, Z. Experimental and Theoretical Investigation of Prefabricated Timber-Concrete Composite Beams with and without Prestress. *Engineering Structures* **2020**, *204*, doi:10.1016/j.engstruct.2019.109901.
88. Zhang, L.; Chui, Y.H.; Tomlinson, D. Experimental Investigation on the Shear Properties of Notched Connections in Mass Timber Panel-Concrete Composite Floors. *Construction and Building Materials* **2020**, *234*, 117375, doi:10.1016/j.conbuildmat.2019.117375.
89. Clouston, P.; Bathon, L.A.; Schreyer, A. Shear and Bending Performance of a Novel Wood–Concrete Composite System. *J. Struct. Eng.* **2005**, *131*, 1404–1412, doi:10.1061/(ASCE)0733-9445(2005)131:9(1404).
90. Rasmussen, P.K.; Sørensen, J.H.; Hoang, L.C.; Feddersen, B.; Larsen, F. Notched Connection in Timber-Concrete Composite Deck Structures: A Literature Review on Push-off Experiments & Design Approaches. *Construction and Building Materials* **2023**, *397*, 131761, doi:10.1016/j.conbuildmat.2023.131761.
91. European Committee for Standardization ILNAS-EN 26891:1991 Timber Structures - Joints Made with Mechanical Fasteners - General Principles for the Determination of Strength and Deformation.
92. Eslami, H.; Yaghma, A.; Jayasinghe, L.B.; Waldmann, D. Comparative Life Cycle Assessment of Light Frame Timber and Reinforced Concrete Masonry Structural Systems for Single-Family Houses in Luxembourg. *Heliyon* **2024**, *10*, doi:10.1016/j.heliyon.2024.e26083.
93. Eslami, H.; Jayasinghe, L.B.; Waldmann, D. Nonlinear Three-Dimensional Anisotropic Material Model for Failure Analysis of Timber. *Engineering Failure Analysis* **2021**, *130*, 105764, doi:10.1016/j.engfailanal.2021.105764.
94. Eslami, H.; Jayasinghe, L.B.; Waldmann, D. Experimental and Numerical Investigation of a Novel Demountable Timber–Concrete Composite Floor. *Buildings* **2023**, *13*, 1763, doi:10.3390/buildings13071763.
95. Eslami, H.; Jayasinghe, L.B.; Waldmann, D. Experimental and Numerical Study on Shear Behavior of a Demountable CLT-Concrete Composite Shear Connection. *Construction and Building Materials* **2024**, *425*, 135982, doi:10.1016/j.conbuildmat.2024.135982.
96. Oh, J.-W.; Park, K.-S.; Kim, H.S.; Kim, I.; Pang, S.-J.; Ahn, K.-S.; Oh, J.-K. Comparative CO₂ Emissions of Concrete and Timber Slabs with Equivalent Structural Performance. *Energy and Buildings* **2023**, *281*, 112768, doi:10.1016/j.enbuild.2022.112768.
97. Shin, B.; Wi, S.; Kim, S. Assessing the Environmental Impact of Using CLT-Hybrid Walls as a Sustainable Alternative in High-Rise Residential Buildings. *Energy and Buildings* **2023**, *294*, 113228, doi:10.1016/j.enbuild.2023.113228.
98. Hafner, A.; Özdemir, Ö. Comparative LCA Study of Wood and Mineral Non-Residential Buildings in Germany and Related Substitution Potential. *Eur. J. Wood Prod.* **2023**, *81*, 251–266, doi:10.1007/s00107-022-01888-2.

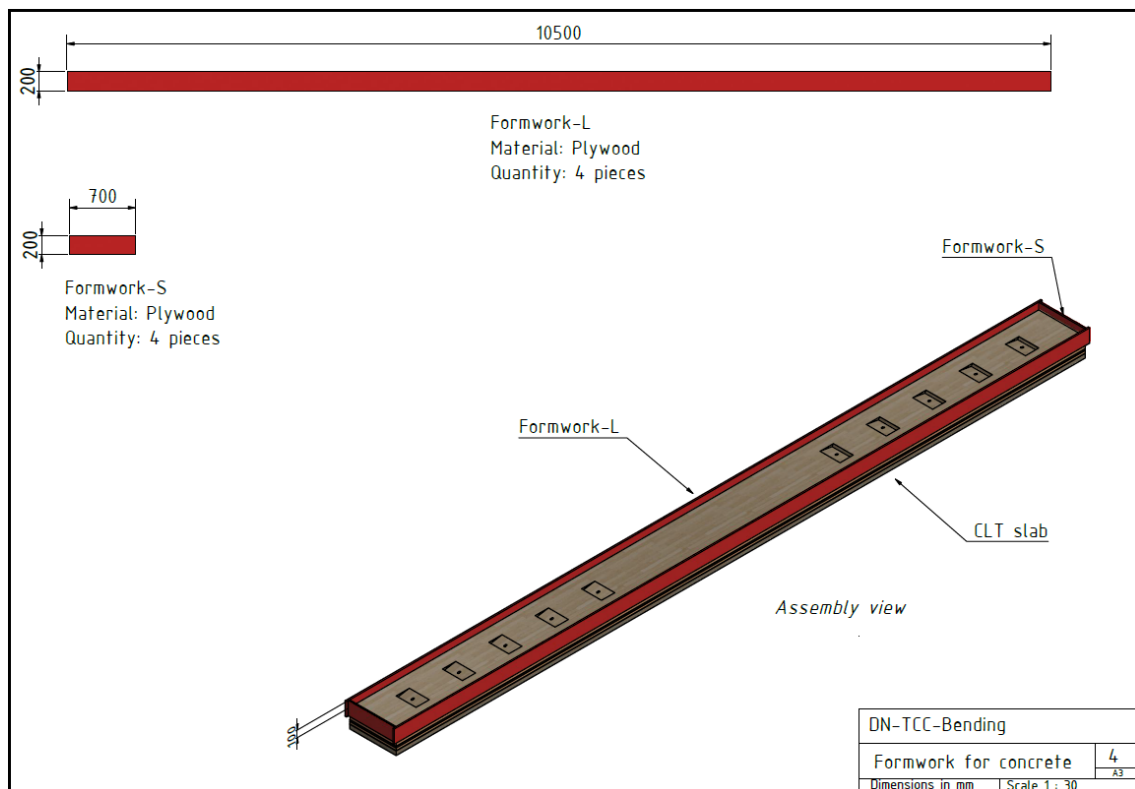
8 Annexes

8.1 Drawings of CCC bending experiment

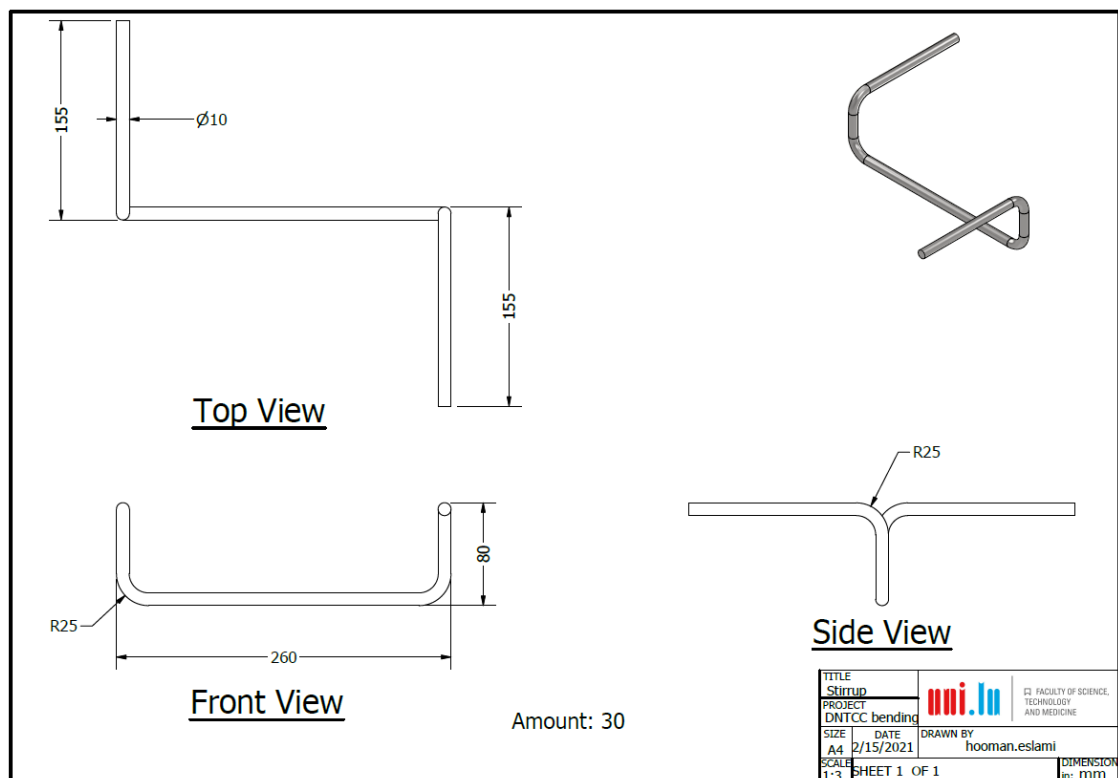
- CLT panel cut for CCC slabs



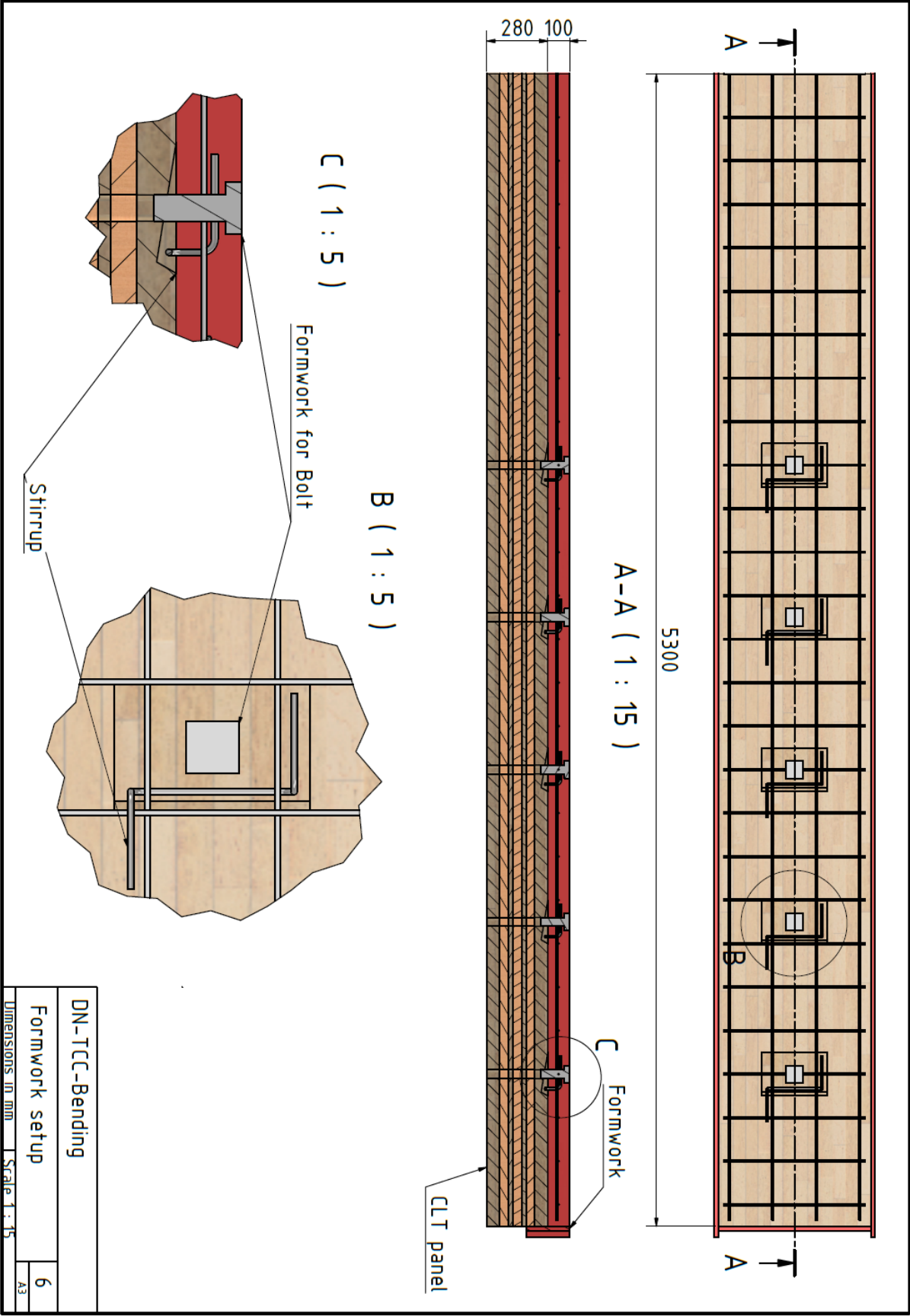
- CCC slab formwork for concreting



- Stirrup used in CCC slab



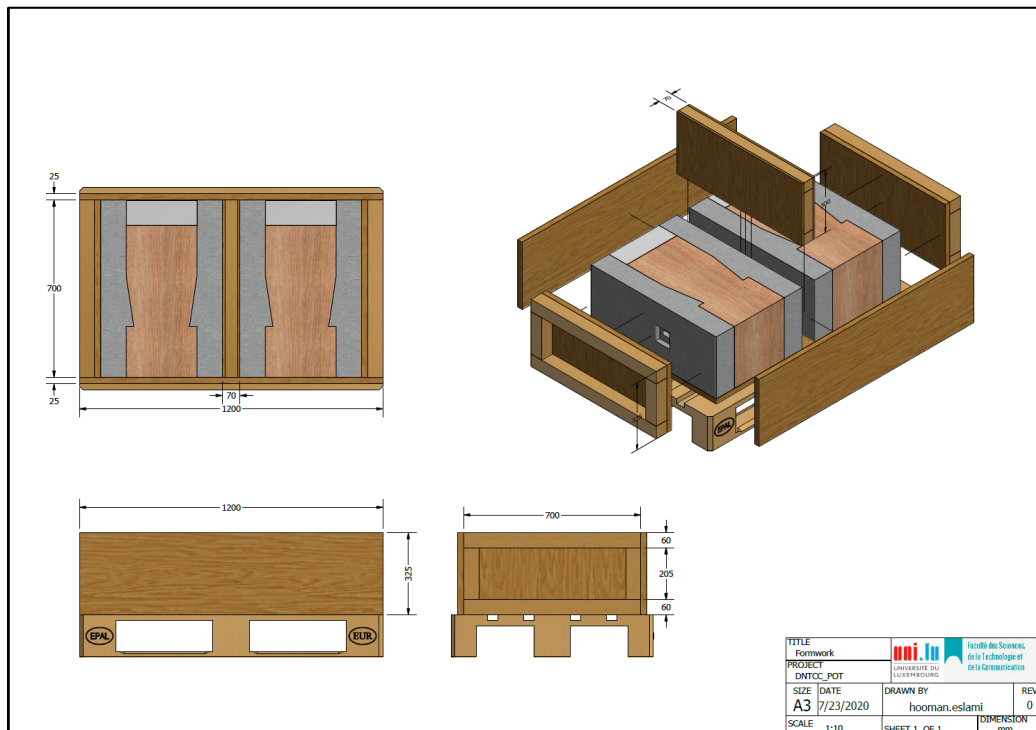
- CCC slabs formwork and reinforcement setup before concreting



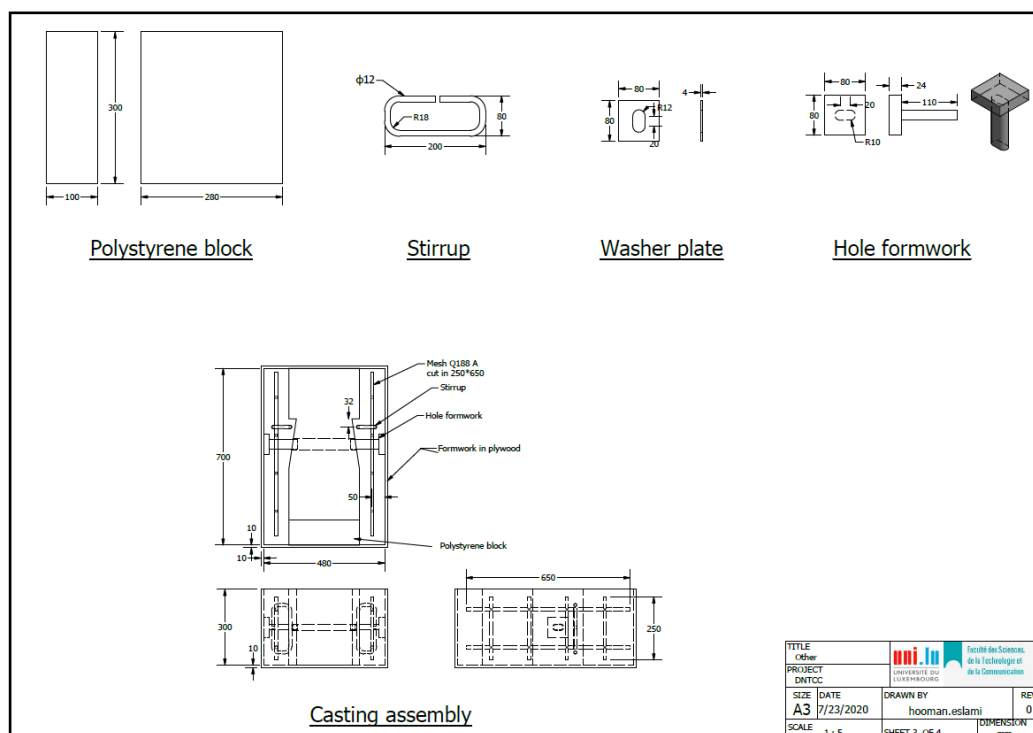
-
- Side View**
- LVDT for Vertical deformation w_1-w_4
- LVDT sensors for vertical gap opening v_1, v_2
- Top View**
- Load plate
- Support plate
- | TABLE | | | |
|--------------|-------------------|--------|---------|
| Sensor | Max. displacement | Amount | comment |
| w_1-w_4 | 200 | 4 | |
| h_1-h_{12} | 50 | 14 | |
| v_1, v_2 | 20 | 2 | |

8.2 Drawings of Push-out experiment

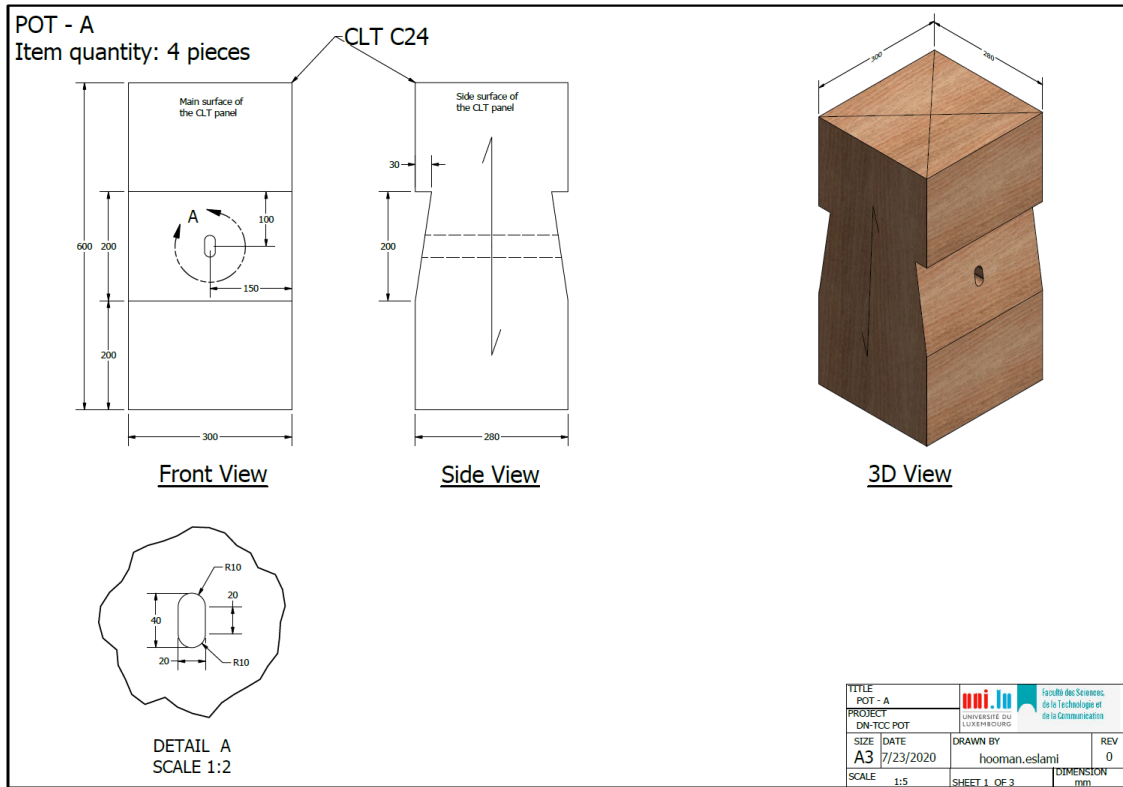
- Push-out test specimens' formwork



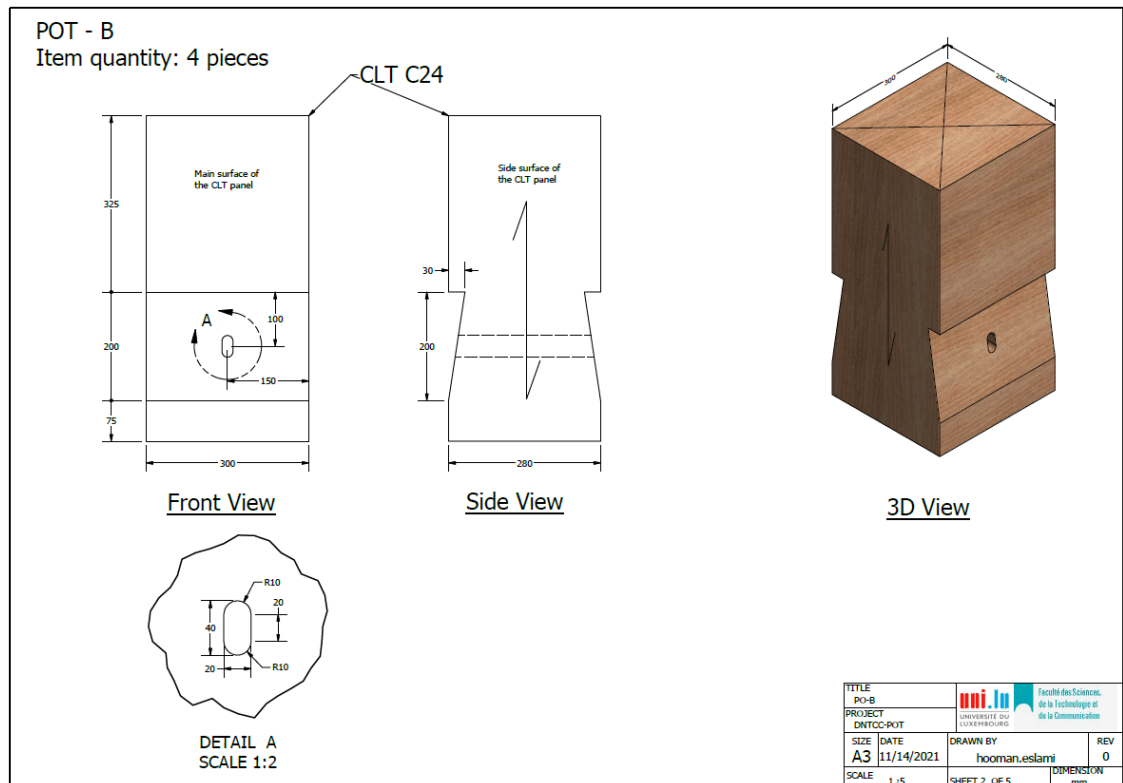
- Push-out test reinforcement and formwork setup



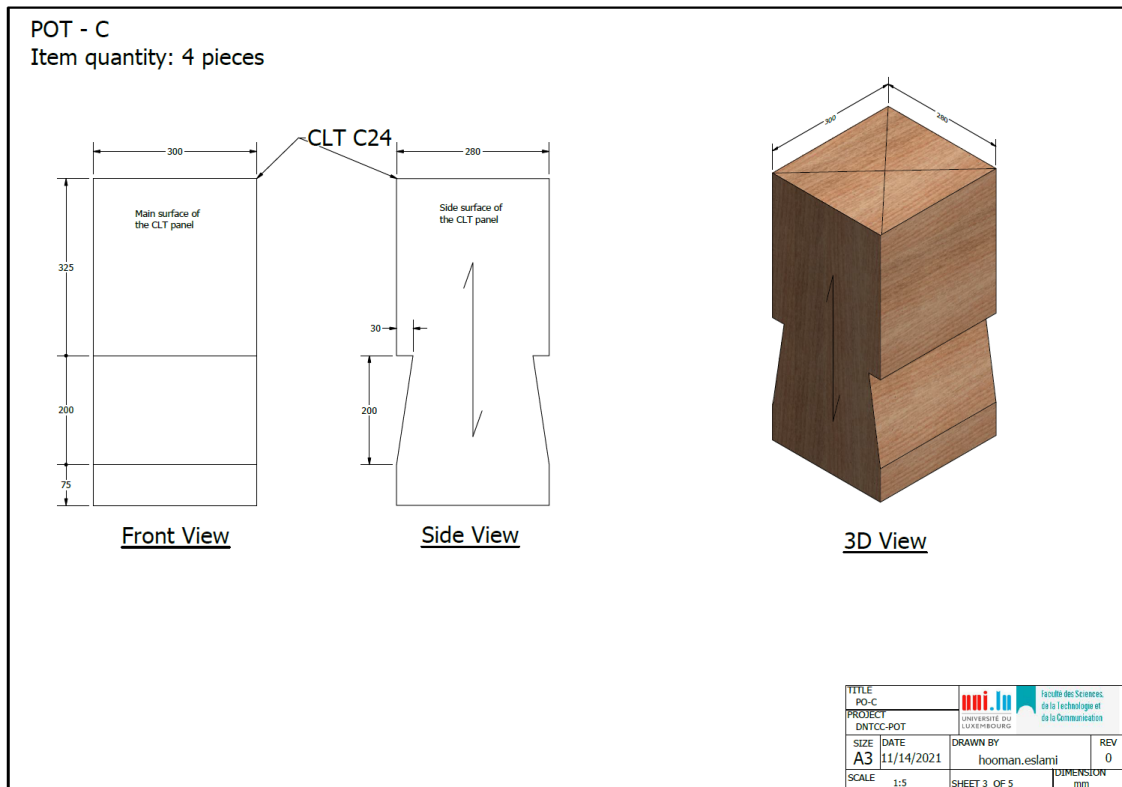
- Push-out test specimen PO-A CLT cut



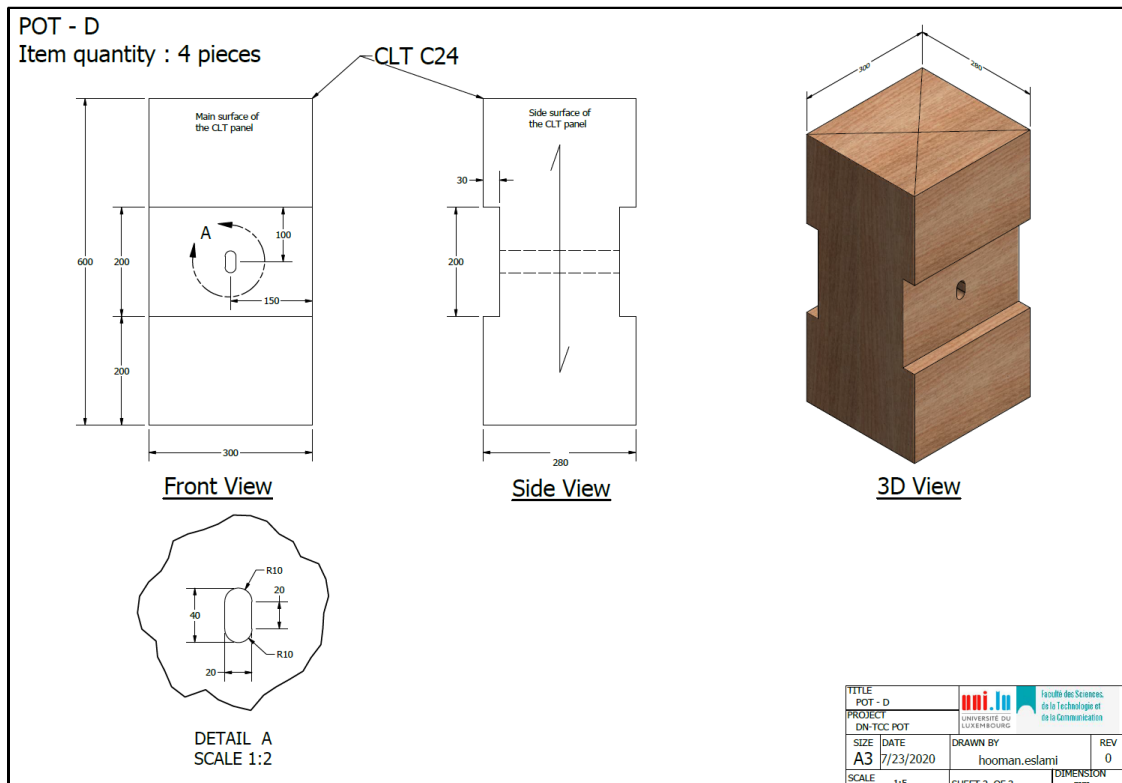
- Push-out test specimen PO-B CLT cut



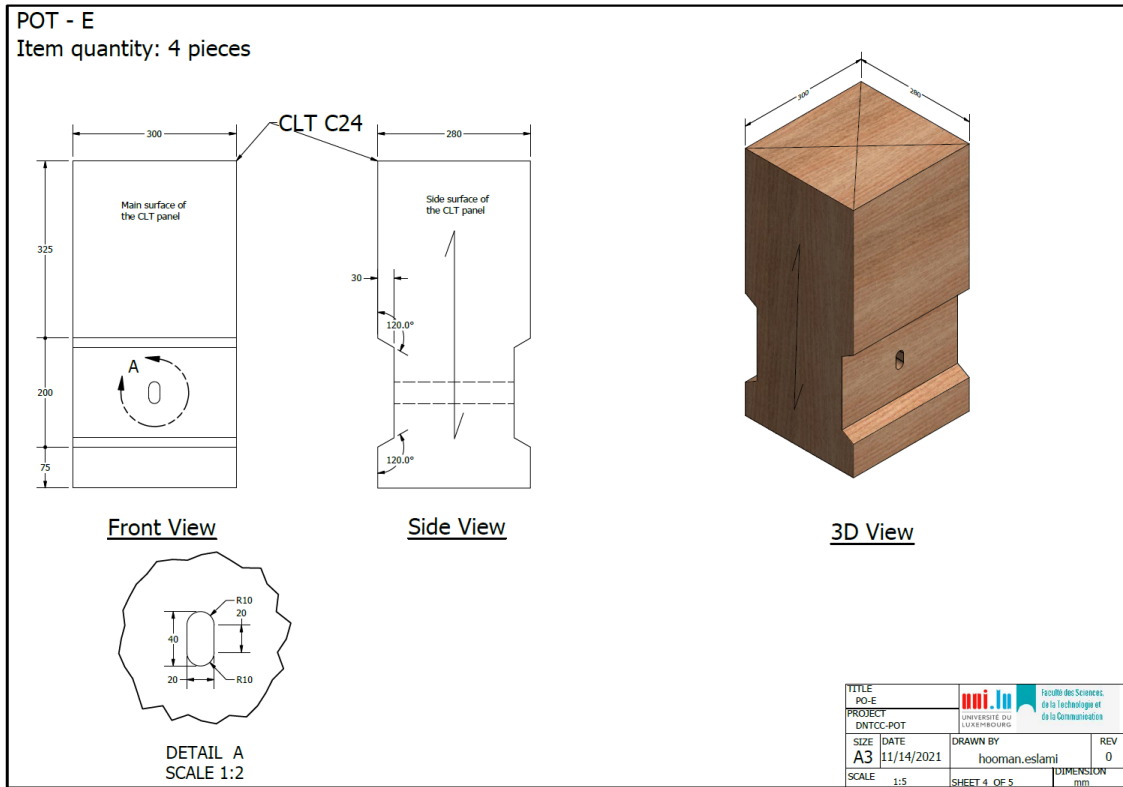
- Push-out test specimen PO-C CLT cut



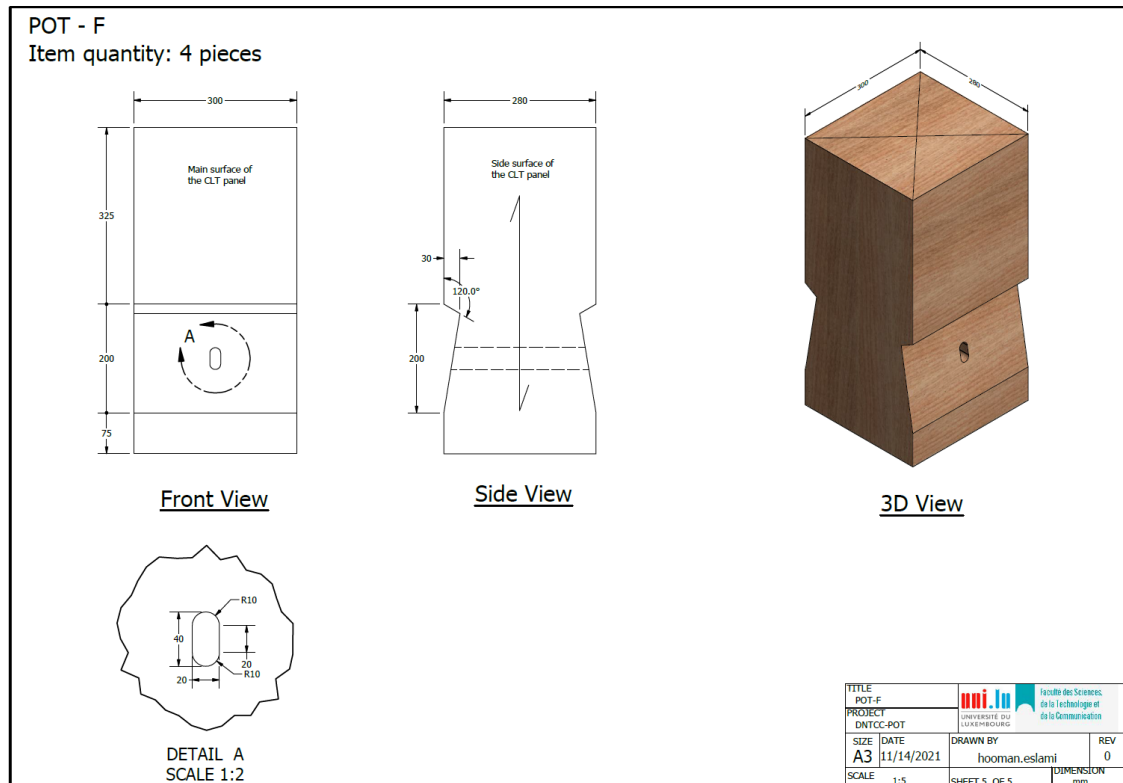
- Push-out test specimen PO-D CLT cut



- Push-out test specimen PO-E CLT cut



- Push-out test specimen PO-F CLT cut



8.3 Drawing of downscaled bending test

